Signaling Analyses of Therapeutic T cells Engineered with Synthetic Receptors

Alexander Isaac Salter

A dissertation

submitted in partial fulfillment of the

requirements for the degree of

Doctor of Philosophy

University of Washington

2018

Reading Committee:

Stanley R. Riddell, Chair

Michael J. Gale Jr.

Edus H. Warren

Program Authorized to Offer Degree:

Molecular and Cellular Biology

University of Washington

Abstract

Signaling Analyses of Therapeutic T Cells Engineered with Synthetic Receptors

Alexander Isaac Salter

Chair of the Supervisory Committee:

Stanley Riddell

Department of Immunology

Revolutionary new cancer therapies are harnessing the power of our immune systems. One type of cancer immunotherapy employs T cells that are genetically re-programmed to efficiently recognize and attack a patient's tumor. Tumor recognition by T cells is normally mediated by T cell receptors (TCRs), but synthetic constructs called chimeric antigen receptors (CARs) are increasingly used in T cell therapies. In simple terms, CARs merge specific protein-binding antibody elements with TCR-related signaling moieties. Clinical trials demonstrate that CAR-engineered T cells can produce dramatic regressions in certain individuals with hematologic malignancies. However, relapses too often occur and, to date, CAR T cell therapy has rarely been effective against solid tumors. Successful cancer-killing activities require that specific activating signals are sent throughout the T cell when the CAR binds to certain proteins on a cancer cell.

Enhancing these signals could optimize antitumor activity, but has proven challenging because we incompletely understand how receptor affinity, structural elements and signaling domains affect T cell effector functions. In my thesis-directed studies, I applied innovative cell signaling analyses to increase our understanding of the molecular events that promote CAR T cell efficacy. I developed an unbiased mass spectrometry technique to comprehensively interrogate signaling proteins in primary human T cells and applied this technique to describe synthetic CAR and natural TCR signaling in detail. By coupling signaling analyses to separate measures of gene transcription, protein-protein interactions, T cell function *in vitro* and therapeutic efficacy in mouse models of cancer, my work provides new insights into how signals delivered by synthetic receptors impact T cell function. Collectively, my findings enhance our understanding of the molecular underpinnings of successful CAR T cell therapy and provide a framework to guide the design of more effective therapeutic receptors.

Table of Contents

List of Figures

Acknowledgements

This thesis would not be possible without the help and support of many individuals. First and foremost, I would like to thank Dr. Stanley (Stan) Riddell for his outstanding mentorship. Stan possesses an infectious enthusiasm for science and critical eye for evaluating scientific work. Stan has high expectations for his trainees, and while it occasionally has been challenging to meet these demands, both me and my science are better for it. I have learned immensely by studying his approach to the scientific process and hope to emulate many of his traits as I work towards my career goal of becoming a physician scientist.

I would also like to thank my thesis committee members – Drs. Edus “Hootie” Warren, Mike Gale, Julie Overbaugh and Martin Prlic – for providing invaluable feedback and advice as I progressed through my training. I sincerely appreciate the time and energy that each of you invested in my scientific development.

Friends and colleagues in the Riddell laboratory, Program in Immunology, and other Fred Hutch departments also provided advice, insight, and technical support instrumental for my success. I would specifically like to acknowledge two Riddell laboratory members – Drs. Shivani Srivastava and Josh Veatch – for serving as a sounding board for both scientific and comical ideas. Graduate school can be an isolating experience, but it was made easier by working with people who I liked and respected.

Finally, thank you to my family and friends. My parents, Andy and Michele, and sister, Hannah, have been there for me every step of the way. Know that it is your support that makes my hard work possible and worthwhile. You motivate me to work fervently so that I may one day improve lives through science and medicine.

Chapter 1
Signaling in the Immune System

In the division of labor within multicellular organisms, the immune system is tasked with protecting the host from damage and infection. Specialized types of immune cells perform different, essential tasks to produce a replete immune response. Neutrophils, macrophages and dendritic cells phagocytose pathogens and tissue debris to protect the host. B lymphocytes, also known as B cells, help direct immune responses against bacterial and viral infections by secreting antibodies when they detect foreign proteins on infected cells. T lymphocytes, or T cells, recognize foreign peptides bound by self major histocompatibility complex (MHC) molecules, based on expression of a large diversity of T-cell receptors (TCRs) that are generated by DNA recombination during thymic development and selection.

One subset of mature T cells expresses the CD8 co-receptor and recognizes 8-11mer peptides bound to class I MHC molecules. If a foreign or non-self pMHC complex is detected, $CD8^+$ T cells become activated, kill the pMHC-expressing cells using cytotoxic chemicals known as perforin and granzyme, secrete pro-inflammatory cytokines, and enter the cell cycle. A second subset of mature T cells called helper T cells express the CD4 co-receptor and support $CD8^+$ T cell and B cell functions by optimizing antigen presentation and providing supplementary cytokines. A unique subpopulation of $CD4^+$ T cells, known as regulatory T cells, can suppress $CD8^+$ T cell responses and thereby limit the development of autoimmune and chronic inflammatory diseases. Importantly, immune activation can give rise to long-lived, memory B and T cells that remember the initial antigen encounter and can be reactivated upon re-exposure to the antigen. Reactivation of memory B and T cells promotes a stronger, faster, and more protective immune response.

To recognize and respond to the early stages of tissue damage or infection, immune cells must process and convert external stimuli into intracellular messages that dictate individual cell behavior. Immune cells must also communicate with both nearby and distant cells to coordinate distinct components of a multifaceted immune response. Immune response-inducing stimuli include the presence of tissue damage-associated and/or pathogen-associated molecular patterns, pH or nutrient levels in the local cellular environment, as well as non-self or altered-self proteins/peptides ‘presented’ by MHC molecules (pMHC).

Cell membrane-spanning surface receptors can sense environmental cues and mediate communication between immune cell subsets. In basic terms, binding of a receptor’s extracellular domain(s) to a soluble or membrane-bound ligand alters the biophysical state of the receptor’s intracellular domain(s), often through dimerization or multimerization of receptor chains. These events initiate biochemical events in the cytoplasm that can be amplified and carried to various organelles to initiate changes in cell behavior, in a process known as

intracellular signal transduction. Signals that reach specific proteins in the cytoplasm and cytoskeleton may induce changes in cell shape, motility, and/or granule release. In the nucleus, biochemical messages can activate transcription factors that alter gene expression and initiate cell division.

Many proteins have evolved to convert extracellular information to intracellular messages and carry these signals to the appropriate intracellular destination(s). G protein coupled receptors (GPCRs) are a prototypical type of signal transducing receptor that possess seven cell membrane-spanning segments (*1*). Upon ligand binding, GPCRs associate with heterotrimeric G protein complexes and activate secondary messengers, including inositol 1,3,5-triphosphate (IP_3) and calcium (Ca^{2+}) flux. IP_3 and Ca^{2+} then carry messages throughout the cell cytoplasm and into the nucleus.

A second type of messenger system involves protein phosphorylation (PO_4), attaching a phosphate group to a free hydroxyl group on serine, threonine or tyrosine amino acids within proteins (*2*). These signal transduction cascades are often initiated by a receptor tyrosine kinase, which is a dimeric transmembrane receptor that links an extracellular ligand-binding domain to an intracellular kinase domain. Extracellular receptor-ligand interactions promote PO_4 of the receptor's intracellular domains and/or of other intracellular signaling proteins. However, protein PO_4 signal transduction cascades can also be initiated by non-receptor kinases. For example, T and B cells recognize foreign antigens with transmembrane receptors that possess no intrinsic kinase capacity, and require close association with neighboring kinases to initiate and regulate signal transduction (*3*).

No matter the source of initiation, protein PO_4 plays an integral role in signal transduction by regulating protein structure, protein activity and protein-protein interactions (*2*). For instance, the negative charge imposed by a PO_4 group can alter protein structure to "unlock" a kinase domain that phosphorylates secondary messenger proteins. Negative charge can also change a protein's subcellular localization or ability to interact with other proteins. With regard to T cells, PO_4 of a transmembrane adapter protein called linker of activation of T cells (LAT) creates docking sites for many cytoplasmic signaling adapters, phospholipases and kinases, which are then recruited to form a large protein signaling complex that transmits messages to other organelles (*4*).

Cell surface receptors can also alter gene expression by transmitting messages directly to the nucleus. In immune cells, Janus kinases (JAKs) and signal transducer and activator of transcription proteins (STATs) transfer cytokine receptor signals directly to the nucleus (*5*). Similar to receptor tyrosine kinases, cytokine binding leads to receptor dimerization, PO_4 of the

receptor chains by associated JAKs, and subsequent PO_4 of STATs. However, instead of forming a large cytoplasmic complex to further propagate protein PO_4 events, STATs dimerize and migrate into the nucleus to alter gene transcription. Notch receptors represent a second mechanism for direct nuclear signaling, in which extracellular ligand binding induces proteolytic cleavage of the receptor's intracellular domain (*6*). Once cleaved, the endodomain migrates to the nucleus and acts as a transcription factor to regulate gene expression. Notch receptors were recently modified to encode orthogonal transcriptional factors and, when applied to genetically modified T cells, synthetic Notch (synNotch) receptors activated transcription of an inducible lentiviral gene expression cassette with binding sites for the orthogonal transcription factor (*7-9*). synNotch receptors represent an advance in synthetic signaling circuit design that could be broadly applied to therapeutic T cells. In Appendix 1, I build upon these proof-of-principle demonstrations by showing that synNotch receptors can regulate chimeric antigen receptor (CAR) expression and reduce off-tumor CAR T cell toxicity to non-malignant cells in the bone marrow and spleen.

T cells use all of these methods of signal transduction to respond to external stimuli in the thymus and peripheral tissues. However, T cells also express proteins that can regulate and inhibit signaling cascades. Phosphatases like SHP-1, SHP-2, and SHIP-1, may dampen protein PO_4 by removing phosphate groups from serine, threonine, and tyrosine residues (*10-14*). Ubiquitin-ligases can be used to degrade signaling proteins and/or multicomponent signaling complexes (*15*). For instance, TCR signaling induces expression of the ubiquitin ligase, Cbl-b, which ubiquitinates a signal-generating molecule called CD3, marking the molecule for degradation and reducing the initiation of new signals (*16*, *17*).

The TCR is a lineage-defining receptor that dictates the specificity of an individual T cell by converting ligand binding into intracellular protein PO_4 signaling and discriminating between potential foreign and host pMHC complexes (*18*). Elucidating key events and regulatory steps in the TCR signal transduction cascade has been the focus of extensive research over the past three decades, and cannot be fully summarized in this thesis (*3*, *19*, *20*). Nonetheless, I will provide a brief primer on key steps in TCR signaling as context for my work on synthetic signaling receptors described in subsequent chapters.

TCR binding to pMHC promotes clustering of TCR-CD3 complexes on the T cell surface, and leads to ordered rearrangement of the TCR and other transmembrane proteins into a supramolecular structure, called an immunological synapse (*21*). This ordered assortment of signaling molecules is believed to be critical for intracellular signal generation because the TCR does not possess intrinsic kinase activity (*3*). Signal generation instead requires close

association with non-receptor kinases, such as Lck, which phosphorylate tyrosine residues in immunoreceptor tyrosine-based activation motifs (ITAMs) on CD3δ, ε, γ, or ζ chains (*22*, *23*). In turn, CD3 PO_4 recruits another signaling kinase, ZAP-70, to the TCR-CD3 complex, where it is phosphorylated and activated by Lck (*24*). ZAP-70 then phosphorylates additional signaling adapters, including SLP-76 and LAT, which go on to form a signalosome that initiates downstream signaling pathways and gene expression programs (*25-29*). Collectively, these events are referred to as signal 1 for T cell activation. Robust T cell growth and division requires a second mitogenic signal, signal 2, which is delivered by surface costimulatory molecules (CD28, 4-1BB, ICOS and others) that bind to ligands on the antigen presenting cell (*30*). Interaction of a costimulatory receptor with its ligand(s) further induces protein PO_4 and/or ubiquitination signals that promote cell growth and division (*31*). Cytokine signals in the local cellular environment can also influence T cell responses, and are known as signal 3 (*32*).

In the late 1980s and early 1990s, researchers asked whether the TCR could be reconfigured to signal in a pMHC-independent manner. Zelig Eshhar and colleagues constructed the first known chimeric T cell receptor by replacing TCR α and β chain variable sequences with immunoglobulin heavy and light chain sequences (*33*). This dimeric receptor provided evidence that T cells could be activated in an MHC-independent manner. Subsequent iterations led to single chain receptors and further demonstrated the CD3ζ signaling endodomain was sufficient for T cell activation (*22*, *34*). With these results, researchers quickly realized that such synthetic chimeric receptors could redirect T cell specificity to target tumor-associated or viral antigens present on the cell surface, without the need for MHC expression or restriction (*35*, *36*).

In the intervening years, CAR structure design has been refined to enhance T cell function in short-term *in vitro* assays and longer-term *in vivo* tumor models, and CARs are now being used to modify autologous T cells to treat cancer patients (reviewed in Chapter 2). However, despite significant investment and enthusiasm for clinical translation, the principles of CAR design are poorly defined and new receptors must be constructed empirically. An incomplete understanding remains regarding (1) how intracellular signals delivered by CARs compare to signals from the natural TCR complexes, and (2) how these synthetic signals impact T cell function and fate. Gaining this knowledge is likely to aid CAR optimization for improved antitumor efficacy and safety.

Upon joining the Riddell laboratory, I focused on addressing these important questions. Because formation of an immunological synapse and initiation of protein PO_4 are critical for canonical TCR activation, I decided to study synapse formation, signaling events and resulting T

cell function(s). I first developed a technique to label CARs with fluorescent proteins. These efforts led to a co-author publication (Appendix 2) and enabled other areas of my dissertation research (Chapters 3 and 5). I then collaborated with Dr. Amanda Paulovich and her laboratory at the Fred Hutch to apply mass spectrometry (MS) to analyze cell signaling in primary T cells. MS was an attractive technique to employ because it quantitates changes in protein PO_4 in an unbiased manner, unlike traditional antibody-based techniques that only permit measurement of pre-defined analytes for which there are commercially-available reagents (*37*). I used MS to compare signaling from two types of CARs in clinical use that contain different intracellular signaling modules (Chapter 3), and to compare signaling from synthetic CARs and natural TCRs (Chapter 4). In Chapter 5, I present findings regarding a second class of chimeric receptor called an immunomodulatory fusion protein (IFP) that blocks and converts negative signals and into positive costimulatory signals. I specifically delve into how IFP affinity impacts T cell function. My ongoing work is focused on using MS data to tune existing CAR signaling domains for improved function and safety, and to design new CAR signaling modules that efficiently recognize tumor cells expressing low levels of CAR antigen.

Chapter 2
A History of Adoptive T Cell Transfer

This chapter was adapted from the following published works:

Shivani Srivastava*, Alexander I. Salter*, and Stanley R. Riddell. “Chapter 19. Adoptive T Cell Transfer.” Cancer Immunotherapy Principles and Practice Textbook. Demos Medical. 2017.

Alexander I Salter, Margot J Pont, and Stanley R Riddell. “Chimeric antigen receptor-modified T cells: CD19 and the road beyond.” *Blood* (2018) 131.24: 2621-9.

***** denotes equal contributions.

Adoptive T cell transfer (ACT) is a personalized cancer therapy that involves the administration of tumor-reactive T lymphocytes derived from the patient's blood or tumor infiltrate, or engineered by gene transfer to recognize tumor antigens. ACT was shown to mediate antitumor activity against transplanted tumors in murine models even before the molecular nature of tumor antigens and the fundamentals of antigen processing and presentation were understood (*38*, *39*). Early evidence supporting the efficacy of T cells in treating human malignancies came from studies in leukemia patients who had relapsed after an allogeneic bone marrow transplant where the infusion of donor lymphocytes was shown to induce remission in a subset of patients (*40*). The strategies for using ACT to treat cancer have evolved as antigens expressed on tumor cells have been characterized and our understanding of regulation and differentiation of T cells has improved. The ability to efficiently deliver, express, and edit genes in T cells has further advanced the applications of ACT, and several ACT strategies are now providing curative therapy for a subset of patients with common epithelial cancers and hematologic malignancies (*41*) (**Figure 2.1**).

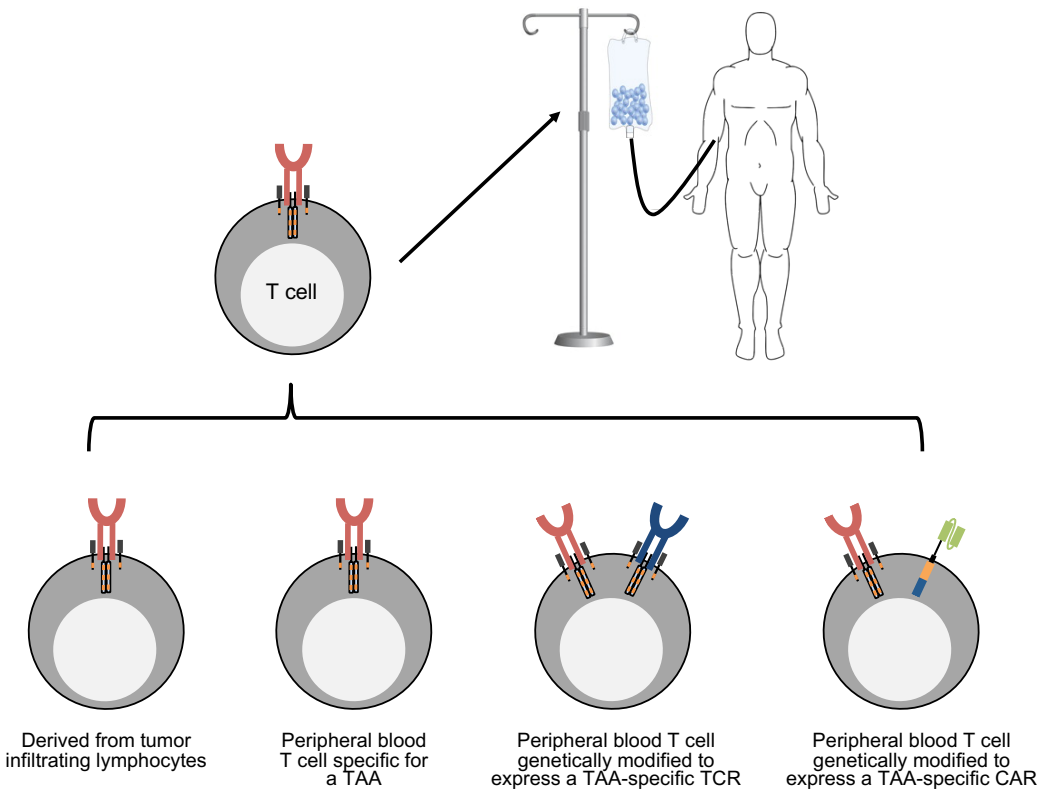

Figure 2.1. Types of tumor-reactive T cells used in adoptive T cell therapy. T cells that are reactive with tumor antigens can be derived from the tumor infiltrate or blood, or modified by gene transfer to express a TCR or CAR that is specific for a tumor-associated antigen.

T CELL RECOGNITION OF TUMOR-ASSOCIATED ANTIGENS

The utility of T cells for cancer therapy is predicated on identifying antigens that are selectively or preferentially expressed on tumor cells and have limited or absent expression on vital normal tissues. $CD8^+$ and $CD4^+$ T cells recognize peptides that are displayed on the cell surface bound to class I and class II major histocompatibility complex (MHC) molecules, respectively (*42*). Following activation by antigen presenting cells (APCs), T cells undergo clonal expansion and progressive differentiation into diverse effector and memory subsets that eliminate cells expressing the antigen and provide long-term protection for the host (*43*, *44*). With regard to cancer, several categories of antigens have been identified and are actively being pursued for ACT. A major category is self-proteins that are overexpressed in transformed cells compared with normal cells or expressed in differentiated normal tissues and tumors originating from those lineages. Examples include Melan-A (MART-1), glycoprotein 100 (gp100), carcinoembryonic antigen (CEA), Wilms tumor antigen 1 (WT-1), and survivin (*45*-*50*). Cancer-testes (C/T) antigens represent another class of self-antigens that are expressed only in normal testes but may be aberrantly expressed in tumors {VanDerBruggen:2002tq}. Tumors that result from oncogenic transformation caused by viruses, such as human papillomavirus (HPV), Epstein–Barr virus (EBV), and Merkel cell polyomavirus, express viral antigens that can be targets for ACT (*51*-*60*). Finally, coding mutations, frameshift mutations, gene fusions, or splice variants of expressed genes can give rise to neoantigens that are presented by MHC molecules on tumor cells (*61*, *62*) (**Table 2.1**).

In some settings, T cells specific for one or more tumor antigens can be detected or expanded from peripheral blood, but more commonly tumor-reactive T cells are present in blood at low frequency and specialized techniques are necessary to reliably extract and expand these cells. The near absence of tumor-reactive T cells in the blood of many cancer patients may reflect thymic deletion of high-avidity T cells reactive with self-antigens, the small number of antigens expressed in tumors that are driven by one or a few oncogenic mutations, a lack of priming of naive T cells to tumor antigens *in vivo*, and/or a loss of functional T cells because of immune regulation and suppression imposed by nascent or progressing tumors (*63*-*66*). Altogether, this poses a significant challenge to using autologous T cells for ACT. Tumor-reactive T cells are more frequent in tumor infiltrates from tumors with a high mutational load and those that have not activated signaling pathways that preclude T cell infiltration or local T cell proliferation (*67*-*72*). This observation led to the first successful clinical applications of ACT with expanded populations of tumor-infiltrating lymphocytes (TILs). As discussed in following sections, it is also now feasible to introduce genes that encode natural or enhanced T cell

receptors (TCRs) or synthetic chimeric antigen receptors (CARs) into T cells from patients that lack readily identifiable tumor-reactive T cells in blood or tumor, and expand the applications of ACT to greater numbers of individuals.

Table 19.1 Representative Examples of Tumor-Associated Antigens That May Serve as Targets for MHC-Restricted T Cells

Class of Tumor Antigen	Examples	Examples of Tumor Type(s)
Self-differentiation antigens	MART-1, gp100 Proteinase 3	Melanoma Leukemia
Self-overexpressed antigens	WT-1 Mesothelin Her2	Leukemia, epithelial cancers Mesothelioma, lung and ovarian cancer Breast, ovarian
Self-cancer-testes (C/T) antigens	NY-ESO-1 MAGE A3 Other C/T members	Melanoma, sarcoma, myeloma, other tumor types Melanoma, many tumors Many tumors
Viral antigens	EBV (LMP-1, 2) HPV (E6, E7) Merkel cell polyoma virus	Lymphoma Cervical cancer, head and neck cancer Merkel cell cancer
Neoantigens from oncogenic mutations	KRAS BRAF	Lung, pancreas, colorectal Melanoma, hairy cell leukemia
Neoantigens from random somatic mutations	Patient specific	Common in melanoma, lung cancer, bladder cancer present in many tumor types

EBV, Epstein–Barr virus; HPV, human papillomavirus; LMP, latent membrane protein; MAGE, melanoma-associated antigen 3; MART, melan-A; MHC, major histocompatibility complex; WT-1, Wilms tumor antigen 1.

ADOPTIVE TRANSFER OF TUMOR INFILTRATING LYMPHOCYTES

Many human tumors are infiltrated with diverse subsets of immune cells, and their presence can positively or negatively affect tumor progression (*73-85*). The amount and location of $CD3^+$ T cell infiltration is an independent predictor of good prognosis in many tumors including colon cancer, ovarian cancer, and breast cancer, and provides inferential evidence that some infiltrating T cells may recognize tumor antigens and regulate tumor growth (*79*, *84*, *86*, *87*). Studies of transplantable tumors in mice showed that tumor-infiltrating T cells were enriched for tumor specificity, and that transferring TILs to syngeneic recipients could mediate antitumor activity against an identical tumor (*88*).

Pioneering studies by investigators in the Surgery Branch at the National Cancer Institute (NCI) examined the use of TILs for ACT in patients with melanoma. To obtain TILs, metastatic melanoma lesions were surgically resected and tumor fragments were cultured in high doses of IL-2, which led to the outgrowth of mixed populations of $CD4^+$ and $CD8^+$ T cells that often specifically recognized tumor cells (*89*, *90*). In a seminal study, expanded TILs were administered to patients in large numbers (10^{10}-10^{11} cells) after low-dose cyclophosphamide and before high-dose systemic IL-2 (*91*). An overall response rate (ORR) of 55% provided the

first evidence that TILs had therapeutic utility in human cancer. Subsequent work using gene marking of TILs showed that the transferred cells persisted only a short time *in vivo* and the antitumor responses were rarely complete or durable (*92*). Moreover, many patients were not eligible for ACT because their tumors lacked vigorous T cell infiltrates and TILs could not be isolated, or because the tumor progressed too rapidly for a therapeutic product to be generated.

Lymphodepleting chemotherapy enhances the efficacy of ACT

Insights into how TIL therapy might be improved initially came from ACT experiments in mice in which administration of cytotoxic chemotherapy before T cell infusion enhanced antitumor efficacy (*93*, *94*). Various cytotoxic regimens for lymphodepletion before TIL infusion were then evaluated in melanoma patients, which increased ORRs to 50-70%, with 11-24% of patients achieving complete and durable remissions (*95-99*). These clinical findings prompted a return to experiments in mice to elucidate precise mechanisms by which chemotherapy enhanced T cell transfer. In addition to reducing tumor burden, chemotherapy was shown to deplete suppressive cell populations, eliminate endogenous lymphocytes that competed for homeostatic cytokines necessary for T cell proliferation and survival, and activate endogenous APC (*100*, *101*). The administration of lymphodepleting chemotherapy followed by TIL infusion and IL-2 for advanced melanoma has now been adopted at several centers, with similar rates of overall response and complete remission (CR) (*102-105*).

Melanoma TILs Have Diverse Antigen Specificity

The efficacy of ACT with TILs provided an opportunity to identify tumor-associated antigens that are recognized in an effective antitumor immune response. T cells specific for epitopes derived from the melanocyte differentiation antigens MART-1, gp100, tyrosinase, and C/T antigens are often present in TILs, and were initially considered the targets responsible for efficacy. Differentiation and C/T antigens are shared among many patients and TCRs specific for these antigens could provide off-the-shelf reagents for engineering T cell specificity in patients with the appropriate MHC allele for the TCR. More recently, whole exome sequencing of melanoma cells from patients has revealed a high mutation load as a consequence of prior ultraviolet light exposure and suggested that neoantigens might be generated (*106*). Indeed, analysis of the specificity of TILs for candidate neoantigens encoded by nonsynonymous mutations in expressed genes identified a diverse response to multiple neoantigens, and these targets are now considered to be important in therapeutic responses to TILs (*107-110*). It is unfortunate that there is significant intratumoral heterogeneity for somatic mutations in

melanoma, and these mutations are not typically shared across patients (*109*, *111*). Mutations in genes, such as BRAF and RAS, that drive oncogenesis are ubiquitous and would be ideal targets; however, T cells specific for these mutations are not commonly found in melanoma TILs.

A critical question is why the tumor-specific T cells that are already present in the patient are not effective in promoting tumor regression. Several factors in the tumor microenvironment (TME) have been identified to inhibit the local function of TILs including a hostile metabolic environment, low levels of class I or II MHC molecules on tumor cells, expression of programmed death-ligand 1 (PD-L1) on tumor and/or infiltrating immune cells, and infiltration with immunosuppressive $CD4^+FoxP3^+$ regulatory T cells and/or myeloid cells (*112*, *113*). Antibodies that target cytotoxic T-lymphocyte-associated protein 4 (CTLA-4), PD-1, or PD-L1 can overcome suppression mediated through these immune checkpoints and are effective in many cancers, particularly those with high mutational burden (*66*, *114*, *115*). However, it is important to note that in melanoma, TILs can be effective in patients who have failed prior treatment with checkpoint-blocking antibodies, suggesting unique benefits in combining lymphodepleting chemotherapy, ACT, and IL-2 for overcoming resistance to immune-mediated tumor eradication. Future combinations of antibodies and/or small molecules that target the immunosuppressive mechanisms operative in the TME may be effective without TIL infusion and narrow the therapeutic applications of TILs. However, the analysis of location, phenotype, specificity, transcriptional, and epigenetic properties of TILs has enriched our understanding of interactions between the tumor and the immune system, and identified opportunities for intervention.

TILs for Solid Tumors Beyond Melanoma

TILs have been expanded from many cancers including cholangiocarcinoma, pancreatic, gastric, renal cell, cervical, and hepatocellular carcinomas, and often show evidence of tumor reactivity. Provocative data from small phase 1 studies of ACT with TILs have been reported in a variety of tumor types, including case reports in cholangiocarcinoma and metastatic colorectal cancer, but this approach has not achieved the uniform success as in melanoma citation (*116-121*). A case report showing regression of metastatic colorectal cancer with the infusion of TILs specific for a mutant epitope of the KRAS oncogene presented by human leukocyte antigen (HLA) C*08:02 illustrates the principle that T cells can recognize oncogenic mutations (*122*). Thus, despite the need for surgical resection to obtain the tumor, the variation in success in culturing TILs, and the complexity, cost, and duration of culture required to prepare a

therapeutic product, important scientific insights with broad implications can be obtained from TILs.

TILs for Hematologic Malignancies

ACT with lymphocytes infiltrating the bone marrow has been investigated in a phase 1 study in patients with myeloma. In this study, marrow infiltrating T cells (MILs) were expanded using anti-CD3/CD28 monoclonal antibody (mAb)-coated beads and then reinfused after myeloablative chemotherapy and autologous $CD34^+$ stem cell transplant (*123*). The approach was feasible, resulted in detectable T cell responses to myeloma antigens after transplant, and provided encouraging evidence for efficacy in a subset of patients. Further study is necessary to confirm these results and determine whether shared and/or mutated antigens are recognized by MILs.

ACT WITH TUMOR-REACTIVE T CELLS ISOLATED FROM BLOOD

Studies in allogeneic stem cell transplant recipients demonstrated that ACT with virus-specific T cell clones or highly enriched polyclonal virus-specific T cells expanded from the blood of the donor could reconstitute protective immunity (*124-129*). With the identification of shared tumor-associated antigens and their MHC-restricting alleles, it was reasonable to apply similar techniques to determine if infrequent tumor-reactive T cells for ACT could be isolated from peripheral blood. Isolating tumor-reactive T cells from blood avoids the need for surgical resection of tumors to derive TILs, but requires complex culture methods that employ autologous APC pulsed with antigenic peptides to expand tumor-reactive T cells to levels sufficient for T cell cloning, and/or sorting with MHC multimers before expansion (*130*).

The first trials of ACT with autologous $CD8^+$ T cell clones targeted the melanocyte differentiation antigens MART-1 or gp100 and administered the T cells without prior lymphodepleting chemotherapy (*131*, *132*). These studies provided evidence of antitumor activity, but responses were rarely complete and transferred T cells did not proliferate or survive long term *in vivo*, even with supplemental IL-2. The addition of lymphodepleting chemotherapy before T cell transfer improved the persistence of T cell clones, but CRs remained infrequent and antitumor effects were usually transient (*133-136*). Given the small number of patients treated in these studies, it is uncertain if the lower efficacy compared with TILs was because of targeting only a single antigen; differences in the avidity, phenotype, or differentiation status of the T cells; or differences in treatment regimens.

Cytokine Modulation of T Cell Differentiation in Culture

ACT with T cell clones or polyclonal T cells has typically required prolonged culture in IL-2 to obtain the numbers of T cells that were perceived to be necessary for efficacy. After culture, the T cells expressed a highly differentiated phenotype, with absent or low expression of CD62L, CD28, and CD27, which, based on our current understanding of T cell differentiation, would be suboptimal for ACT (*137-139*). Investigation of alternative culture conditions for expanding antigen-specific $CD8^+$ T cells from blood demonstrated that IL-21 favored the outgrowth of specific T cells from the naïve pool that retained CD28 expression (*140*). Based on these findings, IL-21 was used during isolation of T cell clones targeting WT-1, which is expressed at high levels in acute myeloid leukemia (AML). Patients with AML that received WT-1 specific T cell clones cultured with IL-21 demonstrated improved persistence compared with those cultured with IL-2, although antitumor efficacy in both groups of patients was limited, perhaps reflecting the low affinity of T cells specific for the self-antigen WT-1 (*141*). More rapid and effective methods for isolating rare tumor-reactive populations without inducing terminal differentiation are likely to improve feasibility, *in vivo* persistence, and efficacy of ACT.

Combining ACT with Checkpoint Inhibitors

Multiple immunotherapeutic modalities have antitumor efficacy, and it is logical to investigate combining these approaches to improve outcomes. Adoptively transferred T cells upregulate molecules, such as CTLA-4 and PD-1, *in vivo*, and administering antibodies that target these immune checkpoints with ACT enhanced efficacy in murine tumor models (*142-144*). A small clinical study in melanoma patients combined the infusion of polyclonal $CD8^+$ MART-1-specific T cells with CTLA-4 blockade. Two of 10 patients achieved a complete remission and T cell responses to additional tumor antigens were evident after therapy, suggesting both improved activity of the transferred T cells and recruitment of new responses (*145*). These results provide encouragement that efficacy of ACT with tumor-reactive T cells derived from the blood can be improved with combination therapy.

T CELL RECEPTOR ENGINEERING OF T CELLS FOR ACT

As previously noted, it is challenging to isolate tumor-reactive T cells from the tumor or blood of many patients. Moreover, generating a cell product for reinfusion often takes several weeks, which is problematic for patients with advanced tumors that progress rapidly. To improve feasibility, a focus in the field has been to identify, clone, and engineer TCRs that are specific for shared tumor-associated antigens presented on common MHC alleles. Such TCRs could

provide off-the-shelf reagents for endowing autologous T cells with tumor reactivity. This approach requires viral or non-viral gene insertion to introduce the TCR into autologous T cells. After *in vitro* expansion, preferably with cytokines such as IL-21 that limit T cell differentiation during culture, the modified T cells can be reinfused back into the patient.

Techniques for genetic modification of primary human T cells

The most well-studied methods for modifying human T cells use retroviral or lentiviral vectors to deliver a transgene that becomes stably integrated into the host cell genome. Early work focused on optimizing the tropism, structure, promoter, and packaging of retroviruses and lentiviruses for obtaining high expression of exogenous TCRs in viable primary T cells (*146-148*). As the TCR is composed of two independent chains (α and β), these studies also sought to determine how best to express two proteins from a single transgene cassette—whether to use two open reading frames with distinct promoters or an internal ribosomal entry site, or one open-reading frame separated by a 2A ribosomal skip element that mediates co-translational polypeptide cleavage (*149*). A disadvantage of two open-reading frames is that the transgene includes a second promoter, which increases the size of the DNA insert and can result in lower viral titer and transduction efficiency. In addition, because promoters vary in strength, the TCR chains encoded in each open-reading frame may not be produced in equimolar amounts, thereby reducing the absolute number of appropriately paired α and β chains on the cell surface. At present, the field has coalesced around the use of 2A ribosomal skip elements to provide for equimolar production of both TCR chains. Several retrovirus and lentivirus vectors have been developed that provide stable expression of exogenous TCRs and other transgenes, and thus far there has been no evidence that gene insertion results in transforming mutations in human T cells (*150*, *151*). This was a relevant issue because clinical studies of retroviral gene transfer into hematopoietic stem cells to correct immunodeficiency syndromes resulted in insertional mutagenesis and leukemia development in a fraction of patients (*152*, *153*). Although this remains a concern, the improved design of viral vectors and apparent intrinsic resistance of T cells to insertional mutagenesis have reassured investigators and regulators alike, and clinical applications of viral gene transfer into T cells have proceeded rapidly.

The production of retrovirus and lentivirus vectors for clinical use poses several challenges for investigators outside of industry or major academic centers (*154*, *155*). First, clinical-grade production of lentiviral or retroviral vectors can take several weeks and is expensive. Second, viral stocks must be tested for safety, including the absence of a replication-competent virus that could be generated by sporadic recombination events during

manufacturing. Third, the size of the transgene payload is limited to ~5 kb by the constraints of packaging viral genomes in retroviral and lentiviral capsids. These limitations have made it difficult thus far to test different TCR designs or multiple TCRs targeting different tumor antigens in a single trial.

Because of the limitations of viral gene delivery, there has been significant interest in using non-viral techniques for modifying T cells. The Sleeping Beauty transposon system for genetic modification uses an engineered transposase to integrate a co-transfected transgene carrying transposon into the genome of human cells (*156*, *157*). Inverted repeat sequences flanking a genetic payload are recognized by the coexpressed transposase, which then catalyzes integration of the transgene-transposon cassette into the genome. Two studies demonstrated the ability of the Sleeping Beauty system to transfer an exogenous TCR into primary human T cells and showed that Sleeping Beauty integrated the transgene into the genome in similar loci as a lentiviral vector (*158*, *159*). Because plasmid DNA can be produced for clinical use more rapidly and inexpensively, there is considerable interest in Sleeping Beauty and other non-viral delivery systems, and phase 1 clinical applications are now being reported (*160*).

T cell receptor mispairing can generate undesired antigen specificities

The initial studies transferring exogenous TCRs into T cells uncovered issues that required further modifications of the transgene. Because the TCR is an $\alpha\beta$ heterodimer and both chains are required for recognition of peptide-MHC (pMHC), the introduction of exogenous α and β chains into a T cell by gene transfer could lead to mispairing of these chains with the endogenous TCR α and β chains (*161*). Mispaired TCR chains diminish the absolute number of correctly paired species on the cell surface and, if expressed in post-thymic T cells, can confer new specificities including self-reactivity. Indeed, when a TCR was transferred into polyclonal murine T cells, mispairing led to systemic autoimmunity resulting in bone marrow failure, pancreatitis, and colitis (*162*). Mispairing was also reported in primary human T cells and led to undesired reactivity against lymphoblastoid cell lines and hematopoietic cell lineages *in vitro*, raising concern that mispairing could lead to toxicity in patients (*163*).

Several strategies have been developed to prevent or minimize TCR mispairing and promote strong TCR expression. One relies on “murinization” or swapping of sequences in the human TCR constant regions not involved in pMHC recognition with those of the murine TCR α and β chains. These efforts began with the observation that a mouse TCR could be expressed in human T cells at higher levels than the endogenous human TCR counterpart (*164*). However,

when murine TCRs specific for human tumor-associated antigens were transduced into human T cells and used for ACT in a clinical trial, a subset of patients developed anti-TCR antibody responses (*165*). This led to the creation of human-mouse hybrid TCRs containing human variable regions and murine α and β constant regions that preferentially pair with each other and not with human constant regions (*166*-*168*). Careful analysis of the murine constant region showed that only nine murine amino acid residues needed to be incorporated into the human constant region to abrogate mispairing (*169*). More recently, it was found that interchanging the constant regions between human TCR α and β chains, so that the α chain contains the β constant region and vice versa, could prevent mispairing (*170*). Thus, domain-swapped TCRs or minimally murinized TCRs should mitigate mispairing and reduce the potential immunogenic space of the transgene.

Other methods to prevent mispairing have been described. In near simultaneous publications, two groups showed that incorporation of cysteine residues at defined positions in the TCR α and β chains led to preferential pairing and increased expression of the exogenous TCR (*171*, *172*). These effects were likely mediated by disulfide bonds formed between the cysteine residues. In the future, the problem of mispairing might be eliminated completely using genome-editing techniques including RNA interference, zinc-finger nucleases (ZFNs), Transcription activator-like effector nucleases, and clustered regularly interspaced short palindromic repeats (CRISPR)/Cas9 to silence, delete, or replace endogenous TCR chains. Silencing of endogenous TCR expression using transgene-encoded endogenous TCR loci-specific inhibitory RNA sequences increased expression of the introduced TCR, improved cytotoxic responses against cells presenting the antigen targeted by the exogenous TCR, and reduced mispairing toxicity in mice (*173*-*176*). ZFNs have been targeted to DNA sequences in the endogenous TCR α and β loci to create DNA double-strand breaks that, when repaired by error-prone nonhomologous end joining (NHEJ), disrupt the coding sequence, resulting in a knockout of endogenous TCR expression (*177*). This approach is cumbersome as it requires sequential delivery of ZFNs targeting each TCR chain, with introduction of the corresponding tumor-specific TCR chain. A logical next step would be to employ CRISPR/Cas9 gene editing with homologous recombination of an insert encoding exogenous TCR α and β chains into the native TCR α and β loci (*178*, *179*). This has the advantage of both preventing mispairing and placing the introduced TCR chains under natural regulatory control to provide for regulated expression of the exogenous TCR at normal levels. A potential limitation of CRISPR/Cas9 is low-editing efficiency in primary T cells when homologous recombination is required, but recent studies demonstrate that homologous recombination can be favored over NHEJ and suggest

the utility of this approach for clinical applications, such as TCR gene transfer, will be improved (*180-182*).

Optimal antigen targets for TCR targeted therapy

Numerous antigens that are selectively or preferentially expressed on cancer cells have been identified and prioritized for clinical translation (*183*). When performing ACT using TCR-modified T cells, it is critical that expression of the target antigen be restricted to transformed or dispensable normal cells. First, the peptide antigen should be a “driver” mutation critical for the oncogenic process or for cell survival so that tumor cells cannot easily downregulate the protein product during T cell therapy. Second, if not associated with oncogenesis or cell survival, the antigen should be uniformly expressed in all tumor cells to minimize the outgrowth of antigen-negative tumor cells, or multiple antigens should be targeted. Third, the antigen should be presented by common HLA alleles so that a maximum number of patients can benefit and a sufficient number of individuals can be treated to obtain robust data on safety and efficacy. Fourth, the peptide must be generated by the proteasome subunits expressed in the tumor cells and bind to the MHC molecule with high affinity (*184*, *185*). Finally, the TCRs that target the antigen should be of sufficiently high avidity to efficiently recognize the level of pMHC expressed on tumor cells (*186*).

Finding, isolating, and engineering TCRs for ACT

Generating TCR-modified T cells requires the development of off-the-shelf TCRs that, when introduced into T cells, reliably and safely redirect T cell specificity to tumor antigens. Exogenous TCRs for self and mutated antigens have been isolated from TIL products that mediated clinically effective antitumor responses, from the endogenous T cell repertoire in the blood of autologous and allogeneic donors, and from TCR and/or HLA-humanized mice that were immunized with peptide antigens (*187-189*). Recent studies have shown that a subset of T cells in tumor infiltrates and blood that express the PD-1 molecule, which is normally upregulated by activation and serves to inhibit T cell signaling, are enriched for tumor reactivity (*190-192*). This observation facilitates a new strategy for isolating tumor-reactive T cells and cloning their TCRs.

High-affinity TCRs that bind strongly to pMHC complexes are believed to be optimal for ACT. However, the affinity of TCRs that can be isolated to self-antigens is limited by thymic negative selection, which deletes T cells with TCRs that bind too strongly to MHC complexes presenting self-peptides (*193*, *194*). To circumvent the effects of central tolerance on TCR

affinity, many groups have sought to enhance the avidity of naturally isolated TCRs. This can be accomplished by mutating complementarity, determining regions in TCR α and β chain genes that define peptide specificity. Simple amino acid substitution as well as selection using phage display or T cell display have been harnessed for affinity enhancement (*195*, *196*). The TCRs produced by these methods can have significantly increased avidity compared with their natural counterparts but come with the potential risk of new undesired and unpredicted reactivities.

TCR gene transfer into $CD8^+$ and $CD4^+$ T Cells

Studies to determine the optimal T cell subsets to engineer for ACT are ongoing. It is established that $CD4^+$ T cells synergize with $CD8^+$ T cells in ACT (*197*, *198*), suggesting it would be advantageous to engineer both tumor-reactive $CD8^+$ and $CD4^+$ T cells with MHC class I- and class II-restricted TCRs, respectively. However, bioinformatics techniques for predicting and immunological reagents for detecting MHC class I antigens are significantly more robust than for MHC class II antigens. As a result, most TCRs that have been isolated for use in ACT are MHC class I-restricted and selected for function in $CD8^+$ T cells.

The CD8 or CD4 coreceptors bind to a conserved region on MHC class I or class II, respectively, and coreceptor binding is important for stabilizing the TCR-pMHC interaction and recruiting Lck, a critical kinase that phosphorylates the TCR-associated CD3 chains and initiates TCR signaling after pMHC engagement (*199*). Thus, placing a class I-restricted TCR into $CD4^+$ T cells disrupts the natural format of TCR recognition because CD4 does not strongly interact with MHC class I molecules. To this end, investigators assessed function of MHC class I-restricted TCRs in $CD4^+$ T cells and found that transducing $CD4^+$ T cells with CD8 α and β chains allows for antigen recognition, but altered effector responses (*200*, *201*). An alternative approach is to use avidity-enhanced TCRs that are not dependent on coreceptor binding for peptide recognition (*202*, *203*).

Clinical trials of TCR-modified T Cells demonstrate antitumor activity

In 2006, Rosenberg *et al*. at the NCI reported the results of a trial in HLA-A*02:01 individuals with progressive metastatic melanoma who received T cells genetically modified to express a MART-1-specific TCR previously isolated from a melanoma patient with a near-complete regression after TIL therapy (*95*, *204*). Two of 15 (13%) patients obtained transient partial responses, demonstrating that TCR-modified T cells could produce therapeutic responses in a subset of individuals with melanoma. None of the patients in this trial experienced off-target or on-target, off-tumor toxicity to normal melanocytes.

The same group later reported that higher avidity TCRs targeting MART-1 and gp100 had antitumor activity in individuals with melanoma (*205*). Objective antitumor responses were achieved in 6 of 20 (30%) patients receiving the anti-MART-1 T cells and 3 of 16 (19%) patients receiving anti-gp100 T cells. Both types of TCR-modified T cells persisted in the blood of all patients for more than 1 month, but a substantial fraction of patients suffered from eye and ear toxicities. Biopsies of affected tissues showed a $CD3^+$ infiltrate, suggesting that the toxicities resulted from on-target off-tumor T cell recognition and destruction of non-transformed melanocytes in these sites. These findings advise caution when using a high-avidity TCR targeting a self-antigen that is also expressed on normal tissues.

Findings from trials evaluating TCR-modified T cells specific for the C/T antigen NY-ESO-1 (aa157-165) in HLA-A*02:01 individuals have also been reported. Individuals with metastatic synovial cell sarcoma and melanoma were treated with a TCR containing two amino acid substitutions in the CDR3 region that enhanced T cell function (*195*, *206*, *207*). Objective responses were observed in 11 of 18 (61%) patients with synovial cell sarcoma and 11 of 20 (55%) patients with melanoma. In a second study, multiple myeloma patients were given an autologous stem cell transplant and infused two days later with TCR-modified T cells expressing an affinity-enhanced NY-ESO-1-specific TCR (*110*). The TCR-modified T cells expanded *in vivo*, trafficked to the bone marrow, and persisted for up to 2 years in some patients. The fact that the T cells were infused immediately after transplant complicates the evaluation of their antitumor efficacy, but the expression level of NY-ESO-1 on tumor cells decreased after treatment and relapses were NY-ESO-1-negative, suggesting that the TCR-modified T cells recognized antigen *in vivo*. Thus, T cells modified to express this NY-ESO-1-specific TCR are safe and can produce antitumor responses in some patients. Collectively these studies establish the principle that TCR-modified T cells can have therapeutic utility.

On-target and off-target toxicities of TCR-modified T cells

In addition to clinical responses, reports of severe toxicities caused by TCR-modified T cells have emerged and are instructive for future applications of this approach. One study evaluated a TCR specific for CEA, which is often overexpressed on tumors of the digestive tract but also expressed by normal colonic epithelial cells (*208*). Dose-limiting transient colitis developed in all three treated individuals soon after infusion of TCR-modified T cells. The colitis was traced to T cell-mediated attack of normal gastrointestinal tract tissues expressing the target antigen, indicating that certain overexpressed antigens may not be viable targets for

TCR-modified T cells (*209*). It remains unknown whether CEA might be safely targeted with T cells modified with a lower affinity TCR.

Toxicity has also been observed with TCR-modified T cells targeting the C/T antigen MAGE-A3, which is a member of the MAGE family of antigens expressed by many tumors (*210*, *211*). In this study, an avidity-enhanced TCR was derived from HLA-A2 transgenic mice by immunizing the mice with two MAGE-A3 peptides and introducing a single amino acid mutation in the CDR3 region of the TCR (*212*). After infusion into nine patients with metastatic melanoma, synovial sarcoma, or esophageal cancer, the T cells persisted for at least 1 month in each patient and 5 of 9 (56%) patients achieved an objective response. However, three patients developed severe neurologic toxicities without major changes in serum cytokine levels after T cell infusion (*213*). In subsequent analyses, the authors failed to find off-target reactivity of their TCR using *in vitro* immunological assays, but discovered that MAGE-A12, which contains a highly homologous peptide sequence to the MAGE-A3 epitope, is expressed in normal human brain. The authors concluded that the neurologic toxicity likely resulted from recognition of MAGE-A12 expressed on a subset of neurons. Their findings speak to the challenges of targeting epitopes that are similar or shared among proteins from the same family and of screening avidity-enhanced TCRs for off-target toxicity.

In 2013, another trial targeting a distinct HLA-A*01:01 restricted epitope of MAGE-A3 with an affinity-enhanced TCR had to be halted after two patients died from cardiogenic shock (*214*). In preclinical testing, the authors enhanced the affinity of the TCR by mutating four residues in the CDR2 region of the α chain. They did not detect cross-reactivity with other known MAGE family members and infused autologous T cells modified to express the affinity-enhanced TCR into individuals with melanoma and multiple myeloma. The first two treated patients developed severe cardiac abnormalities within days of the T cell infusion. Further analysis revealed that the TCR cross-reacted with a peptide derived from titin, which is expressed by cardiomyocytes (*215*, *216*). Although TCR affinity enhancement remains an intriguing strategy for improving the antitumor efficacy of TCR-modified T cells, a more sophisticated understanding of TCR cross-reactivity as well as improved strategies for characterizing affinity-enhanced TCRs and screening for peptides that are cross-reactive are necessary to reduce the likelihood of unanticipated off-target toxicity to normal tissues (*217*, *218*).

Unresolved questions and future directions of TCR-modified T cells

Marked progress has been made in the characterization of TCRs specific for peptide antigens, the optimization of these TCRs *in vitro*, and their testing in clinical trials. Preclinical and clinical data have demonstrated that T cells modified with exogenous TCRs can mediate antitumor responses for some antigens in certain clinical settings. However, a number of questions remain to be addressed in future work. First, clinical trials using TCR-modified T cells suggest that efficacy is partly dependent on the ability of the T cells to persist and *proliferate in vivo*. Fate mapping of T cells after ACT in preclinical models have provided evidence for a model of progressive T cell differentiation whereby naive $CD45RA^{+}CD62L^{+}$ T cells differentiate into long-lived memory stem ($CD45RA^{+}CD62L^{+}CD95^{+}$) and central memory cells ($CD45RO^{+}CD62L^{+}CD95^{+}$) that in turn give rise to shorter lived effector memory ($CD45RO^{+}CD62L^{-}CD95^{+}$) and effector ($CD45RO^{+}CD62L^{-}CD95^{+}$) T cell subsets (*219*-*223*). As discussed earlier, a significant fraction of endogenous tumor-reactive T cells isolated from tumor or blood and cultured *in vitro* become highly differentiated and possess a limited capacity for *in vivo* persistence. Transferring an exogenous TCR into polyclonal T cells partly overcomes this obstacle because the peripheral blood T cell compartment contains many less terminally differentiated T cells. In other systems, clinical trials of CD19-specific CAR T cells have demonstrated that isolating central memory $CD8^{+}$ T cells and $CD4^{+}$ T cells for cell manufacturing and combining the resulting $CD8^{+}$ and $CD4^{+}$ CAR T cells in a 1:1 ratio in the final cell product leads to remissions of refractory leukemia and lymphoma and a predictable dose–effect relationship (*224*, *225*). Therefore, it may be useful for further studies to address how T cell differentiation affects therapeutic efficacy of TCR-modified T cells. To accomplish this, investigators could employ methods for isolating less-differentiated subsets (*226*), genetically modify them to express a TCR, and test how those cells behave after pMHC recognition using *in vitro* measures of proliferation and *in vivo* models of persistence. Separately, it would be interesting to investigate whether other phenotypes, such as expression of certain costimulatory markers or homing receptors, should be selected during manufacturing.

Second, clinical trials of TCR-modified T cells showed that the antitumor responses were highly variable, despite the similarity between the transduction levels and numbers of transduced T cells administered to individual patients. One plausible source of variability is the level of expression of the exogenous TCR in the final cell product. Retroviral, lentiviral, and Sleeping Beauty techniques mediate transgene integration into actively transcribed areas of the genome. However, this process is relatively nonspecific and, in contrast to the tightly regulated TCR locus, each integration site will possess a unique chromatin architecture that is subject to

differential enhancer regulation. Thus, transgene expression can be highly variable from cell to cell. This can affect the functional avidity of the introduced TCR because the avidity of the TCR-pMHC interaction depends not only on the binding affinity but also on the number of TCR molecules that can be engaged. Future studies may use ZFNs or CRISPR/Cas9 to insert an exogenous TCR α and β chain into the endogenous TCR loci and determine how this affects receptor expression and antitumor efficacy in animal models.

Finally, as will be discussed in subsequent sections, it is now possible to engineer additional functions into T cells using synthetic receptors. Fully synthetic proteins that provide additional costimulation or cytokine support as well as resistance to transforming growth factor (TGF)-β signaling and PD-1 signaling have recently been described and tested in T cells (*227*, *228*). Combining them with an exogenous TCR could lead to improved antitumor efficacy.

GENETIC MODIFICATION OF T CELLS WITH SYNTHETIC RECEPTORS

Advances in synthetic biology and genetic modification have led to novel approaches for retargeting T cells to tumor antigens using synthetic CARs. In its most basic design, a CAR links a tumor-specific extracellular recognition domain, typically a single-chain variable fragment (scFv) derived from a monoclonal antibody, to an intracellular signaling domain that induces T cell activation on antigen binding (*34*, *229*, *230*) (**Figure 2.2**). An advantage of CARs over TCRs is that they confer HLA-independent recognition of tumor cells, allowing one receptor to be used regardless of the patient's HLA haplotype. For this reason, CARs recognize tumor cells that have downregulated expression of HLA or antigen-processing molecules, which are common mechanisms of tumor immune evasion (*231*, *232*). Moreover, because of their modular structure, CAR components can be differentially configured to maximize T cell function in various settings. From the recognition domain to the intracellular signaling domain(s), optimization of each CAR component can improve recognition of tumor cells and T cell effector function.

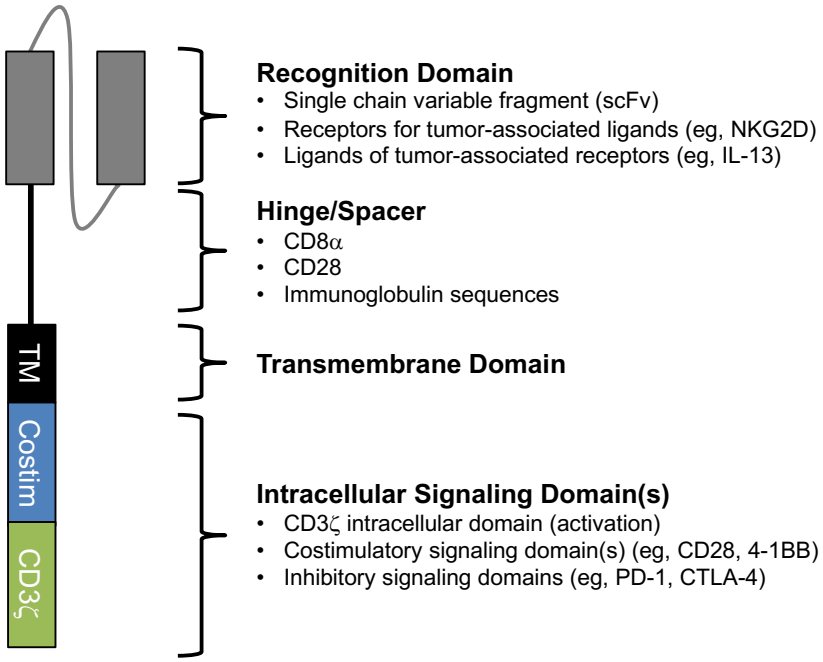

Figure 2.2. Elements of chimeric antigen receptor design. Key structural elements of CARs that can affect sensitivity of antigen recognition and T cell function after ligand engagement include the recognition domain, hinge/spacer, transmembrane domain, and intracellular signaling domains.

Principles of CAR design: the recognition domain

The recognition domain of CARs can be comprised of virtually any molecule that has sufficient binding affinity for a tumor cell surface molecule. CARs that have advanced to clinical testing have been built using scFvs as recognition domains because mAbs to several tumor-associated antigens are readily available, and new mAbs can be obtained by conventional technologies and by screening antibody phage display libraries (*233*, *234*). CARs have been developed from mAbs specific for mutated receptors (eg, epidermal growth factor receptor [EGFR]vIII), cell lineage molecules (eg, CD19, CD20, CD22), developmental molecules (eg, ROR1, GD2) that are expressed on some tumors, and molecules overexpressed in tumors relative to normal tissues (eg, Her2, mesothelin, MUC16) (*235-240*). CARs can also be designed using the ectodomain of natural molecules, such as the NKG2D receptor that binds to stress-induced ligands upregulated on tumor cells (*241-244*). Other groups have exploited the selective expression of the cytokine receptor IL-13Rα2 on glioblastoma by designing CARs using the receptor's natural ligand, the cytokine IL-13, as an ectodomain (*245*, *246*). IL-13 "zetakine" CAR T cells have shown partial efficacy and safety in a phase I clinical trial for glioblastoma (*247*).

Because designing and optimizing a new CAR for each tumor-associated antigen is time consuming and labor intensive, another strategy is to develop a "universal" CAR that can

theoretically target any tumor antigen. One group tested this idea by constructing a CAR specific for the fluorochrome fluorescein isothiocyanate (FITC) molecule. By infusing FITC-labeled antibodies specific for tumor-associated antigens *in vivo*, they could label the tumor with FITC and mark it for killing by FITC-specific CAR T cells (*248*). Similar approaches have been taken using biotinylated antibodies and biotin-specific CAR T cells, or using CARs with a CD16 recognition domain that binds the Fc portion of human immunoglobulins (*249*, *250*). Although "universal" CARs have been effective against multiple tumors in preclinical models, clinical trials are necessary to determine whether they remain effective in patients without binding endogenous biotin or free immunoglobulin and eliciting off-tumor toxicity.

Despite the versatility and plethora of recognition domains, a limitation of current CARs is that they primarily recognize tumor cell surface molecules that are also expressed on normal tissues (**Table 2.2**). Because transcription factors and intracellular signaling molecules are often mutated in tumor cells and represent potential tumor-specific targets, several groups have attempted to develop "TCR-like" antibodies that recognize specific pMHC complexes and could be used as recognition domains for CARs. Investigators are now using phage display and hybridoma strategies to isolate scFvs specific for pMHC, and CARs built from such "TCR-like" antibodies have shown efficacy in preclinical models. For example, T cells expressing TCR-like CARs specific for gp100/HLA-A2, PR1/HLA-A2, and WT1/ HLA-A2 mediate antitumor activity in vitro and in xenograft mouse models (*234*, *251*). Thus, in principle CARs can be designed to target intracellular antigens, although additional study of the biophysical interactions of TCR-like CAR T cells with tumor cells is necessary to optimize specificity, antitumor activity, and safety, and to determine if there are potential advantages over TCRs (*252*).

Several properties of CAR recognition domains are amenable to manipulations that can influence antitumor activity. Receptor affinity for tumor antigens can significantly affect downstream CAR signaling and functionality, and the optimal affinity may be different depending on ligand density and epitope location. Studies evaluating ROR1-specific CARs and folate receptor β-specific CARs found that scFvs with higher affinity exhibited superior antitumor activity against antigen-positive tumor cells in vitro and in vivo (*253*, *254*). Other studies show that there may be an affinity threshold that provides for selective recognition of tumor cells when targeting molecules, such as ErbB2 or EGFR, that are expressed at low levels on some normal tissues (*255*). Even the framework regions of an scFv, which do not participate in antigen binding, can influence CAR signaling and function. When comparing CD19 and GD2 CARs, the framework regions of a GD2 scFv contributed to antigen-independent clustering of the scFvs on the T cell surface, resulting in tonic signaling, early exhaustion, and poor antitumor function both

in vitro and *in vivo* (*256*). Thus, scFvs may need to be screened for both antigen-binding and antigen-independent expression properties.

Table 19.2 Representative Examples of Tumor-Associated Antigens That May Serve as Targets for CAR-T Cells

Class of Tumor Antigen	Examples	Examples of Tumor Type(s)
Cell lineage molecules expressed on tumors and normal cell lineage	CD19 CD20 CD22 BCMA Ig light chain CD123	ALL, NHL, CLL ALL, NHL, CLL ALL, NHL, CLL Multiple myeloma NHL, CLL, myeloma AML
Self-antigen with overexpression on tumors	Her2 CEA	Breast, ovarian Colorectal, breast
Self-antigen with limited normal tissue expression	L1CAM GD2 ROR1 Mesothelin MUC1 MUC16 Folate receptor alpha IL13RA2	Neuroblastoma Neuroblastoma, Ewing sarcoma CLL, Mantle cell lymphoma, ALL NSCLC, triple negative breast cancer, ovarian cancer Mesothelioma, ovarian cancer, pancreatic cancer Ovarian, breast, and pancreatic cancer Ovarian cancer Ovarian, breast, and lung cancer Glioblastoma
Viral antigens	EBV (LMP-1)	Nasopharyngeal carcinoma, lymphoma
Peptide/MHC	HA-1/HLA-A2 PR-1/HLA-A2 WT-1/HLA-A2	Leukemia (allogeneic stem cell transplant) AML, CML AML, epithelial cancers

ALL, acute lymphoblastic leukemia; AML, acute myeloid leukemia; BCMA, B cell maturation antigen; CEA, carcinoembryonic antigen; CLL, chronic lymphocytic leukemia; EBV, Epstein–Barr virus; HLA, human leukocyte antigen; LMP, latent membrane protein; MHC, major histocompatibility complex; NHL, non-Hodgkin lymphoma; MUC1, Mucin 1; NSCLC, non-small cell lung cancer; ROR1, receptor tyrosine kinase–like orphan receptor-1; WT-1, Wilms tumor antigen 1.

Principles of CAR design: the hinge/spacer

CARs often contain a hinge or spacer region derived from CD8α, CD28, or immunoglobulin sequences inserted between the scFv and the transmembrane domain. Notably, the spatial properties of the TCR/pMHC interaction are conserved and have evolved to elicit optimal T cell activation; however, the distance between a CAR and its antigen will vary based on the location of the target epitope and the protrusion of the scFv from the T cell membrane (*257*, *258*). Tailoring the length of the spacer region is one way to modify this distance and maximize T cell activity, and several studies have demonstrated that lengthening the spacer can improve the function of scFvs targeting membrane-proximal epitopes, presumably by adding the flexibility and length needed to access these epitopes (*259*, *260*). It is interesting to note that lengthening the spacer diminishes the function of CARs targeting tumor cell membrane–distal epitopes, suggesting that too much space between the T cell and target cell is suboptimal. Thus, the location of the target epitope may dictate the length of the spacer required for optimal CAR T cell function.

In addition to length, the amino acid sequences of the spacer can affect CAR T cell function *in vivo*. Spacer regions are often derived from the Ig Fc region and CARs designed with IgG1- or IgG4-based spacers can inadvertently bind to and activate FcR^+ innate immune cells *in vivo* (*261*). Binding of the CARs to FcR^+ cells *in vivo* can also activate CAR T cells and induce activation-induced T cell death, thereby compromising antitumor activity (*260*). Mutating five amino acids to abrogate FcR binding in the spacer region improves CAR T cell persistence and antitumor activity for applications that require long spacers.

Principles of CAR design: intracellular signaling domains

Initial CAR designs linked recognition domains to a single signaling module from FcRγ or CD3ζ to induce T cell activation (*34*, *229*, *262*). Expression of these "first-generation" CARs in T cells redirected lytic activity *in vitro*, but provided limited persistence and antitumor activity *in vivo* (*263*, *264*). T cells require two signals for full activation: signal 1 provided by the TCR via CD3ζ and signal 2 provided by costimulatory receptors like CD28 (*265*). In an effort to recapitulate both signals, "second-generation" CARs were designed to carry the signaling endodomains of CD3ζ and CD28 linked in *cis*. A clinical trial directly comparing first- (CD3ζ alone) and second (CD28-CD3ζ)-generation versions of the same CAR demonstrated that CD28 costimulation improved CAR T cell persistence and expansion *in vivo* (*266*). It is interesting to note that although second-generation CAR T cells are generally superior to first-generation CAR T cells, the converse was observed in tumors infiltrated by regulatory T cells (Tregs), and this was linked to greater IL-2 production from second-generation CAR T cells that supported Treg activity (*267*).

Costimulatory domains other than CD28 have also been tested for their ability to support T cell survival and long-term persistence. Most notably, incorporating the 4-1BB (CD137) signaling domain improved CAR T cell persistence, tumor localization, and antitumor activity in some preclinical models compared with CD28/CD3ζ and CD3ζ only CARs (*268*), as well as ameliorated tonic signaling and T cell exhaustion in certain CAR constructs (*256*). Compared with CD28, costimulation through 4-1BB imparts different metabolic phenotypes and supports memory T cell development (*269*). Other signaling domains alone, or in tandem, can be included with CD3ζ in CARs, including OX40, CD27, and ICOS, illustrating the wide range of opportunities to confer unique functions to antitumor T cells through synthetic biology. The importance of the CAR costimulatory domain and its effects on intracellular signaling and T cell fate will be further examined in subsequent chapters.

Considerations for selecting targets for CAR T cell therapy

CARs can be developed to target almost any surface-expressed molecule, and it is important to define which targets will safely elicit antitumor activity. A major consideration when choosing candidate target antigens is the selectivity of their expression on tumors to avoid off-tumor toxicity to vital normal tissues. The most advanced clinical applications of CAR T cells target B cell lineage molecules (CD19, CD20, CD22) expressed on B cell malignancies such as acute lymphoblastic leukemia (ALL), non-Hodgkin lymphoma (NHL), and chronic lymphocytic leukemia (CLL). B cell maturation antigen (BCMA) is another validated CAR target that is expressed by multiple myeloma. As discussed in the following section, CAR T cells targeting these antigens can induce complete remissions, but also eliminate healthy B cell lineages that express the target molecules. This on-target off-tumor toxicity is manageable transiently, but persistent B cell deficiency reduces immunoglobulin titers and increases susceptibility to infections.

Other targets such as L1CAM, GD2, Her2, mesothelin, MUC16, and ROR1 are being pursued as targets for CAR T cells, but have the limitation of being expressed in some normal tissues (*270*-*275*). There is some evidence that GD2-specific CAR T cells can have antitumor activity without on-target toxicity (*276*); however, CAR T cells specific for ErbB2 caused serious pulmonary toxicity in one patient (*240*). Cell surface molecules that are mutated in cancer cells, such as EGFRvIII, which is deleted in exons 2 through 7 and signals constitutively, would provide a true tumor-specific CAR target, but its heterogeneous tumor expression may limit efficacy (*277*). A recent study demonstrated that a cancer-associated glycoform of MUC1 could be targeted with CAR T cells with no recognition of the alternative glycoform in normal cells, suggesting this may be a safe and effective target (*278*). It remains to be determined whether CARs can be designed to discriminate between high and low levels of antigen expression as a means of sparing normal tissues, and trials currently in progress should delineate the risks for individual target molecules.

In addition to selective expression on tumor cells, antigen density and homogeneity of expression on the tumor are important factors. Studies suggest that the threshold for CAR T cell signaling is higher than that for TCRs, which require only 1 to 10 pMHC complexes for activation. For a CD20 CAR, ~200 molecules per target cell were required to induce lytic activity, and the requirement for cytokine production by CAR T cells was 10-fold higher (*279*). Target antigens for CARs should ideally be expressed homogeneously throughout the tumor to minimize the escape of antigen-negative variants. In the case of B cell malignancies, CD19 is expressed homogeneously on tumor cells, and CAR T cells mediate complete remissions in

many patients. Similarly, BCMA is expressed uniformly in at least 60-70% of myeloma cases. Identifying antigens is more difficult for solid tumors, which do not homogeneously express a lineage marker like CD19 on all tumor cells. ROR1 is an attractive target because it is highly and homogeneously expressed on many different types of solid tumors, but this molecule is expressed on a restricted subset of normal tissues and on-target off-tumor toxicity remains a concern despite the safety of ROR1-specific CAR T cells in animal models (*280*).

First generation CAR T cells fail to mediate antitumor responses in patients

Clinical trials testing ACT with T cells modified with first-generation CARs demonstrated feasibility but failed to show objective antitumor responses. In two early studies, patients with NHL, mantle cell, or follicular lymphoma were treated with autologous T cells expressing a CD20- or CD19-specific CAR (*281*, *282*). Both studies used plasmid electroporation for transduction and antibiotic selection to enrich CAR T cells, which required long *in vitro* culture and resulted in highly differentiated “effector” phenotype T cells. CAR T cells were only detectable in the blood by polymerase chain reaction for a short time after transfer and antitumor activity was not observed. Another clinical trial evaluated carbonic anhydrase 9 (CAIX)-specific CAR T cells to treat renal cell carcinoma (*283*). CAR T cell persistence was short and significant off-tumor toxicity occurred because $CAIX^+$ epithelial cells in the liver bile ducts were targeted. No antitumor responses were observed and immune responses to the murine scFv used to construct the CAR were detected in patients after therapy (*284*), which was not surprising given prior studies demonstrating immune responses to foreign transgene products in patients receiving ACT (*285*, *286*). Thus, studies with first-generation CAR T cells highlighted the need to modify the signaling domain, improve gene transfer efficiency, and attenuate immunogenicity.

CD19 CARs incorporating costimulatory domains mediate antitumor responses against B cell malignancies

T cells transduced to express a CD19-specific CAR with one or more costimulatory domains in addition to CD3ζ exhibited more potent antitumor activity in preclinical models(*268*, *287*). In the only clinical trial to directly compare first- and second-generation CAR T cells, superior proliferation and persistence *in vivo* was observed for T cells expressing a CD28/CD3ζ CAR compared with those with a CAR containing only CD3ζ (*266*). Results of large phase I and II clinical trials using autologous T cells expressing CD19-specific CARs containing either 4-1BB/CD3ζ or CD28/CD3ζ signaling domains to treat relapsed or refractory B cell malignancies

are described subsequently and provide insight into the efficacy, toxicities, and current limitations. However, comparing efficacy and toxicity across trials is challenging because of differences in scFvs, construct design, method of gene transfer, T cell culture conditions, composition of T cell products, lymphodepleting chemotherapy regimens, cell dose, and patient heterogeneity.

Acute lymphoblastic leukemia: ACT with CD19-specific 4-1BB/CD3ζ or CD28/CD3ζ CAR T cells after lymphodepleting chemotherapy induced complete remission (CR) in 70% to more than 90% of pediatric and adult patients with relapsed or refractory ALL (*224*, *288-291*). CAR T cell activation and proliferation occurred in a majority of patients and, in those individuals, $CD19^+$ leukemia cells were cleared rapidly from bone marrow, cerebrospinal fluid, and extramedullary sites. Studies in which CAR T cells were formulated with a uniform CD4:CD8 ratio revealed correlations between cell dose, antitumor response, and toxicity, and allowed better definition of the therapeutic window compared with heterogeneous products in other trials (*224*). The degree of CAR T cell proliferation depended on tumor burden, and prolonged CAR T cell persistence of at least 3 to 6 months was associated with superior relapse-free survival (*224*, *289*). Loss of detectable CAR T cells from peripheral blood was shown in some patients to be caused by T cell immune responses directed against epitopes in the murine scFv and other CAR components (*224*, *290*). Many ALL patients that achieved a remission after CAR T cells had a subsequent stem cell transplant, and longer follow-up of patients that did not receive transplant is required to determine if this approach can cure a subset of patients. Notably, relapses with $CD19^-$ leukemia cells caused by mutations, alternative splicing of CD19 mRNA, or a lineage switch to a myeloid phenotype do occur, suggesting that targeting multiple antigens may be important to achieve a higher cure rate (*289*, *292*, *293*). The ELIANA multicenter pivotal trial of 4-1BB/CD3ζ CAR T cells for relapsed ALL in children and young adults enrolled 92 patients, and 75 received CAR T cells (*294*). The overall remission rate in treated patients was 81%, and the relapse free probability at 6 months among responders was 80%. These results formed the basis for the first FDA approved T cell therapy, and represented a breakthrough in the field of ACT.

Non-Hodgkin lymphoma: CD19-specific CAR T cells have also demonstrated significant activity in patients with relapsed or refractory B cell NHL, including patients who relapsed after myeloablative autologous hematopoietic stem cell transplantation. Case reports and small single center trials with CD28/CD3ζ or 4-1BB/CD3ζ CAR T cells demonstrated antitumor activity in follicular lymphoma, transformed follicular lymphoma, diffuse large B cell lymphoma, and primary mediastinal B cell lymphoma (*225*, *266*, *295*, *296*). A multicenter phase

2 trial, which led to FDA approval, administered CD28/CD3ζ CAR T cells to 101 patients with relapsed/refractory NHL and reported objective response and CR rates of 82% and 54% respectively, and an overall survival at 18 months of 52% (*297*). Studies are ongoing to investigate the mechanisms of nonresponse to determine if resistance is at the level of the tumor cell and/or TME, or reflects properties of CAR T cells in individual patients.

Chronic lymphocytic leukemia: The investigation of CD19 CAR T cells in CLL has progressed more slowly than in ALL and NHL due to the efficacy of novel agents such as ibrutinib, idelalisib, and venetoclax in chemotherapy refractory patients (*298-301*). An early trial reported CR in 2 of 3 patients with R/R CLL after treatment with 4-1BB/CD3ζ CAR T cells (*302*). In a follow-up report of this trial, 8 of 14 patients responded to CAR T cells, including 4 patients that achieved a minimal residual disease (MRD) negative CR by deep sequencing for the clonal IgH rearrangement. Turtle *et al.* reported 24 patients treated with 4-1BB/CD3ζ CAR T cells, including 22 patients that progressed on ibrutinib or were ibrutinib intolerant (*303*). Overall response and CR rates by IWCLL criteria were 74% and 21%. Fifty-eight percent of patients that had deep sequencing of bone marrow samples after therapy had no malignant IgH sequences detected. These data demonstrate that CAR T cells can be effective and may have curative potential in patients that have failed chemoimmunotherapy, ibrutinib and venetoclax. Defining a role for CAR T cells earlier in the course of disease may further increase clinical efficacy but will require strategies to mitigate the toxicities of this therapy.

CD19-specific CAR T cells can cause serious toxicities

Toxicities of CD19-specific CAR T cells include cytokine release syndrome (CRS), neurologic toxicity, and persistent B cell aplasia. The clinical features and pathogenesis of these complications are the subject of intense research to identify strategies for prevention and mitigation (*304-306*).

Cytokine release syndrome: The onset of CRS coincides with activation and proliferation of CAR T cells *in vivo*, and typically occurs within the first few days after T cell infusion. CRS is characterized by fever, hypotension, tachycardia, capillary leak syndrome, respiratory compromise and coagulopathy. Serum cytokines including interferon-γ, interleukin 6 (IL-6), interleukin 8, monocyte chemoattractant protein-1, macrophage inflammatory protein 1b, and acute phase reactants such as C-reactive protein and ferritin are commonly elevated after the infusion of CAR T cells (*224*, *225*, *289-292*, *303*, *306*). Rarely, patients will develop fulminant hemophagocytic lymphohistiocytosis (HLH) (*307*). Risk factors for CRS include high tumor burden, higher numbers of $CD19^+$ cells in the bone marrow, pretreatment

thrombocytopenia, and a higher CAR T cell dose (*306*). Treatment of CRS includes administration of tocilizumab to block systemic effects of IL-6, and dexamethasone to inhibit cytokine production by activated CAR T cells and other immune cells. The timing of intervention with tocilizumab and dexamethasone is evolving based on ongoing biomarker studies.

Neurotoxicity: Neurologic symptoms including headache, delirium, aphasia, focal neurologic deficits, seizures, and loss of consciousness are frequently observed in patients treated with CD19 CAR T cells, concurrently or after CRS. Symptoms usually resolve over time, although rare patients have developed fatal cerebral hemorrhage or edema (*305*, *308*). Risk factors for neurotoxicity include high tumor burden or CAR T cell dose, CRS and pre-existing neurologic abnormalities. Neurotoxicity is associated with endothelial activation, disseminated intravascular coagulation, and increased blood brain barrier permeability (*305*). These clinical factors may predict patients at highest risk and guide strategies for prophylaxis or early treatment.

B cell aplasia: The elimination of normal B cells is an expected on-target side effect of targeting CD19. Despite fears that B cell aplasia could compromise immune responses to infection, transient or prolonged loss of normal B cells is well tolerated and B cells eventually recover in most patients as CAR T cells decline in numbers. Vector designs that include a mechanism to accelerate CAR T cell elimination have been developed, including coexpression of a cell surface truncated epidermal growth factor receptor (EGFRt) that can be targeted by cetuximab (*309*). In preclinical models, the administration of cetuximab eliminated CD19 CAR T cells and restored B cell numbers without leukemia relapse {Paszkiewicz:2016vg}. This approach could be applied to patients that achieve durable remission of their malignancy and have persistent B cell aplasia.

CAR T cells for other hematological malignancies

T cell malignancies: The development of CAR T cells for T cell malignancies is more challenging than for B cell malignancies because candidate target antigens are also expressed on normal T cells. To avoid fratricide, it is necessary to combine gene editing to abrogate expression of the target molecule on the T cells that are engineered to express the CAR. CD7 is expressed in T cell leukemia and CRISPR/Cas9-mediated editing has been used to delete CD7 in primary T cells prior to transduction with a CD7-specific CAR (*310*). Edited CD7-specific CAR T cells are functional and mediate antitumor activity in preclinical models. A limitation of this approach not addressed in the preclinical models is the expected elimination of normal $CD7^+$ T and NK cells and their progenitors, which would compromise host immunity. The CAR T cells

could potentially provide some immune function through their endogenous T cell receptor (TCR), however repertoire diversity would be constrained and CAR expression may adversely affect TCR signaling (*311*).

Rather than targeting a lineage-specific molecule on all T cells, an innovative alternative is to employ a CAR specific for only one TCR β chain constant region (TCRBC), analogous to targeting either kappa or lamda Ig light chains in B cell malignancies. Two highly homologous genes (Cβ1 and Cβ2) encode TCR β-chain constant regions, and they are expressed in a mutually exclusive manner (*312*). The clonal nature of T cell malignancies means that the tumor will express either TCRBC1 or TCRBC2, whereas the normal T cell compartment is comprised of T cells expressing either TCRBC chain. Thus, if a CAR targeted only the TCRBC expressed by the malignant T cells, this would not damage normal T cells expressing the alternative TCRBC chain. By screening anti-TCR antibodies, Maciocia *et al*. identified a scFv that selectively bound to TCRBC1, with specificity determined by 2 adjacent amino acid residues that differ between TCRBC1 and TCRBC2 (*312*). Only TCRBC2-positive CAR T cells grew out from cultures transduced with a CD28/OX40/CD3ζ CAR constructed from this scFv, and these CAR T cells specifically recognized TCRBC1-positive T cell leukemia and lymphoma cells *in vitro* and in xenograft models in immunodeficient mice. This approach holds promise for targeted immunotherapy of the subset of T cell malignancies that express TCRBC1 without compromising the entire T cell compartment.

Hodgkin lymphoma (HL) and anaplastic large cell lymphoma (ALCL): CD30 (TNFRSF8) is a member of the tumor necrosis factor (TNF) receptor superfamily expressed at high levels in HL, ALCL, and on activated T and B cells. Clinical trials of an antibody drug conjugate (brentuximab) targeting CD30 have shown antitumor activity in HL without toxicity to normal T and B cells suggesting CD30 is a candidate target for CAR T cells. Wang *et al.* described results of 18 patients with HL treated with autologous T cells engineered by lentiviral transduction to express a 4-1BB/CD3ζ CD30 CAR (*313*). Treatment was well tolerated and 7 of 18 patients achieved a partial response. Ramos *et al*. treated 7 patients with HL and 2 patients with ALCL with T cells expressing a CD28/CD3ζ CD30 CAR (*314*). No toxicity was observed and 3 of the 9 patients achieved a CR, with two of the patients remaining in CR beyond 24 months. These studies demonstrate that targeting CD30 with CAR T cells is safe and can have antitumor activity in $CD30^+$ malignancies.

Multiple myeloma: Multiple myeloma responds initially to immunomodulatory agents, proteasome inhibitors and monoclonal antibodies, but relapse is inevitable and curative therapy remains elusive. ACT with myeloma infiltrating lymphocytes (MILs) or NY-ESO-1 TCR

engineered T cells administered after autologous stem cell transplant have not shown definitive evidence of antitumor efficacy (*123*, *315*). An early effort to treat myeloma with CAR T cells targeting CD19, which is only expressed on rare myeloma cells, was also unsuccessful (*316*). CD38 and SLAMF7 have been successfully targeted with monoclonal antibodies (*317-319*), and CARs specific for these molecules have activity in preclinical models (*320*, *321*). However, CD38 is expressed on other hematopoietic cells and some non-hematopoietic cells raising concern that CAR T cells may be toxic. scFv affinity variants may provide specificity for tumor cells, which have higher levels of CD38 than normal cells (*322*).

The TNF receptor family member BCMA, which is a receptor for BAFF and APRIL, is at present the most attractive CAR T cell target in myeloma. BCMA is expressed on both plasma cells and myeloma cells, but absent on normal tissues (*323-325*). Seckinger *et al*. reported surface BCMA expression in 100% of untreated and relapsed myeloma patients (*326*). A potential limitation of targeting BCMA is that it is cleaved by γ-secretase in myeloma cells leading to variation in surface expression, and increased levels of soluble BCMA that can inhibit CAR recognition (*327*). Nevertheless, BCMA CARs have demonstrated significant clinical efficacy in initial clinical trials. Kochenderfer and colleagues treated 12 patients using unselected T cells engineered with a CD28/CD3ζ BCMA CAR (*328*). A very good partial response (VGPR) was observed in 2 patients, partial response (PR) in 1, and stringent CR (sCR) in 1 patient. Antitumor effects appeared to correlate with CAR T cell dose, although too few patients were treated at each dose level for a definitive conclusion. Toxicity was modest with 2 patients at the highest CAR T cell dose experiencing CRS. Two phase 1 trials of BCMA CAR T cells in relapsed or refractory myeloma were reported at the 2017 American Society of Clinical Oncology Meeting. Although follow-up was short, significant antitumor activity was observed in both studies with a subset of patients achieving CR. These results demonstrate that targeting BCMA with CAR T cells has substantial antitumor activity in myeloma, although much longer follow-up is needed to determine the durability of responses and to identify resistance mechanisms that prevent complete tumor elimination in patients with partial responses. Recent preclinical studies also suggest that CAR T cell efficacy is enhanced in combination with lenalidomide (*329*). Thus, CAR T cells could be combined with other therapeutic regimens for myeloma.

Acute myeloid leukemia (AML): AML is more common than ALL in adults, and patients over the age of 60 respond poorly to conventional therapy. The success of CAR T cells in ALL encouraged efforts to apply this approach in AML, however identifying suitable CAR T cell targets has proven challenging. Lewis Y antigen (LeY), CD33, CD123, and CLL1 have been

studied, but have the disadvantage of having heterogeneous expression on leukemic cells, or being expressed on normal hematopoietic progenitors (*330*). A clinical trial targeting LeY with CAR T cells demonstrated limited antitumor activity and studies targeting CD123 are ongoing. A transcriptomic and proteomic analysis of AML identified three pairs of molecules that are tumor-specific and might be amenable to combinatorial CAR targeting (*331*). CARs incorporating scFvs that bind to HLA/peptide complexes such as HLA-A2/WT1 are also being investigated {Rafiq:2016if}. Further study of the specificity and sensitivity of these reagents is required, but they represent alternatives to targeting broadly-expressed AML surface molecules.

CAR T cells targeting solid tumors mediate incomplete antitumor activity

In contrast to the robust clinical efficacy achieved in B cell malignancies and multiple myeloma, the treatment of solid tumors has produced less-striking results. The efficacy of a first-generation CAR specific for the tumor-associated antigen GD2 was evaluated in 11 neuroblastoma patients, and four of eight (50%) patients with evaluable tumors had evidence of tumor necrosis or regression and no evidence of on-target off-tumor toxicity (*276*, *332*). Mesothelin was targeted in two patients with mesothelioma and pancreatic cancer, respectively, with autologous T cells that expressed a mesothelin-specific CAR after messenger RNA (mRNA) transfection. CAR T cells migrated to sites of disease and transient shrinkage of one lesion was detected by MRI. Despite previous toxicity targeting Her2 with CAR T cells (*240*), a different Her2-specific CAR was tested in 19 patients with sarcoma (*333*). The Her2-specific CAR T cells persisted in some patients for 6 weeks and there were no dose-limiting toxicities, but also no evidence of antitumor efficacy. Most recently, an IL13Rα2-specific CAR produced modest antitumor activity in three glioblastoma patients (*247*). In this study, subjects received up to 12 intracranial infusions in the tumor resection cavity, and two of the patients had evidence of transient antitumor activity with clinically manageable temporary brain inflammation as the only toxicity. Collectively, these results indicate that targeting certain overexpressed surface antigens on solid tumors with CAR T cells can lead to transient antitumor activity without off-tumor toxicity.

BARRIERS TO EFFECTIVE ACT AND POTENTIAL SOLUTIONS

Tumor escape by antigen loss

CAR T cells are MHC-independent and tumors with low MHC expression remain susceptible to recognition. However, loss, downregulation, or differential splicing of the target

antigen or epitope, as observed in some patients that received CD19-specific CAR T cells, are now established mechanisms of tumor escape (*224*, *293*). This problem may be circumvented by targeting multiple antigens at once with multiple cell products or bispecific CARs targeting CD19 and CD20, for example, to reduce the probability of selecting for escape variants that lack expression of multiple antigens (*334*, *335*). This is attractive for B cell malignancies where multiple targets are validated but identifying pairs of tumor-associated antigens coexpressed on the same tumor cell that can be safely targeted may prove challenging for other malignancies.

Toxicity to normal host tissues

CAR T cells can result in toxicity because of off-tumor expression of the antigen on normal tissues. Because few truly tumor-specific antigens exist, developing new methods that enable CAR T cells to discriminate between tumor and normal cells expressing the same antigen would vastly improve both the efficacy and safety of CAR T cell therapy (**Figure 2.3**). Recent studies have demonstrated that tuning the affinity of the scFv for Her2 or EGFR might allow selective recognition of tumor cells that express high levels of these molecules and not normal cells that express lower levels (*333*, *336*, *337*). Whether this ability to discriminate target cells based on level of antigen expression is maintained *in vivo* in relevant settings remains to be determined.

Another strategy to increase tumor specificity is to use “AND” logic gates that require recognition of two distinct tumor-associated antigens on the same target cell to elicit full CAR T cell activation. Such a split-receptor system was designed in which a Her2-specific scFv was linked to the CD3ζ signaling domain and a second MUC1-specific scFv was linked to the CD28 signaling domain (*338*). Both Her2 and MUC1 are commonly overexpressed in many tumors, but have limited overlap in expression in normal tissues. The dual-specific CAR T cells only proliferated in response to Her2/MUC1 double-positive tumor cells that delivered both CD3ζ and CD28 signals, but not in response to Her2 or MUC1 single-positive “normal” cells. These dual-signaling CAR T cells, however, would fail to function against antigen-loss variants, and CD3ζ signaling alone is sufficient to induce some T cell activity against single-positive cells, suggesting that toxicity to single-positive normal tissues may still occur. The latter problem may be addressed by screening low-affinity scFvs that when linked to a CD3ζ signaling domain are incapable of inducing T cell activation without costimulation (*339*). Thus, development of dual-signaling CAR T cells is likely to require further optimization for individual scFvs as well as identification of antigen pairs that are selectively coexpressed in tumor but not in normal tissues.

Tumor specificity can also be increased using a split-receptor system to provide negative signaling in the presence of normal, but not tumor, tissue. This principle is used naturally by the immune system, in which T cells upregulate the inhibitory receptor PD-1 on activation that engages ligands on normal cells to dampen T cell activity (*340*). In principle, this mechanism can be exploited by coexpressing a second inhibitory synthetic receptor that activates PD-1 signaling after engaging an antigen expressed on normal, but not on tumor tissues (*341*). Here again, the utility of this approach will depend on identifying appropriate antigen pairs that are coexpressed on normal cells but where only the activating ligand is on tumor cells.

Sophisticated applications are emerging from the field of synthetic biology to regulate the activity of CAR T cells to minimize toxicity *in vivo*. Constructs have been designed in which CAR expression is regulated by a drug-inducible promoter or in which the recognition domain and signaling domain only associate together in the presence of a small molecule dimerizer (*342-344*). Because CAR expression and/or signaling depend on the presence of an externally supplied drug, their activity can theoretically be halted if toxicity occurs simply by withdrawal of the drug.

Rather than using a drug to induce CAR expression, an inducible dual-receptor system has been described in which engagement of a synthetic Notch receptor specific for one tumor-associated antigen is used to release an orthogonal transcription factor and induce expression of a CAR specific for a second tumor-associated antigen (*9*). The advantage of this approach is that CAR expression is restricted to sites where the synthetic Notch receptor is engaged; in order for a target cell to be lysed, it must also express the CAR ligand. Therefore, this approach can improve tumor selectivity by requiring recognition of two tumor-associated antigens to elicit CAR T cell activity. A drawback of this approach is that it takes ~8 hours for CAR expression to degrade after the first receptor is disengaged; thus, there is a potential window during which the T cells expressing CAR could migrate and engage normal tissues that express the CAR ligand. Nevertheless, this approach illustrates an important new principle that, if refined to relevant CAR targets on solid tumors, might improve the therapeutic index of CAR T cells. Applications of this system to a mouse model of CAR T cell toxicity is described in Appendix 1.

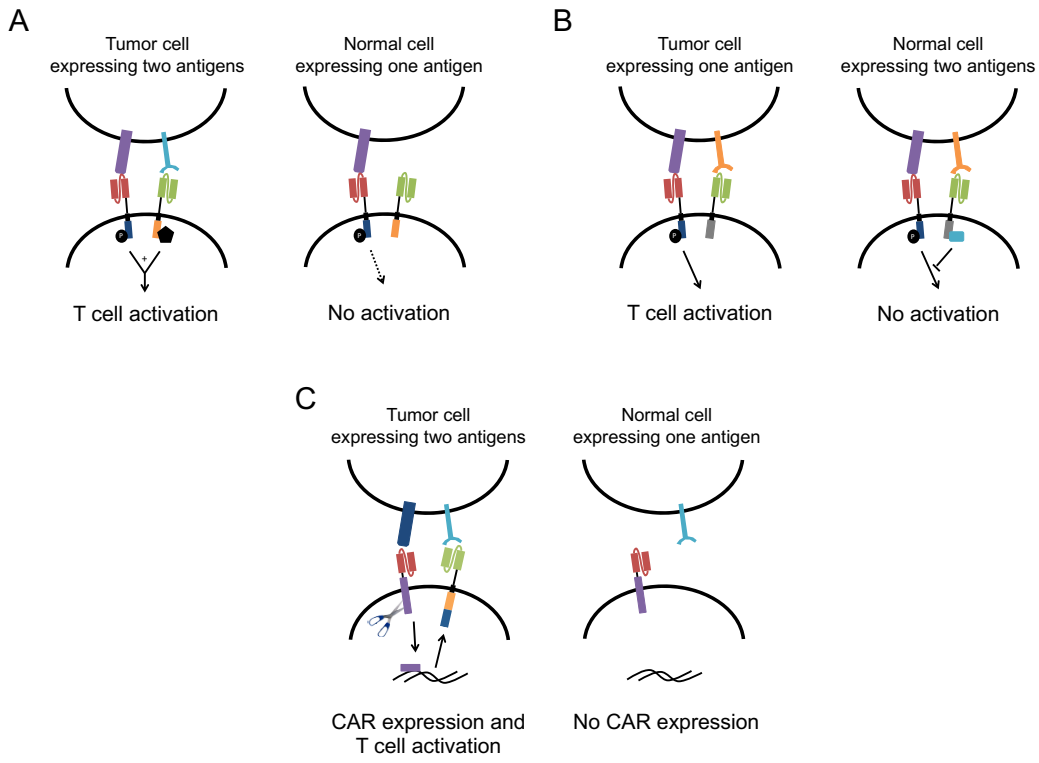

Figure 2.3. Strategies to improve tumor selectivity of CAR T cells. A) T cells may be engineered to express a CAR and a chimeric costimulatory receptor (CCR) specific for two different tumor-associated antigens. The CAR contains the CD3ζ endodomain while the CCR contains a costimulatory (e.g. CD28 or 4-1BB) endodomain such that T cells are only activated when both receptors are simultaneously engaged. Normal cells expressing only one antigen do not induce T cell activation and are spared from toxicity (right); only tumor cells expressing both antigens are capable of fully activating CAR T cells (left). B) T cells may also be engineered to coexpress a CAR capable of fully activating T cells and a chimeric receptor that delivers an inhibitory signal (e.g. via the PD-1 endodomain). Engagement of both targets on normal cells suppresses T cell activation (right), while recognition of only the activating ligand on tumor cells results in T cell activation (left). C) CAR expression may also be tied to inducible systems such as synthetic Notch receptors. Engagement of the Notch receptor specific for one tumor-associated antigen activates a synthetic transcription factor that induces transcription and expression of a CAR specific for a second tumor antigen. Tumor cells that express both antigens are capable of activating CAR T cells and are killed (left); normal tissues expressing either antigen alone cannot activate CAR T cells and are protected from killing (right).

Overcoming the immunosuppressive tumor microenvironment

Although CAR T cells are highly effective for hematologic malignancies, targeting epithelial cancers, which account for 80-90% of all cancers, has proven more challenging due in part to the immunosuppressive TME. Genetic engineering strategies have been used to develop CAR T cells intrinsically capable of resisting or overcoming particular immunosuppressive pathways. For example, several groups have attempted to block inhibitory PD-1 signaling by engineering CAR T cells to secrete anti-PD-L1 antibodies (*345*), to block endogenous expression of PD-1 with short hairpin RNAs (*346*), or to coexpress “switch receptors” linking the

PD-1 ectodomain to the CD28 endodomain such that engagement of PD-L1 delivers an activating rather than inhibitory signal to the T cell (*347*, *348*). Other strategies to genetically enhance CAR T cells include enabling them to secrete extracellular matrix-degrading enzymes that allow them to better infiltrate solid tumors (*349*, *350*), or engineering them to secrete the pro-inflammatory cytokine IL-12, which modulates many different immune cells, such as monocytes and macrophages, to promote antitumor immunity (*351-353*).

A recent focus has been to improve CAR T cell antitumor activity by altering their metabolic profiles to enhance their overall fitness. Memory T cells exhibit distinct metabolic profiles from effector T cells, such as a reliance on oxidative phosphorylation over glycolysis, that endow them with the ability to survive and persist longer *in vivo*. Recent studies have focused on identifying and engineering subsets of T cells with better metabolic profiles that enable them to better resist immunosuppressive mechanisms in the TME. For example, T cells with low mitochondrial membrane potentials demonstrated superior persistence, metabolic fitness, and enhanced antitumor activity when engineered and adoptively transferred into tumor-bearing mice (*354*). Another study identified a master regulator of mitochondrial membrane fusion, Opa1, that when transduced into T cells remodeled their mitochondria and endowed them with superior antitumor activity and memory-like characteristics such as elevated CD62L, CCR7, and CD127 expression; increased mitochondrial mass; and reliance on oxidative phosphorylation over glycolysis (*355*). These studies suggest that new engineering, culturing, or selection methods that enhance the metabolic fitness of CAR T cells can improve efficacy in the immunosuppressive TME of solid tumors.

CELL MANUFACTURING

A limitation for broader application of ACT as a therapeutic modality for cancer is the need to manufacture T cells under current good manufacturing practice (cGMP) conditions. TILs are typically expanded to 10^{10} to 10^{11} cells and manufacturing feasibility would be improved if lower cell doses were effective. The manufacturing of tumor-specific T cells selected from blood or engineered with TCRs has been facilitated by improved clinical cell-sorting capabilities, but cell doses of 10^9 to 10^{10} are routinely employed (*130*, *133*, *141*, *145*). CAR T cells have been shown to be effective in doses of 10^7 to 10^8, which are relatively easy to manufacture, and potency may be further enhanced by engineering naive and central memory T cell subsets that have superior capacity to proliferate and persist *in vivo*, culturing the T cells under cytokine or pharmacologic conditions that limit differentiation in vitro, and/or formulating cell products to contain both tumor-specific $CD8^+$ and $CD4^+$ T cell subsets (*198*, *220*, *224*, *225*, *303*). Further

genetic manipulation to confer superior function in immunosuppressive TMEs and combining T cells with checkpoint inhibitors or small molecules that target specific mechanisms that inhibit T cells should further reduce cell numbers necessary for efficacy. Advances in T cell biology, gene engineering, and synthetic biology suggest that in the near future, ACT will become an established therapeutic modality for a variety of human tumors.

CONCLUSIONS

ACT with unmodified and genetically modified T cells has emerged as a curative modality for a small subset of patients with refractory cancers. Recent advances in synthetic biology, genome engineering, and cell manufacturing have made it possible to develop highly specific and potent tumor-reactive T cells and offer many opportunities for experimentation and broader clinical translation. Extending the success of ACT to broader patient populations will require new strategies to overcome immunosuppression and toxicity to normal tissues. Recent proof-of-principle studies have demonstrated that synthetic signaling systems allow for physician-controllable and/or inducible T cell activity in preclinical models (*8*, *9*, *344*). Advances in genome engineering technologies also have the potential to improve ACT. For example, it was recently reported that targeted insertion of a CAR into the TCR a locus using CRISPR/Cas9 improved CAR T cell antitumor function compared to CAR T cells conventionally generated using retroviral-based gene transfer methods (*180*). Additionally, improvements to cell isolation, culture, and manufacturing are being pursued to improve the phenotype, composition, and potency of infused T cells. With these and other advances, the field is poised for increasingly more effective applications of ACT.

Chapter 3

Phosphoproteomic analysis of CD28/CD3ζ and 4-1BB/CD3ζ CAR signaling reveals kinetic and quantitative differences that impact cell function

A version of this chapter was previously published as:

Alexander I. Salter, Richard G. Ivey, Jacob J. Kennedy, Valentin Voillet, Anusha Rajan, Eva J. Alderman, Uliana J. Voytovich, Chenwei Lin, Daniel Sommermeyer, Lingfeng Liu, Jeffrey R. Whiteaker, Raphael Gottardo, Amanda G. Paulovich, Stanley R. Riddell. “Phosphoproteomic analysis of chimeric antigen receptor signaling reveals kinetic and quantitative differences that impact cell function.” *Sci Signal* (2018) 11: eaat6753.

Abstract

Chimeric antigen receptors (CARs) link an antigen recognition domain to intracellular signaling domains to redirect T cell specificity and function. T cells expressing CARs with CD28/CD3ζ or 4-1BB/CD3ζ signaling domains are effective at treating refractory B cell malignancies but exhibit differences in effector function, clinical efficacy, and toxicity that are assumed to result from activation of divergent signaling cascades. We analyzed stimulation-induced phosphorylation events in primary human $CD8^+$ CD28/CD3ζ and 4-1BB/CD3ζ CAR T cells by mass spectrometry and found that both CAR constructs activated similar signaling intermediates. Stimulation of CD28/CD3ζ CARs activated faster and larger magnitude changes in protein PO_4, which correlated with an effector T cell-like phenotype and function. In contrast, 4-1BB/CD3ζ CAR T cells preferentially expressed T cell memory associated genes and sustained anti-tumor activity against established tumors *in vivo*. Mutagenesis of the CAR CD28 signaling domain demonstrated that increased CD28/CD3ζ CAR signal intensity is partly related to constitutive association of Lck with this domain in CAR complexes. Our data show that CAR signaling pathways cannot be predicted solely by the domains used to construct the receptor, and that signal strength is a key determinant of T cell fate. Tailoring CAR design based on signal strength may lead to improved clinical efficacy and reduced toxicity.

Introduction

Synthetic receptors that mimic natural T cell signaling cascades are being developed as immunotherapeutic reagents for cancer, autoimmunity, and infections. Chimeric antigen receptors (CARs), chimeric costimulatory receptors, and engineered T cell receptors (TCRs) can be introduced into T cells by gene transfer to redirect specificity and promote signaling pathways that initiate effector T cell functions (*230*). The most successful of these novel therapeutics to date are CARs, which are comprised of an extracellular antigen-specific single-chain variable (scFv) immunoglobulin fragment fused to intracellular signaling domains that activate T cells upon ligand binding (*356*). Although treatment with CAR T cells can result in the complete remission of relapsed or refractory B cell malignancies, it can also cause life-threatening toxicities including cytokine release syndrome (CRS) and neurotoxicity (*224*, *225*, *289-291*, *302*, *303*, *305*, *306*, *357*). Both efficacy and toxicity result from activation of intracellular signaling pathways mediated by CAR engagement.

T cell activation occurs following TCR engagement with antigen-specific peptide bound to MHC molecules. TCR binding stimulates intracellular PO_4 of immunoreceptor tyrosine-based activating motifs (ITAMs) found within the CD3δ, ε, γ and ζ chains of the TCR (*18*). Combined

with protein PO_4 signals delivered in *trans* from costimulatory molecules and cytokines, these events alter T cell transcriptional programs, induce proliferation, promote cytotoxic functions, and stimulate cytokine release. Most CARs utilize a simplified format to recapitulate the signals necessary for T cell effector function and proliferation by combining the CD3ζ endodomain in a single chain construct with a costimulatory domain from CD28 or 4-1BB. CD28/CD3ζ or 4-1BB/CD3ζ CAR T cells are both effective for treating patients with B cell malignancies but appear to behave differently *in vivo*. CD28/CD3ζ CAR T cells generally undergo intense proliferation within 7 days of transfer and seldom persist more than 60 days after infusion (*297*, *357*). In contrast, 4-1BB/CD3ζ CAR T cells reach peak levels 7-14 days after transfer and can persist for several months (*224*, *294*). However, variability in patient cohorts, CAR structures, and clinical trial designs impede robust comparisons across trials. Studies comparing CD28/CD3ζ and 4-1BB/CD3ζ CAR T cells *in vitro* and in animal models partially explain these clinical differences by demonstrating that 4-1BB/CD3ζ CAR T cells possess greater mitochondrial mass, a more memory T cell-like surface phenotype, and better retain effector functions in settings of chronic antigen stimulation (*269*, *346*).

It is widely assumed that the differences in phenotype and function of CD28/CD3ζ and 4-1BB/CD3ζ CAR T cells are conferred by activation of divergent signaling pathways through the distinct costimulatory molecules. Analyses of signaling pathways stimulated by 4-1BB/CD3ζ or third-generation CD28/4-1BB/CD3ζ CARs performed using phospho-flow cytometry, Western blot, or blot array do not identify differences between CD28/CD3ζ and 4-1BB/CD3ζ CAR signaling modules and only profile a small number of known signaling events to which there are experimentally-validated antibodies (*358*, *359*). A more comprehensive, unbiased and quantitative approach to examine CAR signaling would be to use liquid chromatography-tandem mass spectrometry (LC-MS/MS). When applied to study TCR signaling, LC-MS/MS uncovered hundreds of novel phosphoprotein signaling events that were missed by antibody-based techniques (*360-364*). We thus reasoned that LC-MS/MS would be valuable to characterize the signaling of CARs being used in clinical trials.

In this study, we analyzed ligation-induced signaling events in primary human $CD8^+$ T cells that express clinically-relevant CD28/CD3ζ and 4-1BB/CD3ζ CARs specific for CD19 or ROR1. We found that stimulation through CD28/CD3ζ and 4-1BB/CD3ζ CARs modulated nearly identical protein PO_4 events. Instead, stimulation of CD28/CD3ζ CAR T cells prompted more rapid and intense PO_4 of signaling intermediates and a more effector cell-like phenotype. CD28/CD3ζ CAR T cells were less potent at eradicating disseminated lymphoma in a xenograft

mouse model than 4-1BB/CD3ζ CAR T cells. Investigation of the basis for the differential signal strength showed that increased basal phosphorylation of the CAR CD3ζ chain and CAR-associated Lck contributed to the rapid kinetics and stronger signal strength of CD28/CD3ζ CARs. Thus, the major distinction between CD28/CD3ζ and 4-1BB/CD3ζ CARs relates not to divergent phosphoprotein signaling pathways, but rather signaling strength and kinetics, which in turn, affect T cell function and fate. These results provide unanticipated insights that can inform the design of new therapeutic receptors.

Results

Primary T cells are a clinically relevant model system for studying CAR signaling

Over the past 30 years, TCR signaling has been extensively studied in Jurkat cells, an immortalized T cell leukemia line, due to the ease at which the cells can be cultured and manipulated with common molecular biology techniques (*365*). For these reasons, we considered using Jurkat cells as a model system in which to analyze CAR signaling, but a comparison of PO_4 of known proximal TCR signaling molecules by LC-MS/MS after anti-CD3 monoclonal antibody (mAb) stimulation revealed that Jurkat and cultured primary human T cells exhibited distinct patterns of protein PO_4 (**Figures 3.1A-B**). In contrast to Jurkat cells, primary T cells displayed prolonged PO_4 of CD3 chains and ZAP-70, and differentially phosphorylated CD28, LAT, LCK, PAK2, SHP1, SOS1, and VAV1 after stimulation. Taken together with the fact that clinical CAR T cell products are formulated from patient-derived primary T cells, we concluded it was necessary to study CAR signaling in primary human T cells.

A

Cell Types	Time	Treatment
Primary T cells	10 min	OKT3 + α-mouse IgG
		α-mouse IgG
	45 min	OKT3 + α-mouse IgG
		α-mouse IgG
Jurkat cells	10 min	OKT3 + α-mouse IgG
		α-mouse IgG
	45 min	OKT3 + α-mouse IgG
		α-mouse IgG

B

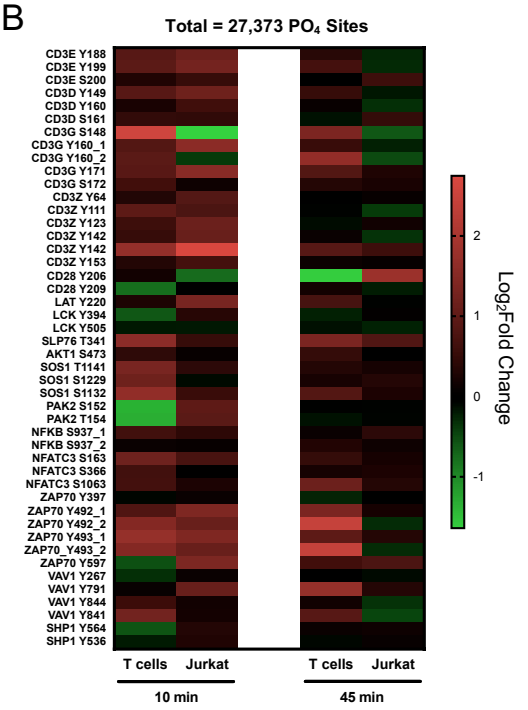

Figure 3.1. Mass spectrometric analysis of TCR signaling in Jurkat cells and primary T cells reveals marked differences in protein phosphorylation. A) Primary $CD8^+$ T cells or Jurkat cells were stimulated with anti-CD3ε mAb and anti-mouse IgG or left unstimulated by treating with anti-mouse IgG alone. B) Heat map showing log_2 fold change of known PO_4 sites in the proximal TCR signaling pathway. One LC-MS/MS experiment was performed.

Stimulating CAR T cells with antigen presenting cells is not amenable to LC-MS/MS analysis

We next sought to develop methods for stimulating CAR signaling in primary T cells. Anti-idiotypic mAbs directed against the single chain variable fragments (scFv) CAR targeting element enable selective CAR cross-linking and signal activation in a manner similar to that of anti-CD3 mAbs (*366*). However, mAbs are often used at saturating concentrations that cross-link the majority of TCR complexes on a given T cell (*360*, *361*). These features are distinct from natural TCR and CAR recognition of a small number of molecules at immunological synapses (*367*). We therefore asked whether co-culture of CAR T cells and antigen presenting cells (APCs) could initiate CAR signaling in a more physiological manner (**Figure 3.2A**). In pilot experiments, we analyzed lysates prepared from co-cultures of CD19-specific 4-1BB/CD3ζ CAR T cells and CD19-transduced or control K562 tumor cells by LC-MS/MS. To enable discrimination of peptides from CAR T cells and K562 cells, we utilized stable isotope labeling by amino acids in cell culture (SILAC) (*368*, *369*). Despite a 4:1 T cell to K562 ratio during co-culture, over 80% of the measured phosphopeptides originated from K562 cells due to their increased cell mass (**Figure 3.2B**). This finding posed a technical impediment to analysis of

CAR signaling since greater mass spectrometry time would be required to characterize the minority of CAR T cell-derived phosphopeptides.

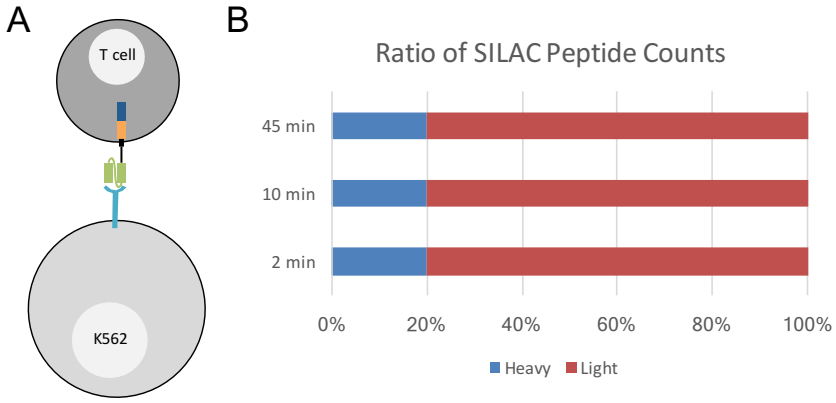

Figure 3.2. Stimulating CAR T cells with K562/CD19 tumor cells contaminates cellular lysates with K562-derived peptides. A) Schematic of a tumor cell-based stimulation technique whereby 'heavy' CAR-T cells are cultured with 'light' K562 tumor cells at a 4:1 effector to target ratio. B) Identification and quantification of peptides by mass spectrometry revealed that 'light' K562-derived peptides comprise about 80% of the lysate. Data representative of 2 independent experiments.

CAR designs containing a Strep-tag II sequence enable selective activation of CAR signaling in primary T cells

To circumvent these drawbacks of cell based-stimulation, we developed a cell-free method for activating CAR signaling. We modified two lentiviral vectors encoding CD19-specific and ROR1-specific 4-1BB/CD3ζ CARs that are currently being tested in clinical trials by adding a nine-amino acid Strep-tag II (STII) sequence to the extracellular CAR hinge. For comparison, we cloned structurally identical CD19-specific and ROR1-specific CD28/CD3ζ CARs containing the STII tag (**Figure 3.3A**). All constructs contained a truncated cell surface EGFR (EGFRt) marker downstream of a T2A ribosomal skip element for purification of CAR-expressing T cells (*309*). Inclusion of the STII sequence does not interfere with CAR T cell recognition or function, and STII CD28/CD3ζ or 4-1BB/CD3ζ CAR T cells are efficiently activated and expanded *in vitro* by simulation with STII microbeads (**Figure 3.3B**) (*370*). Primary $CD8^+$ T cells were transduced with each lentiviral vector, sorted for EGFRt expression, and expanded to $>1.6\times10^8$ cells with a single cycle of stimulation for subsequent analysis of CAR-expressing T cells (**Figure 3.3C**). The abundance of CD28/CD3ζ and 4-1BB/CD3ζ CARs of each scFv specificity was similar on the cell surface as measured by staining with STII mAb (**Figure 3.3D**). CAR T cells also expressed similar amounts of CD45RO, CD62L, CD27, and CD28 (**Figure 3.3E**), indicating that CAR T cells retained markers associated with memory and proliferative potential. We only

detected small frequencies of PD-1- or Tim-3-positive CAR T cells, suggesting the cells were not activated or exhausted after cell culture (**Figure 3.3E**). Accordingly, >85% of CD28/CD3ζ and 4-1BB/CD3ζ CAR T cells were in the G_0/G_1 cell cycle phase, indicating the cells were resting (**Figures 3.3F**).

We evaluated canonical T cell signaling events induced by STII ligation and found that cell-free STII microbead stimulation of CARs was similar to CAR antigen expressing tumor cells. ROR1-specific 4-1BB/CD3ζ CAR T cells were incubated for 45 minutes with increasing amounts of STII microbeads or with ROR1-transduced K562 (K562/ROR1) tumor cells and CD3ζ Tyr^{142} and SLP-76 Ser^{376} were measured by Western blot. At the highest bead to CAR T cell ratio, the phosphorylation of CD3ζ and SLP-76 was similar to that observed in lysates from CAR T cells stimulated with K562/ROR1 cells (**Figures 3.3G**). This bead to cell ratio was used for all subsequent experiments. Thus, STII microbead stimulation provided a precise method to selectively activate CAR signaling in primary T cells.

Mass spectrometry identifies common protein phosphorylation events after stimulation of CD28/CD3ζ or 4-1BB/CD3ζ CAR T cells

We performed tandem LC-MS/MS analysis to interrogate the signaling pathways activated in CD28/CD3ζ or 4-1BB/CD3ζ CARs in an unbiased manner. Human T cells expressing CD28/CD3ζ or 4-1BB/CD3ζ CARs were incubated with STII or uncoated (control) microbeads for 10 or 45 minutes (**Figure 3.4A**). CD19-specific CAR T cells generated from two different donors were used in two independent experiments, and a third independent experiment utilized ROR1-specific CAR T cells derived from one of the two donors (**Figure 3.4B**). Given that ROR1-specific and CD19-specific CARs displayed similar phenotypes across the two donors and were stimulated identically in a ligand-independent manner, the corresponding measurements were considered biological replicates. To provide relative quantitation of phosphopeptides within each experiment, we labeled each trypsin-digested lysate with a unique isobaric Tandem Mass Tag (TMT) and enriched for phosphopeptides by anti-pTyr immunoprecipitation and immobilized metal affinity chromatography (*371*) (**Figure 3.S1B**). We identified a total of 26,804 phosphorylation sites across the three experiments corresponding to 4,849 proteins. Among phosphorylation sites, 571 (2.13%) were pTyr, 4,647 (17.33%) were pThr, and 21,586 (80.53%) were pSer (**Figure 3.4C**). Considering the stochastic limitations inherent in data-dependent acquisition shotgun proteomics, there was considerable overlap in the captured phosphoproteome between replicate experiments (**Figure 3.4D**) (*372*). As

previously described in murine T cells, 99% of PO_4 sites detected in each experiment were present in both unstimulated and stimulated T cell lysates, enabling quantitation of changes induced by CAR activation (*362*, *373*).

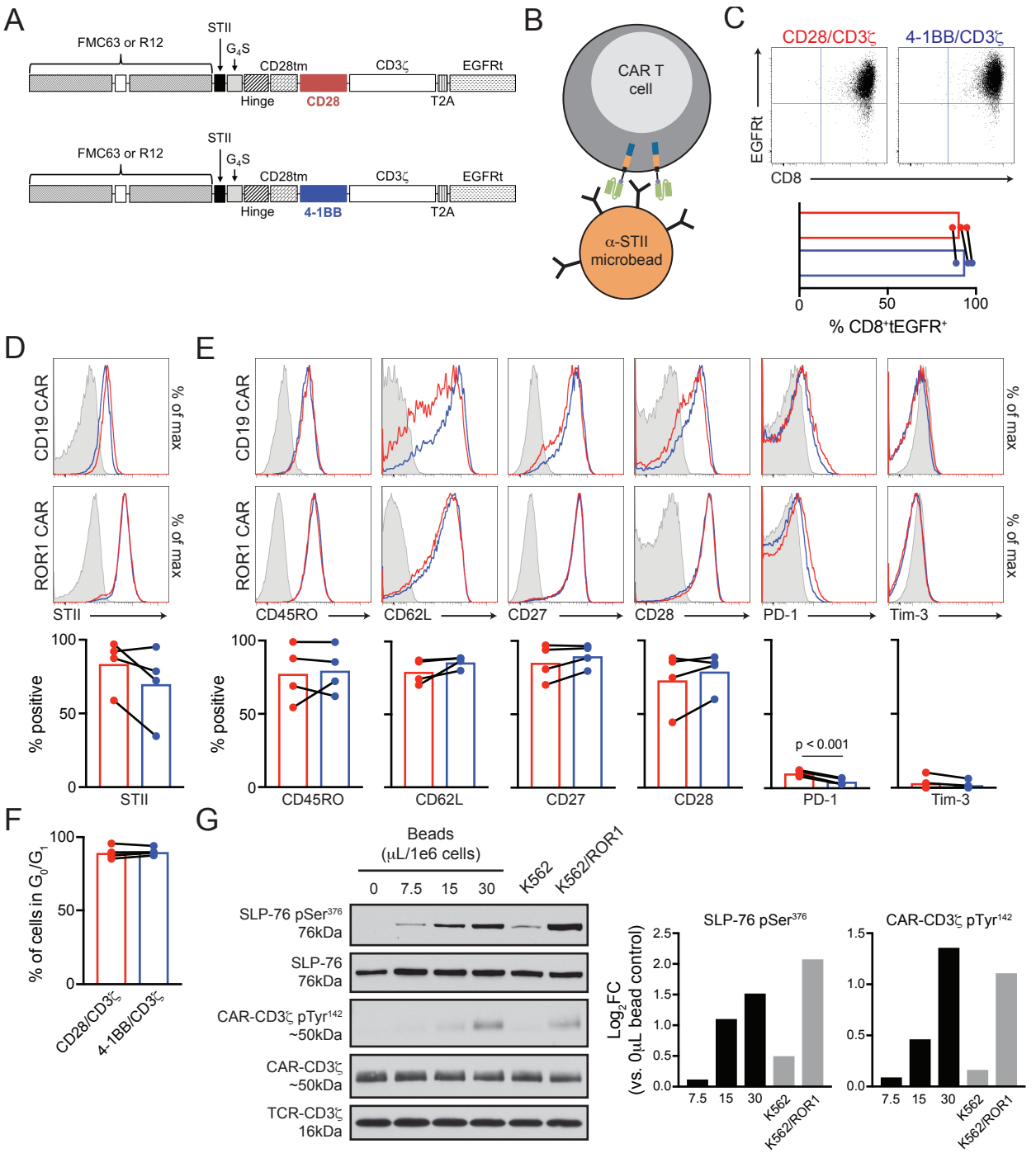

Figure 3.3. Both CD28/CD3ζ and 4-1BB/CD3ζ CAR T cells can be activated through an engineered STII hinge. (**A**) Schematic of CARs incorporating a STII sequence in the extracellular hinge. CARs contained either the CD19-specific FMC63 scFv or ROR1-specific R12 scFv. (**B**) Schematic of CAR T cell

activation through the STII hinge using magnetic beads coated with STII mAb. (**C**) Flow cytometry analysis of CD8 and EGFRt staining on singlet CD19 CAR T cells after expansion. The frequency of $CD8^+EGFRt^+$ cells are means from 3 independent experiments. (**D** and **E**) Flow cytometry analysis of STII staining of cell surface CAR (D) or CD45RO, CD62L, CD27, CD28, PD-1, and Tim-3 phenotypic marker staining (E) on sort-purified CD19-specific or ROR1-specific singlet $CD8^+$ CAR T cells after expansion. Histogram plots of CD28/CD3ζ CAR T cells (red), 4-1BB/CD3ζ CAR T cells (blue), or isotype control staining (grey). The frequency of positive cells are means from 4 independent experiments. (**F**) Flow cytometry analysis of the DNA content of CAR T cells after expansion. The frequency of cells in G_0/G_1 gate are means from 4 independent experiments. (**G**) Western blot analysis for CD3ζ, CD3ζ $pTyr^{142}$, SLP-76, and SLP-76 $pSer^{376}$ in lysates of ROR1 4-1BB/CD3ζ CAR T cells after 45 minutes of co-culture with varying quantities of STII microbeads, K562 cells, or K562/ROR1 cells. Fold change (log_2FC) of normalized band intensity is shown. Blots are representative of 2 independent experiments. The indicated P values were calculated by paired two-tailed t test (E).

A

Signaling Domains	Time	Treatment
CD28/CD3ζ	10min	Stimulation
		Control
	45min	Stimulation
		Control
4-1BB/CD3ζ	10min	Stimulation
		Control
	45min	Stimulation
		Control

B

Experiment	Donor	scFv
1	JD	CD19
2	JD	ROR1
3	JB	CD19

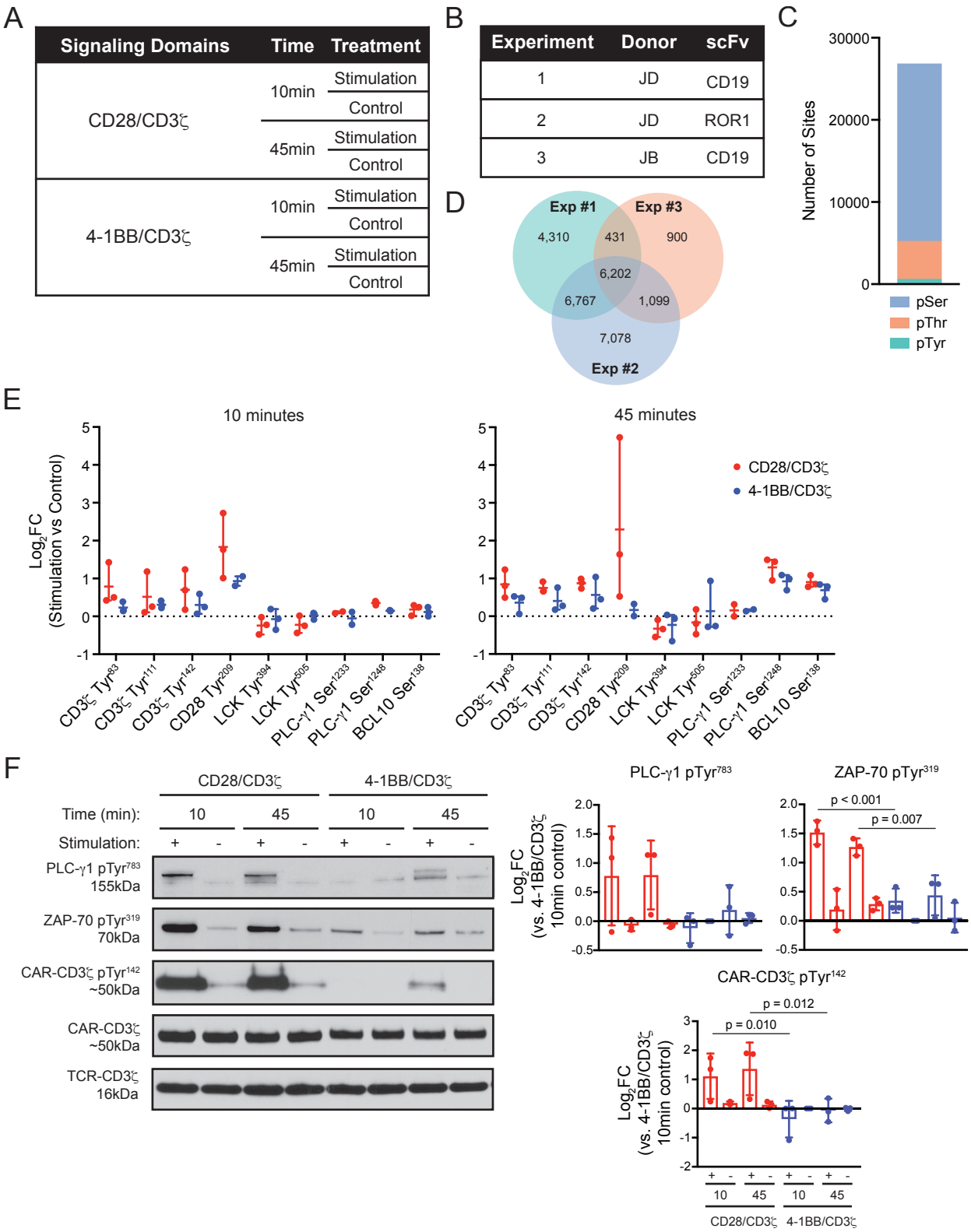

Figure 3.4. CAR T cells signal through endogenous T cell signaling proteins. (**A** and **B**) Human CAR T cell treatment conditions and experimental groups. (**C** to **E**) Tandem MS/MS analysis of phosphorylated peptides from lysates of CAR T cells stimulated as in (A). The total number of pSer, pThr and pTyr peptides identified (C) and the Venn diagram of the overlap among phosphorylation sites (D) are pooled from all

tandem MS/MS experiments. The fold change (log_2FC) in phosphorylation at the indicated times at sites involved in canonical TCR signaling (E) are means ± range from all tandem MS/MS experiments. (**F**) Western blot analysis for CD3ζ, CD3ζ pTyr^{142}, ZAP-70 pTyr^{319}, and PLC-γ1 pTyr^{783} in lysates from CD19-specific CD28/CD3ζ or 4-1BB/CD3ζ CAR T cells at the indicated times after stimulation. Fold change (log_2FC) of normalized band intensity are means ± SD from the 3 tandem MS/MS experiments. The indicated P values were calculated by repeated-measures one-way ANOVA with Tukey's multiple comparisons test comparing CD28/CD3ζ and 4-1BB/CD3ζ CAR samples (F).

We first analyzed well described TCR PO_4 events within the MS dataset to determine sites that were modified by CAR engagement (*18*). We calculated a log_2fold change (log_2FC) value for all phosphorylation sites within each experiment by comparing stimulated samples to appropriate controls (i.e. CD28/CD3ζ CAR 10 minute stimulation vs. CD28/CD3ζ CAR 10 minute control). At 10 minutes, we found increased phosphorylation of CD3ζ at Tyr^{83}, Tyr^{111}, and Tyr^{142} in stimulated CAR T cells (**Figure 3.4E**). All CAR T cells displayed increased phosphorylation of CD28 at Tyr^{209}, which demonstrated that CD28/CD3ζ and 4-1BB/CD3ζ CAR activation both stimulate phosphorylation of CD28. After 45 minutes of stimulation, phosphoprotein signaling spread to downstream TCR nodes and we measured increased PO_4 of PLC-γ1 at Ser^{1248} and BCL10 at Ser^{138} (**Figure 3.4E**) (*374*, *375*). We did not observe reproducible changes at either time point in the PO_4 of CD3δ, ε, or γ ITAMs. Because these sites are phosphorylated after TCR stimulation (*18*), our data indicated that CAR signaling imperfectly mimicked endogenous TCR activation.

The MS data indicated that CD28/CD3ζ CAR stimulation may initiate a greater magnitude log_2FC than 4-1BB/CD3ζ CARs at both 10 and 45 minutes and we confirmed this finding by Western blot. Evaluation of cell lysates for CD3ζ pTyr^{142}, ZAP-70 pTyr^{319} and PLC-γ1 pTyr^{783} demonstrated that both CD28/CD3ζ and 4-1BB/CD3ζ CAR stimulation increased phosphorylation of these sites, but we observed more intense ZAP-70 and CAR CD3ζ phosphorylation in stimulated CD28/CD3ζ CAR T cells compared to 4-1BB/CD3ζ CAR T cells (**Figure 3.4F**). We also detected a low level of basal CAR CD3ζ phosphorylation in unstimulated CD28/CD3ζ CD19 and ROR1 CAR T cells that was not present in 4-1BB/CD3ζ CAR T cells. Western blot analysis of lysates from primary $CD4^+$ T cells transduced with CD19 CARs and stimulated with STII microbeads also demonstrated similar patterns of basal CAR CD3ζ phosphorylation as well as more rapid and robust phosphorylation of CD3ζ and SLP-76 within CD28/CD3ζ CAR T cells (**Figure 3.S2A**). Constitutive phosphorylation of the CAR CD3ζ domain or tonic signaling has been shown to occur with some CARs, including a CD19-specific CD28/CD3ζ CAR being used in the clinic (*180*). Strong tonic signaling has been linked to sequences in the scFv that promote clustering of CAR molecules at the cell surface and results

in the upregulation of T cell exhaustion markers (*256*, *376*). Because we did not observe differences in PD-1 or Tim-3 expression, or evidence of CAR clustering in unstimulated CD28/CD3ζ or 4-1BB/CD3ζ CAR T cells (**Figures 3.3E-F and Figure 3.S2B**), the low level of basal CAR CD3ζ domain phosphorylation detected here may be distinct from more extreme tonic signaling observed in some CARs with different scFv specificities.

Phosphorylation events mediated by CD28/CD3ζ or 4-1BB/CD3ζ CARs differ in kinetics and magnitude

An advantage of shotgun MS is that it can quantitatively and temporally measure thousands of PO_4 events outside of the canonical TCR signaling pathway to which there are no known experimentally validated antibodies. We leveraged the *limma* statistical framework and associated R package to identify PO_4 sites that were up or down modulated after CD28/CD3ζ and 4-1BB/CD3ζ CAR ligation (*377*). We assigned a PO_4 site to be CAR stimulation-responsive if it was detected in at least two of the three experiments, displayed an average $|\log_2 FC| \geq 0.7$ between stimulated and unstimulated conditions at 10 or 45 minutes, and met a 5% FDR cutoff. A $\log_2 FC$ cutoff of 0.7 was chosen because this represents approximately two standard deviations of the distribution of $\log_2 FC$ values (**Figure 3.S3**).

Using these stringent cut-offs, 26 PO_4 sites were identified as stimulation-responsive at 10 minutes after stimulation of CD28/CD3ζ CAR T cells. These sites were enriched for proteins in the KEGG TCR signaling pathway including increased PO_4 of p21 activated kinase 2 (PAK2) at Ser^{64}, CD8 alpha (CD8A) at Ser^{231}, protein kinase C θ (PKCT) at Ser^{370}, and proto-oncogene vav (VAV1) at Ser^{748} and Thr^{749} (**Figure 3.5A and Table 3.S1**). We also detected increased PO_4 of neuroblast differentiation-associated protein (AHNAK) at Ser^{5857}, which activates PLC-γ1 and is required for T cell calcium (Ca^{2+}) mobilization and effector functions (*378*, *379*). In contrast, no sites met $\log_2 FC$ and FDR criteria at the 10 minute time point after stimulation of 4-1BB/CD3ζ CAR T cells (**Figure 3.5A** and **Table 3.S1**). The lack of robust alterations in early protein PO_4 induced by the 4-1BB/CD3ζ CAR was consistent with Western blot data showing a very low level of PO_4 of CAR CD3ζ and PLC-γ1 at 10 minutes after stimulation (**Figure 3.4F**).

After 45 minutes of stimulation, more intense protein PO_4 had occurred and 1,289 PO_4 sites met the $\log_2 FC$ and FDR cutoffs from either CD28/CD3ζ or 4-1BB/CD3ζ CAR samples. These included 1,279 PO_4 sites from 743 genes in CD28/CD3ζ CAR T cells and 522 sites from 346 genes in 4-1BB/CD3ζ CAR T cells (**Figures 3.5A and Tables 3.S2-3**). These data indicate that stimulation of CD28/CD3ζ CAR T cells increased phosphorylation at a greater number of

sites than stimulation of 4-1BB/CD3ζ CAR T cells. However, both CD28/CD3ζ and 4-1BB/CD3ζ CAR activation stimulated highly similar changes in the phosphorylation of activation-responsive sites (**Figure 3.5B**). Only 12 (0.93%) of the 1,289 PO_4 sites that met the cut-offs in CD28/CD3ζ CAR samples exhibited an opposite response after 4-1BB/CD3ζ CAR stimulation, and only 43 (3.3%) sites exhibited a greater magnitude log_2FC after 4-1BB/CD3ζ CAR stimulation. These observations were consistent with our earlier data suggesting signaling downstream of CD28/CD3ζ CAR activation was more intense than downstream of 4-1BB/CD3ζ CAR activation (**Figure 3.5B and Table 3.S2**). Furthermore, these subsets of 12 and 43 PO_4 sites did not map to currently defined 4-1BB signaling networks (*380*).

Finding few differences in protein PO_4 events after stimulation of CD28/CD3ζ and 4-1BB/CD3ζ CARs was unexpected and educed the question of how proteins involved in canonical T cell costimulatory signaling pathways were affected. In agreement with our earlier observation that 4-1BB/CD3ζ CARs activated endogenous CD28, we found that the CD28 signaling intermediates VAV1, PIK3C2A, and PKCT displayed increased PO_4 after stimulation of either CAR (**Figure 3.5C**) (*381*). Within the 4-1BB signaling pathway, lymphocyte-specific protein 1 (LSP1), a direct target of 4-1BB and TRAF2 signaling, was also modulated by both CARs (*382*). Despite similarities in PO_4 sites, CD28/CD3ζ CARs modulated each PO_4 site, including those in the 4-1BB signaling pathway, by a greater magnitude than 4-1BB/CD3ζ CARs. Thus, rather than activating divergent costimulatory pathways, as might be predicted from the distinct costimulatory domains in the receptors, ligation of CD28/CD3ζ and 4-1BB/CD3ζ CARs induced highly similar changes in intracellular protein PO_4 that encompassed both canonical CD28 and 4-1BB signaling intermediates.

A map illustrating the major pathways and individual protein PO_4 events modulated by CD28/CD3ζ and 4-1BB/CD3ζ CAR ligation includes proteins in canonical TCR signaling and MAPK signaling pathways (**Figure 3.6, Table 3.S3**). In addition, stimulation of either CAR affected PO_4 of actin-cytoskeletal regulatory proteins, RNA processing proteins, nuclear pore proteins, and mitochondrial fission regulators such as DRP1 (*383*, *384*). A list of CAR stimulation-responsive PO_4 sites is provided in **Tables 3.S1-2**. Many of these proteins have not been previously associated with TCR or CAR signaling.

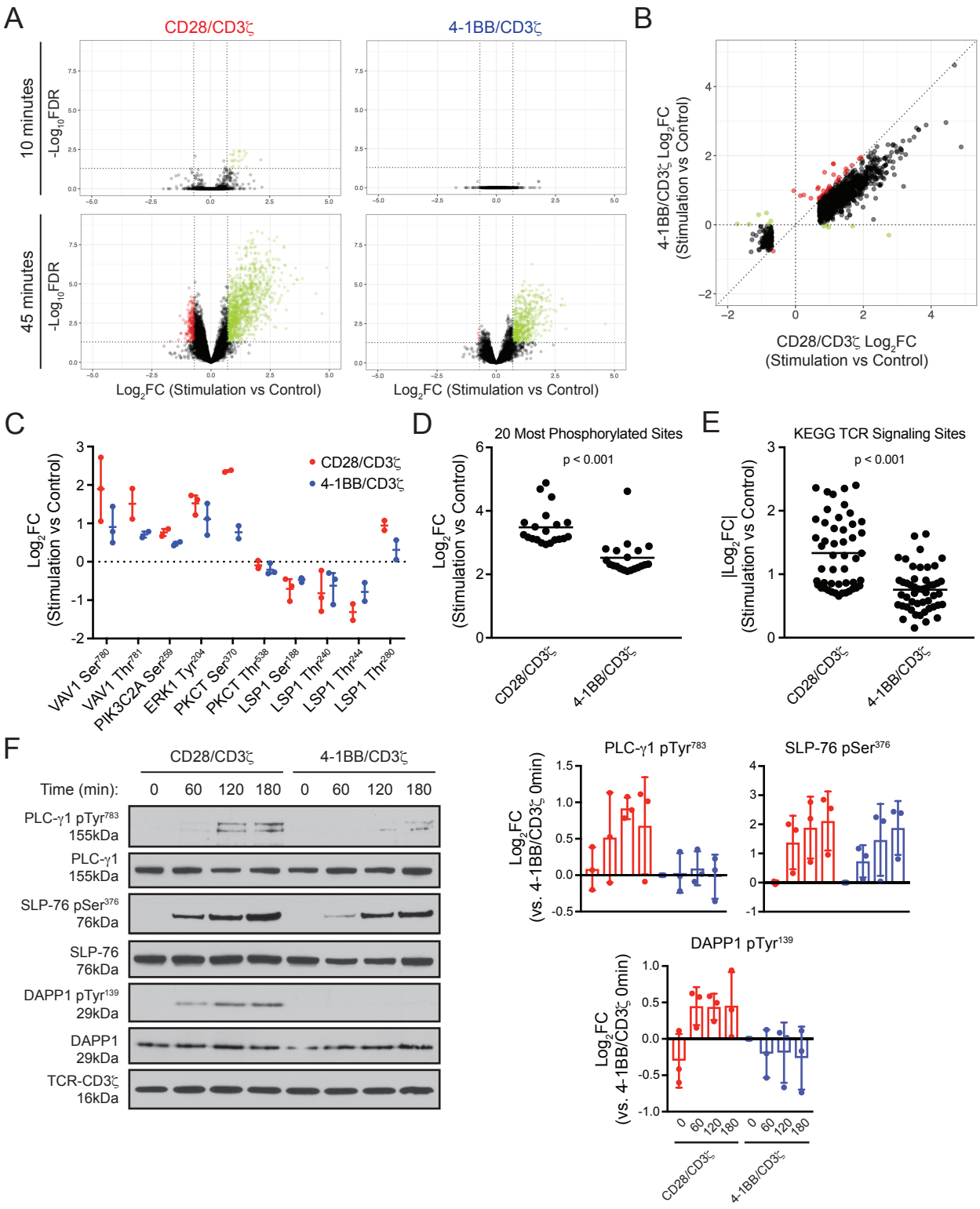

Figure 3.5. The kinetics and strength of signaling vary after stimulation of CD28/CD3ζ or 4-1BB/CD3ζ CAR T cells. (**A**) Volcano plots of fold change (log_2FC) and false discovery rate (FDR) for PO_4 sites identified by tandem MS/MS in Fig 3.4. Green dots indicate sites with increased phosphorylation and red dots indicate sites with decreased PO_4 after CAR stimulation in at least 2 experiments. (**B**) Comparison of stimulation-responsive PO_4 sites identified by tandem MS/MS 45 minutes after activation in either

CD28/CD3ζ and 4-1BB/CD3ζ CAR samples. Green dots specify sites that exhibited opposite responses after CD28/CD3ζ or 4-1BB/CD3ζ CAR activation, whereas red dots indicate sites phosphorylated to a greater extent after stimulation of 4-1BB/CD3ζ CAR T cells in at least 2 tandem MS/MS experiments in Fig 3.4. (**C**) The fold change in PO_4 sites on known CD28 and 4-1BB signaling pathway members at 45 minutes after CAR T cell stimulation. Data are means ± range from the three tandem MS/MS experiments in Fig 3.4. (**D**) The fold change in the 20 most phosphorylated sites identified by tandem MS/MS in Fig 3.4. Data are means from all experiments. (**E**) The absolute fold change of PO_4 sites on known KEGG TCR signaling pathway proteins identified by tandem MS/MS in Fig 3.4. Data are means from all experiments. (**F**) Western blot analysis for CD3ζ, DAPP1, DAPP1 pTyr^{139}, SLP-76, SLP-76 pSer^{376}, PLC-γ1, and PLC-γ1 pTyr^{783} in lysates from ROR1 CAR T cells stimulated with STII microbeads for the indicated times. Fold change of normalized band intensity are means ± SD from 3 independent experiments. The indicated P values were calculated by unpaired two-tailed t test (D and E).

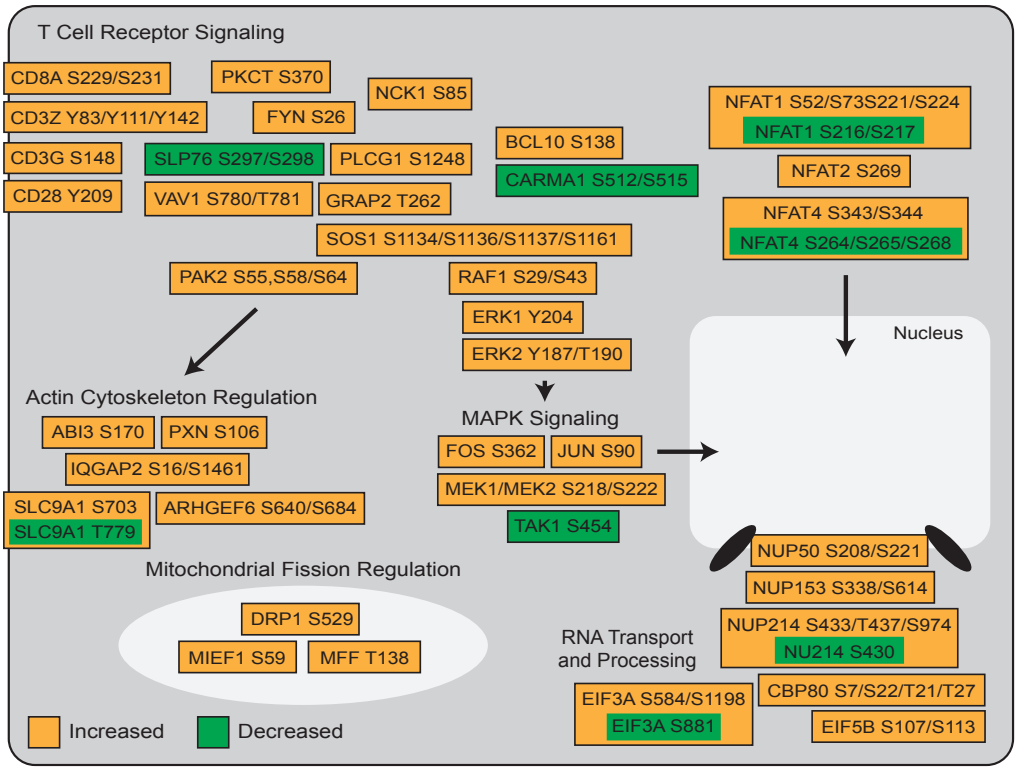

Figure 3.6. Stimulation of CD28/CD3ζ or 4-1BB/CD3ζ CAR T cells alters protein phosphorylation across similar signaling pathways and cellular compartments. Map of select proteins differentially phosphorylated after 45 minutes of CAR T cell stimulation from analysis of all tandem MS/MS experiments in Fig 3.4.

Differences in the magnitude of CD28/CD3ζ and 4-1BB/CD3ζ CAR signaling persist across time

Protein PO_4 mediated by CD28/CD3ζ and 4-1BB/CD3ζ CARs was highly similar but differed in intensity at the vast majority of PO_4 sites. This differential intensity evoked comparisons to work showing that signal strength during T cell activation, measured as a composite of TCR affinity, costimulation and cytokine signals, dictates clonal expansion and the effector capacities of a T cell response (*385-387*). To provide a holistic measure of CAR signal

strength we sorted stimulation-responsive phosphorylation sites at 45 minutes from CD28/CD3ζ and 4-1BB/CD3ζ CAR samples by decreasing log_2FC. In line with results showing both CARs modulated similar phosphorylation sites, 15 of the 20 most phosphorylated sites after stimulation were shared between CD28/CD3ζ and 4-1BB/CD3ζ CAR T cells (**Table 3.S4**). However, PO_4 of the top 20 sites increased by 11.15-fold on average in CD28/CD3ζ CAR samples, but only 5.8-fold on average in 4-1BB/CD3ζ CAR samples (**Figure 3.5D**). Stratifying CAR stimulation-responsive PO_4 sites by signaling pathway further showed that the average PO_4 site within the KEGG TCR signaling pathway was modulated by 2.52-fold in CD28/CD3ζ CAR samples, but only 1.69-fold in 4-1BB/CD3ζ CAR samples (**Figure 3.5E**). To determine if 4-1BB/CD3ζ CAR signals reached a similar intensity to that of CD28/CD3ζ CARs at later times, we stimulated identically prepared $CD8^+$ CAR T cells for 60, 120, or 180 minutes and measured PO_4 of canonical and newly identified signaling intermediates (**Table 3.S4**). CD28/CD3ζ CAR stimulation resulted in more intense PO_4 of SLP-76 Ser^{376}, PLC-γ1 Tyr^{783}, and DAPP1 Tyr^{139} in all samples (**Figure 3.5F**), indicating that 4-1BB/CD3ζ CAR stimulation never rivaled CD28/CD3ζ CAR signal intensity during this time frame.

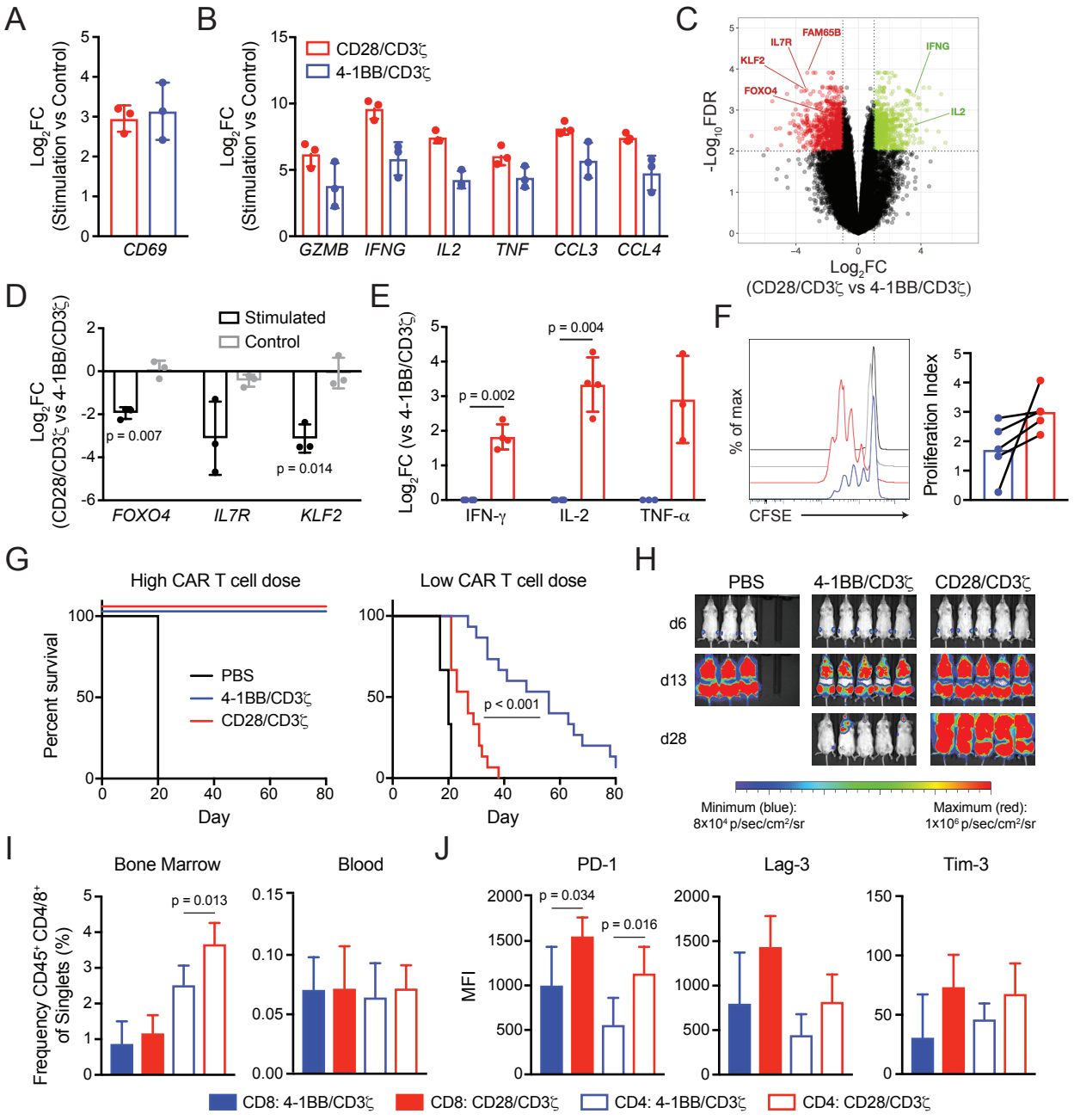

Figure 3.7. Increased CD28/CD3ζ CAR signal intensity is associated with an effector cell-like phenotype and reduced *in vivo* anti-tumor activity. (**A** to **C**) RNA-Seq analysis of RNA expression in CD28/CD3ζ or 4-1BB/CD3ζ CAR T cells with and without stimulation. The fold change values of the indicated transcripts (A and B) are means ± SD from 3 independent experiments. Transcripts shown in (B) met an FDR of 1% for differential expression between CD28/CD3ζ and 4-1BB/CD3ζ CAR T cells. Volcano plot analysis (C) indicates genes with increased expression in CD28/CD3ζ CAR T cells (green) or increased expression in 4-1BB/CD3ζ CAR T cells (red). (**D**) qRT-PCR analysis of IL7R, KLF2, and FOXO4 expression in CD28/CD3ζ and 4-1BB/CD3ζ CAR T cells. Fold change data are means ± SD from 3 independent experiments quantified together in a single qPCR run. (**E**) ELISA analysis of cytokine production 24 hours after co-culture of ROR1-specific CAR T cells with K562/ROR1 cells. Data are means ± SD of 3-4 independent experiments. (**F**) Flow cytometry analysis of T cell proliferation as measured by CFSE dye dilution at 72 hours after STII microbead stimulation. Histogram plot of unstimulated CD28/CD3ζ CAR T cells (grey), unstimulated 4-1BB/CD3ζ CAR T cells (black), stimulated CD28/CD3ζ CAR T cells (red), and

stimulated 4-1BB/CD3ζ CAR T cells (blue). The proliferation index of cells are means from 5 independent experiments. (**G to J**) At 7 days after Raji/ffluc engraftment, NSG mice were treated with a single infusion of the indicated dose of CAR T cells. Survival analyses (G) are pooled from 2-3 independent experiments on 6, 9 or 15 mice per group. Bioluminescence images of Raji/ffluc tumor burden in mice at the indicated time points (H) are representative of all experiments. (**I and J**) Flow cytometry analysis of CAR T cell frequency in bone marrow or peripheral blood (I), or abundance of PD-1, Lag-3, or Tim-3 on CAR T cells in the bone marrow (J) on day 20. Frequency and MFI data are means ± SD of 10 mice per group from 2 independent experiments. The indicated P values were calculated by one sample t test with null hypothesis $H_0 = 0$ (D), paired two-tailed t test (E) or log-rank (Mantel-Cox) test (G), or unpaired two-tailed t test (I and J).

Increased CAR signal intensity is associated with an effector cell-like phenotype and reduced in vivo anti-tumor activity

The strength of T cell activation and signal transduction influences transcriptional programs that regulate effector cell differentiation and memory formation (*386*). We used RNA-seq to analyze changes in transcription in CD28/CD3ζ or 4-1BB/CD3ζ $CD8^+$ CAR T cells at 6 hours after STII bead stimulation. Consistent with the faster and more intense phosphoprotein signal, CD28/CD3ζ CAR stimulation initiated more marked transcriptional changes. A comparison of stimulated to unstimulated CD28/CD3ζ CAR T cells identified 4,894 differentially expressed genes at 6 hours, whereas 4-1BB/CD3ζ CAR stimulation resulted in 197 differentially expressed genes. CD28/CD3ζ or 4-1BB/CD3ζ CAR stimulation increased expression of the canonical T cell activation marker CD69 to a similar degree (**Figure 3.7A**), but greater fold increases in expression of the effector molecules granzyme B (*GZMB*), interferon-γ (*IFNG*), interleukin-2 (*IL2*), tumor necrosis factor-α (*TNF*), macrophage inflammatory protein 1α (*CCL3*), and macrophage inflammatory protein 1β (*CCL4*) were observed in CD28/CD3ζ CAR T cells (**Figure 3.7B**).

Direct comparison of CD28/CD3ζ and 4-1BB/CD3ζ CAR T cells after stimulation identified 1,673 differentially expressed genes (**Table 3.S5**). Of these, Krüppel-like factor 2 (*KLF2*), interleukin-7 receptor (*IL7R*), and Rho family-interacting cell polarization regulator 2 (*RIPOR2*, previously known as *FAM65B*) expression was decreased in CD28/CD3ζ CAR T cells compared to 4-1BB/CD3ζ CAR T cells (**Figure 3.7C**). *KLF2* and *IL7R* are associated with memory T cell formation and are targets of the FOXO family of transcription factors (*388-390*). Consistent with this observation, *FOXO4* expression was reduced in stimulated CD28/CD3ζ CAR T cells when compared to 4-1BB/CD3ζ CAR T cells. qPCR confirmed that some of these T cell memory-associated genes were differentially expressed in stimulated CD28/CD3ζ or 4-1BB/CD3ζ CAR T cells (**Figure 3.7D**).

Because differences in TCR signal quantity affect T cell functions (*386*, *387*), we measured CD28/CD3ζ and 4-1BB/CD3ζ CAR T cell effector functions *in vitro*. We activated CD28/CD3ζ and 4-1BB/CD3ζ CAR T cells with ROR1 and CD19 expressing K562 cells or STII microbeads, and measured cytokine production and proliferation. After 24 hours of co-culture, CD28/CD3ζ CAR T cells secreted markedly more IFN-γ, IL-2, and TNF-α than 4-1BB/CD3ζ CAR T cells (**Figure 3.7E**). By 72 hours, CD28/CD3ζ CAR T cells underwent more divisions than 4-1BB/CD3ζ CAR T cells (**Figure 3.7F**).

We also investigated the function of CD28/CD3ζ and 4-1BB/CD3ζ CAR T cells *in vivo*. For these studies, we utilized a defined 1:1 CD4:CD8 ratio CAR T cell product because we previously demonstrated the combination of $CD8^+$ and $CD4^+$ T cells displayed superior control of xenograft Raji lymphoma in NOD/SCID/$\gamma c^{-/-}$ (NSG) mice and we observed similar basal CAR PO_4 and signaling intensity in $CD8^+$ and $CD4^+$ CAR T cells (**Figures 3.2F and 3.S2A**) (*198*). Adoptive transfer of 3×10^6 CD28/CD3ζ or 4-1BB/CD3ζ CAR T cells into tumor bearing mice mediated complete tumor regression (**Figure 3.7G**). However, when fewer ($7.5\text{-}8\times10^5$) cells were transferred, CD28/CD3ζ CAR T cells were much less potent than 4-1BB/CD3ζ CAR T cells, and all CD28/CD3ζ CAR T cell-treated mice died of tumor progression within 40 days (**Figures 3.7G-H**). Tumor progression occurred in mice treated at the lower CD28/CD3ζ CAR T cell dose despite accumulation of CAR T cells to higher frequencies in tumor-involved bone marrow (**Figure 3.7I**). CD28/CD3ζ CAR T cells in the bone marrow expressed higher levels of PD-1, Lag-3, and Tim-3 (**Figure 3.7J**), consistent with the acquisition of an exhausted phenotype. $CD8^+$ CD28/CD3ζ CAR T cells alone were also less effective in tumor control and exhibited higher levels of PD-1, Lag-3, and Tim-3 than $CD8^+$ 4-1BB/CD3ζ CAR T cells (**Figures 3.S4A-C**). Taken together, the rapid and intense signaling mediated by CD28/CD3ζ CAR activation correlated with an exhausted phenotype in $CD8^+$ and $CD4^+$ CAR T cells and reduced anti-tumor activity.

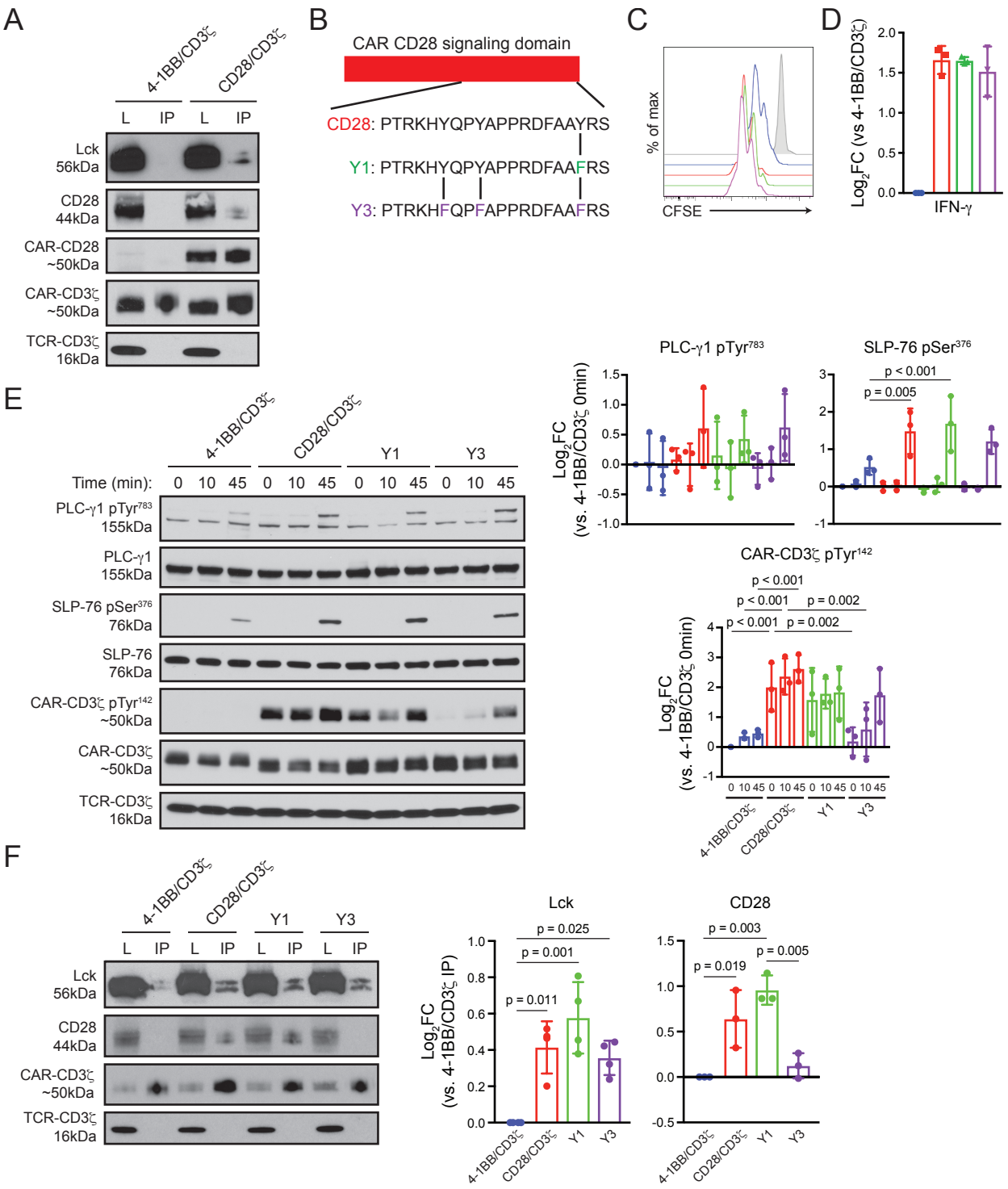

Figure 3.8. CD28/CD3ζ and 4-1BB/CD3ζ CARs differentially associate with endogenous Lck and CD28. (**A**) Western blot analysis for Lck, CD28, and CD3ζ in whole cell lysates (L) and STII immunoprecipitated fractions (IP) from unstimulated ROR1-specific CAR T cells. Blots are representative of 3-4 independent experiments. (**B**) Schematic of mutations made to the CAR CD28 signaling domain. (**C**) Flow cytometry analysis of ROR1-specific CAR T cell proliferation as measured by CFSE dye dilution at 72 hours after co-culture with K562/ROR1 cells. Histograms of untransduced T cells (grey), or 4-1BB/CD3ζ (blue), CD28/CD3ζ (red), Y1 (green), and Y3 CAR T cells (purple) after stimulation are representative of 3 independent experiments. (**D**) ELISA analysis of IFN-γ production by ROR1-specific 4-1BB/CD3ζ (blue),

CD28/CD3ζ (red), Y1 (green), or Y3 CAR T cells (purple) after co-culture with K562/ROR1 cells for 24 hours. Fold change data are means ± SD of 3 independent experiments. (**E**) Western blot analysis for CD3ζ, CD3ζ pTyr^{142}, SLP-76, SLP-76 pSer^{376}, PLC-γ1, and PLC-γ1 pTyr^{783} in lysates from ROR1-specific CAR T cells stimulated for the indicated times with STII microbeads. Fold change of normalized band intensity are means ± SD from 3 independent experiments. (**F**) Western blot analysis for Lck, CD28, and CD3ζ in whole cell lysates (L) and STII immunoprecipitated fractions (IP) from resting CAR T cells. Fold change of normalized band intensity are means ± SD from 3 (CD28) or 4 (Lck) independent experiments. The indicated P values were calculated by repeated-measures one-way ANOVA with Tukey's multiple comparisons test comparing samples at equivalent time points (E and F).

CD28/CD3ζ and 4-1BB/CD3ζ CARs differentially associate with endogenous CD28 and Lck

To interrogate possible causes of increased CD28/CD3ζ CAR signaling kinetics and strength, we immunoprecipitated CAR complexes from CD8$^+$ T cells and probed for differences among associated T cell signaling proteins in the basal state (**Figure 3.8A**). Western blot confirmed efficient CAR pull-down and showed association of endogenous CD28 and Lck with the CD28/CD3ζ CAR, but only minimal CD28 and Lck association with the 4-1BB/CD3ζ CAR (**Figure 3.8B**). Because basal CAR phosphorylation was conferred by the presence of the CD28 costimulatory domain and Tyr^{206}, Tyr^{209}, and Tyr^{218} were intensely phosphorylated after CAR stimulation, we constructed CD28/CD3ζ CARs with tyrosine to phenylalanine mutations at these residues (**Figure 3.8B**). CD19 and ROR1 CARs with mutations of Y218F (Y1) or all three tyrosines (Y3) were efficiently expressed in T cells and led to vigorous IFN-γ production and proliferation in response to co-culture with ROR1$^+$ or CD19$^+$ tumor cells (**Figures 3.8C-D**). We observed partial (Y1) or complete (Y3) abrogation of basal CAR CD3ζ phosphorylation in CARs containing Y to F mutations as compared to CD28/CD3ζ CARs, however Y1 and Y3 CARs still phosphorylated SLP-76 and PLC-γ1 with similar kinetics and intensity as the wild-type CD28/CD3ζ CAR after STII microbead stimulation (**Figure 3.8E**). Immunoprecipitation of each CAR indicated that Lck association was not abrogated by the Y1 and Y3 mutations, although endogenous CD28 did not associate with the Y3 CAR (**Figure 3.8F**). Taken together, these results suggested that neither basal CAR CD3ζ phosphorylation nor endogenous CD28 association were responsible for the increased signal kinetics and strength of CD28/CD3ζ CARs.

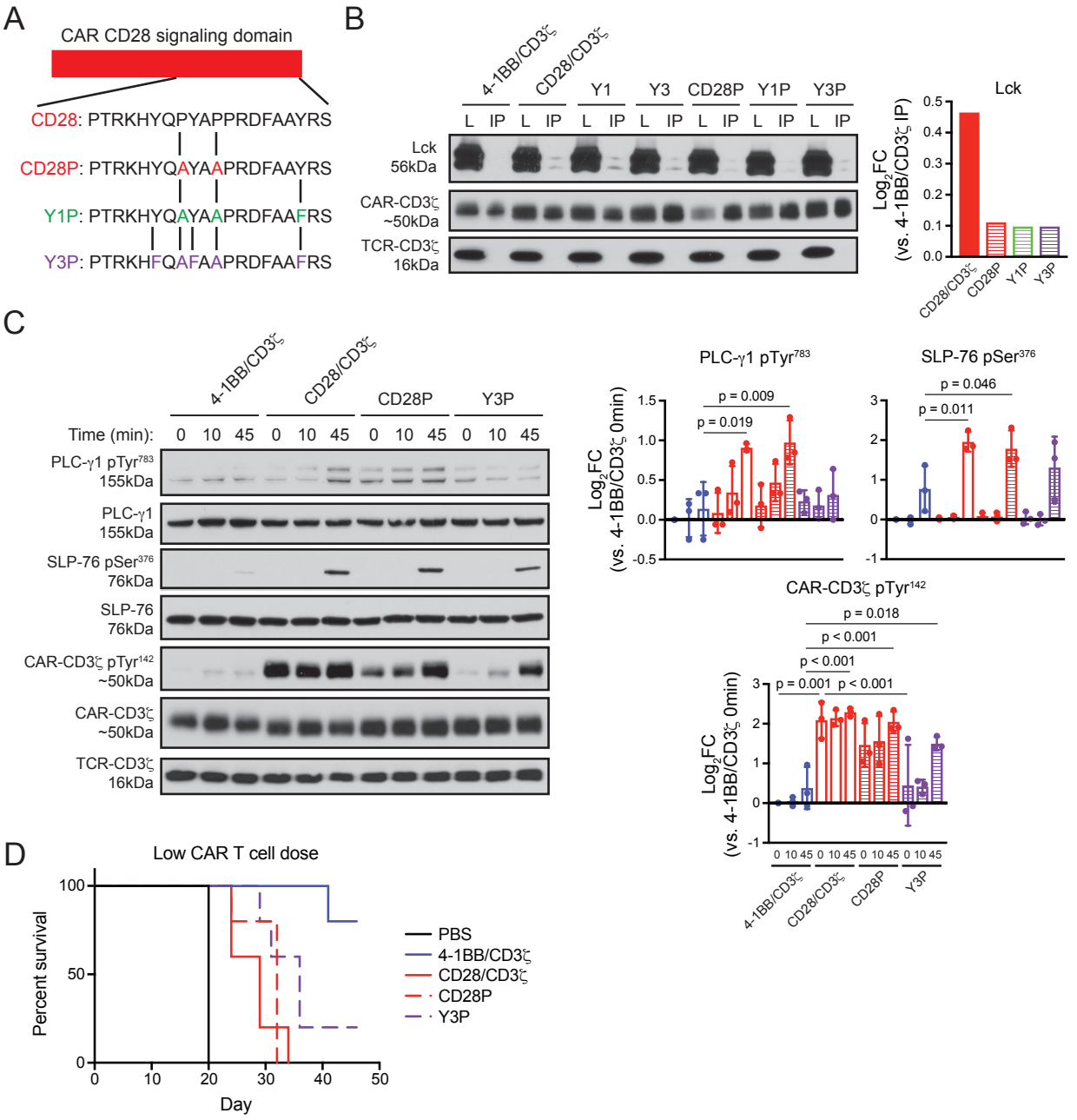

Figure 3.9. Mutations that reduce Lck binding diminish CD28/CD3ζ CAR signal intensity. (**A**) Schematic of mutations made to the CAR CD28 signaling domain. (**B**) Western blot analysis for Lck and CD3ζ within whole cell lysates (L) and STII immunoprecipitated fractions (IP) from resting CAR T cells. Fold change of normalized band intensity data is shown. Blots are representative of 2 independent experiments. (**C**) Western blot analysis for CD3ζ, CD3ζ pTyr^{142}, SLP-76, SLP-76 pSer^{376}, PLC-γ1, and PLC-γ1 pTyr^{783} within lysates from CAR T cells stimulated for the indicated times with STII microbeads. Fold change of normalized band intensity are means ± SD from 3 independent experiments. (**D**) At 7 days after Raji/ffluc engraftment, NSG mice were treated with a single infusion of CAR T cells. Survival analyses are from 1 experiment with 3 or 5 mice per group. The indicated P values were calculated by repeated-measures one-way ANOVA with Tukey's multiple comparisons test comparing samples at equivalent time points (C).

Constitutive Lck activation promotes T cell effector functions (*391*, *392*). Therefore, we tested whether association of Lck with CD28/CD3ζ CARs mediated rapid and robust phosphorylation of signaling intermediates after CAR activation. We generated proline to alanine mutations at the Lck binding site of CD28 (**Figure 3.9A**) (*393*, *394*). Immunoprecipitation of the wild-type and mutant CD28/CD3ζ CARs showed that Lck association was absent in CARs with proline to alanine mutations (**Figures 3.9B and 3.S5**). Signaling analyses of these constructs demonstrated mutation of proline residues alone in CD28P CARs partially abrogated basal CAR CD3ζ phosphorylation but did not reduce signal intensity (**Figure 3.9C**). However, simultaneous mutation of proline and tyrosine residues in Y3P CARs fully abrogated basal CAR phosphorylation and reduced the magnitude of SLP-76 and PLC-γ1 phosphorylation after stimulation (**Figure 3.9C**). In a preliminary experiment, adoptive transfer of 8×10^5 Y3P CAR T cells into Raji tumor bearing mice also prolonged median survival compared to CD28/CD3ζ CAR T cells (**Figure 3.9D**). Thus, differences in CAR signal intensity between CD28/CD3ζ CARs and 4-1BB/CD3ζ CARs were in part related to greater Lck association with CD28/CD3ζ CARs. These data suggest that CAR signal intensity can be altered by mutating tyrosine and proline residues in the CD28 signaling domain and that altering signal strength may lead to more effective therapeutic receptors.

Discussion

The adoptive transfer of CD28/CD3ζ or 4-1BB/CD3ζ CD19 CAR T cells is an effective therapy for patients with certain B cell malignancies, but can cause serious toxicities that originate from CAR signaling after ligand binding (*230*). However, CD28/CD3ζ or 4-1BB/CD3ζ CAR signaling modules confer differences in effector functions and metabolic profiles, and both types of CAR T cells can cause serious toxicities that originate from CAR signaling after ligand binding (*269*, *346*). Crafting safer and more effective CAR T cells might be accomplished by modifying CAR design, but optimization is hindered by the rudimentary understanding of how signaling by synthetic CARs directs T cell functional outputs and cell fate decisions.

We used mass spectrometry to study changes in the phosphoproteome of T cells after CAR ligation and captured 26,804 unique PO_4 sites that describe changes induced by CD28/CD3ζ and 4-1BB/CD3ζ CARs in detail. Our experiments utilized structurally-identical CARs specific for two target antigens being pursued in clinical trials. In contrast to the current perception of how costimulatory domains function in CARs, our data show that, in the space of this dataset, CD28/CD3ζ and 4-1BB/CD3ζ CAR activation initiated nearly identical directional

changes in protein PO_4. Notably, both CARs altered PO_4 of proteins involved in canonical TCR, CD28, and 4-1BB signaling pathways. Only 12 of 1,289 (0.93%) CAR stimulation-responsive PO_4 sites at the 45 minute time point exhibited opposite responses to stimulation when comparing CAR constructs at 45 minutes after activation, and these few sites are not known to be directly linked to either CD28 or 4-1BB signaling pathways. Therefore, our data refute the notion that CD28/CD3ζ and 4-1BB/CD3ζ CARs activate divergent signaling cascades and indicate that one cannot predict the signaling cascades initiated synthetic CARs by focusing solely on the domains encoded by the receptor polypeptide. Rather, synthetic CARs initiate a plethora of signals that both encompass and surpass those of the natural molecules on which the synthetic receptors are based.

Instead, our data demonstrate that a major difference between CD28/CD3ζ and 4-1BB/CD3ζ CARs is that CD28/CD3ζ receptors signal with markedly increased kinetics and intensity. Within 45 minutes, CD28/CD3ζ CAR stimulation altered the PO_4 state of hundreds of proteins involved in TCR signaling, MAP kinase signaling, actin-cytoskeleton rearrangement, and RNA processing pathways. Alterations in protein PO_4 after 4-1BB/CD3ζ CAR stimulation affected identical proteins as CD28/CD3ζ CAR stimulation but proceeded more slowly and with reduced intensity. Subsequent analysis of CAR binding partners demonstrated more Lck in immunoprecipitates from unstimulated CD28/CD3ζ CAR T cells than 4-1BB/CD3ζ CAR T cells. Mutational analysis of the CAR CD28 signaling domain identified residues responsible for basal CAR CD3ζ PO_4 as well as Lck association, and showed that abrogation of these features reduced CAR signal intensity. Thus, future analyses of novel CAR designs should consider how interactions with potential binding partners might affect signaling.

Our data also show that the more rapid and intense phosphoprotein signaling in CD28/CD3ζ CAR T cells induced an effector-cell like transcriptional profile and more robust T cell cytokine production and proliferation early after CAR ligation, but less potent anti-tumor function in an *in vivo* tumor model of disseminated lymphoma. These data are consistent with prior findings that intense TCR signaling and IL-2 production promote differentiation of short-lived effector $CD8^+$ T cells (*395*, *396*), and also support a model by which TCR and costimulatory signals sum linearly to impact cell fate (*387*). Some amount of CD28 signaling is beneficial for T cell memory formation (*397*), and we found the 4-1BB/CD3ζ CARs used in this study phosphorylated endogenous CD28 and activated the CD28 signaling pathway. However, encoding a fully-functional CD28 signaling domain on a CAR polypeptide chain may yield excessive stimulation that increases the incidence of cytokine release syndrome, promotes T

cell exhaustion and reduces persistence. Indeed, analyses of acute lymphoblastic leukemia patients who were in morphologic relapse at the time of treatment with CD28/CD3ζ CAR T cells showed poor long-term CAR T cell persistence and low overall survival due to frequent relapse with $CD19^+$ disease (*398*).

CARs are often currently selected to maximize measures *in vitro* T cell effector functions and proliferation, and our findings indicate that these selection criteria may not be optimal for predicting *in vivo* efficacy. Future optimizations to CAR design should consider both the signaling domains contained within the receptor, interactions with potential binding partners, and how modifications of costimulatory domains might tailor overall signal strength for downstream T cell functional outputs. Mutating the CAR CD28 signaling domain is a logical approach for reducing excessive signal strength and further studies of mutated CAR signaling domains are warranted. However, variability in CAR structural features outside of the costimulatory CD28 or 4-1BB and CD3ζ signaling domains may limit the universality of this approach. Most CARs possess a unique combination of scFv, hinge, and transmembrane domain and this structural variation can affect CAR signaling and may alter association with endogenous T cell signaling molecules. For instance, the CAR CD28 transmembrane domain utilized in this study may have influenced association with endogenous CD28 and Lck. Further immunoprecipitation analysis of CARs with CD8α transmembrane domains and other structural features could answer this question (*302*).

Our approach evaluating CD28/CD3ζ and 4-1BB/CD3ζ CAR signaling using a cell free stimulation method has the advantage of identifying PO_4 events induced by the synthetic receptors in isolation. While this approach did not integrate the multitude of other events that may occur when CAR T cells encounter tumor cells *in vivo* (*340*), it could be extended to interrogate cross-talk between CAR signaling and costimulatory or inhibitory pathways by immobilizing various ligands onto the magnetic beads. Our approach was also not designed to compare TCR and CAR signaling. A direct comparison of TCR and CAR ligation-induced phosphoprotein signaling is likely to be valuable and is described in Chapter 4. Thus, MS analysis can provide important insights into CAR signaling that will impact next-generation CAR designs.

Materials and Methods

Acquisition of peripheral blood T cells from healthy donors
Healthy adults (>18 years-old) were enrolled in an Institutional Review Board-approved study for peripheral blood collection. Informed consent was obtained from all enrollees. Researchers were blinded to all personally-identifiable information about study participants, and were provided only donor age and a nondescript donor ID number. 400cc of peripheral blood was collected by venipuncture and mononuclear cells (PBMC) were isolated by density gradient using Lymphocyte Separation Media (Corning). $CD4^+$ and $CD8^+$ T cells were isolated using the EasySep Human $CD4^+$ and $CD8^+$ T Cell Isolation Kits (StemCell Technologies); For the three shotgun mass spectrometry experiments, $CD8^+CD62L^+$ T cells were further enriched by staining with CD62L-PE (DREG56, ThermoFisher) followed by the EasySep Human PE Selection Kit (StemCell Technologies). Isolations were performed in accordance with manufacturer's instructions.

Cell Culture
LentiX cells (Clontech) were cultured in DMEM (Gibco) supplemented with 10% fetal bovine serum, 1mM L-glutamine (Gibco), 25mM HEPES (Gibco), and 100U/mL penicillin/streptomycin (Gibco). K562 (CCL-243), Jurkat (TIB-152), and Raji (CCL-86) cells were obtained from American Type Culture Collection and cultured in RPMI-1640 (Gibco) supplemented with 5% fetal bovine serum, 1mM L-glutamine, 25mM HEPES, and 100U/mL penicillin/streptomycin. Primary human T cells were cultured in CTL medium consisting of RPMI-1640 supplemented with 10% human serum, 2mM L-glutamine, 25mM HEPES, 100U/mL penicillin/streptomycin, 50μM β-Mercaptoethanol (Sigma), and 50 U/mL IL-2 (Prometheus). All cells were cultured at 37°C and 5% CO_2, and tested bi-monthly for the absence of mycoplasma using MycoAlert Mycoplasma Detection Kit (Lonza).

Generation of chimeric antigen receptors (CARs) and recombinant lentiviral vectors
CD19-specific and ROR1-specific CAR constructs have been previously described (*198*, *253*). For work in this manuscript, a single Strep-tag II sequence and two G_4S linkers were inserted between the FMC63 or R12 single chain variable fragment and IgG4 hinge (*370*). These were linked to the 27 amino acid transmembrane domain of human CD28 (UniProt: P10747) and to a signaling module comprising either (i) the 41 amino acid cytoplasmic domain of human CD28 with an LL→GG substitution located at positions 186-187 of the native CD28 protein (*399*), or (ii) the 42 amino acid cytoplasmic domain of human 4-1BB (UniProt: Q07011), each of which was linked to the 112 amino acid cytoplasmic domain of isoform 3 of human CD3ζ (UniProt: P20963-3). Mutant CD28/CD3ζ CARs with tyrosine to phenylalanine substitutions at CD28 UniProt positions 206, 209, and 218 and/or proline to alanine substitutions at CD28 UniProt positions 208 and 211 were generated by site-direct mutagenesis. All CAR constructs were linked by T2A sequence to a truncated epidermal growth factor receptor (EGFRt), codon-optimized, and cloned into a HIV7 lentiviral vector. For fluorescence microscopy, the CD3ζ endodomain was directly fused to eGFP. To make CAR antigen-expressing K562 cells, amino acids 1-325 of human CD19 (UniProt: P15391) were cloned into a HIV7 lentiviral vector and amino acids 1-937 of human ROR1 (UniProt: Q01973) were cloned into a mp71 retroviral vector which was a gift of Dr. Wolfgang Uckert, Max Delbruck Center for Molecular Medicine. All cloning was performed by PCR, enzyme digest, and/or Gibson assembly. Plasmids were verified by capillary sequencing and restriction digest.

Lentivirus preparation and transduction

To prepare CAR T cells, LentiX cells were transiently transfected with the HIV7 CAR vector, as well as psPAX2 (Addgene Cat # 12260) and pMD2.G (Addgene Cat # 12259) packaging plasmids. One day later (day 1), primary T cells were activated using Dynabeads Human T-Activator CD3/CD28 (ThermoFisher) and cultured in CTL supplemented with 50 U/mL IL-2. The next day (day 2), lentiviral supernatant was harvested from LentiX cells, filtered using 0.45μm PES syringe filters (Millipore), and added to activated T cells. Polybrene (Millipore) was added to reach a final concentration of 4.4μg/mL and cells were spinoculated at 800×g and 32°C for 90 minutes. Viral supernatant was replaced 8 hours later with fresh CTL supplemented with 50 IU/mL IL-2. Half-media changes were then performed every 48 hours using CTL supplemented with 50 U/mL IL-2. Dynabeads were removed on day 6; $CD8^+EGFRt^+$ transduced T cells were FACS-sorted on a FACSAria II (BD Biosciences) on day 9.

To prepare K562/CD19 cells, LentiX cells were transiently transfected with psPAX2, pMD2.G, and an HIV7 lentiviral vector encoding CD19. To prepare K562/ROR1 cells, LentiX cells were transiently transfected with MLV g/p, 10A1, and a mp71 retroviral vector encoding ROR1. To prepare Raji/ffluc cells, LentiX cells were transiently transfected with psPAX2, pMD2.G, and an HIV7 lentiviral vector encoding GFP and firefly luciferase. Two days later, viral supernatant was filtered using a 0.45μm PES syringe filter and added to K562 or Raji cells. Five days later, transduced cells were stained monoclonal antibodies specific for CD19 (HIB19, Biolegend) or ROR1 (2A2, Miltenyi Biotec) and FACS-sorted on a FACSAria II to greater than 97% purity.

T cell expansion for mass spectrometric and functional analyses
FACS-sorted $CD8^+EGFRt^+$ cells were expanded over a single stimulation cycle prior to MS and/or functional analyses. CD19-specific CAR T cells were expanded by co-culture with irradiated $CD19^+$ lymphoblastoid cell lines (LCL) in a 1:7 (T cell:LCL) ratio and assayed 8 days after stimulation. ROR1-specific CAR T cells were expanded using a rapid expansion protocol containing purified OKT3, irradiated LCL, and irradiated PBMC, and assayed 11 days after stimulation. During expansion, cultures were fed with fresh CTL media containing 50 IU/mL IL-2 every 2-3 days.

Flow cytometry and cell phenotyping
T cells were stained with a 1:100 dilution of fluorophore-conjugated monoclonal antibodies specific for human CD4 (RPA-T4), CD8 (SK1), CD27 (M-T271), CD28 (CD28.2), CD45 (HI30), CD45RO (UCHL1), CD62L (DREG56), CD223 (3DS223H), CD279 (eBioJ105), or CD366 (F38-2E2) purchased from BD Biosciences, ThermoFisher, or Biolegend. T cells were also stained with isotype control fluorophore-conjugated antibodies when appropriate. Cetuximab (anti-EGFR, Bristol Myers Squibb) and 3E8 (anti-STII, FHCRC) mAb were biotinylated using the EZ-Link Sulfo-NHS-Biotin kit (ThermoFisher) followed by cleanup with a Zeba Spin Desalting Column (ThermoFisher) and used to stain T cells in conjunction with Streptavidin-APC (ThermoFisher). DNA content staining was performed by fixing T cells with 70% ice-cold ethanol, permeabilizing cells with 1% Triton-X (Sigma), degrading RNA with 100μg/mL RNAse A (ThermoFisher), and staining DNA with 20μg/mL Propidium Iodide (ThermoFisher). All data was collected on a FACSCanto II or FACSAria II (BD Biosciences).

Anti-STII and control bead preparation
1mL Streptavidin Coated Magnetic Particles (Spherotech) was washed once in excess 1× PBS supplemented with 100 U/mL penicillin/streptomycin (PBS+P/S) using a benchtop magnet. Anti-STII beads were prepared by resuspending beads in 1mL PBS+P/S and then slowly adding 16.67μg anti-STII biotin mAb (GenScript) while vortexing the bead solution. Beads and anti-STII antibody were incubated overnight at 4°C on a 3D orbital shaker, washed three times with

excess PBS+P/S using a benchtop magnet, and resuspended in 4mL PBS+P/S. To make control beads, 1mL Streptavidin Coated Magnetic Particles were washed once using a benchtop magnet and the bead pellet was resuspended in 4mL PBS+P/S. Beads were stored at 4°C.

Cell stimulations, protein lysates, RNA isolation
CAR T or Jurkat cells were washed and resuspended in warm CTL medium. For OKT3 stimulations, cells were incubated for 5 minutes on ice with 1.25μg/mL OKT3 (Biolegend) and then with 5μg/mL anti-mouse IgG (ThermoFisher) for 10 minutes on ice. Cells were transferred to a 37°C water bath to initiate signaling. For K562 cell-based stimulations, CAR T cells were co-cultured with K562 or K562/ROR1 cells at a 4:1 effector to target ratio in a 37°C water bath. For bead-based stimulations, T cells were brought to a concentration of 2×10^7 cells per mL and incubated with STII or control microbeads at a ratio of 30μL beads per 1×10^6 cells in a 37°C water bath. After the allotted time, cells were quickly washed twice using ice-cold PBS, then lysed in a 6M Urea, 25mM Tris (pH 8.0), 1mM EDTA, 1mM EGTA solution supplemented with protease (Sigma) and phosphatase inhibitors (Sigma) at a 1:100 dilution, hereon referred to as lysis buffer. Lysates were sonicated for 15 seconds prior to centrifuging at 10,000×g and 4°C for 10 minutes. Beads were removed during lysate clearing. After 6 hours of stimulation, RNA isolations were performed using a NucleoSpin RNA kit (Macherey-Nagel) according to manufacturer's instructions. Beads were removed using a benchtop magnet prior to cell lysis and RNA extraction.

Protein digestion, TMT labeling, and phosphotyrosine (pTyr) peptide immunoprecipitation
Protein was quantified in lysates by Micro BCA Assay (ThermoFisher), and lysates were diluted to 2mg/mL using lysis buffer. Lysates were reduced in 24mM TCEP (ThermoFisher) for 30 minutes at 37°C with shaking, followed by alkylation with 48mM iodoacetamide (Sigma) in the dark at room temperature for 30 minutes. Lysates were then diluted with 200mM Tris (pH 8.0), to a urea concentration of 2M. Lys-C (Wako) was dissolved in 25mM Tris (pH 8.0) at 200ug/mL and added to lysates at 1:100 (enzyme:protein) ratio by mass and incubated for 2 hours at 37°C with shaking. Samples were further diluted with 200mM Tris (pH 8.0) to a urea concentration of 1M before adding trypsin at a 1:50 trypsin:protein ratio. After 2 hours, a second trypsin aliquot was added at a 1:100 trypsin:protein ratio. Digestion was carried out overnight at 37°C with shaking. After 16 hours, the reaction was quenched with formic acid to a final concentration 1% by volume. Samples were desalted using Oasis HLB 96-well plates (Waters) and a positive pressure manifold (Waters). The plate wells were washed with 3 x 400μL of 50% MeCN/0.1% FA, and then equilibrated with 4 x 400μL of 0.1% FA. The digests were applied to the wells, then washed with 4 x 400μL 0.1% FA before being eluted drop by drop with 3 x 400μL of 50% MeCN/0.1% FA. The eluates were lyophilized, followed by storage at -80°C until use. For TMT labeling (ThermoFisher), desalted peptides were resuspended in 50 mM HEPES at 1mg/mL based on starting protein mass. TMT reagents were resuspended in 257μL MeCN and transferred to the peptide sample. Samples were incubated at room temperature for 1 hour with mixing. Labeling reactions were quenched by the addition of 50μL of 5% hydroxyl Amine (Sigma) and incubated for 15 minutes at room temperature with mixing. The independent labeling reactions were then pooled together and lyophilized. The labeled peptides were desalted as above and then lyophilized and stored at -80°C. Immunoprecipitation of pTyr peptides was performed using the PTMScan P-Tyr-1000 Kit (Cell Signaling). The enriched pTyr peptide fraction was purified using a C18 Spin Tip (ThermoFisher), lyophilized, and stored at -80°C until analysis. The flow-through fraction was desalted, lyophilized, and stored at -80°C.

Basic (high pH) reverse phase liquid chromatography

The desalted and pTyr peptide-depleted flow-through was fractionated by high-pH reverse phase (RP) liquid chromatography. 4mg of the protein digest was loaded onto a LC system consisting of an Agilent 1200 HPLC with mobile phases of 5mM NH_4HCO_3 (pH 10) (A) and 5mM NH_4HCO_3 in 90% MeCN (pH 10) (B). The peptides were separated by a 4.6mm x 250mm Zorbax Extend-C18, 3.5µm, column (Agilent) over 96 minutes at a flow rate of 1.0mL/min by the following timetable: hold 0% B for 9 minutes, gradient from 0 to 10% B for 4 minutes, 10 to 28.5% B for 50 minutes, 28.5 to 34% B for 5.5 minutes, 34 to 60% B for 13 minutes, hold at 60% B for 8.5 minutes, 60 to 0% B for 1 minute, re-equilibrate at 0% B for 5 minutes. 1 minute fractions were collected from 0-96 minutes by the shortest path by row in a 1 mL deep well plate (ThermoFisher). The high pH RP fractions were concatenated into 24 samples by every other plate column starting at minute 15 (e.g.: sample 1 contained fractions from wells B10, D10, F10, etc.). The remaining fractions were combined such that fractions from 12 to 14 minutes were added to sample 1, all fractions after 86 minutes were added to sample 24, and all fractions from 0 to 11 minutes were combined into sample 'A'. 95% of every 12th fraction of the 24 samples was combined (1,13; 2,14; ...) to generate 12 more samples, which were dried down and stored at -80°C prior to phosphopeptide enrichment by immobilized metal affinity chromatography.

Immobilized metal affinity chromatography (IMAC)
IMAC enrichment was performed using Ni-NTA-agarose beads (Qiagen) stripped with EDTA and incubated in a 10mM $FeCl_3$ solution to prepare Fe^{3+}-NTA-agarose beads. Fractionated lysate was reconstituted in 200µL of 0.1% TFA in 80% MeCN and incubated for 30 minutes with 100µL of the 5% bead suspension while mixing at room temperature. After incubation, beads were washed 3 times with 300µL of 0.1% TFA in 80% MeCN. Phosphorylated peptides were eluted from the beads using 200µL of 70% ACN, 1% Ammonium Hydroxide for 1 minute with agitation at room temperature. Samples were transferred into a fresh tube containing 60µL of 10% FA, dried down and re-suspended in 0.1% FA, 3% MeCN. Samples were frozen at -80°C until analysis.

Nano-liquid chromatography-tandem mass spectrometry
Phosphopeptide-enriched samples were analyzed by LC-MS/MS on an Easy-nLC 1000 (ThermoFisher) coupled to an LTQ-Orbitrap Fusion mass spectrometer (ThermoFisher) operated in positive ion mode. The LC system, configured in a vented format consisted of a fused-silica nanospray needle (PicoTip emitter, 50µm ID x 20cm, New Objective) packed in-house with ReproSil-Pur C18-AQ, 3µm and a trap (IntegraFrit Capillary, 100µm ID x 2 cm, New Objective) containing the same resin as in the analytical column with mobile phases of 0.1% FA in water (A) and 0.1% FA in MeCN (B). The peptide sample was diluted in 20 µL of 0.1% FA, 3% MeCN, and 8.5µL was loaded onto the column and separated over 210 minutes at a flow rate of 300 nL/min with a gradient from 5 to 7% B for 2 minutes, 7 to 35% B for 150 minutes, 35 to 50% B for 1 minute, hold 50% B for 9 minutes, 50 to 95% B for 2 minutes, hold 95% B for 7 minutes, 95 to 5% B for 1 minute, re-equilibrate at 5% B for 38 minutes. A spray voltage of 2000 V was applied to the nanospray tip. MS/MS analysis occurred over a 3 second cycle time consisting of 1 full scan MS from 350-1500 m/z at resolution 120,000 followed by data dependent MS/MS scans using HCD activation with 27% normalized collision energy of the most abundant ions. Selected ions were dynamically excluded for 45 seconds after a repeat count of 1.

Immunoprecipitation
Protein G Dynabeads (ThermoFisher) were incubated with purified anti-STII antibody (GenScript) for 60 minutes, cross-linked for 30 minutes using 20mM dimethyl pimelimidate

(ThermoFisher) diluted in 200 mM triethanolamine (ThermoFisher), quenched with 150mM monoethanolamine (Fisher Scientific), and washed three times with 1× PBS. T cells were lysed in NP40 Cell Lysis Buffer (ThermoFisher) supplemented with protease and phosphatase inhibitors. Lysates were incubated on ice for 15 minutes and then centrifuged at 10,000×g and 4°C for 10 minutes. Equal masses of cleared lysates were incubated with Dynabeads for 90 minutes at room temperature. Immunoprecipitations were then performed according to manufacturer's instructions.

Western blotting
Equal masses of protein lysate or equal volumes of immunoprecipitation eluents were loaded into 4-12% Bis-Tris NuPAGE Gels (ThermoFisher) or 3-8% Tris-Acetate NuPAGE Gels (ThermoFisher). After protein transfer onto nitrocellulose membranes (ThermoFisher), membranes were blocked with Western Blocking Reagent (Sigma). Membranes were stained with primary and secondary antibodies diluted in SuperBlock (ThermoFisher) supplemented with 0.1% Tween. The following antibodies were used: anti-human CD247 (8D3, BD Biosciences), anti-human CD247 $pTyr^{142}$ (K25-407.69, BD Biosciences), anti-ZAP-70 $pTyr^{319}$ (65E4, Cell Signaling), anti-SLP-76 (polyclonal, Cell Signaling), anti-SLP-76 $pSer^{376}$ (D9D6E, Cell Signaling), anti-PLC-γ1 (D9H10, Cell Signaling), anti-PLC-γ1 $pTyr^{783}$ (D6M9S, Cell Signaling), anti-DAPP1 (D9K4O, Cell Signaling), anti-DAPP1 $pTyr^{139}$ (D7G4G, Cell Signaling), anti-Lck (D88, Cell Signaling), anti-CD28 (D2Z4E, Cell Signaling), anti-mouse horseradish peroxidase (HRP) (polyclonal, Cell Signaling), and anti-rabbit HRP (polyclonal, Cell Signaling). Typical antibody dilutions ranged from 1:10,000 to 1:2500. Band intensities were quantified using ImageJ (NIH); normalized to total protein, loading control, or immunoprecipitation input; and then renormalized to a control sample.

RNA sequencing (RNA-seq)
RNA was extracted from 24 samples from three donors. Total RNA integrity was checked using an Agilent 4200 TapeStation (Agilent) and quantified using a Trinean DropSense96 spectrophotometer (Caliper Life Sciences). RNA-seq libraries were prepared from total RNA using the TruSeq RNA Sample Prep Kit v2 (Illumina) and a Sciclone NGSx Workstation (PerkinElmer). Library size distributions were validated using an Agilent 4200 TapeStation. Additional library quality control, blending of pooled indexed libraries, and cluster optimization were performed using a Qubit 2.0 Fluorometer (ThermoFisher). RNA-seq libraries were pooled (6-8-plex) and clustered onto a flow cell lane. Sequencing was performed using an Illumina HiSeq 2500 in rapid mode employing a paired-end, 50 base read length (PE50) sequencing strategy.

Quantitative PCR
RNA was extracted and total RNA integrity was verified using an Agilent 4200 TapeStation (Agilent Technologies). 500ng RNA was used to prepare cDNA with SuperScript III (ThermoFisher). 15ng cDNA was added to a reaction with TaqMan Universal Master Mix II with UNG (ThermoFisher) and one of the following ThermoFisher TaqMan assay probes: Hs00172973_m1 (*FOXO4*), Hs00902234_m1 (*IL7R*), Hs00360439_g1 (*KLF2*), or Hs99999907_m1 (*B2M*). Reactions were run in duplicate or triplicate on one 384-well plate. ΔCt values were calculated by dividing mean Ct of technical replicates from *FOXO4*, *IL7R*, and *KLF2* probes by the mean Ct of the housekeeping gene β2 microglobulin (*B2M*). CD28/CD3ζ versus 4-1BB/CD3ζ ratios for each donor were calculated and subjected to a $\log_2$ transformation.

In vitro functional assays

CAR T cells were co-cultured with K562, K562/CD19, or K562/ROR1 cells at a T cell to tumor cell ratio of 2:1. In some experiments, CAR T cells were also incubated with control or anti-STII beads at a ratio of 30μL beads per million cells. Cytokine concentrations in cellular supernatant were quantified by ELISA (ThermoFisher) 24 hours after stimulation. T cell proliferation was quantified by staining CAR T cells with a 0.2μM solution of carboxyfluorescein succinimidyl ester (CFSE) dye (ThermoFisher) and incubating CAR T cells with K562/CD19, K562/ROR1 cells, control beads, or anti-STII beads for 72 hours.

Transfer of T cells in NOD/SCID/γc$^{-/-}$ (NSG) mice
Six- to eight-week-old male or female NSG mice were obtained from the Jackson Laboratory or bred in-house. Mice were engrafted via tail vein with 5×10^5 CD19$^+$ Raji/ffluc cells, and 7 days later, injected intravenously with PBS or a defined product of purified CD8$^+$ and CD4$^+$ CD19-specific CAR T cells mixed together in a 1:1 ratio. Bioluminescence imaging was performed as described (*198*). Mice were either followed for survival or sacrificed on day 20 for analysis of T cell frequencies and phenotypes by flow cytometry. Peripheral blood was extracted, red blood cells were lysed using ACK Lysing Buffer (ThermoFisher), and remaining cells were stained with fluorochrome-labeled mAbs. Bone marrow was isolated from hind-limbs by mechanical disruption followed by red blood cell lysis, and staining with fluorochrome-labeled mAbs. Mice handlers were blinded to group allocation. The Fred Hutchinson Cancer Research Center Institutional Animal Care and Use Committee approved all experimental procedures.

Fluorescence microscopy
CD8$^+$ T cells from healthy donors were transduced as previously described. Instead of FACS-purification on day 9, cells were imaged on a Deltavision Elite microscope (GE Healthcare). At least 8 cells were visualized per condition. Raw images were subjected to a linear adjustment of brightness and contrast using ImageJ (NIH).

Shotgun mass spectrometry data analysis
Raw MS/MS spectra from each replicate experiment were searched together against the reviewed Human Universal Protein Resource (UniProt) sequence database (release 2016_01) with common laboratory contaminants using the MaxQuant/Andromeda search engine version 1.6.0.1 (*400*). The search was performed with a tryptic enzyme constraint for up to two missed cleavages. Variable modifications were oxidized methionine, phosphorylated serine, phosphorylated threonine, and phosphorylated tyrosine. Carbamidomethylated cysteine was set as a static modification. Peptide MH+ mass tolerances were set at 20 ppm. The overall FDR was set at ≤ 1% using a reverse database target decoy approach.

For the three TMT experiments, phosphopeptide site localization was determined by MaxQuant and converted to phosphorylation sites using Perseus version 1.6.0.7 (*401*). At this step, reverse hits and potential contaminants were excluded from further analysis. Data normalization was performed by scaling each TMT channel to the channel median, followed by a $\log_2$transformation. Stimulation vs. control ratios were calculated by subtracting the appropriate control channels from stimulated channels. Due to incomplete MS sampling, some phosphorylation sites (features) were only found in one or two replicate experiments, and a much smaller minority (< 1%) of sites were not found in every TMT channel.

Differential expression analyses over PO_4 sites were performed using the limma statistical framework and associated R package (*377*, *402*). For these analyses, we chose to keep only features that had values in at least two experiments and all TMT channels, leaving us with 14,490 quantified phosphorylation sites. A linear model was fitted to each PO_4 site, and empirical Bayes moderated t-statistics were used to assess differences in

expression/abundance. Contrasts comparing stimulation vs control treatments were tested. Intraclass correlations were estimated using the duplicateCorrelation function of the limma package to account for measures originating from the same patients and the same antigens (*403*). An absolute log_2fold change cutoff (stimulation versus control) of 0.7 and a false discovery rate (FDR) cutoff of 5% were used to determine differentially expressed PO_4 sites. Analyses of signaling networks and KEGG Pathways were performed using StringDB.

RNA sequencing data analysis
Image analysis and base calling were performed using Illumina's Real Time Analysis v1.18 software, followed by 'demultiplexing' of indexed reads and generation of FASTQ files, using Illumina's bcl2fastq Conversion Software v1.8.4. The RNA-seq data were aligned to the human genome (UCSC Human Genome Assembly GRCh38 reference) using STAR, and gene quantification was performed using RSEM (*404*, *405*). Genes with less than 10 non-zero read counts (taking into account technical replicates) were discarded, leaving 18,498 expressed genes. All libraries passed the quality control criteria (libraries with more than 200,000 reads, 12,000 detected genes and an exon range > 60%). Raw count data were imported into R. edgeR was used to calculate the normalization factors to scale the raw library sizes, followed by a voom transformation from the limma Bioconductor package (*406*, *407*). It transforms count data to log_2counts per million and estimates the mean-variance relationship to compute appropriate observation-level weights. Linear models with subject random effects were again used for differential gene expression analysis as described above in *Shotgun mass spectrometry data analysis*. Contrasts comparing treatments (control versus stimulation) or CARs (CD28/CD3ζ versus 4-1BB/CD3ζ) were tested. An absolute log_2fold change cutoff of 1 and a FDR cutoff of 1% were used to determined differentially expressed genes.

Analysis of T cell phenotype, function, and in vivo experiments
FlowJo version 9 (Treestar) was used to analyze flow cytometry files and calculate proliferation indices. Prism version 7 (GraphPad) was used to plot data and calculate statistics. P values meeting an $\alpha = 0.05$ level of significance are indicated in the figures. The precise statistical tests used are indicated in the figure legends.

Supplementary Figures

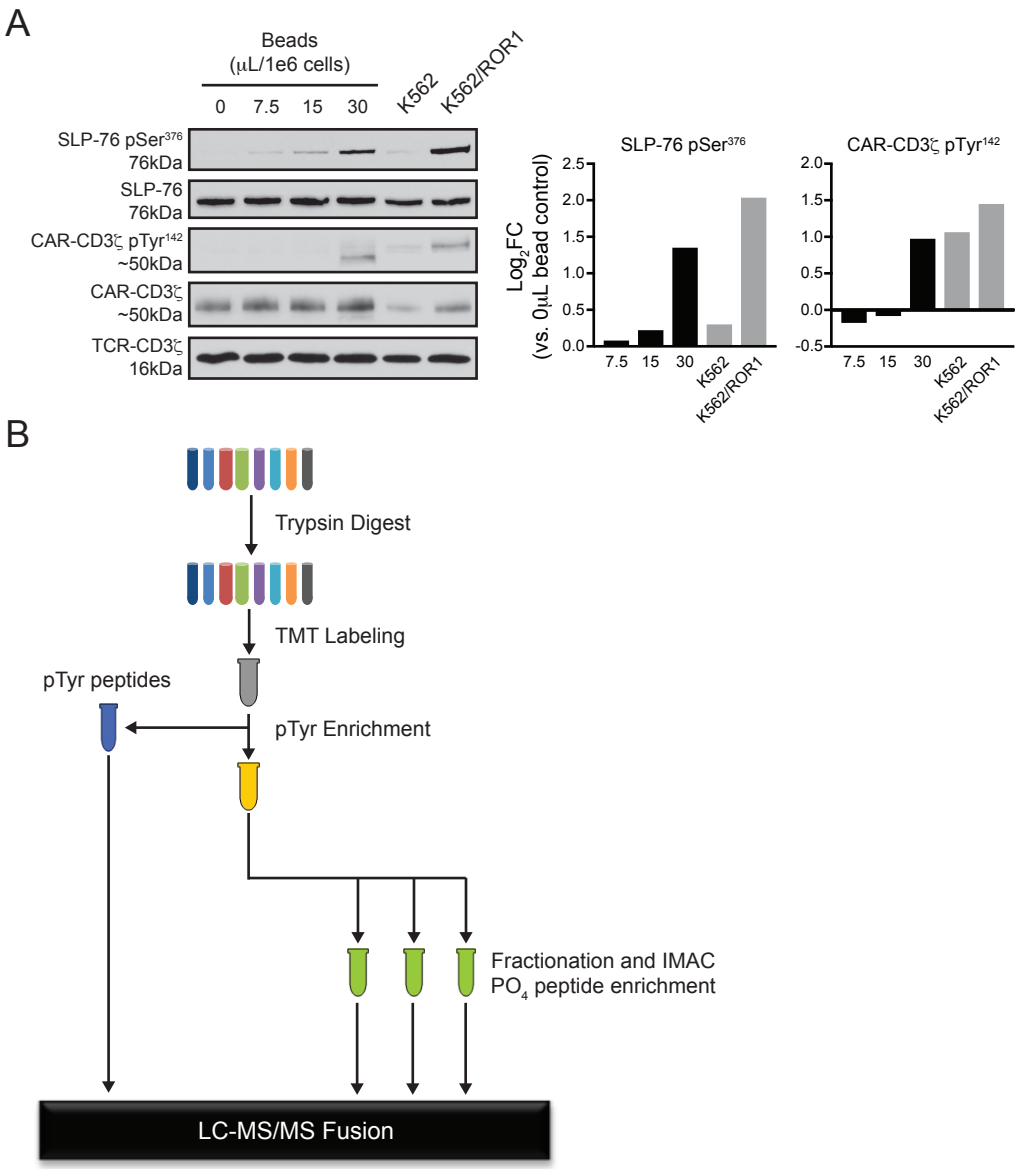

Figure 3.S1. CAR designs containing a STII sequence enable selective activation of CAR signaling in primary T cells. (**A**) Western blot analysis for CD3ζ, CD3ζ pTyr^{142}, SLP-76, and SLP-76 pSer^{376} in lysates of ROR1 4-1BB/CD3ζ CAR T cells after 45 minutes of co-culture with varying quantities of STII microbeads, K562 cells, or K562/ROR1 cells. Fold change of normalized band intensity data is shown. Blots are representative of 2 independent experiments. (**B**) Schematic of phosphopeptide enrichment strategy using tandem mass tag (TMT) reagents and multistep phosphopeptide enrichments.

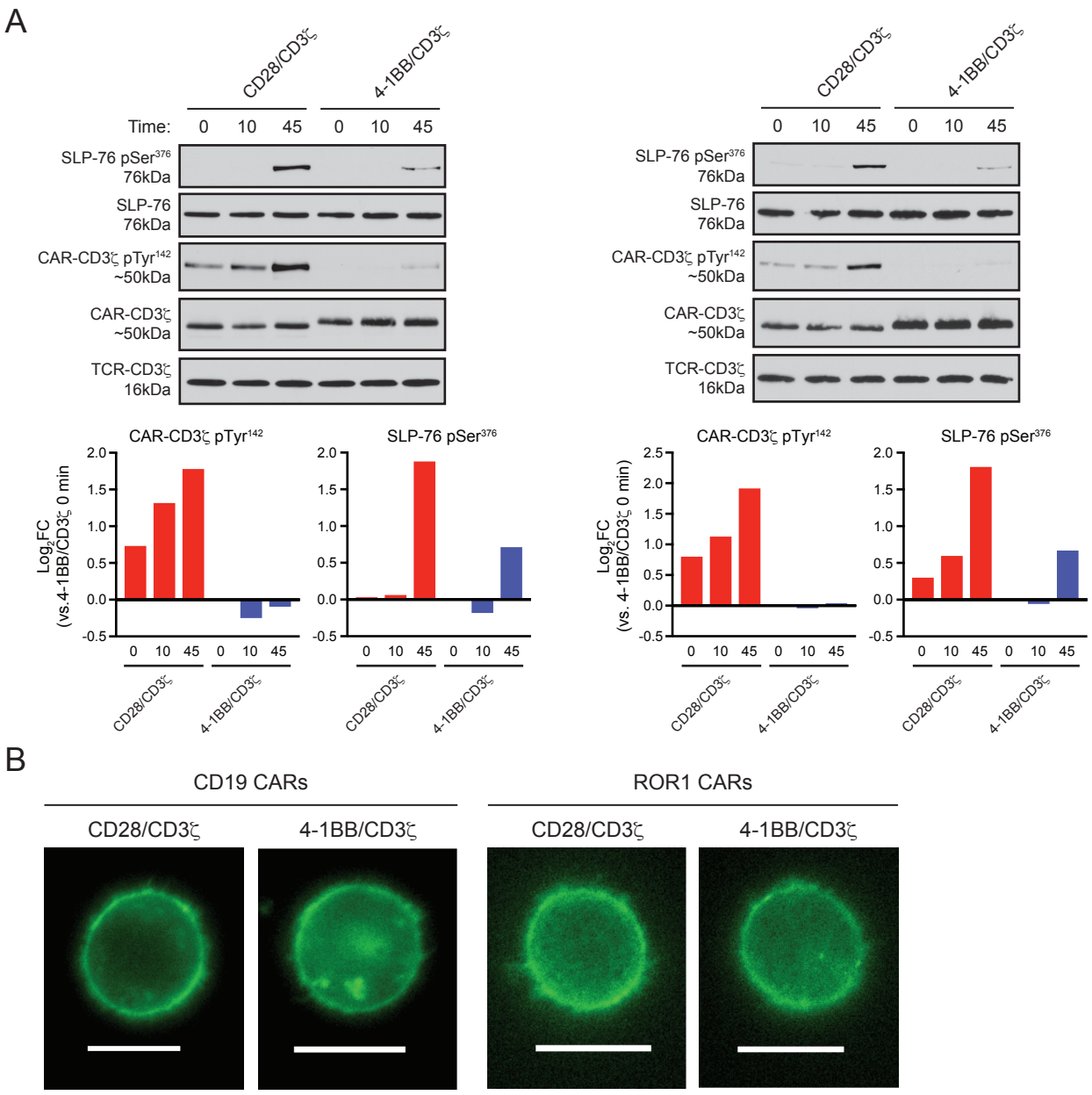

Figure 3.S2. CD19-specific and ROR1-specific CD28/CD3ζ and 4-1BB/CD3ζ CARs signal similarly in CD4⁺ T cells and are uniformly expressed on the cell surface. (**A**) Western blot analysis for CD3ζ, CD3ζ pTyr^{142}, SLP-76, and SLP-76 pSer^{376} in lysates of CD4⁺ CD19 CAR T cells. Blots and normalized band intensity data are shown from 2 independent experiments. (**B**) Fluorescence microscopy analysis of CARs tagged with eGFP on the C-terminus of CAR CD3ζ. Images are representative of 2 independent experiments with at least 8 CAR T cells visualized per experiment. Scale bar = 10 micrometers.

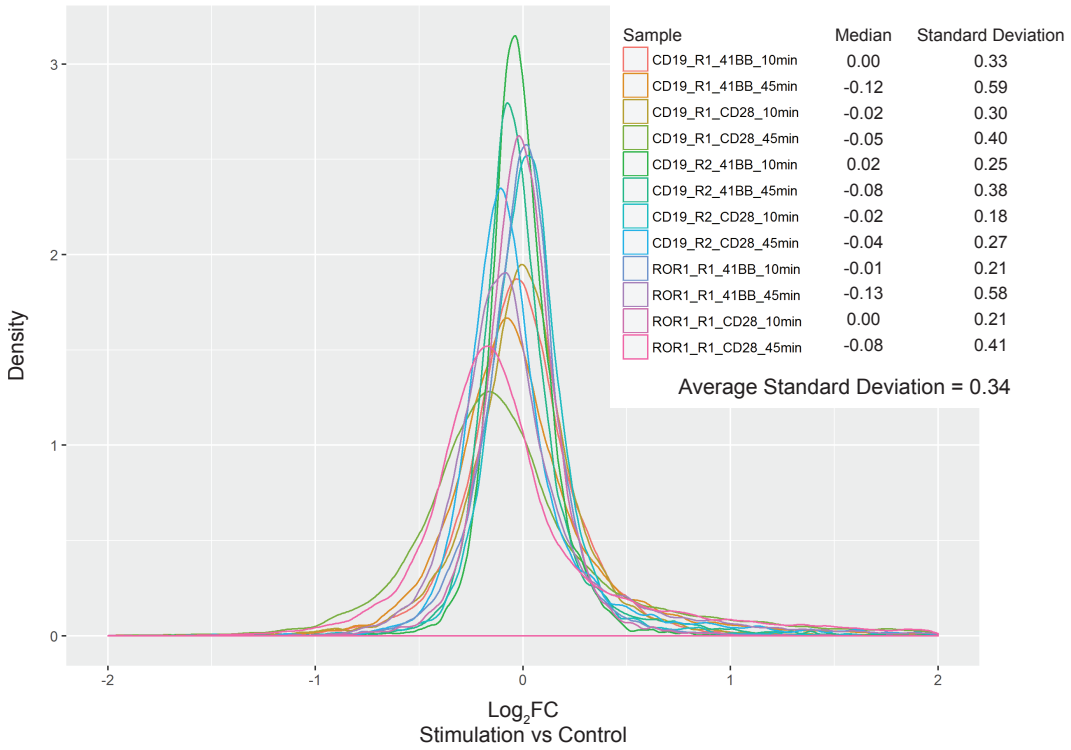

Figure 3.S3. Log$_2$fold change summary statistics. Histogram shows the distribution of log$_2$fold change (Log$_2$FC) values across three LC-MS/MS experiments. Standard deviations are noted in the key.

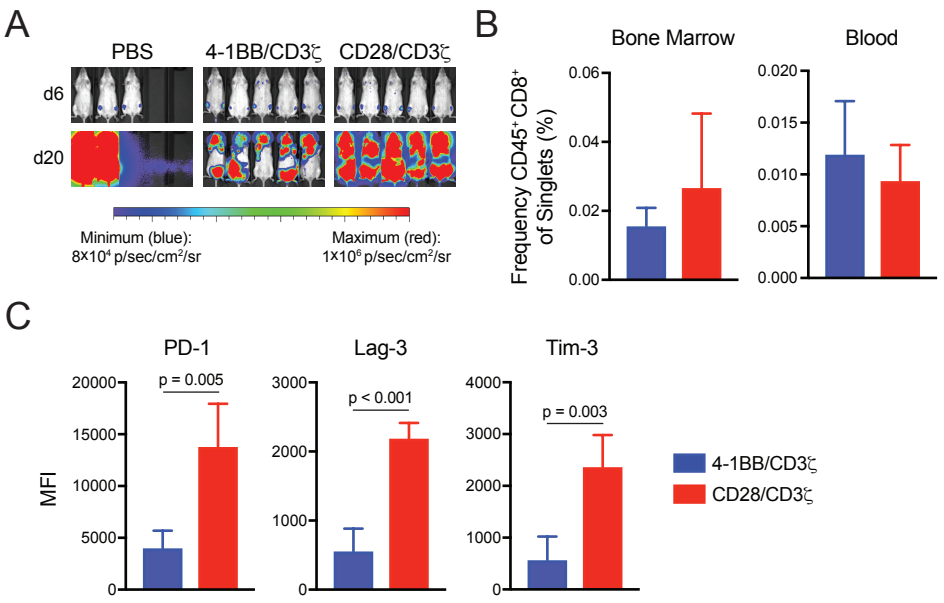

Figure 3.S4. CD8⁺ CD28/CD3ζ CAR T cells display reduced anti-tumor activity and an exhausted phenotype in vivo compared to CD8⁺ 4-1BB/CD3ζ CAR T cells. (**A**) Representative bioluminescence analysis of total radiance (p/sec/cm^2/sr) in mice at the indicated time points. Images are representative of 1 independent experiment. (**B** and **C**) Flow cytometry analysis of CAR T cell frequency in bone marrow or peripheral blood (B), or mean fluorescence intensity (MFI) of PD-1, Lag-3, or Tim-3 expression on CAR T cells in the bone marrow (C) on day 20. Data are means ± SD of 4 mice per group from 1 independent experiment. An unpaired two-tailed t test was used to compare groups.

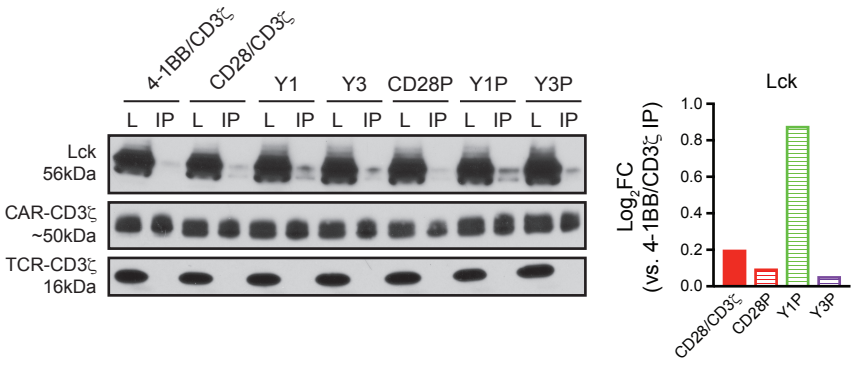

Figure 3.S5. Mutations to the CAR CD28 domain abrogate Lck binding. Western blot analysis for Lck and CD3ζ within whole cell lysates (L) and STII immunoprecipitated fractions (IP) from resting CAR T cells. Fold change of normalized band intensity is shown. Blots are representative of 2 independent experiments.

Chapter 4

Phosphoproteomic analysis of TCR and CAR signaling uncovers key T cell signaling adaptors weakly activated by CAR stimulation

This chapter will be prepared for submission to a peer-reviewed journal after final analysis of data.

Abstract

CAR T cell therapy is FDA-approved for individuals with relapsed/refractory B cell malignancies but therapeutic efficacy can be limited by outgrowth of tumor cells expressing little or none of the CAR target antigen. CAR T cell therapy is also presently ineffective for solid tumors, where tumor-associated antigens are often expressed at lower levels than hematological malignancies. In contrast to synthetic CARs, natural TCRs are capable of recognizing minute amounts of peptide/MHC antigen on the surface of a tumor cell or antigen presenting cell. Enhancing CAR T cell recognition of low-density tumor antigens may both improve initial antitumor efficacy and reduce the risk of relapse, but achieving this goal is challenging because the field incompletely understands how signaling in T cells after CARs engage antigen compares to that after TCRs engage peptide/MHC. We used MS to study the similarities and differences between TCR and CAR recognition-induced signaling events. On a global scale, TCR and CAR signaling events were quite similar, but key T cell signaling adaptors, including CD3δ, ε, and γ, LAT, ITK and NCK1/2, were either not phosphorylated or more weakly phosphorylated by CAR stimulation than TCR stimulation. We hypothesized that CARs capable of engaging these signaling adaptors may enhance recognition of low-density tumor antigens and are currently testing novel CAR designs with CD3ε signaling motifs and/or LAT binding motifs *in vitro* and in pre-clinical mouse models of cancer.

Introduction

CAR T cells are a highly effective immunotherapy for certain individuals with relapsed or refractory B cell malignancies. Generally, greater than 70% of acute lymphocytic leukemia patients who are treated with CD19- or CD22-specific CAR T cells achieve a complete response. However, a significant proportion relapse with leukemia blasts expressing little to no detectable CD19 or CD22 (*224*, *294*, *398*, *408*). A clinical trial of BCMA-specific CAR T cells in relapsed or refractory multiple myeloma also demonstrates that outgrowth of BCMA-negative myeloma cells is a potential cause of relapse (*409*). As CAR T cell therapy is further applied to solid epithelial tumors that lack homogenously or highly expressed antigens like CD19, CD22, or BCMA, selection of antigen low or negative tumor cells is likely to limit complete and durable response rates (*230*, *410*).

It is becoming apparent that CAR T cells less efficiently recognize small amounts of target antigen than the TCR upon which CARs are based. For a CD20-specific CAR, about two hundred CD20 molecules per target cell are required for lytic CAR T cell activity and the requirement for CAR T cell cytokine production is approximately ten-fold higher (*279*). For an

anaplastic lymphoma kinase-specific (ALK) CAR, >10,000 ALK molecules are required for optimal CAR T cell effector functions and tumor eradication *in vivo* (*411*). In contrast, the natural TCR possesses exquisite sensitivity for peptide antigens presented by MHC molecules. As few as one to ten agonist pMHC complexes among thousands of self-pMHC molecules can trigger T cell activation through the TCR (*412*, *413*). Whether increased antigen density requirements for CAR T cell recognition can be improved upon is an open question.

CARs have been designed to mimic fundamental processes of TCR recognition but differ in several aspects (*356*). First, most TCRs bind agonist peptide-MHC with micromolar affinity (*19*), but CARs with a scFv targeting domain often bind MHC-independent ligands with nanomolar affinities (*253*, *414*). This increased binding affinity may alter receptor off-rate and serial triggering. Second, upon antigen engagement, the TCR and its associated CD3δ, ε, γ, and ζ chains assemble multi-component signaling complexes where each protein contributes to a signal transduction cascade (*3*). CARs, by contrast, generally encode only the CD3ζ signaling endodomain and a costimulatory domain from CD28, 4-1BB, and ICOS. While CARs do associate with canonical TCR signaling proteins (Chapter 3), variation in the stoichiometric ratios of signaling molecules or the absence of certain signaling components at the immunological synapse could alter antigen sensitivity and signal intensity. Indeed, initial images of CAR synapses were distinct from those formed by TCRs (*415*). How faithfully CAR signaling recapitulates TCR signaling is unknown.

We compared TCR and CAR ligation-induced phosphoprotein signaling events with the intention of using our results to inform the design of new CAR signaling domains and structures that may more efficiently recognize low-density antigens. We first developed techniques to isolate a pure population of primary T cells possessing a mono-specific TCR or CAR as well as novel reagents for selective TCR or CAR stimulation. We then coupled these reagents to the MS platform developed in Chapter 3 to study TCR and CAR signaling in a single population of T cells. Our results show that TCR and CAR stimulation generated highly similar protein PO_4 events, but CAR stimulation failed to phosphorylate key signal transduction intermediates. MS data was used to inform modification of CAR structural elements and signaling domains for engagement of additional TCR signaling adaptors. *In vitro*, these modified CARs more efficiently recognized tumor cells expressing low levels of antigen.

Results

Protein-coated microbeads selectively activate TCR and CAR signaling in bi-specific T cells

CAR T cells are often generated from polyclonal T cells with diverse TCR specificities. If virus-specific T cells are used as a starting medium for cell manufacturing, one can generate bi-specific T cells that possess a TCR and CAR of known specificity (*358*). We harnessed bi-specific T cells expressing an endogenous EBV-specific TCR and transduced ROR1-specific CAR to comprehensively compare TCR and CAR induced phosphoprotein signaling (**Figure 4.1A**). Bi-specific T cells offer the advantages of: 1) comparing TCR and CAR function in the identical cell population with a single culture history and phenotype, and 2) utilizing the endogenous TCR, which negates potential effects of reduced TCR expression or TCR α and β chain mispairing after transduction of an engineered TCR (reviewed in Chapter 2). We formulated bi-specific T cells by stimulating $CD8^+CD45RO^+$ memory T cells from HLA-$B8^+$ EBV seropositive donors with autologous irradiated and EBV peptide-pulsed peripheral blood mononuclear cells, and transducing cells with a lentiviral vector encoding a CD28/CD3ζ ROR1-specific CAR. T cells that bound an HLA-B8/EBV tetramer and expressed the CAR transduction marker, tCD19, were purified by fluorescence-activated cell sorting (FACS) and expanded for subsequent assays (**Figure 4.1B**).

Stimulating EBV/ROR1 bi-specific T cells with tumor cells expressing TCR or CAR antigens was an attractive strategy to initiate phosphoprotein signaling but our previous work demonstrated that antigen presenting cells contaminated the cellular lysate and were not amenable for MS analysis (Chapter 3). We therefore generated microbeads coated with a recombinant single chain timer (SCT) consisting of EBV RAKFKQLL (RAK) peptide, HLA-B8, and β2 microglobulin, or recombinant ROR1 ectodomain (**Figure 4.S1A**) (*416*). SCT or ROR1 beads selectively activated TCR or CAR signaling, as evidenced by PO_4 of CD3ζ Tyr^{142} and PLC-γ1 Tyr^{783}, and we titrated down the amount of protein coated on the beads (**Figure 4.S1B**) as well as the bead to cell ratio (**Figure 4.S1C**) to levels that reduced reagent costs while still saturating PO_4 of the CAR, TCR, and PLC-γ1. To make TCR stimulation functionally equivalent to CD28/CD3ζ CAR stimulation that delivers 'signal 1' and 'signal 2' for T cell activation, we added CD28 mAb to the SCT beads. Consistent with the known additive role of CD28 costimulation, SCT/CD28 bead stimulation increased PLC-γ1 Tyr^{783} PO_4 and T cell proliferation compared to SCT bead stimulation (**Figure 4.S1D**) (*30*).

We next sought to study whether microbead-based TCR or CAR stimulation could substitute for antigen presenting cell-based stimulation of the TCR or CAR. Expanded bi-specific T cells were incubated with either SCT/CD28 or ROR1 microbeads at the previously identified saturating ratio, or K562 cells expressing HLA-B8 alongside endogenously processed

EBV peptides or full-length human ROR1 at a 2:1 T cell to K562 cell ratio. TCR stimulation using SCT/CD28 beads elicited greater cytokine production and cell proliferation than CAR stimulation using ROR1 beads (**Figures 4.1C-E**). Similarly, TCR stimulation using K562/B8/EBV cells elicited greater effector responses than CAR stimulation with K562/B8/ROR1 cells. These data were consistent with prior work that TCR stimulation initiates more rapid and potent effector functions than CAR stimulation (*252*, *358*). Notably however, bead-based TCR or CAR stimulation induced less cytokine production and proliferation than cell-based stimulation despite incubating T cells with levels of beads that saturated phosphoprotein signaling. We attributed the weaker effector responses to the absence of adhesion and costimulatory molecules on magnetic beads that are present on K562 cells (*417*). Thus, bead-based stimulation mirrored cell-based stimulation and represented a viable strategy to stimulate bi-specific T cells for MS analysis.

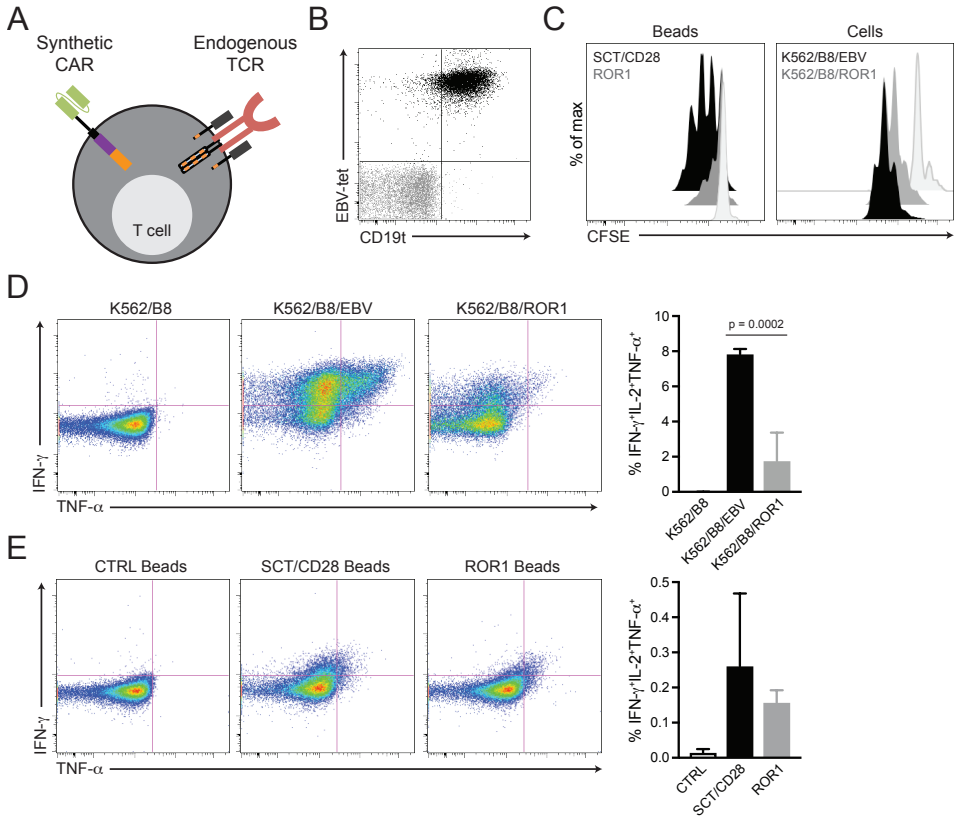

Figure 4.1. Bi-specific T cells enable selective analysis of TCR and CAR induced signaling and effector functions in a single cell population. (**A**) Schematic of bi-specific T cells possessing a TCR and CAR of known specificity. (**B**) Flow cytometry analysis of EBV-tetramer binding and CD19t expression in expanded T cells. FACS plot shows stained (black) and isotype (grey) $CD8^+$ singlet lymphocytes. (**C**) Flow cytometry analysis of T cell proliferation as measured by CFSE dye dilution at 72 hours after co-culture with K562/B8 cells on control beads (light grey), K562/B8/EBV cells or SCT/CD28 beads (black), or K562/B8/ROR1 cells or ROR1 beads (dark grey). Histogram plots show $CD8^+$ lymphocytes and are

representative of 2-3 independent experiments. (**D** and **E**) Flow cytometry analysis IFN-γ, IL-2, and TNF-α production 5 hours after co-culture of bi-specific T cells with K562/B8 cells, K562/B8/EBV cells, K562/B8/ROR1 cells, control beads, SCT/CD28 beads, or ROR1 beads. FACS plots show $CD45^+$ singlet lymphocytes. The frequency of IFN-g^+IL-2^+TNF-a^+ cells is shown. Data are means ± SD of 2-3 independent experiments. The indicated P values were calculated by unpaired two-tailed t test (D).

MS identifies common protein phosphorylation events after TCR or CAR stimulation

To measure protein PO_4 signaling events initiated by TCR or CAR stimulation, we performed three independent experiments in which EBV/ROR1 bi-specific T cells were incubated with SCT/CD28, ROR1, or uncoated (control) magnetic beads for 10, 45, or 90 minutes prior to cell lysis (**Figures 4.2A**). Bi-specific T cells generated from two different donors were used in two experiments; a third experiment utilized bi-specific T cells independently derived from one of the two donors. Cell phenotyping prior to TCR (SCT/CD28) or CAR (ROR1) microbead stimulation showed that bi-specific T cells expressed CD45RO, CD62L, and CD28, and >83% of cells were in the G_0/G_1 cell cycle phase, consistent with a resting memory phenotype (**Figure 4.S2**). Using identical phosphopeptide labeling and enrichment techniques as in Chapter 3, a total of 30,669 PO_4 sites corresponding to 4,997 gene products were detected from these three experiments (**Figure 4.2B**). Among PO_4 sites, 715 (2.3%) were phosphotyrosines, 5,056 (16.5%) were phosphothreonines, and 24,898 (81.2%) were phosphoserines (**Figure 4.2C**). For each PO_4 site, $\log_2$FC values comparing TCR stimulation to control treatment or CAR stimulation to control treatment were similar across replicate experiments (**Figure 4.2D**).

Phosphorylation events mediated by TCRs and CARs differ in kinetics and magnitude

We leveraged limma in the R statistical computing framework to identify PO_4 sites that were up or down modulated by TCR or CAR stimulation. We assigned a PO_4 site to be CAR stimulation-responsive if it was detected in at least two of the three experiments, displayed an average $|\log_2 FC| \geq 1$ between stimulated and unstimulated conditions at 10 or 45 minutes, and met a 5% FDR cutoff. Few PO_4 sites met $\log_2$FC and false discovery rate (FDR) cutoffs after 10 minutes of TCR or CAR stimulation, but hundreds of PO_4 sites were up or down modulated after 45 or 90 minutes of TCR and CAR stimulation (**Figure 4.2E and Table 4.S1**). On a global level, TCR stimulation induced greater fold changes in protein PO_4 at the 10 minute time point compared to CAR stimulation. These differences became less apparent after 45 and 90 minutes of stimulation. Network analysis of stimulation-responsive PO_4 sites revealed that both TCR and CAR stimulation altered the PO_4 of proteins in the KEGG T cell receptor signaling, RNA transport, and actin cytoskeleton regulatory pathways (**Table 4.S2**).

To confirm that bead stimulation activated TCR and CAR signaling intermediates, we searched the dataset for PO_4 sites on CD3ζ, CD28, and ZAP-70. PO_4 of all three CD3ζ ITAMs, CD28 tyrosine residues, and ZAP-70 regulatory sites increased after TCR or CAR stimulation (**Figures 4.2F-H**). CD3ζ and CD28 were more intensely phosphorylated by CAR stimulation than TCR stimulation at the 10 and 45 minute time points. However, the more robust PO_4 of CD3ζ and CD28 after CAR stimulation did not translate into substantially greater ZAP-70 PO_4 as ZAP-70 PO_4 sites displayed similar increases in PO_4 after TCR and CAR stimulation (**Figure 4.2H**). These results suggested that CAR stimulation using ROR1 beads led to more intense CAR PO_4 but that this strong signal intensity was not as efficiently converted into ZAP-70 PO_4 as after TCR stimulation.

A limitation of these analyses was that bi-specific T cells possessed two identical copies of CD3ζ and CD28 proteins derived from either the endogenous gene or the CAR transgene and MS cannot differentiate identical peptides derived from distinct sources. Because CARs and TCRs are of different molecular mass, we analyzed undigested whole cell lysates by Western blot. Western blot analysis confirmed selective TCR and CAR activation as well as more intense PO_4 of the CAR CD3ζ domain after CAR ligation than the TCR CD3ζ domain after TCR ligation (**Figure 4.2I**). In contrast, SLP-76 Ser^{376} and PLC-γ1 Tyr^{783} were more intensely phosphorylated after TCR stimulation than after CAR stimulation. These data demonstrated that TCR stimulation more efficiently converted small amounts of CD3ζ PO_4 into intense ZAP-70, SLP-76, and PLC-γ1 PO_4 and suggested that CAR stimulation requires greater receptor PO_4 to initiate intracellular signaling than TCR stimulation.

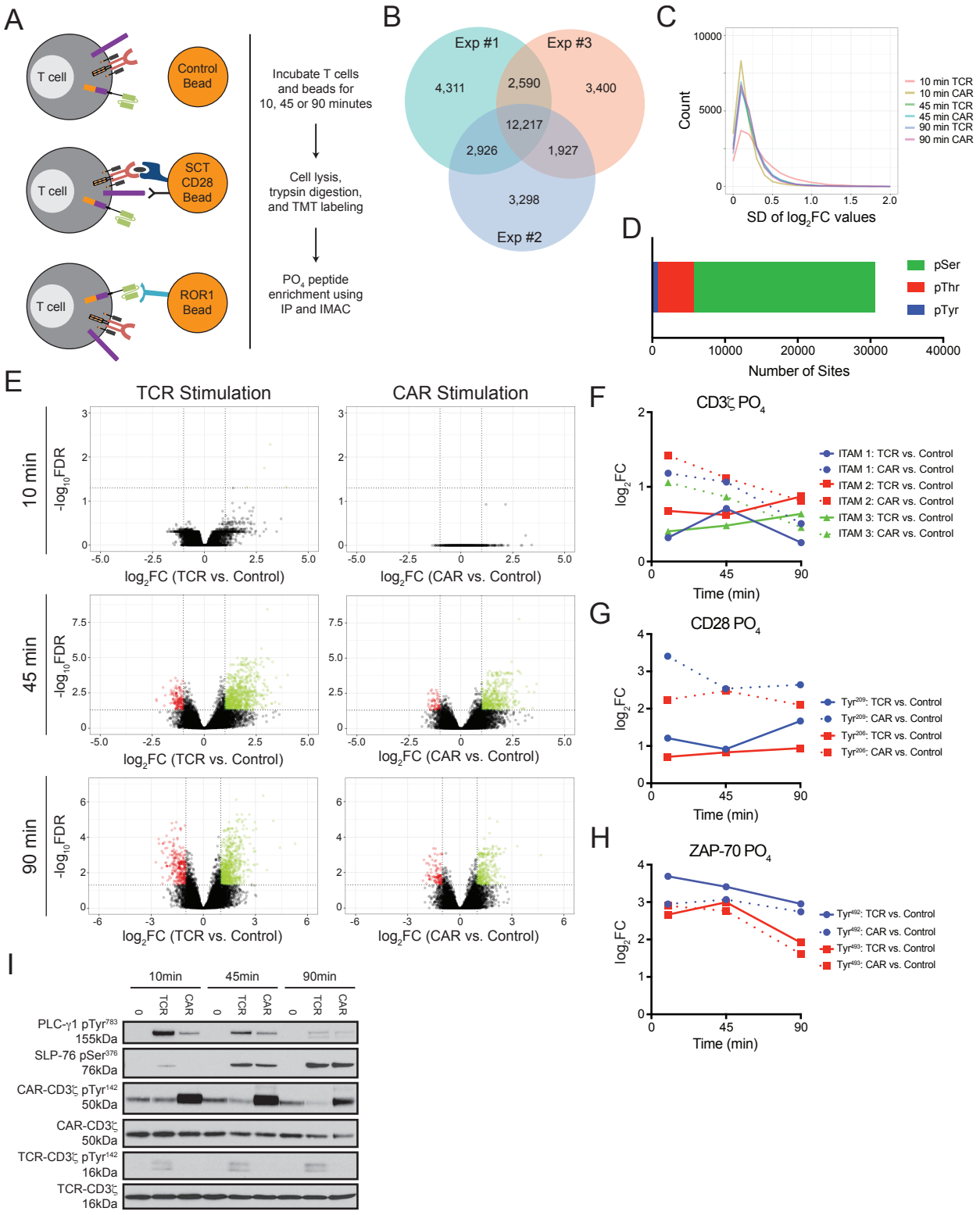

Figure 4.2. MS identifies common protein phosphorylation events after TCR or CAR stimulation. (**A**) Schematic of experimental design stimulating bi-specific T cells with microbeads coated with TCR or CAR antigens. (**B** to **D**) Tandem MS/MS analysis of phosphorylated peptides from lysates of bi-specific T cells stimulated as in (A). Venn diagram of the overlap among PO_4 sites (B), histogram of the SD of the fold

change (log_2FC) values across all tandem MS/MS experiments (C), and the total number of pSer, pThr and pTyr peptides identified (D) are pooled from all tandem MS/MS experiments. (**E**) Volcano plots of log_2FC and false discovery rate (FDR) for PO_4 sites identified by tandem MS/MS. Green dots indicate sites with increased PO_4 and red dots indicate sites with decreased phosphorylation after stimulation in at least 2 experiments. (**F** to **H**) The fold change of the indicated PO_4 sites identified by tandem MS/MS. Data are means from all experiments. (**I**) Western blot analysis for CD3ζ, CD3ζ pTyr^{142}, SLP-76 pSer^{376}, and PLC-γ1 pTyr^{783} in bi-specific T cell lysates at the indicated times after stimulation. Blots are representative of all tandem MS/MS experiments.

CAR stimulation promotes less intense PO_4 of CD3 chains and signaling adaptors

Our functional and signaling data suggested that TCR stimulation more efficiently converts initial receptor PO_4 into downstream signals that give rise to more potent effector functions. We therefore directly compared changes in protein PO_4 after CAR or TCR stimulation. At the earliest 10 minute stimulation time point, hundreds of PO_4 sites were more intensely modulated by TCR than CAR stimulation (**Figure 4.3A, left**). Many of these differentially phosphorylated sites mapped to proteins involved in TCR and immunological signaling (**Table 4.S1**). After 45 minutes and 90 minutes, we observed a strong correlation between PO_4 site changes in TCR and CAR stimulated samples. Only 30 sites at the 45 minute time point possessed fold change values that differed by more than 2-fold between TCR and CAR treated samples (**Figure 4.3A, middle**). Among these, CD3D, CD3E, CD3G, LAT, LAX1 and PAG1 were all more intensely phosphorylated by TCR than CAR stimulation (**Figures 4.3A-C**). After 90 minutes of stimulation, 41 sites possess fold change values that differed by more than 2-fold between TCR and CAR treated samples. CD3E and CD3G remained more intensely phosphorylated by TCR than CAR stimulation, and we also detected preferential PO_4 of TAGAP, SOS1, STAT3, STAT5A/B, and NR4A1 after TCR but not CAR stimulation (**Figure 4.3A, right**). Plotting individual sites across time further demonstrated that signaling adaptors known to be critical for TCR signaling were less intensely phosphorylated by CAR stimulation than TCR stimulation (**Figures 4.3B-E**). These differences were consistent with our earlier observations of weaker SLP-76 Ser^{376} and PLC-γ1 Tyr^{783} PO_4 after CAR stimulation (**Figure 4.2H**) and indicated that CARs did not faithfully recapitulate all TCR-induced signaling events.

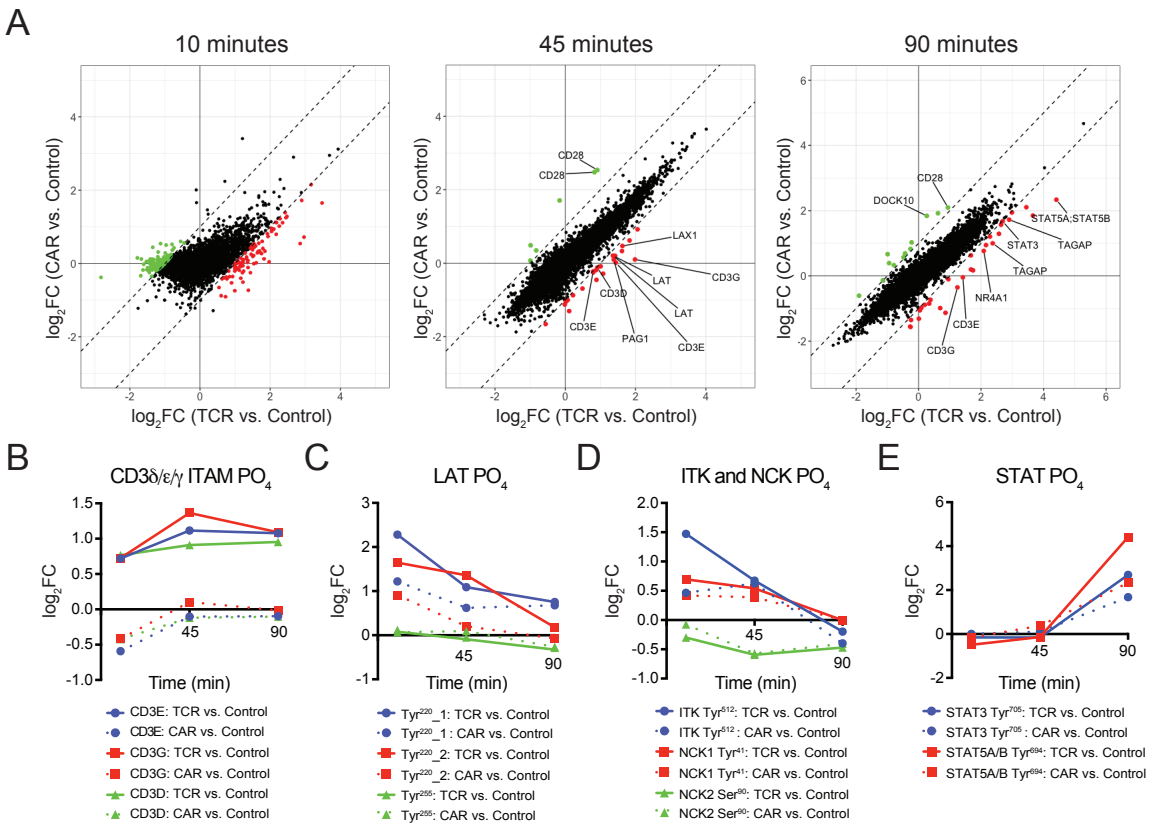

Figure 4.3. CAR stimulation promotes less intense phosphorylation of CD3 chains and proximal signaling adaptors. (**A**) Comparison of the log_2FC of PO_4 sites identified by tandem MS/MS after TCR or CAR stimulation. Green and red dots specify sites that possessed mean log_2FC values differing by ≥ 1 between TCR and CAR stimulated samples in at least 2 tandem MS/MS experiments. (**B** to **E**) The fold change of the indicated PO_4 sites identified by tandem MS/MS. Data are means from all experiments.

CD3ε sequences improve CAR T cell recognition of ROR1^{lo} tumor cells

Our MS data indicated that CARs stimulation promoted weaker PO_4 signaling adaptors and no PO_4 of CD3δ/ε/γ chains. We asked whether engineering additional ITAMs and/or protein recruitment domains on the CAR backbone would enhance antigen sensitivity. Because CD3ε cross-linking is frequently used to activate T cells (*418*), we incorporated the CD3ε endodomain into existing CAR backbones. The CD3ε endodomain has three known signaling motifs – a membrane-adjacent basic residue-rich sequence (BRS) that binds Lck (*419*), a proline-rich sequence (PRS) further within the endodomain that is thought to enhance TCR sensitivity to low-affinity antigens by interacting with Nck1 (*420*, *421*), and an ITAM that activates ZAP-70 (*18*). We also designed a CAR variant containing only the CD3ε PRS and ITAM because our earlier data indicated that additional Lck increases CAR signal strength (Chapter 3). We believed this construct would increase signaling capacities without additional CAR-Lck association due to the CD3ε BRS.

We placed all or part of the CD3ε endodomain either before or after the CD3ζ domain in CD19-specific or ROR1-specific CD28/CD3ζ and 4-1BB/CD3ζ CARs (**Figure 4.4A**). CD19-specific CARs bearing the entire CD3ε or only $CD3\varepsilon_{PRS\_ITAM}$ domains efficiently activated T cells after STII microbead crosslinking, although placing the entire CD3ε endodomain between the 4-1BB and CD3ζ domains led to relatively weaker SLP-76 Ser^{376} and PLC-γ1 Tyr^{783} PO_4 after stimulation (**Figure 4.4B**). Further assessment of CD3ε-containing $CD8^+$ and $CD4^+$ CAR T cells in NSG mice with disseminated $CD19^+$ Raji lymphoma demonstrated that adding the complete CD3ε domain reduced antitumor function compared to parental CD28/CD3ζ or 4-1BB/CD3ζ CAR T cells (**Figure 4.4C**). Inclusion of only the $CD3\varepsilon_{PRS\_ITAM}$ domains in a 4-1BB/CD3ζ CAR backbone slightly reduced median survival compared to mice treated with conventional 4-1BB/CD3ζ CAR T cells, although $CD3\varepsilon_{PRS\_ITAM}$ CAR T cells were superior to CD28/CD3ζ CAR T cells. Taken together, increasing the number of signaling domains and CAR signal intensity appeared to reduce median survival, consistent with our prior hypothesis that CAR signal strength is a determinant of antitumor function *in vivo* (Chapter 3).

Signal strength is influenced by both the signaling endodomains encoded by the CAR, as well as the density of target antigen and/or number of CARs bound to the target antigen. We suspected that the density of CD19 molecules on the surface of $K562/CD19^{lo}$, $K562/CD19^{hi}$ and Raji cells was more than sufficient for CAR recognition and turned to the solid tumor-associated antigen, ROR1, to study CAR T cell recognition at lower target antigen densities more relevant to solid tumors. ROR1 is endogenously expressed at varying levels by the MDA-MB-231 breast adenocarcinoma and NCI-H358 lung adenocarcinoma cell lines (**Figure 4.S3**). In agreement with our hypothesis, 4-1BB/$CD3\varepsilon_{PRS\_ITAM}$/CD3ζ CAR T cells produced modestly more IFN-γ, IL-2, and TNF-α compared to conventional 4-1BB/CD3ζ CAR T cells upon co-culture with $ROR1^{int}$ MDA-MB-231 cells (**Figure 4.4D**). In addition, 4-1BB/$CD3\varepsilon_{PRS\_ITAM}$/CD3ζ CAR T cells proliferated to a greater extent upon co-culture with $ROR1^{int}$ MDA-MB-231 and $ROR1^{lo}$ NCI-H358 cells (**Figure 4.4E**).

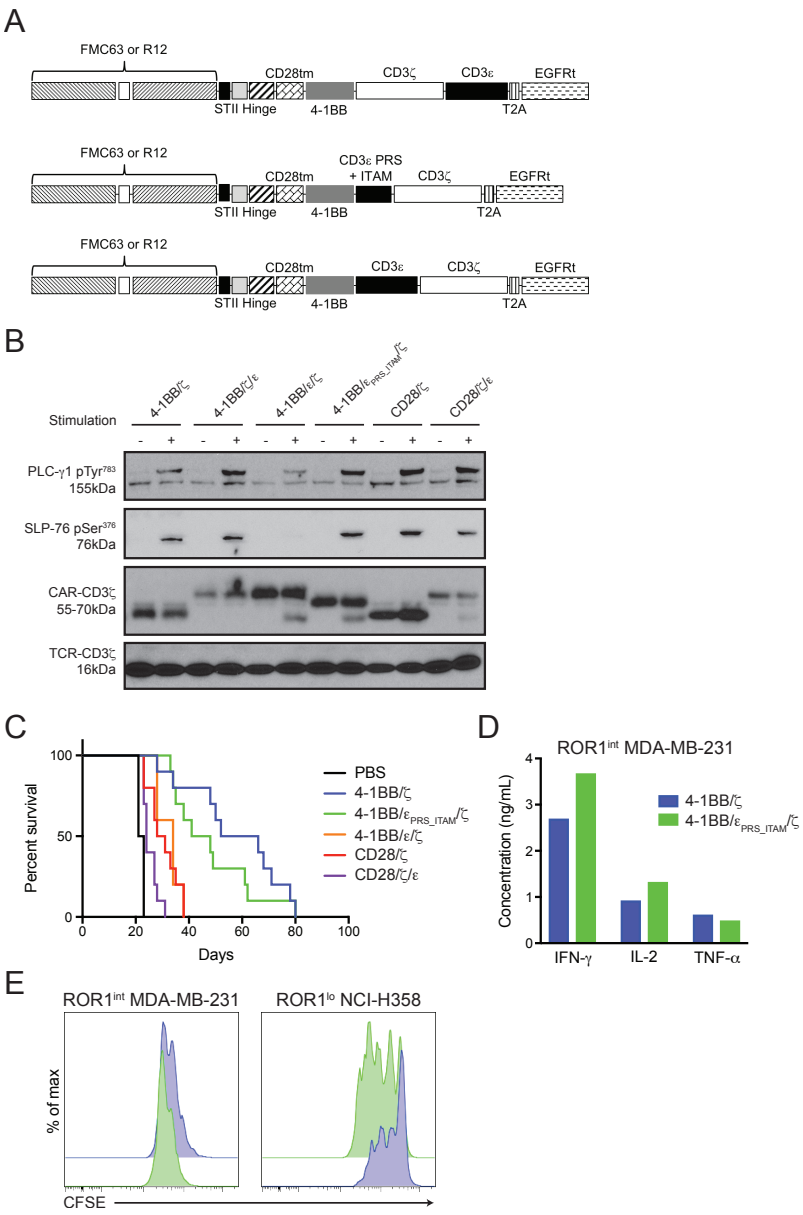

Figure 4.4. CARs incorporating CD3ε sequences enhance recognition of tumor cells with low antigen density. (**A**) Schematic of CD3ε CAR designs containing a CD19-specific FMC63 scFv or ROR1-specific R12 scFv. (**B**) Western blot analysis for CD3ζ, SLP-76 pSer^{376}, and PLC-γ1 pTyr^{783} in CAR T cell lysates after 45 minutes of stimulation with STII microbeads or control microbeads. Blots are representative of 2 independent experiments. (**C**) At 7 days after Raji/ffluc engraftment, NSG mice were treated with a single infusion of CAR T cells. Survival analyses are pooled from 2 independent experiments on 6 or 10 mice per group. (**D**) ELISA analysis of cytokine production 24 hours after co-culture of the indicated CAR T cells and tumor cells. Data are means from 1 experiment. (**E**) Flow cytometry analysis of CAR T cell proliferation as measured by CFSE dye dilution at 72 hours after co-culture with the indicated tumor cells. Histogram plots show 4-1BB/CD3ζ (blue) and 4-1BB/CD3ε_{PRS_ITAM}/CD3ζ (green) CD8^{+} lymphocytes and are representative of 1 experiment.

Discussion

CD19 and CD22 CAR T cells are an effective therapy for acute lymphocytic leukemia but many patients relapse with tumor cells expressing little or no antigen expression (*410*). One strategy to address this problem is to design CAR T cells that attack multiple antigens at once (*335*, *408*). The basic premise is that selection of treatment-resistant tumor cells is less likely to occur during a multi-pronged therapeutic regimen. Clinical trials testing this strategy for the B cell leukemia antigens CD19, CD20, and CD22 are now underway (NCT03330691, NCT03468153, NCT03398967, NCT02315612, NCT03593109). However, signaling is not fully understood for monovalent CARs, and might differ (positively or negatively) for multivalent CARs. Therefore, multiplexing current CAR designs may continue to insufficiently detect low antigen expressing tumor cells.

Natural TCRs are capable of recognizing minute amounts of antigen and we reasoned that detailed analyses of the signaling events initiated by TCR and CAR recognition might inform optimizations to CAR design that permit efficient recognition of low-density antigens (*412*, *413*). We used shotgun MS to study TCR and CAR stimulation-induced phosphoprotein signaling events and collected a comprehensive dataset describing how 30,669 PO_4 sites corresponding to 4,997 gene products were changed by stimulation. Importantly, our approach analyzed TCR and CAR stimulation-induced signaling events in a single T cell population with a defined culture history and phenotype.

Our data demonstrate that TCR and CAR stimulation induced similar changes in protein PO_4 at a global level and within the KEGG TCR signaling pathway. However, TCR stimulation more efficiently phosphorylated proximal members of the canonical TCR signaling pathway than did CAR stimulation. After 10 minutes of stimulation, hundreds of PO_4 sites both within and outside of the canonical TCR signaling pathway were more intensely modulated by TCR stimulation than CAR stimulation. After 45 and 90 minutes, CAR- and TCR-stimulated samples grew more similar as >99% of PO_4 sites exhibited similar responses to TCR or CAR stimulation. However, key TCR signaling adapters, including LAT, ITK, NCK1/2, and STAT proteins, remained more intensely phosphorylated by TCR than CAR stimulation. Notably, CD3 δ, ε, and γ chains were not phosphorylated by CAR stimulation at any time point. These findings are consistent with our prior work (Chapter 3) and published work that CARs do not typically associated with the endogenous TCR (*422*). The initial reduction in signal intensity and inefficient engagement of key signaling molecules could lead to differential transcriptional programs by modifying NFAT and NF-κB transcriptional factor activation. Differential signaling could also alter T cell differentiation during sustained contact with antigen-expressing tumor

cells, such as in *in vivo* models. Thus, our phosphoproteomic data warrant further evaluation of the transcriptional and functional differences between TCR and CAR stimulated samples.

Incorporating additional signaling domains and/or protein recruitment domains into CARs is an established approach to engage additional signaling adapters (*423*). We asked whether inclusion of all or part of the CD3ε endodomain into an existing 4-1BB/CD3ζ CAR backbone would augment recognition of low-density antigens. In a preliminary experiment, CD3ε-containing CARs enhanced *in vitro* recognition of ROR1^{int} MDA-MB-231 and ROR1^{lo} NCI-H358 tumor cell lines. To better determine whether the CD3ε endodomain improves tumor cell recognition or signal generation, we are measuring the effector functions initiated by ROR1 CAR T cells after co-culture with additional ROR1^{int} and ROR1^{lo} tumor lines. We are also employing xenograft mouse models of ROR1^{+} breast and lung adenocarcinoma to study how CD3ε-containing CARs behave *in vivo*.

A caveat of modifying CAR structure for improved recognition of low-density antigens is that revised CAR designs could increase the risk of toxicity and reduce the therapeutic window for CAR T cell therapy. Two studies have linked life-threatening toxicities after CAR T cell infusions to recognition and destruction of healthy, non-transformed cells expressing the target antigen (*240*, *283*). Further enhancing CAR recognition of low-density antigens could increase the risk for on-target off-tumor toxicities stemming from recognition of healthy tissues. A possible method to mitigate or circumvent the increased risk for on-target off-tumor toxicity is to devise logic-gated tumor targeting systems that require multiple antigen inputs for full-fledged T cell activation and killing (*9*, *339*, *341*). We expand on one method utilizing synthetic Notch receptors in Appendix II and show that logic-gated CAR expression can mitigate CAR T cell destruction of healthy bone marrow progenitor cells expressing low levels of ROR1. Thus, MS offers a valuable resource to interrogate immunological signaling and guide the design of new CAR signaling domains for improved therapeutic efficacy.

Finally, a potential limitation of our approach to study signaling was that many unique TCR sequences were present in the tetramer-specific T cell population (*424*). An alternative strategy to study TCR and CAR signaling in one cell population is to transduce CD8^{+} T cells with a CAR and a single virus- or tumor-specific MHC class I-restricted TCR. However, TCR transduction can lead to altered TCR expression and/or α and β chain mispairing that occurs with the endogenous TCR (Chapter 2). Our approach has the benefit of utilizing a cell's endogenous TCR that is expressed at physiological levels. Thus, we believe our approach presented fewer concerns than available alternatives.

Materials and Methods

Acquisition of peripheral blood T cells from healthy donors
Healthy adults (>18 years-old) were enrolled in Institutional Review Board-approved studies for peripheral blood collection or leukapheresis. Informed consent was obtained from all enrollees. Researchers were provided only donor age and a nondescript donor ID number and blinded to all personally-identifiable information about study participants. $CD4^+$, $CD8^+$, and memory $CD8^+$ T cells were isolated using the EasySep Human $CD4^+$, $CD8^+$, and Memory $CD8^+$ T Cell Isolation Kits (StemCell Technologies). Isolations were performed in accordance with manufacturer's instructions.

Cell Culture
LentiX cells (Clontech) were cultured in DMEM (Gibco) supplemented with 10% fetal bovine serum, 1mM L-glutamine (Gibco), 25mM HEPES (Gibco), and 100U/mL penicillin/streptomycin (Gibco). K562 (CCL-243), NCI-H358 (CRL-5807), MDA-MB-231 (HTB-26), and Raji (CCL-86) cells were obtained from American Type Culture Collection and cultured in RPMI-1640 (Gibco) supplemented with 5% fetal bovine serum, 1mM L-glutamine, 25mM HEPES, and 100U/mL penicillin/streptomycin. The generation of K562/CD19 and K562/ROR1 cells was previously described (*425*). Primary human T cells were cultured in CTL medium consisting of RPMI-1640 supplemented with 10% human serum, 2mM L-glutamine, 25mM HEPES, 100U/mL penicillin/streptomycin, 50μM β-mercaptoethanol (Sigma), and 50 U/mL IL-2 (Prometheus). All cells were cultured at 37°C and 5% CO_2, and tested bi-monthly for the absence of mycoplasma using MycoAlert Mycoplasma Detection Kit (Lonza).

Generation of chimeric antigen receptors (CARs) and recombinant lentiviral vectors
CD19-specific and ROR1-specific 4-1BB/CD3ζ and CD28/CD3ζ CAR constructs with an R12 scFv and IgG4 hinge have been previously described (*198*, *253*). CD3ε CARs were constructed using the STII CARs described in Chapter 3. The entire CD3ε endodomain (UniProt: P07766) or a truncated endodomain (amino acids 179-207) containing PRS and ITAM components was inserted either immediately before or after the CD3ζ endodomain. CAR constructs were linked by T2A sequence to a truncated CD19 (CD19t) or epidermal growth factor receptor (EGFRt), codon-optimized, and cloned into a HIV7 lentiviral vector. All cloning was performed by PCR, enzyme digest, and/or Gibson assembly. Plasmids were verified by capillary sequencing and restriction digest.

Lentivirus preparation and transduction
Lentivirus was generated by transient transfection of LentiX cells using psPAX2, pMD2.G, and a CAR encoding lentiviral vector. To prepare bi-specific T cells, memory $CD8^+$ T cells were stimulated one day later (day 1) using irradiated autologous peripheral blood mononuclear cells that had been pulsed with EBV-RAK (RAKFKQLL, Elim Biopharmaceuticals) peptide. The next day (day 2), lentiviral supernatant was harvested from LentiX cells, filtered using 0.45μm PES syringe filters (Millipore), and added to activated T cells. Polybrene (Millipore) was added to reach a final concentration of 4.4μg/mL and cells were spinoculated at 800×g and 32°C for 90 minutes. Viral supernatant was replaced 8 hours later with fresh CTL supplemented with 50 IU/mL IL-2. Half-media changes were then performed every 48 hours using CTL supplemented with 50 U/mL IL-2. $CD8^+$tetramer$^+$t$CD19^+$ transduced T cells were FACS-sorted on a FACSAria II (BD Biosciences) on day 11. Conventional CAR T cells were prepared as described in Chapter 3 (*425*).

To prepare K562 cells expressing HLA-B8, LentiX cells were transiently transfected with psPAX2, pMD2.G, and an HIV7 lentiviral vector encoding HLA-B8. To prepare K562/B8 cells expressing EBV antigens or ROR1, LentiX cells were transiently transfected with MLV g/p, 10A1, and a mp71 retroviral vector encoding GFP and an EBV peptide minigene, or human ROR1. To prepare Raji/ffluc cells, LentiX cells were transiently transfected with psPAX2, pMD2.G, and an HIV7 lentiviral vector encoding GFP and firefly luciferase. Two days later, viral supernatant was filtered using a 0.45μm PES syringe filter and added to K562 or Raji cells. Five days later, transduced cells were stained monoclonal antibodies specific for HLA-B8 (REA145, Miltenyi Biotec) and ROR1 (2A2, Miltenyi Biotec) and FACS-sorted on a FACSAria II to greater than 97% purity.

T cell expansion for mass spectrometric and functional analyses
FACS-sorted $CD8^+$tetramer$^+CD19t^+$ or $CD8^+EGFRt^+$ cells were expanded over a single stimulation cycle prior to MS and/or functional analyses. Bi-specific and ROR1-specific CAR T cells were expanded using a rapid expansion protocol containing purified OKT3, irradiated LCL, and irradiated PBMC, and assayed 11 days after stimulation. CD19-specific CAR T cells were expanded by co-culture with irradiated $CD19^+$ lymphoblastoid cell lines (LCL) in a 1:7 (T cell:LCL) ratio and assayed 8 days after stimulation. During expansion, cultures were fed with fresh CTL media containing 50 IU/mL IL-2 every 2-3 days.

Flow cytometry and cell phenotyping
T cells were stained with a 1:100 dilution of fluorophore-conjugated monoclonal antibodies specific for human CD4 (RPA-T4), CD8 (SK1), CD19 (HIB19), CD28 (CD28.2), CD45 (HI30), CD45RO (UCHL1), CD62L (DREG56) or CD279 (eBioJ105) purchased from BD Biosciences, ThermoFisher, or Biolegend. Phycoerythrin (PE)-conjugated HLA-B8/EBV tetramer was generated by the Immune Monitoring Core Facility at the Fred Hutchinson Cancer Research Center. T cells were also stained with isotype control fluorophore-conjugated antibodies when appropriate. Cetuximab (anti-EGFR, Bristol Myers Squibb) was biotinylated using the EZ-Link Sulfo-NHS-Biotin kit (ThermoFisher) followed by cleanup with a Zeba Spin Desalting Column (ThermoFisher) and used to stain T cells in conjunction with Streptavidin-APC (ThermoFisher). DNA content staining was performed by fixing T cells with 70% ice-cold ethanol, permeabilizing cells with 1% Triton-X (Sigma), degrading RNA with 100μg/mL RNAse A (ThermoFisher), and staining DNA with 20μg/mL Propidium Iodide (ThermoFisher). All data was collected on a FACSCanto II or FACSAria II (BD Biosciences).

SCT, SCT/CD28, ROR1, STII and control microbead preparation
Recombinant single chain trimer (SCT) and human ROR1 were produced at the Fred Hutchinson Cancer Research Center. 1mL Streptavidin Coated Magnetic Particles (Spherotech) was washed once in excess 1× PBS supplemented with 100 U/mL penicillin/streptomycin (PBS+P/S) using a benchtop magnet. SCT and ROR1 microbeads were prepared by resuspending beads in 1mL PBS+P/S and then slowly adding recombinant protein while vortexing the solution. Protein was added at the indicated molar ratios according to manufacturer's predetermined molar binding capacities. SCT/CD28 microbeads were prepared by resuspending beads in 1mL PBS+P/S and then slowly adding recombinant SCT protein and biotinylated CD28 mAb (CD28.2, ThermoFisher) at a 3:1 molar ratio. STII microbeads were prepared by resuspending beads in 1mL PBS+P/S and then slowly adding 16.67μg anti-STII biotin mAb (GenScript) while vortexing the bead solution. All microbeads were incubated overnight at 4°C on a 3D orbital shaker, washed three times with excess PBS+P/S using a benchtop magnet, and resuspended in 4mL PBS+P/S for STII microbeads or 1mL PBS+P/S for control, SCT, SCT/CD28 and ROR1 beads. To make control beads, 1mL Streptavidin Coated

Magnetic Particles was washed once using a benchtop magnet and the bead pellet was resuspended in 1mL PBS+P/S. All beads were stored at 4°C.

Cell stimulations, protein lysates, RNA isolation
CAR T were washed and resuspended in warm CTL medium. T cells were brought to a concentration of 2×10^7 cells per mL and incubated with control, SCT, SCT/CD28, ROR1, or STII microbeads in a 37°C water bath. After the allotted time, cells were quickly washed twice using ice-cold PBS, then lysed in a 6M Urea, 25mM Tris (pH 8.0), 1mM EDTA, 1mM EGTA solution supplemented with protease (Sigma) and phosphatase inhibitors (Sigma) at a 1:100 dilution, hereon referred to as lysis buffer. Lysates were sonicated for 15 seconds prior to centrifuging at 10,000×g and 4°C for 10 minutes. Beads were removed during lysate clearing.

Protein digestion, TMT labeling, and phosphotyrosine (pTyr) peptide immunoprecipitation
Protein was quantified in lysates by Micro BCA Assay (ThermoFisher), and lysates were diluted to 2mg/mL using lysis buffer. Lysates were reduced in 24mM TCEP (ThermoFisher) for 30 minutes at 37°C with shaking, followed by alkylation with 48mM iodoacetamide (Sigma) in the dark at room temperature for 30 minutes. Lysates were then diluted with 200mM Tris (pH 8.0), to a urea concentration of 2M. Lys-C (Wako) was dissolved in 25mM Tris (pH 8.0) at 200ug/mL and added to lysates at 1:100 (enzyme:protein) ratio by mass and incubated for 2 hours at 37°C with shaking. Samples were further diluted with 200mM Tris (pH 8.0) to a urea concentration of 1M before adding trypsin at a 1:50 trypsin:protein ratio. After 2 hours, a second trypsin aliquot was added at a 1:100 trypsin:protein ratio. Digestion was carried out overnight at 37°C with shaking. After 16 hours, the reaction was quenched with formic acid to a final concentration 1% by volume. Samples were desalted using Oasis HLB 96-well plates (Waters) and a positive pressure manifold (Waters). The plate wells were washed with 3 x 400μL of 50% MeCN/0.1% FA, and then equilibrated with 4 x 400μL of 0.1% FA. The digests were applied to the wells, then washed with 4 x 400μL 0.1% FA before being eluted drop by drop with 3 x 400μL of 50% MeCN/0.1% FA. The eluates were lyophilized, followed by storage at -80°C until use. For TMT labeling (ThermoFisher), desalted peptides were resuspended in 50 mM HEPES at 1mg/mL based on starting protein mass. TMT reagents were resuspended in 257μL MeCN and transferred to the peptide sample. Samples were incubated at room temperature for 1 hour with mixing. Labeling reactions were quenched by the addition of 50μL of 5% hydroxyl Amine (Sigma) and incubated for 15 minutes at room temperature with mixing. The independent labeling reactions were then pooled together and lyophilized. The labeled peptides were desalted as above and then lyophilized and stored at -80°C. Immunoprecipitation of pTyr peptides was performed using the PTMScan P-Tyr-1000 Kit (Cell Signaling). The enriched pTyr peptide fraction was purified using a C18 Spin Tip (ThermoFisher), lyophilized, and stored at -80°C until analysis. The flow-through fraction was desalted, lyophilized, and stored at -80°C.

Basic (high pH) reverse phase liquid chromatography
The desalted and pTyr peptide-depleted flow-through was fractionated by high-pH reverse phase (RP) liquid chromatography. 4mg of the protein digest was loaded onto a LC system consisting of an Agilent 1200 HPLC with mobile phases of 5mM NH_4HCO_3 (pH 10) (A) and 5mM NH_4HCO_3 in 90% MeCN (pH 10) (B). The peptides were separated by a 4.6mm x 250mm Zorbax Extend-C18, 3.5μm, column (Agilent) over 96 minutes at a flow rate of 1.0mL/min by the following timetable: hold 0% B for 9 minutes, gradient from 0 to 10% B for 4 minutes, 10 to 28.5% B for 50 minutes, 28.5 to 34% B for 5.5 minutes, 34 to 60% B for 13 minutes, hold at 60% B for 8.5 minutes, 60 to 0% B for 1 minute, re-equilibrate at 0% B for 5 minutes. 1 minute fractions were collected from 0-96 minutes by the shortest path by row in a 1 mL deep well plate (ThermoFisher). The high pH RP fractions were concatenated into 24 samples by every other

plate column starting at minute 15 (e.g.: sample 1 contained fractions from wells B10, D10, F10, etc.). The remaining fractions were combined such that fractions from 12 to 14 minutes were added to sample 1, all fractions after 86 minutes were added to sample 24, and all fractions from 0 to 11 minutes were combined into sample 'A'. 95% of every 12th fraction of the 24 samples was combined (1,13; 2,14; ...) to generate 12 more samples, which were dried down and stored at -80°C prior to phosphopeptide enrichment by immobilized metal affinity chromatography.

Immobilized metal affinity chromatography (IMAC)
IMAC enrichment was performed using Ni-NTA-agarose beads (Qiagen) stripped with EDTA and incubated in a 10mM $FeCl_3$ solution to prepare Fe^{3+}-NTA-agarose beads. Fractionated lysate was reconstituted in 200μL of 0.1% TFA in 80% MeCN and incubated for 30 minutes with 100μL of the 5% bead suspension while mixing at room temperature. After incubation, beads were washed 3 times with 300μL of 0.1% TFA in 80% MeCN. Phosphorylated peptides were eluted from the beads using 200μL of 70% ACN, 1% Ammonium Hydroxide for 1 minute with agitation at room temperature. Samples were transferred into a fresh tube containing 60μL of 10% FA, dried down and re-suspended in 0.1% FA, 3% MeCN. Samples were frozen at -80°C until analysis.

Nano-liquid chromatography-tandem mass spectrometry
Phosphopeptide-enriched samples were analyzed by LC-MS/MS on an Easy-nLC 1000 (ThermoFisher) coupled to an LTQ-Orbitrap Fusion mass spectrometer (ThermoFisher) operated in positive ion mode. The LC system, configured in a vented format consisted of a fused-silica nanospray needle (PicoTip emitter, 50μm ID x 20cm, New Objective) packed in-house with ReproSil-Pur C18-AQ, 3μm and a trap (IntegraFrit Capillary, 100μm ID x 2 cm, New Objective) containing the same resin as in the analytical column with mobile phases of 0.1% FA in water (A) and 0.1% FA in MeCN (B). The peptide sample was diluted in 20 μL of 0.1% FA, 3% MeCN, and 8.5μL was loaded onto the column and separated over 210 minutes at a flow rate of 300 nL/min with a gradient from 5 to 7% B for 2 minutes, 7 to 35% B for 150 minutes, 35 to 50% B for 1 minute, hold 50% B for 9 minutes, 50 to 95% B for 2 minutes, hold 95% B for 7 minutes, 95 to 5% B for 1 minute, re-equilibrate at 5% B for 38 minutes. A spray voltage of 2000 V was applied to the nanospray tip. MS/MS analysis occurred over a 3 second cycle time consisting of 1 full scan MS from 350-1500 m/z at resolution 120,000 followed by data dependent MS/MS scans using HCD activation with 27% normalized collision energy of the most abundant ions. Selected ions were dynamically excluded for 45 seconds after a repeat count of 1.

Western blotting
Equal masses of protein lysate were loaded into 4-12% Bis-Tris NuPAGE Gels (ThermoFisher). After protein transfer onto nitrocellulose membranes (ThermoFisher), membranes were blocked with Western Blocking Reagent (Sigma). Membranes were stained with primary and secondary antibodies diluted in SuperBlock (ThermoFisher) supplemented with 0.1% Tween. The following antibodies were used: anti-human CD247 (8D3, BD Biosciences), anti-human CD247 $pTyr^{142}$ (K25-407.69, BD Biosciences), anti-SLP-76 $pSer^{376}$ (D9D6E, Cell Signaling), anti-PLC-γ1 $pTyr^{783}$ (D6M9S, Cell Signaling), anti-mouse horseradish peroxidase (HRP) (polyclonal, Cell Signaling), and anti-rabbit HRP (polyclonal, Cell Signaling). Typical antibody dilutions ranged from 1:10,000 to 1:2500. Band intensities were quantified using ImageJ (NIH); normalized to total protein, loading control, or immunoprecipitation input; and then renormalized to a control sample.

In vitro functional assays
CAR T cells were co-cultured with tumor cells at a T cell to tumor cell ratio of 2:1 or beads at a ratio of 7.5μL beads per 1×10^6 cells. Intracellular cytokine staining was performed by incubating T cells with tumor cells or beads and GolgiStop (BD Biosciences) for 5 hours. Cells were fixed and permeabilized using FoxP3/Transcription Factor Staining Buffers (ThermoFisher) and stained with fluorochrome-labeled monoclonal antibodies specific for IFN-γ (B27), IL-2 (MQ1-17H12), and TNF-α (Mab11) purchased from Biolegend and BD Biosciences. Cytokine concentrations in cellular supernatant were quantified by ELISA (ThermoFisher) 24 hours after stimulation. T cell proliferation was quantified by staining CAR T cells with a 0.2μM solution of carboxyfluorescein succinimidyl ester (CFSE) dye (ThermoFisher) and incubating T cells with tumor cells or beads for 72 hours.

Transfer of T cells in NOD/SCID/γc$^{-/-}$ (NSG) mice
Six- to eight-week-old male or female NSG mice were obtained from the Jackson Laboratory or bred in-house. Mice were engrafted via tail vein with 5×10^5 CD19$^+$ Raji/ffluc cells, and 7 days later, injected intravenously with PBS or a defined product of purified CD8$^+$ and CD4$^+$ CD19-specific CAR T cells mixed together in a 1:1 ratio. Bioluminescence imaging was performed as described and mice were followed for survival (*198*). Mice handlers were blinded to group allocation. The Fred Hutchinson Cancer Research Center Institutional Animal Care and Use Committee approved all experimental procedures.

Shotgun mass spectrometry data analysis
Raw MS/MS spectra from each replicate experiment were searched together against the reviewed Human Universal Protein Resource (UniProt) sequence database (release 2016_01) with common laboratory contaminants using the MaxQuant/Andromeda search engine version 1.6.0.1 (*400*). The search was performed with a tryptic enzyme constraint for up to two missed cleavages. Variable modifications were oxidized methionine, phosphorylated serine, phosphorylated threonine, and phosphorylated tyrosine. Carbamidomethylated cysteine was set as a static modification. Peptide MH+ mass tolerances were set at 20 ppm. The overall FDR was set at ≤ 1% using a reverse database target decoy approach.

For the three TMT experiments, phosphopeptide site localization was determined by MaxQuant and converted to phosphorylation sites using Perseus version 1.6.0.7 (*401*). At this step, reverse hits and potential contaminants were excluded from further analysis. Data normalization was performed by scaling each TMT channel to the channel median, followed by a $\log_2$transformation. Stimulation vs. control ratios were calculated by subtracting the appropriate control channels from TCR or CAR stimulated channels. Due to incomplete MS sampling, some phosphorylation sites (features) were only found in one or two replicate experiments, and a much smaller minority (< 1%) of sites were not found in every TMT channel.

Differential expression analyses over PO_4 sites were performed using the limma statistical framework and associated R package (*377*, *402*). For these analyses, we chose to keep only features that had values in at least two experiments and all TMT channels, leaving us with 19,608 quantified PO_4 sites. A linear model was fitted to each PO_4 site, and empirical Bayes moderated t-statistics were used to assess differences in expression/abundance. Contrasts comparing stimulation vs control treatments were tested. Intraclass correlations were estimated using the duplicateCorrelation function of the limma package to account for measures originating from the same patients and the same antigens (*403*). An absolute $\log_2$fold change cutoff (stimulation versus control) of 1 and a false discovery rate (FDR) cutoff of 5% were used

to determine differentially expressed PO_4 sites. Analyses of signaling networks and KEGG Pathways were performed using StringDB.

Analysis of T cell phenotype, function, and in vivo experiments
FlowJo version 9 (Treestar) was used to analyze flow cytometry files. Prism version 7 (GraphPad Software) was used to plot data and calculate statistics. P values meeting an α = 0.05 level of significance are indicated in the figures. The precise statistical tests used are indicated in the figure legends.

Supplementary Figures

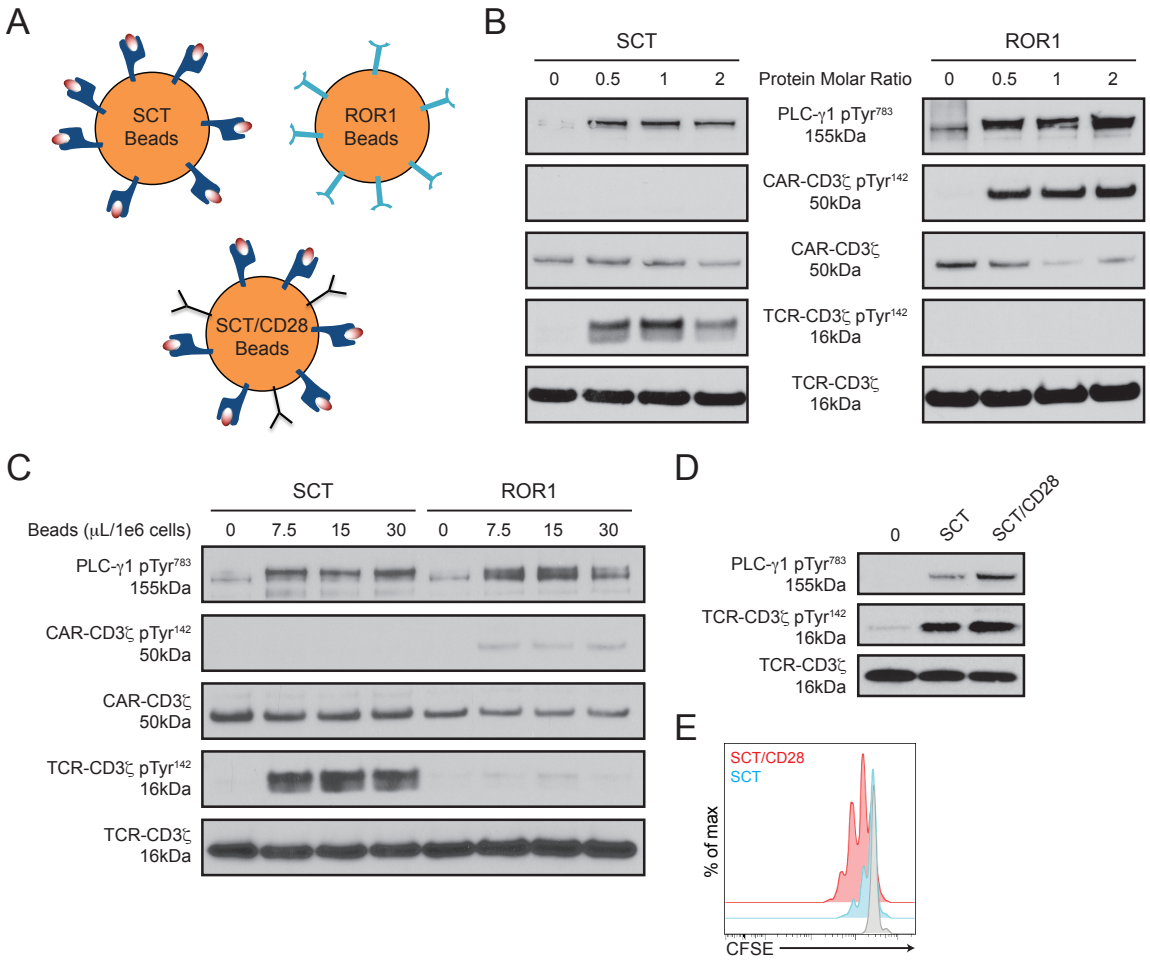

Figure 4.S1. Optimization of bead stimulation parameters. (**A**) Schematic of magnetic beads coated with HLA-B8/EBV-RAK single chain trimer (SCT), ROR1 ectodomain, or SCT and CD28 mAb. (**B**) Western blot analysis for CD3ζ, CD3ζ pTyr^{142}, and PLC-γ1 pTyr^{783} in lysates from T cells incubated for 45 minutes with microbeads coated with various molar ratios of SCT or ROR1. 30μL beads were used per million cells. (**C**) Western blot analysis for CD3ζ, CD3ζ pTyr^{142}, and PLC-γ1 pTyr^{783} in lysates from T cells incubated for 45 minutes with various amounts SCT or ROR1 microbeads (molar ratio = 0.5). (**D**) Western blot analysis for CD3ζ, CD3ζ pTyr^{142}, and PLC-γ1 pTyr^{783} in lysates from T cells incubated for 45 minutes with uncoated (0), SCT, or SCT/CD28 microbeads. 7.5μL beads were used per million cells. (**E**) Flow cytometry analysis of T cell proliferation as measured by CFSE dye dilution at 72 hours after microbead stimulation. Histogram plot of CD8^{+} lymphocytes treated with uncoated (black), SCT (blue) or SCT/CD28 (red) microbeads.

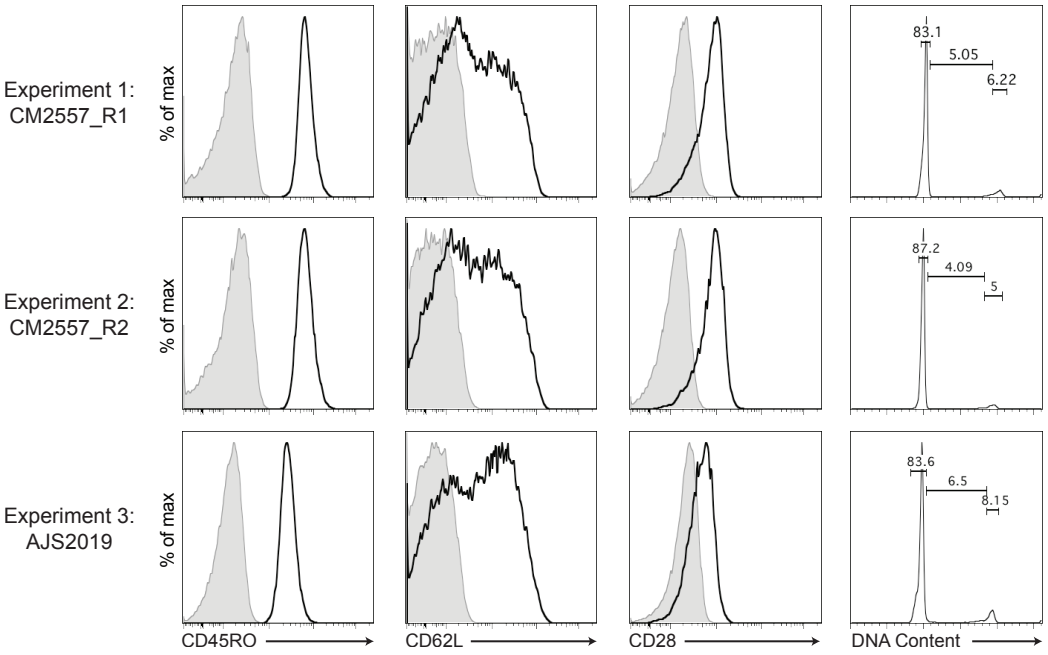

Figure 4.S2. EBV/ROR1 bi-specific T cells express T cell memory markers and are resting after cell culture. Flow cytometry analysis of CD45RO, CD62L, CD28 and DNA content in expanded T cells prior to MS signaling analysis. Histograms show stained (black) and isotype (grey) $CD8^+$ singlet lymphocytes. DNA content was measured by staining with propidium iodide after fixation and permeabilization. Frequencies of cells in G0/G1, S, and G2 phases (from left to right) are indicated by the gates.

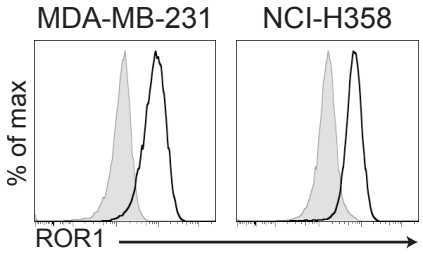

Figure 4.S3. ROR1 is expressed by MDA-MB-231 and NCI-H358 tumor lines. Flow cytometry analysis of ROR1 expression on the indicated tumor lines. Histograms show stained (black) and isotype (grey) singlets.

Chapter 5
High-affinity PD-1/CD28 immunomodulatory fusion proteins augment the function of genetically modified T cells

This chapter is being prepared for submission to a peer-reviewed journal:

Alexander I. Salter, Shannon K. Oda, Anusha Rajan, Nicolas M. Garcia, Pranali Ravikumar, Andrew W. Daman, Eva J. Alderman, Alexandra Cabanov, Philip D. Greenberg, Stanley R. Riddell. “High-affinity PD-1/CD28 immunomodulatory fusion proteins augment the function of genetically modified T cells.”

Abstract

The adoptive transfer of genetically modified T cells can be an effective cancer therapy for some individuals with leukemia or lymphoma. Unfortunately, many patients with either lymphoma or epithelial cancer do not respond to therapy. Elements of the tumor microenvironment are among the possible obstacles to success and can limit therapeutic T cell efficacy, as when T cell signaling is inhibited by the programmed cell death protein 1 (PD-1). One strategy to subvert this inhibitory signal employs immunomodulatory fusion proteins (IFPs) that link the PD-1 ectodomain to the activating CD28 signaling endodomain, but IFPs have produced only modest benefits in pre-clinical testing to date. We hypothesized that PD-1/CD28 IFPs may compete poorly with endogenous PD-1 on the T cell surface because interactions between PD-1 and its PD-L1/L2 ligands on the antigen-presenting cells are of low affinity and/or are inefficiently recruited into immunological synapses. We therefore constructed IFPs, using mutated PD-1 ectodomains with higher affinity for PD-L1. High-affinity IFPs improved T cell function after co-culture with PD-L1^{+} tumor cells and outcompeted both wild-type IFPs and full-length PD-1 for entry into immunological synapses, but did not improve the *in vivo* antitumor activity of genetically modified T cells. In some tumor models, high-affinity IFP^{+} T cells displayed detrimental effects in a tumor PD-L1 expression-independent manner. We speculate that high-affinity PD-1/CD28 IFPs may be binding to endogenous cells expressing murine PD-L1 and thus are not be a viable strategy to circumvent PD-1/PD-L1 signaling. Receptor-ligand expression patterns should be carefully considered when designing high-affinity immunomodulatory receptors.

Introduction

T cells that are genetically modified to express tumor-associated antigen (TAA) targeting receptors can provide clinical benefits for some patients after adoptive transfer (*230*). The mechanisms for therapeutic failure in non-responding patients are complex, but include suppression of T cell function (*426*). In addition to redirecting T cell specificity, genetic modification of T cells can be used to endow resistance to immunosuppression (*227*, *427*, *428*). One such technique is to design an IFP that connects a costimulatory signaling endodomain to an inhibitory ectodomain, thereby promoting T cell effector functions upon binding of otherwise inhibitory ligands.

Programmed cell death 1 (PD-1) is an immunoreceptor that inhibits T cell function when engaged by programmed cell death 1 ligand 1 (PD-L1) or 2 (PD-L2) (*340*). PD-L1 and PD-L2 are frequently expressed by malignant and infiltrating immune cells in numerous solid tumors

and on non-Hodgkin lymphomas. Ligation of PD-1 activates the inhibitory phosphatase, SHP-2, which in turn, dephosphorylates CD28 and quantitatively suppress T cell receptor signaling (*14*, *30*, *387*, *429*, *430*). Notably, administration of PD-1 or PD-L1 blocking antibodies produces tumor regressions in subsets of patients with melanoma, non-small cell lung cancer and bladder cancer (*431*). Crystal structures of murine or human PD-1/ligand complexes have revealed contact sites important for ligand binding and enabled the design of small protein therapeutics that interfere with this inhibitory interaction (*432-436*).

PD-1 signaling also regulates adoptively transferred T cells (*346*, *347*, *437*), and we are currently conducting a clinical trial combining CD19-targeting CAR T cell therapy with PD-L1 antibody blockade (NCT02706405). While this combination has the potential to improve the efficacy of the CAR T therapy, systemic PD-1/PD-L1 blockade could increase rates of off-tumor toxicity, cytokine release syndrome and/or autoimmunity (*307*). In light of recent data showing that PD-1 directly dephosphorylates CD28, we reasoned that an IFP linking the PD-1 ectodomain to the CD28 endodomain might be harnessed to increase the efficacy of adoptive T cell therapy by simultaneously blocking PD-1 signaling and boosting CD28 signaling. PD-1/CD28 IFPs have been utilized in genetically modified T cells, but only modestly improved T cell function *in vitro* and *in vivo* (*228*, *347*, *348*, *438*, *439*). Because interactions between PD-1 and its ligands are only of low micromolar affinity and possess a high off-rate (*432*, *435*, *436*), we hypothesized that increasing IFP binding affinity for PD-1 ligands may enhance IFP function.

Herein, we describe optimizations to PD-1/CD28 IFP structure and affinity that promote efficient binding to physiological levels of PD-L1. We show that the amount of PD-L1 expression on the tumor cell is a critical determinant of IFP function, and that mutated PD-1 protein ectodomains can be incorporated to increase affinity for PD-L1 (*432*, *435*). High-affinity IFPs significantly enhanced the *in vitro* function of CAR T or TCR-modified T (TCR-T) cells, compared to conventional CAR T or TCR-T cells. However, adoptive transfer of IFP-expressing (IFP^+) CAR or TCR transgenic T cells in multiple mouse models of cancer either decreased or did not impact median survival. Therefore, high-affinity PD-1/CD28 IFPs do not generally enhance the function of genetically modified T cells *in vivo,* and may sometimes even inhibit T cell function by binding to host, non-tumor $PD\text{-}L1^+$ cells.

Results

PD-1/PD-L1 interactions restrain CAR T cell antitumor activity in vivo

PD-1 ligation reduces CAR T cell antitumor functions (*346*, *347*), and we established an *in vivo* model in which to test methods for overcoming this immuno-suppression. We used the well-characterized Raji lymphoma cell line because it is susceptible to CAR T cell therapy, does not natively express PD-L1 and does not upregulate PD-L1 expression upon treatment with IFN-γ (*198*, *440*, *441*). Raji lymphoma cells were transduced with human ROR1, a TAA frequently overexpressed in Mantle cell lymphoma, triple-negative breast cancer, and lung adenocarcinoma (*270*), as well as firefly luciferase (ffluc) and human PD-L1 genes. Raji/ROR1/ffluc or Raji/ROR1/PD-L1/ffluc tumor cells were purified by fluorescence-activated cell sorting (FACS) and engrafted into NSG mice. One week later, a non-curative dose of $CD8^+$ and $CD4^+$ ROR1-specific 4-1BB/CD3ζ CAR T cells was administered (**Figure 5.1A**) (*198*). Mice treated with untransduced (UT) $CD8^+$ and $CD4^+$ T cells died from lymphoma by day 21 post-tumor engraftment; the presence of PD-L1 did not affect tumor growth kinetics or survival. However, forced expression of PD-L1 on Raji tumor cells reduced median survival of CAR T cell-treated mice (**Figure 5.1B**). Tumor PD-L1-mediated reductions in CAR T cell function could be overcome by combining CAR T cells with PD-1 blocking mAb. Treating Raji/ROR1/PD-L1/ffluc tumor-bearing mice with both CAR T cells and PD-1 mAb delayed tumor progression and prolonged median survival, although cessation of PD1 mAb therapy on day 25 allowed rapid tumor outgrowth (**Figures 5.1C-E**). Thus, PD-1/PD-L1 interactions negatively regulated CAR T cells *in vivo,* and CAR T cell function could be improved by blocking this interaction.

Optimization of the PD-1/CD28 fusion site increases IFP surface expression

Previous work indicates that IFPs linking a PD-1 ectodomain to a CD28 signaling domain enhance T cell function in various contexts (*228*, *347*, *348*, *438*, *439*). To build upon this work, we sought to optimize the PD-1/CD28 fusion site. We constructed three PD-1/CD28 IFP iterations described by others containing either the 1) first 155 amino acids of the PD-1 ectodomain linked to the hinge, transmembrane and intracellular domains of the CD28 costimulatory molecule (155aa), 2) the first 165 amino acids of the PD-1 ectodomain linked to the CD28 transmembrane and intracellular domains (165aa), or 3) the entire PD-1 ectodomain and transmembrane domain linked to the CD28 intracellular domain (PD-1tm). These IFPs were expressed in a tricistronic lentiviral vector, with a ROR1-targeting CAR and a truncated CD19 (tCD19) insert for tracking (**Figure 5.2A**) (*228*, *347*, *348*, *438*, *439*, *442*). Notably, the 155aa construct contained a cysteine residue that increased function of a CD200R/CD28 IFP (*427*).

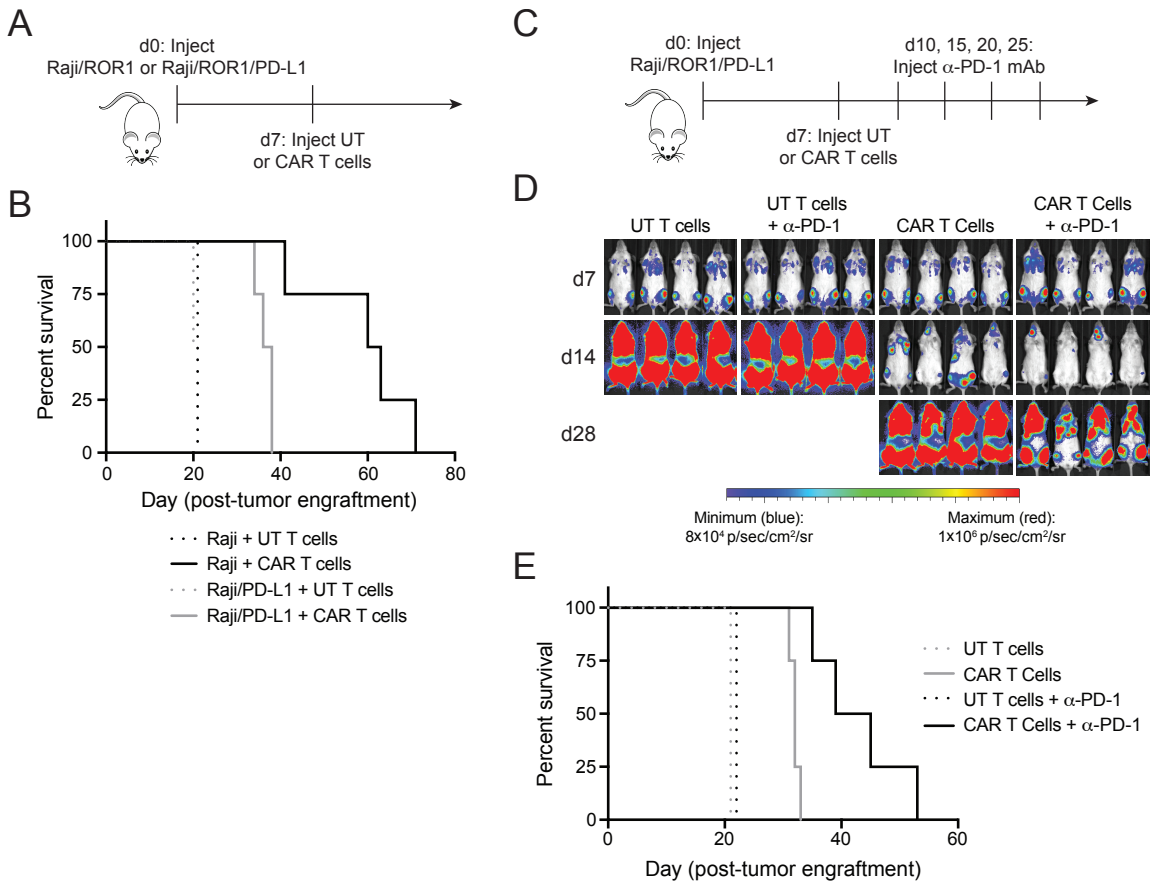

Figure 5.1. PD-1/PD-L1 interactions restrain CAR T cell antitumor activity in vivo. (**A**) Experimental outline showing engraftment of NSG mice with Raji/ROR1 or Raji/ROR1/PD-L1 tumor cells followed by treatment with untransduced (UT) or ROR1 CAR T cells. (**B**) Survival analysis of mice treated as per A. n = 2 mice per group for groups receiving UT T cells and 4 mice per group for groups receiving CAR T cells. (**C**) Experimental outline showing engraftment of NSG mice with Raji/ROR1/PD-L1 tumor cells followed by treatment with a combination of untransduced (UT) or ROR1 CAR T cells and anti-PD-1 blocking antibody. (**D**) Bioluminescence images of Raji/ROR1/PD-L1/ffluc tumor burden in mice at the indicated time points treated as per C. (**E**) Survival analysis of mice treated as per C. n = 4 mice per group.

For initial testing, we expressed the PD-1/CD28 IFPs with a first-generation CAR, containing only CD3ζ as an T cell activation signal, to determine if the IFP provided an additive costimulatory signal. We transduced primary human $CD8^+$ T cells with these constructs, FACS-purified $tCD19^+$ transduced cells, and expanded sorted cells *in vitro*. Conventional CAR T cells lacking an IFP were $PD\text{-}1^-$ after expansion, but all IFP^+ CAR T cells were $PD\text{-}1^+$, confirming IFP surface expression (**Figure 5.2B**). Cells transduced with the PD-1tm IFP stained with a lower fluorescence intensity than cells transduced with the 155aa and 165aa IFPs. This indicates that the PD-1tm IFP containing the PD-1 transmembrane domain was expressed at lower levels than the IFPs containing the CD28 transmembrane domain. These results are consistent with a recent report from Schlenker *et al*., but differ from Kobold *et al*. who found that the PD-1

transmembrane domain increased surface expression of murine PD-1/CD28 IFPs (*228*, *439*). Additional Western blot analyses confirmed reduced PD-1tm IFP expression and revealed that all IFPs migrated between 47 and 52kDa in reducing conditions (**Figure 5.2C**). The 44-52kDa bands were far from the predicted 26kDa molecular weight of monomeric IFPs, but near the molecular weight of the IFP dimers (52kDa) and endogenous CD28 dimers (44kDa). Thus, all IFP variants may dimerize and/or associate with CD28.

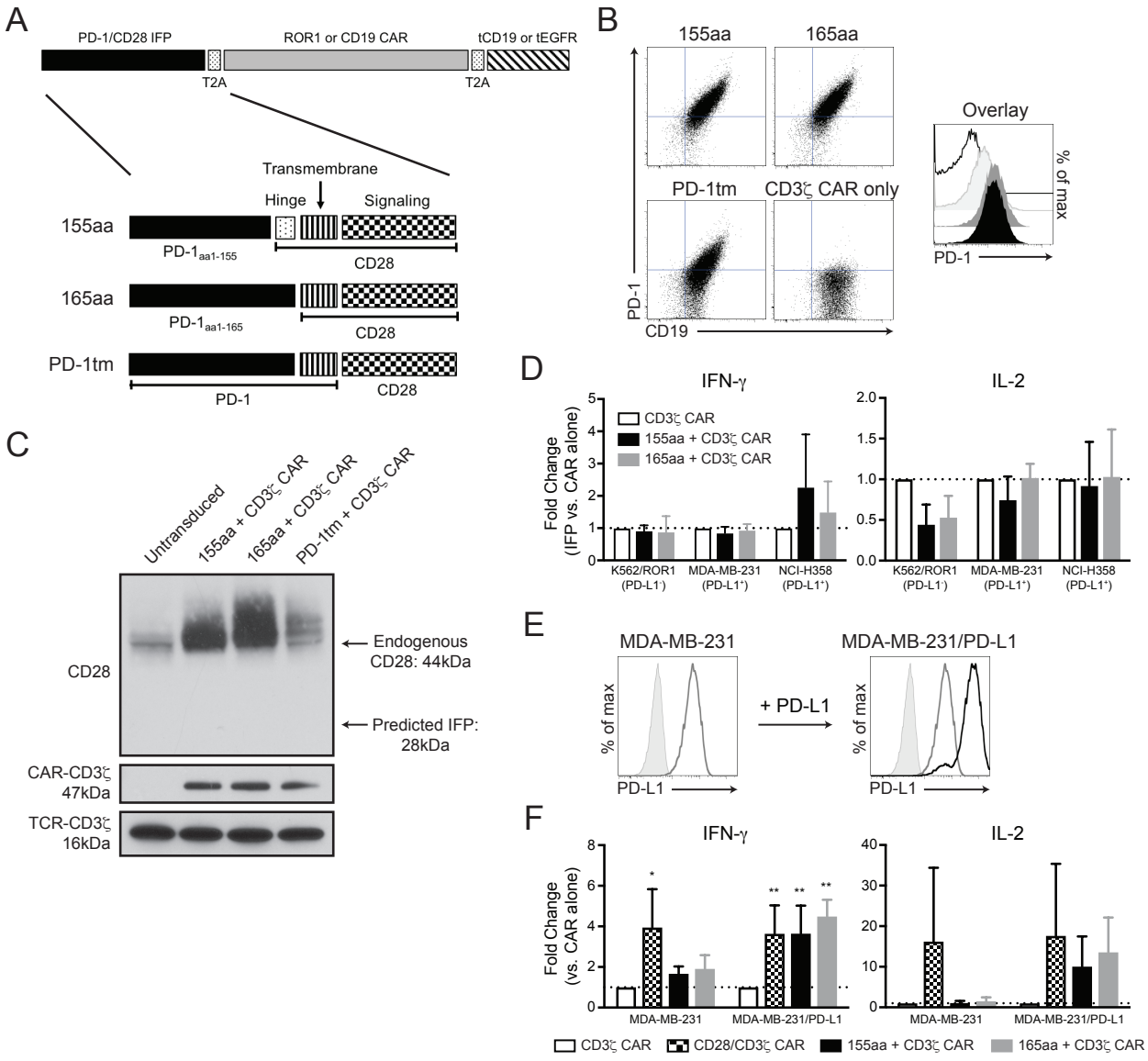

Figure 5.2. Optimization of the PD-1/CD28 fusion site increases IFP expression but does not augment CAR T cell effector functions. (**A**) Schematic of a tri-cistronic lentiviral construct encoding an IFP, CAR, and truncated CD19 or EGFR selection marker. Three IFPs with different PD-1/CD28 fusion sites are depicted. (**B**) Flow cytometry analysis of CD19 and PD-1 staining on $CD8^+$ singlet lymphocytes. Data representative of 3 independent experiments. (**C**) Western blot analysis for CD3ζ and CD28 in T cell lysates after sorting and expansion. Blots representative of n=3 independent experiments. (**D**) ELISA

analysis of cytokine production 24 hours after co-culture of ROR1-targeting CAR T cells with tumor cells. Data are means + SD of 3 independent experiments. (**E**) Flow cytometry analysis of PD-L1 expression. Histogram plots show isotype control (grey filled), MDA-MB-231 (grey open), and MDA-MB-231/PD-L1 (black open) singlets. (**F**) ELISA analysis of cytokine production 24 hours after co-culture of ROR1 CAR T cells with tumor cells. Data are means + SD of 3 independent experiments. The indicated *P* values were calculated by repeated-measures one-way ANOVA with Dunnett's multiple comparisons test comparing samples to CD3ζ CAR. * denotes $P \leq 0.05$ and ** denotes $P \leq 0.01$.

PD-1/CD28 IFPs do not enhance CAR T cell effector functions unless PD-L1 is overexpressed

We proceeded to measure the functional activity of the highly-expressed 155aa and 165aa IFPs by co-culturing purified and expanded $CD8^+tCD19^+$ ROR1-targeting CAR T cells with ROR1-transduced, $PD\text{-}L1^-$ K562 chronic myelogenous leukemia cells, or with endogenously $ROR1^+PD\text{-}L1^+$ MDA-MB-231 breast cancer and NCI-H358 lung cancer cell lines (**Figure 5.S1A**). Surprisingly, neither IFP enhanced *in vitro* CAR T cell cytokine production or proliferation against MDA-MB-231 or NCI-H358 cells (**Figure 5.2D**), which contradicted a previous report on IFP function (*347*). However, the tumor cells in our assays expressed PD-L1 endogenously and the target cells used by Liu *et al*. were rendered strongly $PD\text{-}L1^+$ using lentivirus. Single cell suspensions of primary solid tumors are difficult to procure, but PD-L1 staining of circulating $CD138^+$ plasma cells from individuals with refractory multiple myeloma demonstrated modest PD-L1 expression, below the levels on MDA-MB-231 and NCI-H358 cells (**Figures 5.S1A-B**). Thus, the results obtained by Liu *et al*. may not accurately describe the effects of IFPs in the setting of physiological ligand expression.

We tested whether PD-L1 expression level impacts IFP function by transducing MDA-MB-231 cells with a lentivirus encoding human PD-L1 (**Figure 5.2E**). IFP^+ CAR T cells only displayed higher cytokine production than conventional IFP^- CAR T cells when co-cultured with MDA-MB-231 cells overexpressing PD-L1 (**Figure 5.2F**). IFP^+ T cells expressing a first generation ROR1 CAR produced IFN-γ at levels rivaling those of second-generation ROR1 CD28/CD3ζ CAR T cells (*443*). These data suggest that PD-L1 expression levels are critical for IFP function and that additional modifications would be necessary for IFPs to promote improved T cell function when PD-L1 is expressed at relatively low levels.

PD-1/CD28 IFPs constructed with mutated PD-1 ectodomains enhance PD-L1 binding

We hypothesized that the utility of PD-1/CD28 IFPs for tumors with physiological PD-L1 expression might be improved if receptor affinity was increased. To enhance PD-L1 binding, we made a single point mutation (A132L) in the wild-type (WT) 155aa IFP, which decreases the equilibrium dissociation constant (K_d) for binding to human PD-L1 or PD-L2 by 15-fold or 30-fold, respectively (*436*). We also constructed two higher affinity ectodomains – G1-41 and HAC

– with nanomolar and picomolar affinity, using sequences identified by directed evolution of PD-1 (*435*). All modifications were made to the 155aa IFP, because it contained fewer potentially immunogenic peptides at the fusion site between PD-1 and CD28 than the 165aa IFP (data not shown). With this work, we obtained a panel of chimeric PD-1/CD28 receptors spanning more than a 100,000-fold range of affinity (**Figure 5.3A**).

We cloned each mutant into our tricistronic lentiviral vector, transduced and expanded FACS-purified $CD8^{+}tCD19^{+}$ T cells. After expansion, flow cytometric analysis demonstrated that high-affinity IFPs enhanced binding to soluble human PD-L1 compared to the WT IFP (**Figure 5.3B**). The HAC IFP stained with the greatest MFI, followed by the A132L, G1-41, and WT IFPs. Notably, despite possessing a higher theoretical affinity than A132L, the G1-41 variant did not stain as brightly as A132L, suggesting that the G1-41 mutant may have folded improperly or aggregated on the T cell surface, as previously described (*435*).

Additional IFP expression analyses were performed using three PD-1 mAb clones (eBioJ105, MIH4, and EH12.1 that bind different epitopes) to address possible disruption of antibody binding to mutant PD-1 ectodomains (*444*, *445*). Each mAb displayed different staining patterns, but the A132L and HAC IFPs stained similarly to the WT IFP with at least one mAb (**Figures 5.S1C**). The G1-41 IFP stained weakly with all three mAbs, further suggesting it had not folded properly on the cell surface (*435*). Based on these data, we reasoned that A132L and HAC IFPs were expressed at similar levels to the WT IFP and possessed enhanced PD-L1 binding capacities.

A

Ectodomain	PD-L1 Affinity (K_d)
Wild-type (WT)	3.88-6.36μM
A132L	140nM
G1-41	7.78nM
HAC	110pM

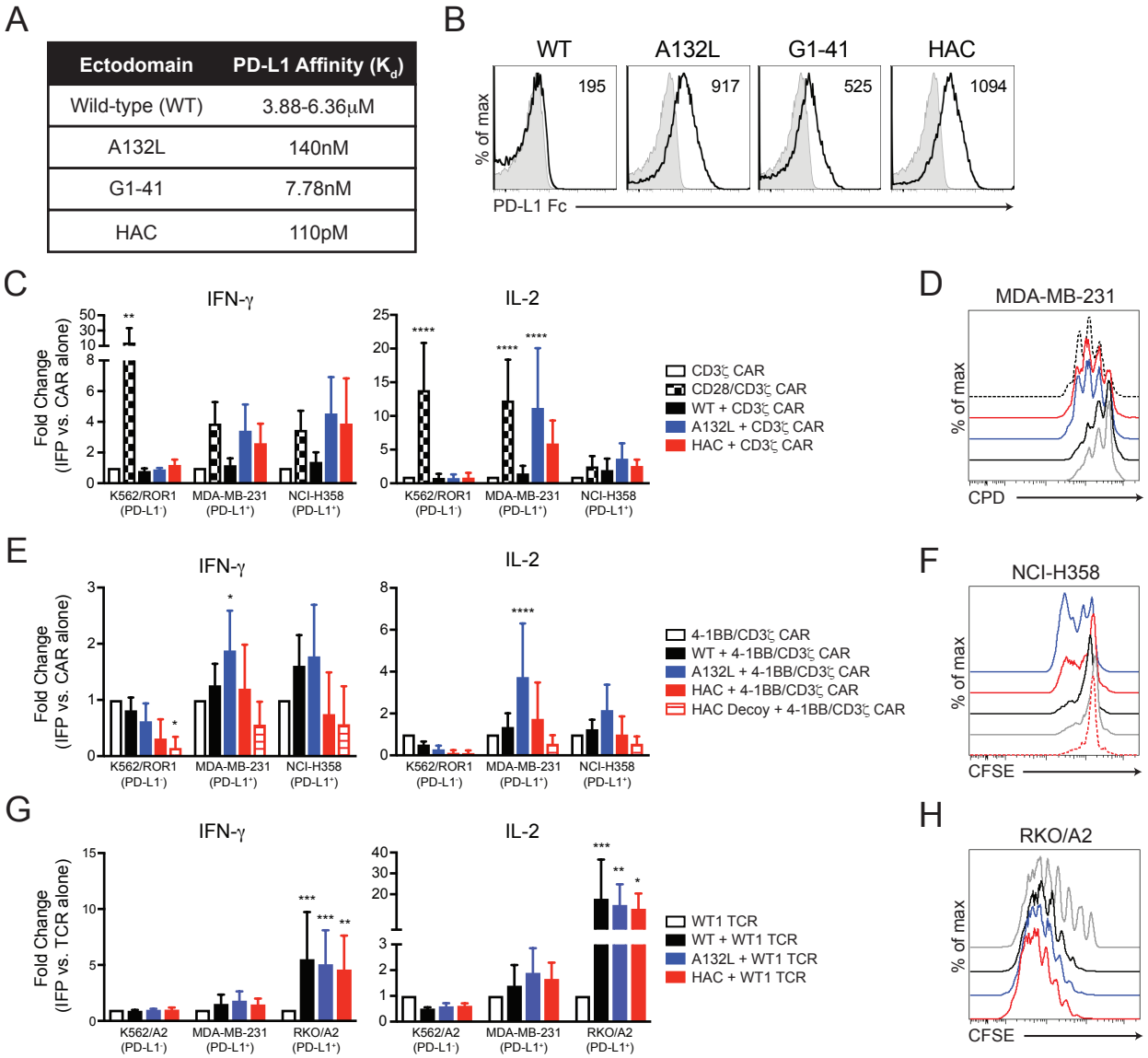

Figure 5.3. IFPs bearing mutated PD-1 ectodomains increase PD-L1 binding and improve CAR and TCR-T cell cytokine production and proliferation. (**A**) Table shows theoretical PD-L1 binding affinity of PD-1 ectodomain mutants. (**B**) Flow cytometry analysis of PD-L1 Fc staining. Histogram plots show IFP$^+$ CAR T cells (black) and IFP$^-$ CAR T cells (grey) singlets. Data representative of 2 independent experiments. (**C, E, and G**) ELISA analysis of cytokine production 24 hours after co-culture of ROR1 CAR T cells or WT1 TCR-modified T cells with tumor cells. Data are means + SD of 3 (C), 5 (E), or 3 (G) independent experiments. (**D, F, and H**) Flow cytometry analysis of T cell proliferation as measured by CFSE or CPD dilution at 72 hours after co-culture with the indicated tumor cells. Histogram plot of IFP$^-$ T cells (grey), WT IFP$^+$ T cells (black), A132L IFP$^+$ T cells (blue), HAC IFP$^+$ T cells (red), IFP$^-$ CD28/CD3ζ CAR T cells (black dotted), and HAC Decoy$^+$ CAR T cells (red dotted). Data representative of 4 (D), 5 (F), or 3 (H) independent experiments. The indicated *P* values were calculated by two-way ANOVA with Dunnett's multiple comparisons test comparing samples to CD3ζ CAR (C), 4-1BB/CD3ζ CAR (E) or WT1 TCR (G). * denotes $P \leq 0.05$, ** denotes $P \leq 0.01$, *** denotes $P \leq 0.001$, and **** denotes $P \leq 0.0001$.

High-affinity PD-1/CD28 IFPs significantly enhance CAR T and TCR-T cell cytokine production and proliferation

We next asked whether more efficient IFP PD-L1 binding translated into improved $CD8^+$ T cell functionality *in vitro*. Co-culture of high-affinity IFP+ CD3ζ ROR1-targeting CAR T cells with $ROR1^+PD\text{-}L1^+$ MDA-MB-231 and NCI-H358 tumor lines led to marked increases in IFN-γ and IL-2 production that were not observed with the WT IFP, or upon co-culture with $PD\text{-}L1^-$ K562/ROR1 cells (**Figure 5.3C**). The A132L IFP, with a 45-fold increased affinity for PD-L1, outperformed both the WT and HAC IFPs, and markedly increased IL-2 production to a level equivalent to or greater than that from a second-generation CD28/CD3ζ ROR1-targeting CAR. Consistent with these results, we observed increased proliferation among T cells expressing A132L or HAC IFPs, after 72 hours of co-culture with $PD\text{-}L1^+$ MDA-MB-231 cells (**Figure 5.3D**). We did not detect any differences in T cell cytotoxicity, at effector-to-target ratios from 30:1 to 1:1, when IFP^+ CAR T cells were incubated with $PD\text{-}L1^-$ K562/ROR1, or $PD\text{-}L1^+$ MDA-MB-231 or NCI-H358 cells (data not shown).

Second-generation CARs possessing a costimulatory domain promote increased T cell persistence and more robust antitumor responses than first-generation CAR T cells possessing only a CD3ζ endodomain (*266*). To ascertain whether high-affinity IFPs would enhance the function of second-generation CAR T cells where costimulatory signals are already provided by the CAR itself, we modified the tricistronic lentiviral vector to encode a second-generation 4-1BB/CD3ζ ROR1-targeting CAR after the IFP, and transduced and expanded FACS-purified transduced ($CD8^+tCD19^+$) T cells (*253*). Upon co-culture with $PD\text{-}L1^+$ tumor cells, A132L IFP^+ CAR T cells produced markedly more IFN-γ and IL-2, and proliferated to a greater extent than conventional CAR T cells (**Figures 5.3E-F**). WT and HAC IFP^+ CAR T cells also displayed enhanced cytokine production and proliferation, although to lesser degrees than A132L IFP^+ CAR T cells. Similar results were observed with $CD4^+$ T cells (**Figure 5.S2**). We also tested a PD-1 decoy receptor, bearing the HAC ectodomain but no CD28 signaling endodomain, but this decoy receptor failed to increase cytokine production or cell proliferation. We concluded that IFP CD28 signaling enhanced CAR T cell functionality.

T cells modified to express tumor-specific TCRs have also demonstrated antitumor activity in clinical trials, and we asked whether high-affinity IFPs would improve the functionality of TCR-T cells. We constructed a tricistronic lentiviral vector encoding a WT, A132L, or HAC IFP linked by T2A sequence to the β and α chains from a high-affinity HLA-A2-restricted Wilms tumor antigen 1 (WT1)-targeting TCR (*427*). Transduced $CD8^+$ cells were FACS-purified with fluorescent WT1 peptide/HLA-A2 tetramers, expanded *in vitro*, and co-cultured with WT1

peptide-pulsed HLA-A2-transduced PD-L1$^-$ K562 (K562/A2) cells, peptide-pulsed HLA-A2$^+$PD-L1$^+$ MDA-MB-231 cells or peptide-pulsed HLA-A2$^+$PD-L1$^+$ RKO/A2 colon carcinoma cells (**Figure 5.S1A**). Inclusion of any IFP enhanced the cytokine production and proliferation of WT1-specific TCR-T cells upon co-culture with PD-L1$^+$ tumor cells (**Figures 5.3G-H**). Minimal increases in cytokine production were detected when WT1-specific IFP$^+$ TCR-T cells were co-cultured with PD-L1$^-$ K562/A2 cells. Notably, both WT and high-affinity IFPs enhanced T effector functions upon co-culture with RKO/A2 cells, which express high levels of both PD-L1 and PD-L2. Taken together, our data indicated that high-affinity PD-1/CD28 IFPs enhanced the antitumor functions of genetically modified T cells in multiple contexts, and that PD-1 ligand expression impacted the degree of functional enhancement.

High-affinity IFPs efficiently cluster and outcompete endogenous PD-1 into immunological synapses

Endogenous PD-1 and CD28 modulate T cell signaling in the immunological synapse formed between T cells and antigen presenting cells and/or tumor cells (*30*, *340*). High-affinity PD-1/CD28 IFPs could alter receptor distribution and/or biophysical interactions with tumor cells. To enable detection of the receptors by live-cell fluorescence microscopy, we fused mCherry to the C-terminus of WT, A132L and HAC IFPs, and fused eGFP to the C-terminus of a CD3ζ ROR1-specific CAR (**Figure 5.4A**). Transduced CD8$^+$eGFP$^+$mCherry$^+$ cells were FACS-purified and imaged using fluorescence microscopy. In the absence of tumor cells, IFPs and the ROR1-specific CAR were present on the T cell surface and in intracellular vesicles (**Figure 5.4A, top row**). Upon co-culture with K562/ROR1 cells (**Figure 5.4A, middle row**) or ROR1$^+$ MDA-MB-231 (**Figure 5.4A, bottom row**) cells, we detected synapse formation as fluorescent CAR clustering at the T cell:tumor cell interface. However, only the high-affinity A132L and HAC IFPs were recruited to the synapses formed with MDA-MB-231 cells expressing physiological PD-L1 levels. We rarely observed WT IFP clustering in the synapse formed between CAR T cells and MDA-MB-231 cells, and only witnessed efficient WT IFP clustering when PD-L1 was overexpressed in transduced MDA-MB-231 cells (**Figure 5.4B**).

A limitation of this microscopy was that the CAR T cells did not express endogenous PD-1 at the start of the co-culture. CAR T cells in immunosuppressive tumor microenvironments are likely to express endogenous PD-1, and any IFP would need to compete with endogenous PD-1 for binding to PD-L1. To determine whether IFPs could outcompete full-length PD-1 for entry into the T cell:tumor cell interface, we co-transduced CD8$^+$ T cells with a PD-1/eGFP fusion protein-encoding construct alongside a bicistronic lentiviral vector encoding a mCherry-tagged

IFP and non-fluorescent first-generation ROR1-specific CAR (**Figure 5.4C**). In this experiment, PD-1/eGFP served as a highly expressed competitor for PD-L1 binding. Notably, the A132L, but not WT, IFP efficiently clustered at the T cell:tumor cell interface upon co-culture with PD-L1$^+$ MDA-MB-231 tumor cells (**Figure 5.4C**). The A132L IFP occasionally even excluded PD-1/eGFP from the interface, demonstrating that high-affinity PD-1/CD28 IFPs can outcompete full-length PD-1 for PD-L1 binding.

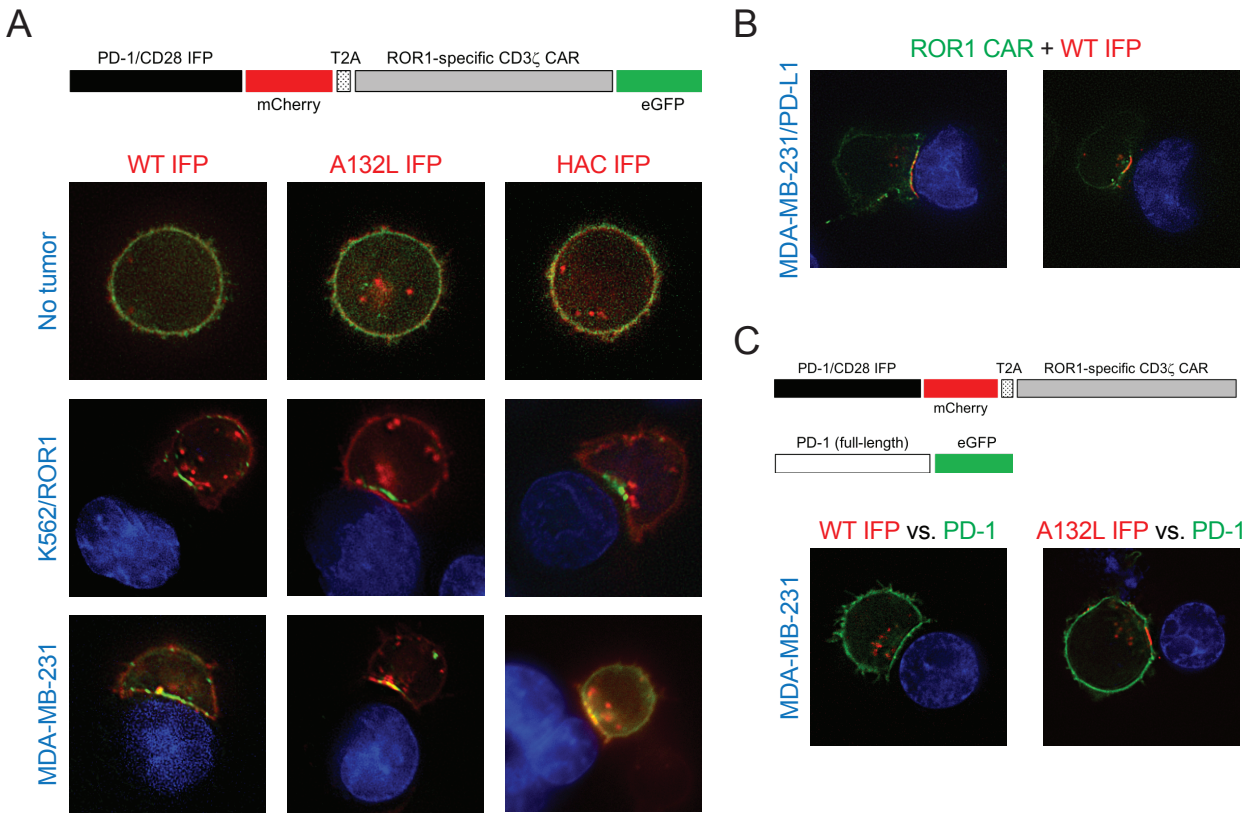

Figure 5.4. High-affinity IFPs efficiently cluster and outcompete endogenous PD-1 into immunological synapses. (**A**) Schematic of IFP-mCherry-T2A-CAR-eGFP construct and representative images of IFP$^+$ CAR T cells either alone (top row), or co-cultured with PD-L1$^-$ K562/ROR1 cells (middle row) or PD-L1$^+$ MDA-MB-231 cells (bottom row). (**B**) Representative images of WT IFP$^+$ CAR T cells co-cultured with MDA-MB-231/PD-L1 cells as in A. (**C**) Schematic of IFP-mCherry, unlabeled CAR, and PD-1-eGFP constructs, and representative images of IFP$^+$ CAR T cells co-cultured with MDA-MB-231 cells. Images are representative of 3 independent experiments with at least 6 cells/synapses visualized per condition.

PD-1/CD28 IFPs do not improve CAR T cell antitumor function in vivo

The marked functional enhancements mediated by high-affinity IFPs *in vitro* beckoned the question as to whether IFPs could improve T cell function in transplantable mouse tumor models. We first employed a xenograft model of MDA-MB-231 cells, in which NSG mice were engrafted with firefly luciferase-labeled MDA-MB-231 cells expressing endogenous levels of

ROR1 and PD-L1, and treated with a sub-curative dose of 5×10^6 $CD8^+$ T cells. Tumor burden decreased markedly in a preliminary experiment when PD-1 blocking mAb was combined with conventional IFP^- 4-1BB/CD3ζ CAR T cells (**Figure 5.S3A**). However, infusion of WT, A132L or HAC IFP^+ CAR T cells did not reduce tumor burden, compared to conventional IFP^- CAR T cells, and tumors grew in all mice after a 30-day period of partial tumor control (**Figure 5.5A**). IFP^+ and IFP^- CAR T cells accumulated to similar numbers in tumors and displayed similar frequencies of proliferating cells (**Figures 5.5B-C**). Thus, in contrast to our earlier observations that high-affinity IFP^+ CAR T cells displayed more potent effector functions *in vitro*, IFPs did not improve tumor control by CAR T cells *in vivo*.

To determine if high-affinity IFPs might enhance CAR T cell antitumor functions in other models, we treated mice bearing Raji/ROR1/PD-L1 lymphoma xenografts with a sub-curative dose of $CD4^+$ and $CD8^+$ IFP^+ or conventional IFP^- ROR1-specific or CD19-specific CAR T cells. IFP^+ ROR1-specific CAR T cells again failed prolong survival compared to conventional IFP^- CAR T cells (**Figures 5.5D-E**). Survival was lower among mice treated with CAR T cells expressing a HAC IFP, or especially with HAC or A132L IFP decoys lacking the CD28 signaling domain. We hypothesized that our results could reflect outgrowth of Raji cells that had downregulated ROR1 expression, and therefore repeated the experiment using IFP^+ and IFP^- CAR T cells specific for the CD19 antigen that is natively expressed on Raji cells. Nevertheless, mice treated with IFP^+ CD19-targeting CAR T cells displayed lower survival than mice treated with conventional CD19-targeting CAR T cells, regardless of IFP affinity or the presence of the CD28 signaling domain (**Figure 5.5F**). In both experiments, IFP^+ and IFP^- CAR T cells were detected at similar frequencies in peripheral blood after transfer (data not shown). Taken together, our data suggest that detrimental effects seen with high-affinity IFP^+ CAR T cells were not specific to the antigen target, IFP CD28 signaling or decreased T cell persistence.

PD-1/CD28 IFPs do not improve TCR-T cell antitumor function in vivo

PD-1/CD28 IFPs modestly increase the *in vivo* antitumor function of T cells that signal through their TCR (*228*, *438*, *439*). We asked whether high-affinity IFPs would increase survival after adoptive immunotherapy with transgenic gag-specific TCR-transgenic (TCR_{gag}) T cells in an immunocompetent model of murine $PD\text{-}L1^+$ FBL leukemia (*427*, *446*). Murine PD-1/CD28 IFPs were constructed by fusing the first 155aa of murine wild-type PD-1, murine wild-type PD-1 with an A132L mutation, or human HAC sequence to murine CD28 hinge, transmembrane and intracellular segments. High-affinity IFPs displayed enhanced binding to murine PD-L1 (**Figure 5.S3B**), but adoptive transfer of IFP^+ TCR_{gag} T cells into leukemia-bearing mice slightly reduced

the frequency of mice surviving to day 100, compared to transfer of control-transduced IFP$^-$ TCR$_{gag}$ T cells (**Figure 5.5G**). Thus, IFP expression also failed to improve the antitumor function of transgenic T cells that signaled through their TCR.

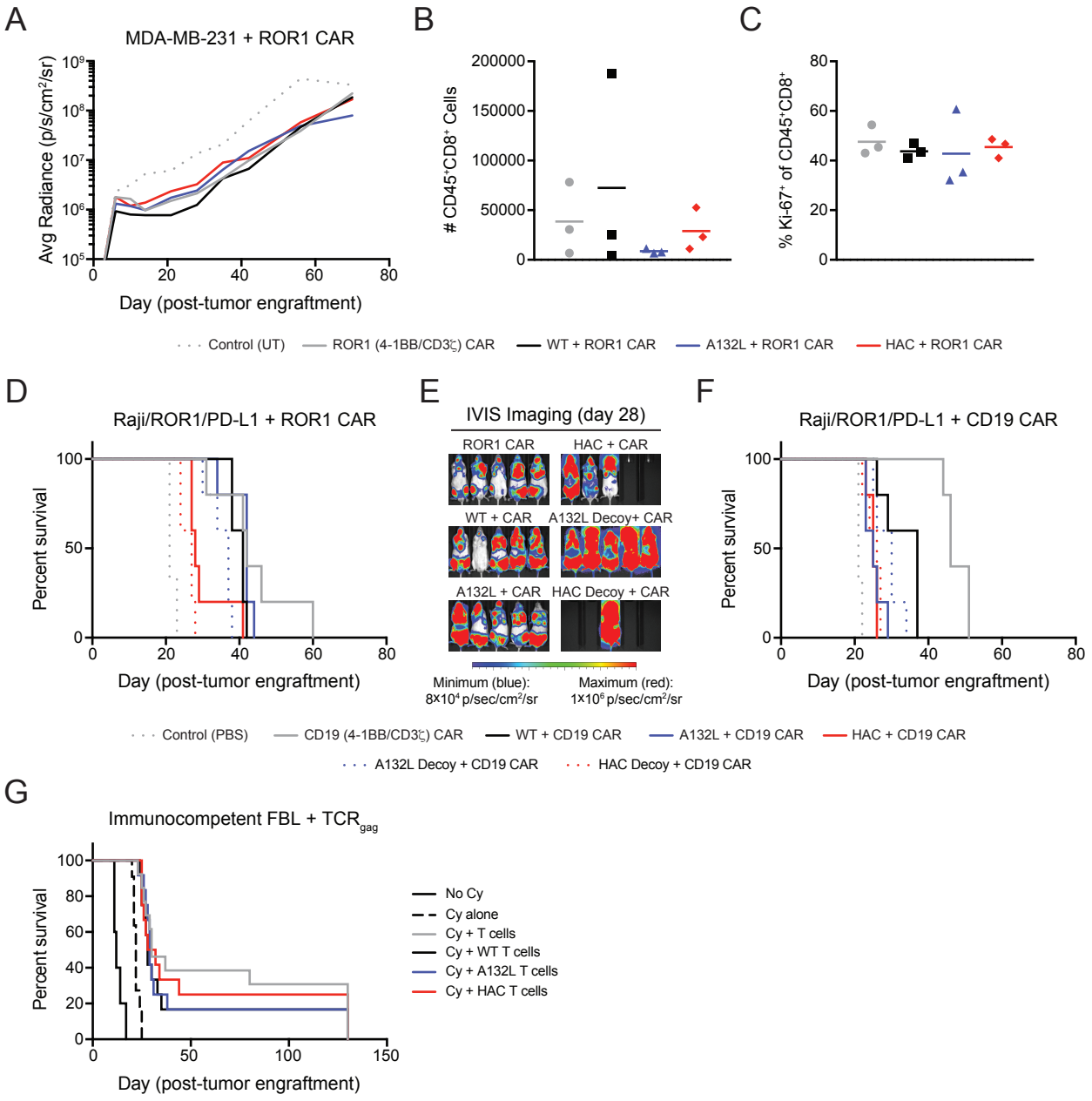

Figure 5.5. PD-1/CD28 IFPs do not improve CAR T cell or TCR-T cell antitumor function *in vivo*. (**A**) Bioluminescence analysis of NSG mice engrafted with MDA-MB-231/ffluc cells and treated with untransduced (UT) or ROR1 CAR T cells on day 7. (**B** and **C**) Flow cytometry analysis of total CD45$^+$CD8$^+$ T cell counts (B) or frequency of Ki67$^+$ cells among CD45$^+$CD8$^+$ singlets (C) from 3 mice per group treated as in A and sacrificed on day 43. (**D**) Survival curve of NSG mice engrafted with Raji/ROR1/PD-L1 tumors and treated with untransduced (UT) or ROR1 CAR T cells. (**E**) Bioluminescence images of Raji/ROR1/PD-L1/ffluc tumor burden in mice at the indicated time points. (**F**) Survival curve of NSG mice engrafted with Raji/ROR1/PD-L1 tumors and treated with phosphate buffered saline (PBS) or CD19 CAR T cells. (**G**)

Survival curve of C57BL/6 mice engrafted with FBL leukemia and left untreated (No Cy), treated with Cytoxan (Cy) alone, or Cy and IFP^+ or control IFP^- TCR_{gag} T cells. For panels A, D and F, n = 3 mice for groups receiving UT T cells or PBS and 5 mice for groups receiving CAR T cells. For panel G, n = 14 mice for groups receiving control-transduced TCR_{gag} T cells, and 12 mice per group for groups receiving IFP^+ TCR_{gag} T cells.

PD-L1 expression by non-transformed host cells may cause IFP^+ CAR T cell dysfunction

Finding that IFPs reduced the antitumor effects of both CAR and transgenic TCR T cells contradicted previously published data. We investigated possible reasons for this discrepancy, using Raji lymphoma-bearing mice as a model of IFP^+ T cell dysfunction. We first flipped the order of the lentiviral expression cassette to rule out possible differences in CAR expression stemming from placement of the IFP in front of the CAR. Despite equivalent levels of CAR expression, IFP^+ CAR T cells continued to reduce median survival (**Figures 5.S3C-D**). A separate experiment utilizing IFPs with the PD-1 transmembrane domain also demonstrated reduced survival (**Figure 5.S3E**). Therefore, reduced survival was not due to the ordering of the lentiviral cassette or the identity of the IFP transmembrane domain.

We noted that survival in some earlier experiments inversely correlated with IFP affinity, as higher affinity A132L and HAC IFP^+ CAR T cells displayed greater deficits in antitumor activity. In addition to increased affinity for human PD-L1 and PD-L2, the A132 point mutation confers enhanced binding to mouse PD-L1 and PD-L2 (*432*, *436*); the HAC ectodomain also binds murine PD-L1 (**Figure 5.6A**) (*435*). We hypothesized that IFPs constructed with affinity-enhanced PD-1 ectodomains may have inhibited the antitumor activity of CAR T cells by binding to murine PD-L1 or PD-L2 expressed on non-tumor cells in NSG mice. We inoculated mice with $PD\text{-}L1^-$ Raji cells that had not been transduced with PD-L1 lentivirus and treated tumor-bearing mice with IFP^+ CD19-specific CAR T cells. Consistent with our hypothesis, we observed reduced survival among IFP^+ CAR T cell-treated mice, even as Raji cells remained $PD\text{-}L1^-$ in the peripheral blood (**Figures 5.6B-C**). Thus, tumor cell expression of human PD-L1 was not responsible for the diminished survival.

To look for sources of murine PD-L1 expression, we harvested bone marrow and lung from non-tumor bearing NSG mice. Bone marrow $CD45^+CD11b^+Ly6G^+$ neutrophil progenitors, but not $CD45^+CD11c^+$ dendritic cell progenitors, expressed high levels of PD-L1 (**Figure 5.6D**). $CD45^+CD11b^+Ly6G^+$ neutrophils remained $PD\text{-}L1^+$ in the lung, and we also detected PD-L1 expression on $EpCAM^+$ epithelial cells (**Figure 5.6E**). We hypothesized that these endogenous cells may directly interact with adoptively transferred IFP^+ CAR T cells to influence their antitumor function. However, we were unable to further study how the endogenous cells were impacting CAR T cell function due to a lack of available PD-L1 knockout NSG mice.

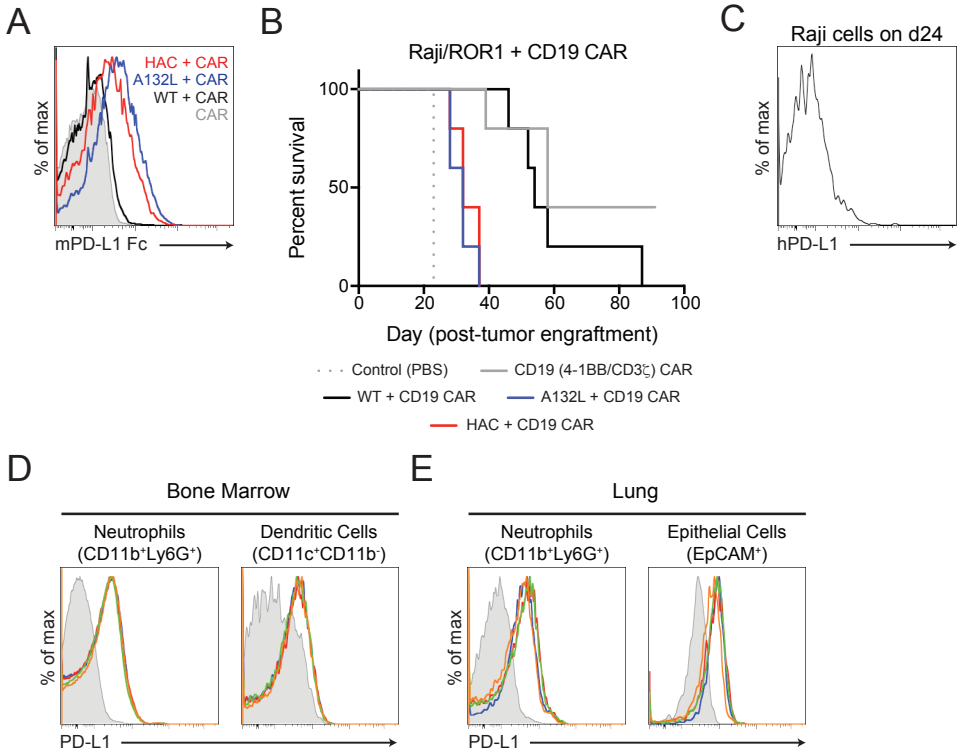

Figure 5.6. IFP dysfunction is not related to tumor cell PD-L1 expression. (**A**) Flow cytometry analysis of mouse PD-L1 Fc staining. Histogram plots show IFP$^-$ CAR T cells (grey) and WT (black), A132L (blue), and HAC (red) IFP$^+$ CAR T cell CD8$^+$ singlet lymphocytes. (**B**) Survival curve of NSG mice engrafted with Raji/ROR1 tumors and treated with PBS or CD19 CAR T cells. n = 3 mice for groups receiving UT T cells or PBS and 5 mice for groups receiving CAR T cells. (**C**) Flow cytometry analysis of PD-L1 expression on circulating Raji/ROR1 cells in peripheral blood 24 days after tumor inoculation as in A. Histogram plot shows CD45$^+$GFP$^+$ singlets and is representative of 23 mice. (**D** and **E**) Flow cytometry analysis of PD-L1 staining on neutrophils, dendritic cells, or epithelial cells in the bone marrow (C) or lung (D) of NSG mice. Histogram plot of fluorescence minus one control (grey), or four mice (red, green, blue, orange).

Discussion

A potential strategy to circumvent immunosuppressive regulation of CAR T or TCR-T cells is to add an IFP that converts inhibitory signals into positive costimulatory signals. Compared to conventional IFP$^-$ CAR T cells, PD-1/CD28 IFPs enhance CAR T cell antitumor function *in vitro* and in a xenograft model of pancreatic cancer (*347*). IFPs also slightly improve *in vitro* and *in vivo* function when added to transgenic or TCR-T cells that signal through a TCR, especially when the tumor-specific TCR is of low-affinity (*228*, *438*, *439*). Two limitations of the prior studies are that IFPs produced marginal benefits and that the majority of functional analyses utilized recombinant PD-L1 or tumor cells transduced to overexpress PD-L1.

In our hands, PD-1/CD28 IFPs based on the wild-type PD-1 sequence did not enhance CAR T cell cytokine production or proliferation in co-culture assays with tumor cells expressing

endogenous levels of PD-L1. By modulating the amount of PD-L1 on tumor cells, we show that PD-L1 expression levels influenced IFP activity. IFPs containing PD-1 ectodomain variants with increased affinity for PD-L1 and PD-L2 enhanced T cell function in settings where tumor cells expressed low levels of PD-L1 and/or PD-L2. In contrast, IFPs based on the low affinity wild-type PD-1 sequence required high endogenous PD-L1 or PD-L2 expression (as on RKO/A2 cells) or PD-L1 overexpression (as on MDA-MB-231/PD-L1 cells) to increase T cell function.

When tested in transplantable tumor models expressing different amounts of PD-L1, inclusion of WT or high-affinity IFPs failed to improve CAR T cell or TCR-transgenic T cell antitumor function. Raji tumor-bearing mice treated with IFP^+ CAR T cells died even earlier than mice receiving conventional IFP^- CAR T cells. While Raji cells were not an ideal target due to forced PD-L1 overexpression, the addition of PD-1 mAb to IFP^- CAR T cell therapy had improved survival in a separate experiment and we expected to find improved survival among mice treated with IFP^+ CAR T cells. Investigation of the basis for reduced survival demonstrated that tumor PD-L1 expression was irrelevant for IFP^+ T cell dysfunction and suggested that endogenous $PD\text{-}L1^+$ or $PD\text{-}L2^+$ expressing cells may interfere with IFP^+ T cell function.

High-affinity binders have been used in CARs specific for tumor-association antigens and are frequently pursued as a strategy to confer tumor selectivity and binding to lowly-expressed TAAs (*447*). This strategy appears to be valid when targeting TAAs with limited tissue expression, but PD-L1 and PD-L2 are widely expressed on hematopoietic and epithelial cells (*340*). High-affinity PD-L1 binders expressed on the T cell surface may bind to endogenous non-transformed cells, such as $PD\text{-}L1^+$ neutrophil progenitors in the bone marrow, and thereby reduce intended contact with $ROR1^+$ or $CD19^+$ lymphoma cells. Viable NSG mice with homozygous mutations in PD-L1 are not commercially available, which limited our ability to test this hypothesis. Nevertheless, ongoing work is focused on developing an *in vitro* co-culture system with murine $PD\text{-}L1^+$ tumor cells and murine PD-L1 blocking antibody to more comprehensively assess the effects of murine PD-L1 expression on human IFP^+ CAR T cells.

The lack of improved antitumor function observed with membrane-expressed PD-L1 binders contrasts with previous demonstrations of soluble PD-1/PD-L1 mAbs and high-affinity PD-L1 binders based on the same A132L and HAC ectodomains (*435*, *436*, *448*). Thus, our data suggest that designing high-affinity IFPs directed against widely-expressed target molecules like PD-L1 and PD-L2 may have limited translational utility due to unpredictable *in vivo* effects. Engineering T cells to secrete high-affinity binders that block immunosuppressive pathways may produce greater functional benefits when combined with existing T cell immunotherapies.

Materials and Methods

Vector construction

CD19- and ROR1-specific second-generation CD28/CD3ζ and 4-1BB/CD3ζ CARs with a FMC63 or R12 scFv and 12aa IgG4 hinge were previously described (*253*, *260*). A first-generation CAR with R12 scFv, IgG4 hinge, CD4 transmembrane domain (UniProt: P01730), and CD3ζ endodomain was constructed using fusion PCR. Human IFPs were assembled by fusing the first 155 amino acids of human PD-1 (UniProt: Q15116) to amino acid 141 of human CD28 (Uniprot: P10747), the first 165 amino acids of PD-1 to amino acid 153 of CD28, or the first 191 amino acids of PD-1 to amino acid 180 of CD28. Murine IFPs were constructed by fusing the first 155 amino acids of mouse PD-1 (UniProt: Q02242) to amino acid 139 of mouse CD28 (UniProt: P31041). IFPs with alanine to leucine mutations at amino acid 132 of human or murine PD-1 were constructed by site-directed mutagenesis. Codon-optimized G1-41 or HAC ectodomains were synthesized and cloned using Gibson assembly. Human IFPs were linked by T2A ribosomal skip elements to a CAR and truncated human CD19 (tCD19) molecule or truncated epidermal growth factor receptor (EGFRt). Human IFPs were linked by P2A ribosomal skip sequence to WT1-specific TCR β and α chains (*427*). For fluorescence microscopy, CARs and/or IFPs were fused to eGFP or mCherry. Murine IFPs were linked by P2A ribosomal skip element to a truncated mouse CD19 (mtCD19) molecule. Human IFP and CAR constructs were cloned into a HIV7 lentiviral vector, murine IFPs were cloned into a mp71 retroviral vector. All plasmids were verified by capillary sequencing and restriction enzyme digest.

Acquisition of primary human T cells and CD138$^+$ plasma cells

Healthy adults (>18 years-old) or individuals with multiple myeloma were enrolled in Institutional Review Board-approved studies for peripheral blood collection or bone marrow aspiration. Informed consent was obtained from all enrollees and researchers were blinded to personally-identifiable information about study participants. Peripheral blood was collected by venipuncture and mononuclear cells were isolated by density gradient. CD4$^+$ and CD8$^+$ T cells were further isolated from healthy donors using EasySep Human CD4 or CD8 T Cell Isolation Kits (StemCell Technologies). CD138$^+$ plasma cells were isolated from multiple myeloma patients using CD138 Microbeads (Miltenyi Biotec).

Cell Culture

293T LentiX cells were purchased from Clontech. K562 (CCL-243), NCI-H358 (CRL-5807), MDA-MB-231 (HTB-26), Raji (CCL-86), and RKO (CRL-2577) cells were obtained from American Type Culture Collection and cultured in appropriate media. K562/ROR1 and Raji/ROR1 cells were prepared by transducing parental cells with retroviral supernatant generated from transient transfection of LentiX cells with MLV g/p, 10A1, and a retroviral vector encoding human ROR1. Cell lines expressing HLA-A2, firefly luciferase (ffluc), and/or human PD-L1 were prepared by transducing parental cells with lentiviral supernatant generated from transient transfection of LentiX cells with psPAX2, pMD2.G, and lentiviral vectors encoding HLA-A2, GFP-tagged ffluc, or human PD-L1. Five days after transduction, cells were stained for ROR1, HLA-A2, and/or PD-L1 and sorted on a FACSAria II (BD Biosciences) to >97% purity. psPAX2 and pMD2.G packaging plasmids were gifts from Didier Trono (Addgene Plasmid #s 12259 and 12260). Primary human T cells were cultured in CTL medium consisting of RPMI-1640 supplemented with 10% human serum, 2mM L-glutamine, 25mM HEPES, 100U/mL penicillin/streptomycin, 50μM β-mercaptoethanol, and 50 U/mL IL-2. All cells were cultured at 37°C and 5% CO_2, and tested bi-monthly for the absence of mycoplasma.

Lentivirus preparation and human T cell transduction

Lentivirus was generated by transient transfection of LentiX cells using psPAX2, pMD2.G, and a lentiviral vector encoding IFP and CAR or TCR genes. Primary human T cells were activated and transduced as described (*425*). Transduced (tCD19$^+$, EGFRt$^+$, or tetramer$^+$) T cells were purified on day 9 and expanded over a single stimulation cycle prior to functional analyses. CD19-specific CAR T cells were expanded by co-culture with irradiated CD19$^+$ lymphoblastoid cell lines (LCL) in a 1:7 (T cell:LCL) ratio and assayed 8 days after stimulation. ROR1-specific CAR T cells were expanded using a rapid expansion protocol containing purified OKT3, irradiated LCL, and irradiated PBMC, and assayed 11 days after stimulation. During expansion, cultures were fed every 2-3 days with CTL supplemented with 50 U/mL IL-2.

Retrovirus preparation and mouse T cell transduction
Plat-E cells (Cell-Bio Labs) were transfected using Effectene transfection reagent (Qiagen) and viral supernatant was collected 48 and 72 hours later. One day prior to transfection, TCR_{gag} T cells were stimulated with anti-CD3/CD28 and 100 IU/mL human IL-2. Transduction of TCR_{gag} T cells was performed in 12 well plates in the presence of IL-2 and Polybrene by spinoculation for 90 minutes at 1000*g*. Transduced cells were restimulated 7 days post stimulation in the presence of irradiated splenocytes (5×10^6), irradiated FBL (3×10^6), and IL-2.

Immunophenotyping
Cells were stained with combinations of the following conjugated monoclonal antibodies at a 1:100 dilution: CD4 (RPA-T4), CD8 (SK1), CD19 (HIB19), CD273 (MIH18), CD274 (29E.2A3), CD279 (eBioJ105, EH12.1, and MIH4), HLA-A2 (BB7.2), ROR1 (2A2), and matched isotype controls. HLA-A2/WT1 tetramer was generated by the Immune Monitoring Lab at the Fred Hutchinson Cancer Research Center. PD-L1 binding capacity was assessed by staining with 100nM biotinylated human PD-L1/Fc (RND Biosystems) or 100nM mouse PD-L1/Fc (RND Biosystems), followed by washing and secondary staining with streptavidin-allophycocyanin (ThermoFisher Scientific) or anti-human IgG (Biolegend). Samples were acquired on a FACSCanto II or Celesta (BD Biosciences) and analyzed with FlowJo (Treestar).

Western blotting
Purified CD8$^+$ T cells were lysed using NP40 Cell Lysis Buffer (ThermoFisher Scientific) containing protease and phosphatase inhibitors (Sigma). Equal masses of protein lysate were loaded into 4-12% Bis-Tris NuPAGE Gels (ThermoFisher Scientific) and transferred onto nitrocellulose membranes (ThermoFisher Scientific). Membranes were blocked with Western Blocking Reagent (Sigma) and stained with anti-human CD247 (8D3, BD Biosciences), anti-CD28 (D2Z4E, Cell Signaling), anti-mouse HRP (polyclonal, Cell Signaling), and anti-rabbit HRP (polyclonal, Cell Signaling) diluted in SuperBlock (ThermoFisher Scientific) with 0.1% Tween-20. Typical antibody dilutions ranged from 1/10,000 to 1/4000. For experiments showing simultaneous staining with CD28 and CD247, two identical gels were loaded using one master loading mix.

In vitro functional assays
CAR T cells were co-cultured with irradiated K562/ROR1, MDA-MB-231, or NCI-H358 tumor cells at a T cell to tumor cell ratio of 2:1. WT1 TCR-modified T cells were co-cultured with irradiated and peptide-pulsed (0.2μg/mL WT1 peptide, RMFPNAPYL) K562/A2, MDA-MB-231, or RKO/A2 cells at a T cell to tumor cell ratio of 1:1. After 24 hours of stimulation, cytokine concentrations in cellular supernatant were quantified by ELISA (ThermoFisher Scientific). T cell proliferation was quantified by staining T cells with a 0.2μM solution of carboxyfluorescein succinimidyl ester (CFSE) dye (ThermoFisher Scientific) or 0.5μM solution of Cell Proliferation Dye (ThermoFisher Scientific) and incubating T cells with irradiated tumor cells for 72 hours.

Fluorescence microscopy
$CD8^+$ T cells from healthy donors were transduced and FACS-purified. Cells were cultured for 72 hours in CTL supplemented with 50 U/mL IL-2 and then imaged on a Deltavision Elite microscope (GE Healthcare). At least 5 cells were visualized per condition and 3 independent experiments were performed. ImageJ (NIH) was used to split raw images into individual color channels, perform linear adjustments of brightness and contrast, and merged channels into a composite image.

MHC binding prediction
Binding affinities of 8- to 14-mer peptides derived from IFP sequences that are not encoded by the human genome were predicted using NetMHC (*449*).

Adoptive immunotherapy of human tumor xenografts in NOD/SCID/$\gamma c^{-/-}$ (NSG) mice
Six- to eight-week-old male and female NSG mice were obtained from The Jackson Laboratory or bred in house. Mice were engrafted with 5×10^5 MDA-MB-231/ffluc cells in the right flank using subcutaneous injection, or 5×10^5 Raji/ROR1/ffluc cells using intravenous injection. Seven days after tumor engraftment, mice were injected intravenously with genetically modified T cells, untransduced (UT) T cells, or saline (PBS). Bioluminescence imaging and retro-orbital blood collection was performed as described (*198*). For PD-1 blocking experiments, 10 mg/kg anti-PD1 antibody (2H12.EH7, Biolegend) was injected intraperitoneally on days 10, 15, 20, and 25. Mouse handlers were blinded to group allocation.

Adoptive immunotherapy of disseminated FBL leukemia in immunocompetent mice
C57BL/6J mice were purchased from The Jackson Laboratory. TCR_{gag} transgenic mice express in $CD8^+$ T cells a TCR specific for the Friend virus gag epitope (peptide CCLCLTVFL) of the B6 Friend virus induced erythroleukemia (FBL) (*450*, *451*). Eight-week-old mice were injected intraperitoneally with 4×10^6 FBL cells. After 5 days to allow FBL to disseminate, mice received 180 mg/kg cyclophosphamide (Cy) intraperitoneally 6 hours before intravenous transfer of the 1×10^5 IFP-transduced or empty vector control-transduced TCR_{gag} T cells. T cells were stimulated twice *in vitro* prior to adoptive transfer. Mice were regularly monitored for increasing tumor burden and euthanized if the evidence of tumor progression predicted that mortality would occur within 24 to 48 hours.

Statistics
Appropriate statistical tests with post-hoc multiple comparisons testing were performed using Prism Software version 7.0d (GraphPad).

Supplementary Figures

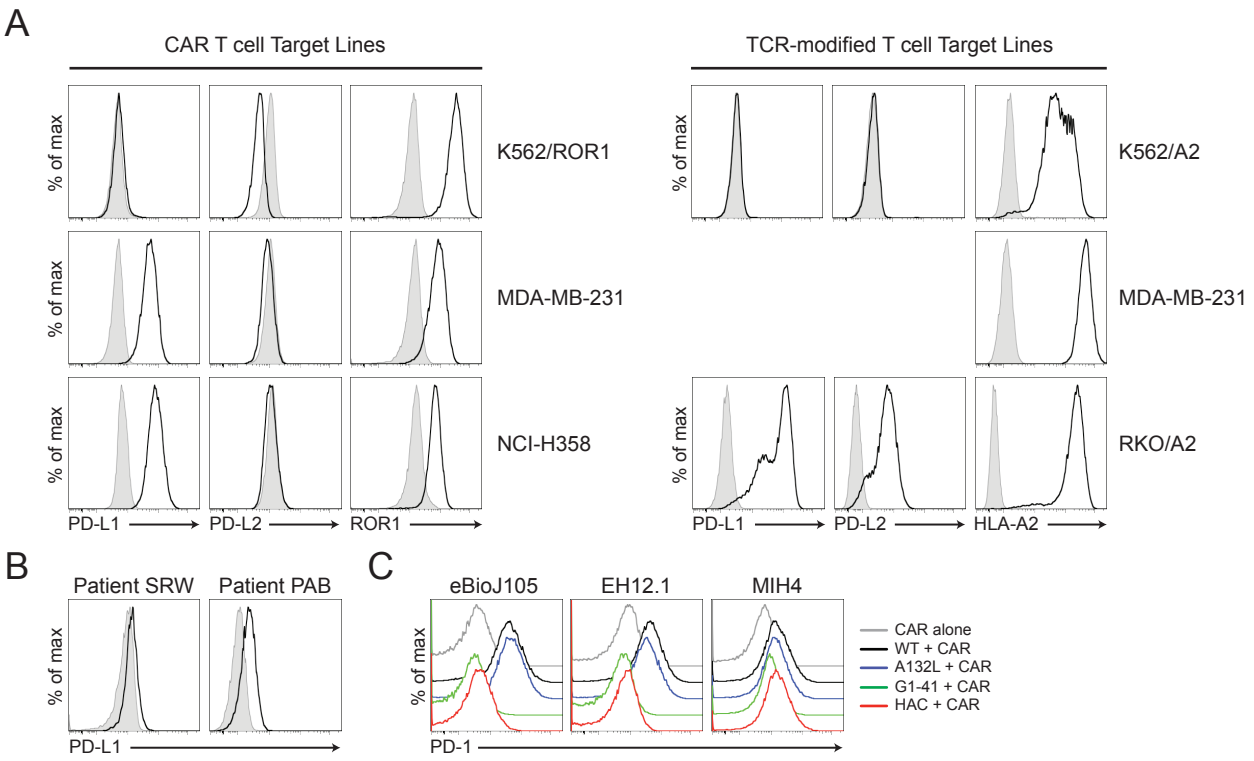

Figure 5.S1. Tumor cell antigen and T cell IFP expression patterns. (**A**) Flow cytometric analysis of HLA-A2, ROR1, PD-L1, and PD-L2 expression on tumor cell lines. Histogram plots show stained (black) and isotype control (grey) singlets. (**B**) Flow cytometric analysis of PD-L1 expression on primary myeloma samples. Histogram plots show stained (black) and isotype control (grey) $CD138^+$ singlet lymphocytes. (**C**) Flow cytometric analysis of PD-1 expression by IFP^+ CAR T cells after sorting and expansion using three different antibody clones - eBioJ105, EH12.1, and MIH4. Histogram plots show $CD8^+$ singlet lymphocytes and are representative of 2 independent experiments.

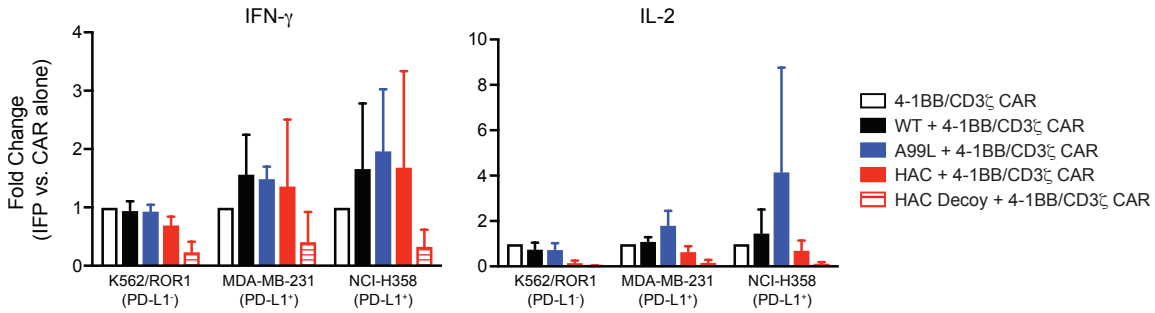

Figure 5.S2. High-affinity PD-1/CD28 IFPs improve CD4⁺ CAR T cell cytokine secretion. ELISA analysis of cytokine production 24 hours after co-culture of CD4⁺ CAR T cells with tumor cells. Data are means + SD of 4 independent experiments.

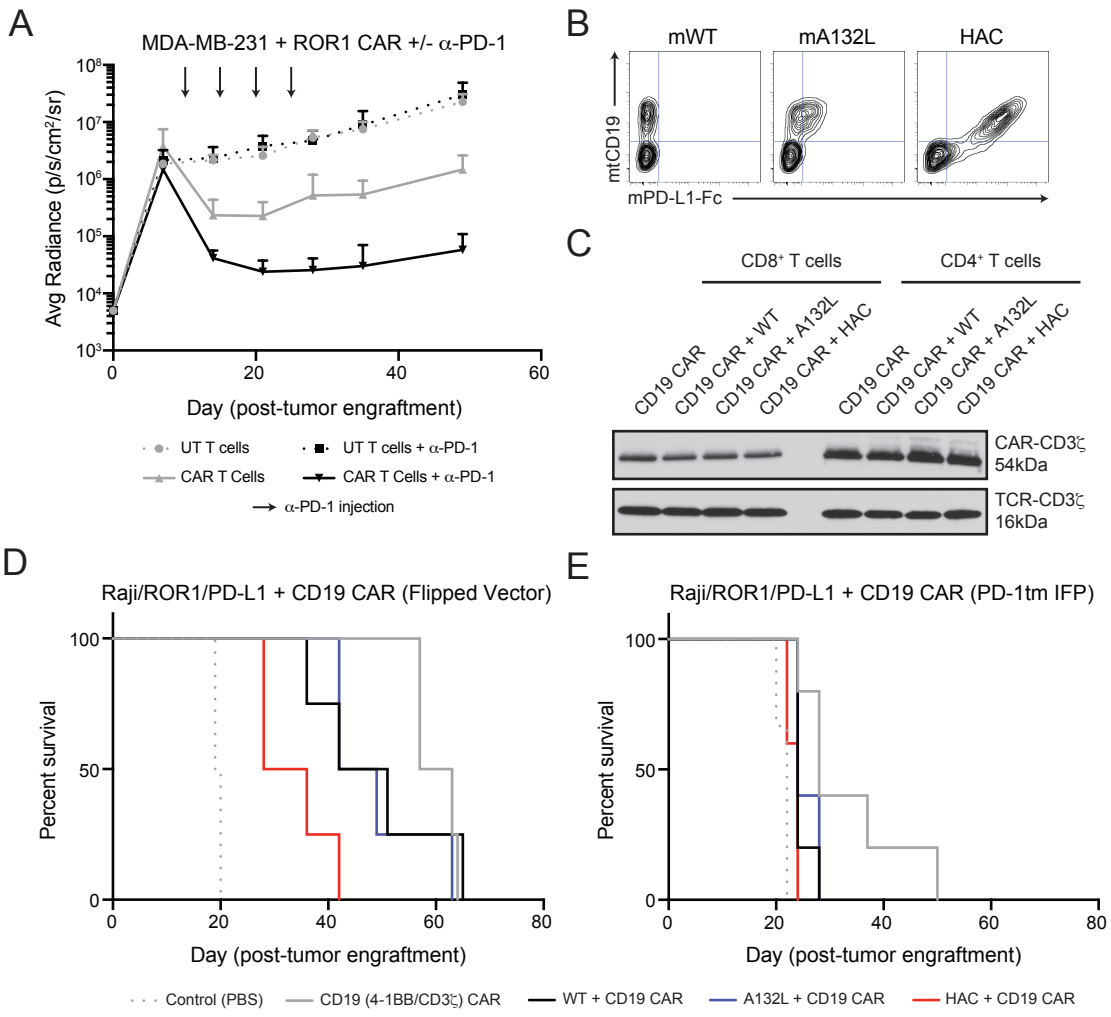

Figure 5.S3. PD-1/CD28 IFPs do not enhance CAR T cell functionality in murine xenograft tumor models. (**A**) Graph shows mean and standard deviation of bioluminescence imaging of NSG mice engrafted with MDA-MB-231/ffluc cells and treated with ROR1 CAR T cells and anti-PD-1 mAb. Vertical arrows denote dates of anti-PD-1 mAb injection. n = 4 mice per group. (**B**) Representative FACS plots of murine T cells after transduction show all live CD8$^+$ singlet lymphocyte events. C) Western blot analysis of CAR expression in CD4$^+$ and CD8$^+$ IFP-expressing CAR T cells used in panel D. D) Survival analysis of NSG mice engrafted with Raji/ROR1/PD-L1 cells and treated with the indicated CAR T cells. n = 2 mice for groups receiving a control PBS injection and 4 mice for groups receiving CAR T cells. E) Survival analysis of NSG mice engrafted with Raji/ROR1/PD-L1 cells and treated with various CAR T cells. n = 3 mice for groups receiving a control PBS injection and 5 mice for groups receiving CAR T cells.

Chapter 6
Concluding Remarks

Adoptive T cell therapies employ tumor-reactive T lymphocytes that have either been isolated from a patient's blood or tumor, and/or genetically modified to express a tumor-specific TCR or CAR. After years of slow but steady progress, the field took off with the advent of 'second-generation' CARs that combined a costimulatory signaling domain with the CD3ζ T cell activating domain (*443*). Striking results emerged from the first clinical trials of second-generation CD19-specific CAR T cells in 2011. Greater than 75% of children and adults with advanced chemotherapy refractory acute lymphoblastic leukemia achieved a complete response (*224*, *289-291*, *302*). Complete response rates were more modest for patients with non-Hodgkin's lymphoma and chronic lymphocytic leukemia (*225*, *297*, *303*, *357*), but real successes in dire clinical settings highlighted CAR T cells as proof of immunotherapy's promise.

Since 2011, there has been an urgency to apply CAR T cell therapy to other hematological and epithelial malignancies, and potential pitfalls were arguably overlooked amid the excitement. First, a significant fraction of patients who initially responded to CD19 CAR T cell therapy later relapse (*224*, *294*, *398*, *408*). Second, CAR T cell therapies have to date not generated similarly dramatic responses in solid tumors, like breast carcinoma, lung carcinoma, or glioblastoma (*426*). It is now apparent that what works for B cell malignancies is imperfect and may not translate to other clinical settings. Thus, additional research including a focus on understanding the function of current CAR designs is necessary to improve safety and optimize efficacy for B cell malignancies and other types of cancer.

The rapid applications of current CAR designs to new clinical settings left many unanswered questions about the biological mechanisms underpinning successful CAR T cell therapy. We, as a field, do not know precisely: 1) how CARs with different signaling modules direct T cell functions and fate, 2) how CAR signaling compares to TCR signaling, or 3) how synthetic receptor affinity and signaling can contribute to toxicity and immediate versus long-term efficacy. My dissertation research sought to add to our understanding of how various receptor attributes influence T cell function and fate, with the ultimate goal of guiding optimization in the design of future synthetic receptors.

In Chapter 3, I described the development of a shotgun MS platform for interrogating phosphoprotein signaling events in primary human T cells. This approach has heretofore not been used for primary human T cells and required the development of novel techniques for activating signaling through the CAR using ligand coated beads to ensure downstream signaling events resulted only from the CAR. I applied this technology to compare the two most common types of CAR T cells in clinical use containing either CD28/CD3ζ or 4-1BB/CD3ζ signaling domains. My results showed that both receptor types altered protein phosphorylation in highly

similar fashions, dispelling a previous assumption in the field that CARs with different costimulatory domains signal through different pathways, which has guided CAR design. Instead, the data showed that CD28/CD3ζ CARs signaled with faster kinetics and greater signal intensity than 4-1BB/CD3ζ CAR T cells. These differences in signal strength persisted across time and led to divergent cell fates; 4-1BB/CD3ζ CAR T cells expressed genes associated with T cell memory at higher levels that CD28/CD3ζ CAR T cells and adopted a more memory cell-like phenotype. Moreover, 4-1BB/CD3ζ CAR T cells were more potent in a tumor xenograft model of disseminated lymphoma and expressed lower levels of molecules associated with T cell exhaustion. Further analyses revealed selective Lck kinase association with the CAR CD28 signaling domain and not with 4-1BB, which we determined to be partly responsible for the increased downstream signal strength. Mutating the putative binding motif reduced Lck association with CD28/CD3ζ CARs and reduced CAR signal intensity. Notably, mutant CD28/CD3ζ CAR T cells retained antitumor function despite reduced Lck binding and were more effective than traditional CD28/CD3ζ CAR T cells *in vivo*. This work revealed the importance of endogenous T cell proteins that are important in signal transduction and associate differently with CARs with different costimulatory molecules.

While 4-1BB/CD3ζ CAR T cells displayed superior function in a model of disseminated lymphoma, the heightened activation and effector function of CD28/CD3ζ CAR T cells may be more appropriate in other settings. CD28/CD3ζ CAR T cells produce markedly more pro-inflammatory cytokines after receptor ligation and initiating inflammatory responses could be beneficial against solid tumors, which typically have an immunosuppressive microenvironment. One might envision a mixed T cell product composed of CD28/CD3ζ plus 4-1BB/CD3ζ CAR T cells as a multipronged attack, where CD28/CD3ζ CAR T cells rapidly infiltrate the tumor, initiate an inflammatory response and mediate immediate effector function, while longer-acting 4-1BB/CD3ζ CAR T cells kill residual tumor cells and provide long-term immunosurveillance. Formulating a multi-component T cell product has many challenges, but represents a possible future direction for CAR T cell therapy, particularly for solid tumors where efficacy has been more difficult to achieve. Finally, CAR T cells bearing mutated CD28/CD3ζ signaling domains might be tested in future trials. Dr. Riddell and I hold a patent covering applications of mutant CD28/CD3ζ for adoptive cell therapy.

In subsequent work, I applied MS to comprehensively compare TCR and CAR signaling. This required developing bi-specific human T cells expressing a mono-specific TCR and the CAR, and a new set of reagents to engage either the TCR or CAR in isolation in the same cell.

TCRs and CARs differ in their ability to recognize limiting antigen concentrations; designing CARs that efficiently recognize low-density antigens may improve therapeutic efficacy by reducing relapse rates and enabling the targeting of newly discovered tumor-associated antigens (*279*, *412*, *413*). At saturating antigen densities, my data revealed that TCRs and CARs initiate highly similar signaling events, but that certain key T cell signaling adapters were either not phosphorylated or less intensely phosphorylated by CAR stimulation. I concluded that CARs did not recapitulate all aspects of TCR signaling and hypothesized that these disparities may account for the observed differences in antigen sensitivity. Based on insights from the MS data, I am currently testing new CAR designs incorporating additional activation motifs and protein recruitment domains. Importantly, I have worked with the Paulovich lab to develop a targeted MS assay for 192 analytes, which will enable faster, quantitative and less expensive analysis of certain signaling events in T cells. I have also established collaborations with Dr. David Baker's laboratory at the University of Washington and Dr. Sarah Veatch's laboratory at the University of Michigan to test whether additional protein recruitment domains could enhance CAR sensitivity specifically for low-density antigens. I anticipate that continuation of this work before returning to medical school clerkships will further inform CAR design.

Finally, I studied the effects of increasing receptor affinity in the context of IFPs that augment how T cells process inhibitory signals. I asked whether using PD-1 ectodomain mutants to increase the affinity of PD-1/CD28 IFPs would enhance T cell function against tumor lines expressing low levels of the PD-1 ligand, PD-L1. While high-affinity IFPs improved T cell function *in vitro*, they reduced the antitumor function of CAR- and TCR-modified T cells *in vivo*. I was unable to fully untangle the reasons for these reductions, due to a lack of appropriate mouse models, but my data is consistent with the hypothesis that high-affinity IFPs bound to non-tumor PD-L1$^+$ cells *in vivo*, thereby reducing access to contact with ROR1$^+$ or CD19$^+$ lymphoma cells. Thus, my data indicate that significantly enhancing receptor affinity can have unintended consequences. Affinity enhancement has been pursued with both TCRs and CARs to improve peptide-MHC recognition or recognition of low-density cell surface antigens, respectively. In a notable case, TCR affinity enhancement resulted in a fatal off-target toxicity due to recognition of a cross reactive epitope, and my data adds to growing concerns that this approach should be undertaken cautiously (*215*, *240*, *283*, *452*). Detailed preclinical models are necessary to ensure that any on-target off-tumor effects are identified prior to clinical translation.

The *in vivo* antitumor function of genetically modified T cells primarily reflects how environmental stimuli are sensed and acted upon by synthetic receptors, but we know just enough about these processes to design successful receptors for a few clinical settings. It is still

widely assumed that synthetic receptors signal in isolation, but recent publications and the data presented in this thesis argue otherwise (*19*, *387*, *453*). Signaling pathways contain many shared components, and signaling from a single transgene is likely to have pleiotropic effects. Furthermore, the balance of positive and negative signaling can have profound impacts on cellular function1. As written in the quintessential textbook, *Janeway's Immunobiology*, "Signaling is usually not a simple 'on or off' switch, but frequently involved quantitative aspects of thresholds, amplitude, duration, and regulation. These features are often merged into the simple term 'signal strength.'" Whether we think of signaling initiated by a TCR, CAR, IFP, or natural cytokine or chemokine receptor, the sum of many individual signals through the receptor and associated molecules clearly determines overall signal strength, and the totality needs to be better understood.

The cancer immunotherapy field currently uses relatively simple approaches to co-opt cell signaling circuits, redirect T cell specificity and alter T cell behavior. Synthetic receptors like CARs and IFPs repurpose whole signaling domains from natural proteins, but new synthetic biology tools are becoming available. For example, signaling domains containing small binding motifs instead of entire endodomains could be used to more precisely tailor signaling outputs. Synthetic Notch receptors and new types of logic-gated proteins could also be used to enable T cells to sense and interpret multiple environmental cues (Appendix 1) (*428*). Moving forward, the field can apply these tools to design entirely novel synthetic receptors for T cell therapy.

However, we may harm patients if we do not learn more about how immune cells respond and signal. Designing safer and more effective cellular therapies that can benefit additional patients may require a change in how we perceive synthetic receptors interacting with endogenous proteins and signaling networks. Fundamental scientific research must improve our understanding of immunological signaling and how it can be manipulated for therapeutic benefit. I look forward to continuing my own efforts toward this important goal.

References

1. K. Newton, V. M. Dixit, Signaling in innate immunity and inflammation. *Cold Spring Harb Perspect Biol*. **4** (2012), doi:10.1101/cshperspect.a006049.

2. J. Schlessinger, Cell signaling by receptor tyrosine kinases. *Cell*. **103**, 211–225 (2000).

3. A. K. Chakraborty, A. Weiss, Insights into the initiation of TCR signaling. *Nat. Immunol.* **15**, 798–807 (2014).

4. W. Zhang, J. Sloan-Lancaster, J. Kitchen, R. P. Trible, L. E. Samelson, LAT: the ZAP-70 tyrosine kinase substrate that links T cell receptor to cellular activation. *Cell*. **92**, 83–92 (1998).

5. J. S. Rawlings, K. M. Rosler, D. A. Harrison, The JAK/STAT signaling pathway. *J. Cell. Sci.* **117**, 1281–1283 (2004).

6. R. A. Kovall, B. Gebelein, D. Sprinzak, R. Kopan, The Canonical Notch Signaling Pathway: Structural and Biochemical Insights into Shape, Sugar, and Force. *Dev. Cell*. **41**, 228–241 (2017).

7. L. Morsut *et al.*, Engineering Customized Cell Sensing and Response Behaviors Using Synthetic Notch Receptors. *Cell*. **164**, 780–791 (2016).

8. K. T. Roybal *et al.*, Engineering T Cells with Customized Therapeutic Response Programs Using Synthetic Notch Receptors. *Cell*. **167**, 419–432.e16 (2016).

9. K. T. Roybal *et al.*, Precision Tumor Recognition by T Cells With Combinatorial Antigen-Sensing Circuits. *Cell*. **164**, 770–779 (2016).

10. B. G. Neel, H. Gu, L. Pao, The “Shp”ing news: SH2 domain-containing tyrosine phosphatases in cell signaling. *Trends Biochem Sci*. **28**, 284–293 (2003).

11. J. Zhang *et al.*, Involvement of the SHP-1 tyrosine phosphatase in regulation of T cell selection. *J. Immunol.* **163**, 3012–3021 (1999).

12. C. C. Fowler, L. I. Pao, J. N. Blattman, P. D. Greenberg, SHP-1 in T cells limits the production of CD8 effector cells without impacting the formation of long-lived central memory cells. *J Immunol*. **185**, 3256–3267 (2010).

13. C. K. Anderson *et al.*, Role of SHIP1 in Invariant NKT Cell Development and Functions. *The Journal of Immunology*. **195**, 2149–2156 (2015).

14. E. Hui *et al.*, T cell costimulatory receptor CD28 is a primary target for PD-1-mediated inhibition. **355**, 1428–1433 (2017).

15. K. Iwai, Diverse ubiquitin signaling in NF-κB activation. *Trends Cell Biol.* **22**, 355–364 (2012).

16. M. D. Myers *et al.*, Src-like adaptor protein regulates TCR expression on thymocytes by linking the ubiquitin ligase c-Cbl to the TCR complex. *Nat Immunol*. **7**, 57–66 (2006).

17. H. Y. Wang *et al.*, Cbl promotes ubiquitination of the T cell receptor zeta through an adaptor function of Zap-70. *J. Biol. Chem.* **276**, 26004–26011 (2001).

18. R. J. Brownlie, R. Zamoyska, T cell receptor signalling networks: branched, diversified and bounded. *Nature Reviews Immunology*. **13**, 257–269 (2013).

19. K. A. Hogquist, S. C. Jameson, The self-obsession of T cells: how TCR signaling thresholds affect fate “decisions” and effector function. *Nat. Immunol.* **15**, 815–823 (2014).

20. M. N. Navarro, D. A. Cantrell, Serine-threonine kinases in TCR signaling. *Nat. Immunol.* **15**, 808–814 (2014).

21. M. L. Dustin, What counts in the immunological synapse? *Mol. Cell*. **54**, 255–262 (2014).

22. B. A. Irving, A. Weiss, The cytoplasmic domain of the T cell receptor zeta chain is sufficient to couple to receptor-associated signal transduction pathways. *Cell*. **64**, 891–901 (1991).

23. Q.-J. Li *et al.*, CD4 enhances T cell sensitivity to antigen by coordinating Lck accumulation at the immunological synapse. *Nat. Immunol.* **5**, 791–799 (2004).

24. H. Wang *et al.*, ZAP-70: an essential kinase in T-cell signaling. *Cold Spring Harb Perspect Biol*. **2**, a002279 (2010).

25. M. Iwashima, B. A. Irving, N. S. van Oers, A. C. Chan, A. Weiss, Sequential interactions of the TCR with two distinct cytoplasmic tyrosine kinases. *Science*. **263**, 1136–1139 (1994).

26. A. C. Chan *et al.*, Activation of ZAP-70 kinase activity by phosphorylation of tyrosine 493 is required for lymphocyte antigen receptor function. *EMBO J.* **14**, 2499–2508 (1995).

27. J. Alberola-Ila, S. Takaki, J. D. Kerner, R. M. Perlmutter, Differential signaling by lymphocyte antigen receptors. *Annu. Rev. Immunol.* **15**, 125–154 (1997).

28. L. E. Samelson, Signal transduction mediated by the T cell antigen receptor: the role of adapter proteins. *Annu. Rev. Immunol.* **20**, 371–394 (2002).

29. S. J. F. Cronin, J. M. Penninger, From T-cell activation signals to signaling control of anti-cancer immunity. *Immunol. Rev.* **220**, 151–168 (2007).

30. O. Acuto, F. Michel, CD28-mediated co-stimulation: a quantitative support for TCR signalling. *Nature Reviews Immunology*. **3**, 939–951 (2003).

31. F. Michel *et al.*, CD28 utilizes Vav-1 to enhance TCR-proximal signaling and NF-AT activation. *J Immunol*. **165**, 3820–3829 (2000).

32. J. M. Curtsinger, M. F. Mescher, Inflammatory cytokines as a third signal for T cell activation. *Current Opinion in Immunology*. **22**, 333–340 (2010).

33. G. Gross, T. Waks, Z. Eshhar, Expression of immunoglobulin-T-cell receptor chimeric molecules as functional receptors with antibody-type specificity. *Proceedings of the National Academy of Sciences*. **86**, 10024–10028 (1989).

34. Z. Eshhar, T. Waks, G. Gross, D. G. Schindler, Specific activation and targeting of cytotoxic lymphocytes through chimeric single chains consisting of antibody-binding domains and the gamma or zeta subunits of the immunoglobulin and T-cell receptors. *Proc. Natl. Acad. Sci. U.S.A.* **90**, 720–724 (1993).

35. Z. Eshhar, From the mouse cage to human therapy: a personal perspective of the emergence of T-bodies/chimeric antigen receptor T cells. *Hum. Gene Ther.* **25**, 773–778 (2014).

36. C. Romeo, B. Seed, Cellular immunity to HIV activated by CD4 fused to T cell or Fc receptor polypeptides. *Cell*. **64**, 1037–1046 (1991).

37. F. Meissner, M. Mann, Quantitative shotgun proteomics: considerations for a high-quality workflow in immunology. *Nat. Immunol.* **15**, 112–117 (2014).

38. A. Fefer, Immunotherapy and chemotherapy of Moloney sarcoma virus-induced tumors in mice. *Cancer Res*. **29**, 2177–2183 (1969).

39. S. A. Rosenberg, Adoptive immunotherapy of cancer: accomplishments and prospects. *Cancer Treat Rep*. **68**, 233–255 (1984).

40. H. J. Kolb *et al.*, Donor leukocyte transfusions for treatment of recurrent chronic myelogenous leukemia in marrow transplant patients. *Blood*. **76**, 2462–2465 (1990).

41. C. H. June, S. R. Riddell, T. N. Schumacher, Adoptive cellular therapy: A race to the finish line. *Sci Transl Med*. **7**, 280ps7 (2015).

42. R. H. Schwartz, T-lymphocyte recognition of antigen in association with gene products of the major histocompatibility complex. *Annu Rev Immunol*. **3**, 237–261 (1985).

43. W. Cui, S. M. Kaech, Generation of effector CD8+ T cells and their conversion to memory T cells. *Immunol. Rev.* **236**, 151–166 (2010).

44. V. R. Buchholz, P. Gräf, D. H. Busch, The origin of diversity: studying the evolution of multi-faceted CD8+ T cell responses. *Cell. Mol. Life Sci.* **69**, 1585–1595 (2012).

45. Y. Oka *et al.*, Human cytotoxic T-lymphocyte responses specific for peptides of the wild-type Wilms' tumor gene (WT1) product. *Immunogenetics*. **51**, 99–107 (2000).

46. P. G. Coulie *et al.*, A new gene coding for a differentiation antigen recognized by autologous cytolytic T lymphocytes on HLA-A2 melanomas. *J Exp Med*. **180**, 35–42 (1994).

47. M. Schmitz *et al.*, Generation of survivin-specific CD8+ T effector cells by dendritic cells pulsed with protein or selected peptides. *Cancer Res*. **60**, 4845–4849 (2000).

48. M. H. Andersen, L. O. Pedersen, J. C. Becker, P. T. Straten, Identification of a cytotoxic T lymphocyte response to the apoptosis inhibitor protein survivin in cancer patients. *Cancer Res*. **61**, 869–872 (2001).

49. C. Arber *et al.*, Survivin-specific T cell receptor targets tumor but not T cells. *J. Clin. Invest.* **125**, 157–168 (2015).

50. Y. Kawakami *et al.*, Cloning of the gene coding for a shared human melanoma antigen recognized by autologous T cells infiltrating into tumor. *Proceedings of the National Academy of Sciences*. **91**, 3515–3519 (1994).

51. H. Hohn *et al.*, CD4+ tumor-infiltrating lymphocytes in cervical cancer recognize HLA-DR-restricted peptides provided by human papillomavirus-E7. *J Immunol*. **163**, 5715–5722 (1999).

52. G. G. Kenter *et al.*, Vaccination against HPV-16 oncoproteins for vulvar intraepithelial neoplasia. *N Engl J Med*. **361**, 1838–1847 (2009).

53. L. M. Draper *et al.*, Targeting of HPV-16+ Epithelial Cancer Cells by TCR Gene Engineered T Cells Directed against E6. *Clin. Cancer Res.* **21**, 4431–4439 (2015).

54. C. A. Ramos *et al.*, Human papillomavirus type 16 E6/E7-specific cytotoxic T lymphocytes for adoptive immunotherapy of HPV-associated malignancies. *J. Immunother.* **36**, 66–76 (2013).

55. R. Khanna, S. R. Burrows, J. Nicholls, L. M. Poulsen, Identification of cytotoxic T cell epitopes within Epstein-Barr virus (EBV) oncogene latent membrane protein 1 (LMP1): evidence for HLA A2 supertype-restricted immune recognition of EBV-infected cells by LMP1-specific cytotoxic T lymphocytes. *Eur. J. Immunol.* **28**, 451–458 (1998).

56. H. M. Long *et al.*, CD4+ T-cell clones recognizing human lymphoma-associated antigens: generation by in vitro stimulation with autologous Epstein-Barr virus-transformed B cells. *Blood*. **114**, 807–815 (2009).

57. T. A. Haigh *et al.*, EBV latent membrane proteins (LMPs) 1 and 2 as immunotherapeutic targets: LMP-specific CD4+ cytotoxic T cell recognition of EBV-transformed B cell lines. *J Immunol*. **180**, 1643–1654 (2008).

58. X. Lin *et al.*, CD4 and CD8 T cell responses to tumour-associated Epstein-Barr virus antigens in nasopharyngeal carcinoma patients. *Cancer Immunol. Immunother.* **57**, 963–975 (2008).

59. J. G. Iyer *et al.*, Merkel cell polyomavirus-specific CD8(+) and CD4(+) T-cell responses identified in Merkel cell carcinomas and blood. *Clin. Cancer Res.* **17**, 6671–6680 (2011).

60. R. Lyngaa *et al.*, T-cell responses to oncogenic merkel cell polyomavirus proteins distinguish patients with merkel cell carcinoma from healthy donors. *Clin. Cancer Res.* **20**, 1768–1778 (2014).

61. S. Ilyas, J. C. Yang, Landscape of Tumor Antigens in T Cell Immunotherapy. *The Journal of Immunology*. **195**, 5117–5122 (2015).

62. P. Kvistborg, M. M. van Buuren, T. N. Schumacher, Human cancer regression antigens. *Current Opinion in Immunology*. **25**, 284–290 (2013).

63. L. Klein, B. Kyewski, P. M. Allen, K. A. Hogquist, Positive and negative selection of the T cell repertoire: what thymocytes see (and don't see). *Nature Reviews Immunology*. **14**, 377–391 (2014).

64. G. Willimsky, T. Blankenstein, Sporadic immunogenic tumours avoid destruction by inducing T-cell tolerance. *Nature*. **437**, 141–146 (2005).

65. A. Schietinger *et al.*, Tumor-Specific T Cell Dysfunction Is a Dynamic Antigen-Driven Differentiation Program Initiated Early during Tumorigenesis. *Immunity*. **45**, 389–401 (2016).

66. S. L. Topalian, C. G. Drake, D. M. Pardoll, Immune Checkpoint Blockade: A Common Denominator Approach to Cancer Therapy. *Cancer Cell*. **27**, 450–461 (2015).

67. S. Spranger, R. Bao, T. F. Gajewski, Melanoma-intrinsic beta-catenin signalling prevents anti-tumour immunity. *Nature*. **523**, 231–235 (2015).

68. L. B. Alexandrov *et al.*, Signatures of mutational processes in human cancer. *Nature*. **500**, 415–421 (2013).

69. N. Seki, T. Hoshino, M. Kikuchi, A. Hayashi, K. Itoh, HLA-A locus-restricted and tumor-specific CTLs in tumor-infiltrating lymphocytes of patients with non-small cell lung cancer. *Cell. Immunol.* **175**, 101–110 (1997).

70. Y. Shimizu, E. Weidmann, S. Iwatsuki, R. B. Herberman, T. L. Whiteside, Characterization of human autotumor-reactive T-cell clones obtained from tumor-infiltrating lymphocytes in liver metastasis of gastric carcinoma. *Cancer Res*. **51**, 6153–6162 (1991).

71. E. J. Stevens *et al.*, Generation of tumor-specific CTLs from melanoma patients by using peripheral blood stimulated with allogeneic melanoma tumor cell lines. Fine specificity and MART-1 melanoma antigen recognition. *J Immunol*. **154**, 762–771 (1995).

72. S. C. Casey *et al.*, MYC regulates the antitumor immune response through CD47 and PD-L1. *Science*. **352**, 227–231 (2016).

73. A. S. Berghoff *et al.*, Density of tumor-infiltrating lymphocytes correlates with extent of brain edema and overall survival time in patients with brain metastases. *Oncoimmunology*. **5**, e1057388 (2016).

74. D. I. Gabrilovich, S. Ostrand-Rosenberg, V. Bronte, Coordinated regulation of myeloid cells by tumours. *Nature Reviews Immunology*. **12**, 253–268 (2012).

75. C. Gu-Trantien *et al.*, CD4(+) follicular helper T cell infiltration predicts breast cancer survival. *J. Clin. Invest.* **123**, 2873–2892 (2013).

76. V. Kumar, S. Patel, E. Tcyganov, D. I. Gabrilovich, The Nature of Myeloid-Derived Suppressor Cells in the Tumor Microenvironment. *Trends in Immunology*. **37**, 208–220 (2016).

77. B. Mlecnik *et al.*, Functional network pipeline reveals genetic determinants associated with in situ lymphocyte proliferation and survival of cancer patients. *Sci Transl Med*. **6**, 228ra37 (2014).

78. B. Mlecnik *et al.*, The tumor microenvironment and Immunoscore are critical determinants of dissemination to distant metastasis. *Sci Transl Med*. **8**, 327ra26 (2016).

79. F. Pages *et al.*, Effector memory T cells, early metastasis, and survival in colorectal cancer. *N Engl J Med*. **353**, 2654–2666 (2005).

80. B. Ruffell *et al.*, Leukocyte composition of human breast cancer. *Proc. Natl. Acad. Sci. U.S.A.* **109**, 2796–2801 (2012).

81. B. Shang, Y. Liu, S. J. Jiang, Y. Liu, Prognostic value of tumor-infiltrating FoxP3+ regulatory T cells in cancers: a systematic review and meta-analysis. *Sci Rep*. **5**, 15179 (2015).

82. G. Stoll *et al.*, Immune-related gene signatures predict the outcome of neoadjuvant chemotherapy. *Oncoimmunology*. **3**, e27884 (2014).

83. J. R. Webb, K. Milne, P. Watson, R. J. Deleeuw, B. H. Nelson, Tumor-Infiltrating Lymphocytes Expressing the Tissue Resident Memory Marker CD103 Are Associated with Increased Survival in High-Grade Serous Ovarian Cancer. *Clin. Cancer Res.* **20**, 434–444 (2014).

84. M. C. A. Wouters *et al.*, Treatment Regimen, Surgical Outcome, and T-cell Differentiation Influence Prognostic Benefit of Tumor-Infiltrating Lymphocytes in High-Grade Serous Ovarian Cancer. *Clin. Cancer Res.* **22**, 714–724 (2016).

85. W. H. Fridman *et al.*, Prognostic and predictive impact of intra- and peritumoral immune infiltrates. *Cancer Res.* **71**, 5601–5605 (2011).

86. P. Savas *et al.*, Clinical relevance of host immunity in breast cancer: from TILs to the clinic. *Nature Reviews Clinical Oncology 2018 15:4*. **13**, 228–241 (2016).

87. K. N. Townsend *et al.*, Markers of T Cell Infiltration and Function Associate with Favorable Outcome in Vascularized High-Grade Serous Ovarian Carcinoma. *PLoS ONE*. **8**, e82406 (2013).

88. S. A. Rosenberg, P. Spiess, R. Lafreniere, A new approach to the adoptive immunotherapy of cancer with tumor-infiltrating lymphocytes. *Science*. **233**, 1318–1321 (1986).

89. L. M. Muul, P. J. Spiess, E. P. Director, S. A. Rosenberg, Identification of specific cytolytic immune responses against autologous tumor in humans bearing malignant melanoma. *J Immunol*. **138**, 989–995 (1987).

90. S. L. Topalian, L. M. Muul, D. Solomon, S. A. Rosenberg, Expansion of human tumor infiltrating lymphocytes for use in immunotherapy trials. *J. Immunol. Methods*. **102**, 127–141 (1987).

91. S. A. Rosenberg *et al.*, Use of tumor-infiltrating lymphocytes and interleukin-2 in the immunotherapy of patients with metastatic melanoma. A preliminary report. *N Engl J Med*. **319**, 1676–1680 (1988).

92. S. A. Rosenberg *et al.*, Gene transfer into humans--immunotherapy of patients with advanced melanoma, using tumor-infiltrating lymphocytes modified by retroviral gene transduction. *N Engl J Med*. **323**, 570–578 (1990).

93. R. J. North, Cyclophosphamide-facilitated adoptive immunotherapy of an established tumor depends on elimination of tumor-induced suppressor T cells. *J Exp Med*. **155**, 1063–1074 (1982).

94. P. D. Greenberg, M. A. Cheever, A. Fefer, Eradication of disseminated murine leukemia by chemoimmunotherapy with cyclophosphamide and adoptively transferred immune syngeneic Lyt-1+2- lymphocytes. *J Exp Med*. **154**, 952–963 (1981).

95. M. E. Dudley *et al.*, Cancer regression and autoimmunity in patients after clonal repopulation with antitumor lymphocytes. *Science*. **298**, 850–854 (2002).

96. M. E. Dudley *et al.*, Adoptive cell therapy for patients with metastatic melanoma: evaluation of intensive myeloablative chemoradiation preparative regimens. *J. Clin. Oncol.* **26**, 5233–5239 (2008).

97. S. L. Goff *et al.*, Randomized, Prospective Evaluation Comparing Intensity of Lymphodepletion Before Adoptive Transfer of Tumor-Infiltrating Lymphocytes for Patients With Metastatic Melanoma. *J. Clin. Oncol.* **34**, 2389–2397 (2016).

98. M. E. Dudley *et al.*, CD8+ enriched “young” tumor infiltrating lymphocytes can mediate regression of metastatic melanoma. *Clin. Cancer Res.* **16**, 6122–6131 (2010).

99. S. A. Rosenberg *et al.*, Durable complete responses in heavily pretreated patients with metastatic melanoma using T-cell transfer immunotherapy. *Clin. Cancer Res.* **17**, 4550–4557 (2011).

100. L. Gattinoni *et al.*, Removal of homeostatic cytokine sinks by lymphodepletion enhances the efficacy of adoptively transferred tumor-specific CD8+ T cells. *J Exp Med*. **202**, 907–912 (2005).

101. C. Wrzesinski *et al.*, Hematopoietic stem cells promote the expansion and function of adoptively transferred antitumor CD8+ T cells. *J. Clin. Invest.* **117**, 492–501 (2007).

102. M. J. Besser *et al.*, Adoptive Transfer of Tumor-Infiltrating Lymphocytes in Patients with Metastatic Melanoma: Intent-to-Treat Analysis and Efficacy after Failure to Prior Immunotherapies. *Clin. Cancer Res.* **19**, 4792–4800 (2013).

103. R. Andersen *et al.*, Long-Lasting Complete Responses in Patients with Metastatic Melanoma after Adoptive Cell Therapy with Tumor-Infiltrating Lymphocytes and an Attenuated IL2 Regimen. *Clin. Cancer Res.* **22**, 3734–3745 (2016).

104. P. Kvistborg *et al.*, TIL therapy broadens the tumor-reactive CD8(+) T cell compartment in melanoma patients. *Oncoimmunology*. **1**, 409–418 (2012).

105. L. G. Radvanyi *et al.*, Specific lymphocyte subsets predict response to adoptive cell therapy using expanded autologous tumor-infiltrating lymphocytes in metastatic melanoma patients. *Clin. Cancer Res.* **18**, 6758–6770 (2012).

106. E. Hodis *et al.*, A landscape of driver mutations in melanoma. *Cell*. **150**, 251–263 (2012).

107. N. van Rooij *et al.*, Tumor exome analysis reveals neoantigen-specific T-cell reactivity in an ipilimumab-responsive melanoma. *J. Clin. Oncol.* **31**, e439–42 (2013).

108. C. Linnemann *et al.*, High-throughput epitope discovery reveals frequent recognition of neo-antigens by CD4+ T cells in human melanoma. *Nature Medicine*. **21**, 81–85 (2015).

109. E. M. E. Verdegaal *et al.*, Neoantigen landscape dynamics during human melanoma–T cell interactions. *Nature*. **536**, 91–95 (2016).

110. T. D. Prickett *et al.*, Durable Complete Response from Metastatic Melanoma after Transfer of Autologous T Cells Recognizing 10 Mutated Tumor Antigens. *Cancer Immunol Res*. **4**, 669–678 (2016).

111. K. Harbst *et al.*, Multiregion Whole-Exome Sequencing Uncovers the Genetic Evolution and Mutational Heterogeneity of Early-Stage Metastatic Melanoma. *Cancer Res.* **76**, 4765–4774 (2016).

112. A. Arina, L. Corrales, V. Bronte, Enhancing T cell therapy by overcoming the immunosuppressive tumor microenvironment. *Semin. Immunol.* **28**, 54–63 (2016).

113. J. M. Pitt *et al.*, Resistance Mechanisms to Immune-Checkpoint Blockade in Cancer: Tumor-Intrinsic and -Extrinsic Factors. *Immunity*. **44**, 1255–1269 (2016).

114. M. A. Postow, M. K. Callahan, J. D. Wolchok, Immune Checkpoint Blockade in Cancer Therapy. *J. Clin. Oncol.* **33**, 1974–1982 (2015).

115. D. S. Shin, A. Ribas, The evolution of checkpoint blockade as a cancer therapy: what“s here, what”s next? *Current Opinion in Immunology*. **33**, 23–35 (2015).

116. V. Baldan, R. Griffiths, R. E. Hawkins, D. E. Gilham, Efficient and reproducible generation of tumour-infiltrating lymphocytes for renal cell carcinoma. *Br. J. Cancer*. **112**, 1510–1518 (2015).

117. A. Belldegrun, L. M. Muul, S. A. Rosenberg, Interleukin 2 expanded tumor-infiltrating lymphocytes in human renal cell cancer: isolation, characterization, and antitumor activity. *Cancer Res*. **48**, 206–214 (1988).

118. M. Hall *et al.*, Expansion of tumor-infiltrating lymphocytes (TIL) from human pancreatic tumors. *J Immunother Cancer*. **4**, 61 (2016).

119. S. S. Jiang *et al.*, A phase I clinical trial utilizing autologous tumor-infiltrating lymphocytes in patients with primary hepatocellular carcinoma. *Oncotarget*. **6**, 41339–41349 (2015).

120. S. Stevanovic *et al.*, Complete regression of metastatic cervical cancer after treatment with human papillomavirus-targeted tumor-infiltrating T cells. *J. Clin. Oncol.* **33**, 1543–1550 (2015).

121. S. Turcotte *et al.*, Tumor-Reactive CD8+ T Cells in Metastatic Gastrointestinal Cancer Refractory to Chemotherapy. *Clin. Cancer Res.* **20**, 331–343 (2014).

122. E. Tran *et al.*, T-Cell Transfer Therapy Targeting Mutant KRAS in Cancer. *N Engl J Med*. **375**, 2255–2262 (2016).

123. K. A. Noonan *et al.*, Adoptive transfer of activated marrow-infiltrating lymphocytes induces measurable antitumor immunity in the bone marrow in multiple myeloma. *Sci Transl Med*. **7**, 288ra78 (2015).

124. S. R. Riddell, P. D. Greenberg, Principles for adoptive T cell therapy of human viral diseases. *Annu Rev Immunol*. **13**, 545–586 (1995).

125. S. R. Riddell *et al.*, Restoration of viral immunity in immunodeficient humans by the adoptive transfer of T cell clones. *Science*. **257**, 238–241 (1992).

126. E. A. Walter *et al.*, Reconstitution of cellular immunity against cytomegalovirus in recipients of allogeneic bone marrow by transfer of T-cell clones from the donor. *N Engl J Med*. **333**, 1038–1044 (1995).

127. A. M. Leen *et al.*, Monoculture-derived T lymphocytes specific for multiple viruses expand and produce clinically relevant effects in immunocompromised individuals. *Nat Med*. **12**, 1160–1166 (2006).

128. C. M. Rooney, L. K. Aguilar, M. H. Huls, M. K. Brenner, H. E. Heslop, Adoptive immunotherapy of EBV-associated malignancies with EBV-specific cytotoxic T-cell lines. *Curr. Top. Microbiol. Immunol.* **258**, 221–229 (2001).

129. C. M. Rooney *et al.*, Infusion of cytotoxic T cells for the prevention and treatment of Epstein-Barr virus-induced lymphoma in allogeneic transplant recipients. *Blood*. **92**, 1549–1555 (1998).

130. S. M. Pollack *et al.*, Tetramer guided, cell sorter assisted production of clinical grade autologous NY-ESO-1 specific CD8(+) T cells. *J Immunother Cancer*. **2**, 36 (2014).

131. C. Yee *et al.*, Adoptive T cell therapy using antigen-specific CD8+ T cell clones for the treatment of patients with metastatic melanoma: in vivo persistence, migration, and antitumor effect of transferred T cells. *Proc. Natl. Acad. Sci. U.S.A.* **99**, 16168–16173 (2002).

132. C. Yee *et al.*, Melanocyte destruction after antigen-specific immunotherapy of melanoma: direct evidence of t cell-mediated vitiligo. *J Exp Med*. **192**, 1637–1644 (2000).

133. A. G. Chapuis *et al.*, Transferred melanoma-specific CD8+ T cells persist, mediate tumor regression, and acquire central memory phenotype. *Proc. Natl. Acad. Sci. U.S.A.* **109**, 4592–4597 (2012).

134. M. E. Dudley *et al.*, Adoptive transfer of cloned melanoma-reactive T lymphocytes for the treatment of patients with metastatic melanoma. *J. Immunother.* **24**, 363–373 (2001).

135. N. N. Hunder *et al.*, Treatment of metastatic melanoma with autologous CD4+ T cells against NY-ESO-1. *N Engl J Med*. **358**, 2698–2703 (2008).

136. S. S. Chandran *et al.*, Persistence of CTL clones targeting melanocyte differentiation antigens was insufficient to mediate significant melanoma regression in humans. *Clin. Cancer Res.* **21**, 534–543 (2015).

137. C. Berger, C. J. Turtle, M. C. Jensen, S. R. Riddell, Adoptive transfer of virus-specific and tumor-specific T cell immunity. *Current Opinion in Immunology*. **21**, 224–232 (2009).

138. L. Gattinoni *et al.*, Acquisition of full effector function in vitro paradoxically impairs the in vivo antitumor efficacy of adoptively transferred CD8+ T cells. *J. Clin. Invest.* **115**, 1616–1626 (2005).

139. D. H. Busch, S. P. Fräßle, D. Sommermeyer, V. R. Buchholz, S. R. Riddell, Role of memory T cell subsets for adoptive immunotherapy. *Semin. Immunol.* **28**, 28–34 (2016).

140. Y. Li, M. Bleakley, C. Yee, IL-21 influences the frequency, phenotype, and affinity of the antigen-specific CD8 T cell response. *J Immunol*. **175**, 2261–2269 (2005).

141. A. G. Chapuis *et al.*, Transferred WT1-Reactive CD8+ T Cells Can Mediate Antileukemic Activity and Persist in Post-Transplant Patients. *Sci Transl Med*. **5**, 174ra27 (2013).

142. D. A. Mahvi *et al.*, Ctla-4 blockade plus adoptive T-cell transfer promotes optimal melanoma immunity in mice. *J. Immunother.* **38**, 54–61 (2015).

143. S. J. P. Blake *et al.*, Blockade of PD-1/PD-L1 promotes adoptive T-cell immunotherapy in a tolerogenic environment. *PLoS ONE*. **10**, e0119483 (2015).

144. S. Pilon-Thomas, A. Mackay, N. Vohra, J. J. Mule, Blockade of programmed death ligand 1 enhances the therapeutic efficacy of combination immunotherapy against melanoma. *The Journal of Immunology*. **184**, 3442–3449 (2010).

145. A. G. Chapuis *et al.*, T-Cell Therapy Using Interleukin-21-Primed Cytotoxic T-Cell Lymphocytes Combined With Cytotoxic T-Cell Lymphocyte Antigen-4 Blockade Results in Long-Term Cell Persistence and Durable Tumor Regression. *J. Clin. Oncol.* **34**, 3787–3795 (2016).

146. B. A. Bunnell, L. M. Muul, R. E. Donahue, R. M. Blaese, R. A. Morgan, High-efficiency retroviral-mediated gene transfer into human and nonhuman primate peripheral blood lymphocytes. *Proceedings of the National Academy of Sciences*. **92**, 7739–7743 (1995).

147. W. Uckert *et al.*, Efficient gene transfer into primary human CD8+ T lymphocytes by MuLV-10A1 retrovirus pseudotype. *Hum. Gene Ther.* **11**, 1005–1014 (2000).

148. B. Engels *et al.*, Redirecting human T lymphocytes toward renal cell carcinoma specificity by retroviral transfer of T cell receptor genes. *Hum. Gene Ther.* **16**, 799–810 (2005).

149. M. Leisegang *et al.*, Enhanced functionality of T cell receptor-redirected T cells is defined by the transgene cassette. *J Mol Med (Berl)*. **86**, 573–583 (2008).

150. J. Scholler *et al.*, Decade-long safety and function of retroviral-modified chimeric antigen receptor T cells. *Sci Transl Med*. **4**, 132ra53 (2012).

151. S. Newrzela *et al.*, Resistance of mature T cells to oncogene transformation. *Blood*. **112**, 2278–2286 (2008).

152. S. Hacein-Bey-Abina *et al.*, LMO2-associated clonal T cell proliferation in two patients after gene therapy for SCID-X1. *Science*. **302**, 415–419 (2003).

153. M. Bosticardo, F. Ferrua, M. Cavazzana, A. Aiuti, Gene therapy for Wiskott-Aldrich Syndrome. *Curr Gene Ther*. **14**, 413–421 (2014).

154. A. McCarron, M. Donnelley, C. McIntyre, D. Parsons, Challenges of up-scaling lentivirus production and processing. *J. Biotechnol.* **240**, 23–30 (2016).

155. O.-W. Merten, M. Hebben, C. Bovolenta, Production of lentiviral vectors. *Mol Ther Methods Clin Dev*. **3**, 16017 (2016).

156. A. M. Geurts *et al.*, Gene transfer into genomes of human cells by the sleeping beauty transposon system. *Mol Ther*. **8**, 108–117 (2003).

157. X. Huang *et al.*, Stable gene transfer and expression in human primary T cells by the Sleeping Beauty transposon system. *Blood*. **107**, 483–491 (2006).

158. A. C. Field *et al.*, Comparison of lentiviral and sleeping beauty mediated alphabeta T cell receptor gene transfer. *PLoS ONE*. **8**, e68201 (2013).

159. D. C. Deniger *et al.*, Stable, Nonviral Expression of Mutated Tumor Neoantigen-specific T-cell Receptors Using the Sleeping Beauty Transposon/Transposase System. *Mol Ther*. **24**, 1078–1089 (2016).

160. P. Kebriaei *et al.*, Phase I trials using Sleeping Beauty to generate CD19-specific CAR T cells. *J. Clin. Invest.* **126**, 3363–3376 (2016).

161. M. H. Heemskerk *et al.*, Efficiency of T-cell receptor expression in dual-specific T cells is controlled by the intrinsic qualities of the TCR chains within the TCR-CD3 complex. *Blood*. **109**, 235–243 (2007).

162. G. M. Bendle *et al.*, Lethal graft-versus-host disease in mouse models of T cell receptor gene therapy. *Nature Medicine*. **16**, 565–70– 1p following 570 (2010).

163. M. M. van Loenen *et al.*, Mixed T cell receptor dimers harbor potentially harmful neoreactivity. *Proc. Natl. Acad. Sci. U.S.A.* **107**, 10972–10977 (2010).

164. J. Kuball *et al.*, Cooperation of human tumor-reactive CD4+ and CD8+ T cells after redirection of their specificity by a high-affinity p53A2.1-specific TCR. *Immunity*. **22**, 117–129 (2005).

165. J. L. Davis *et al.*, Development of human anti-murine T-cell receptor antibodies in both responding and nonresponding patients enrolled in TCR gene therapy trials. *Clin. Cancer Res.* **16**, 5852–5861 (2010).

166. C. J. Cohen, Y. Zhao, Z. Zheng, S. A. Rosenberg, R. A. Morgan, Enhanced antitumor activity of murine-human hybrid T-cell receptor (TCR) in human lymphocytes is associated with improved pairing and TCR/CD3 stability. *Cancer Res.* **66**, 8878–8886 (2006).

167. R.-H. Voss *et al.*, Redirection of T Cells by Delivering a Transgenic Mouse-Derived MDM2 Tumor Antigen-Specific TCR and its Humanized Derviative Is Governed by the CD8 Coreceptor and Affects Natural Human TCR Expression. *Immunol. Res.* **34**, 67–87 (2006).

168. D. Sommermeyer *et al.*, Designer T cells by T cell receptor replacement. *Eur. J. Immunol.* **36**, 3052–3059 (2006).

169. D. Sommermeyer, W. Uckert, Minimal amino acid exchange in human TCR constant regions fosters improved function of TCR gene-modified T cells. *The Journal of Immunology*. **184**, 6223–6231 (2010).

170. M. T. Bethune *et al.*, Domain-swapped T cell receptors improve the safety of TCR gene therapy. *Elife*. **5** (2016), doi:10.7554/eLife.19095.

171. J. Kuball *et al.*, Facilitating matched pairing and expression of TCR chains introduced into human T cells. *Blood*. **109**, 2331–2338 (2007).

172. C. J. Cohen *et al.*, Enhanced antitumor activity of T cells engineered to express T-cell receptors with a second disulfide bond. *Cancer Res*. **67**, 3898–3903 (2007).

173. S. Okamoto *et al.*, Improved expression and reactivity of transduced tumor-specific TCRs in human lymphocytes by specific silencing of endogenous TCR. *Cancer Res.* **69**, 9003–9011 (2009).

174. S. Okamoto *et al.*, A Promising Vector for TCR Gene Therapy: Differential Effect of siRNA, 2A Peptide, and Disulfide Bond on the Introduced TCR Expression. *Mol Ther Nucleic Acids*. **1**, e63 (2012).

175. T. Ochi *et al.*, Novel adoptive T-cell immunotherapy using a WT1-specific TCR vector encoding silencers for endogenous TCRs shows marked antileukemia reactivity and safety. *Blood*. **118**, 1495–1503 (2011).

176. M. Bunse *et al.*, RNAi-mediated TCR knockdown prevents autoimmunity in mice caused by mixed TCR dimers following TCR gene transfer. *Mol Ther*. **22**, 1983–1991 (2014).

177. E. Provasi *et al.*, Editing T cell specificity towards leukemia by zinc finger nucleases and lentiviral gene transfer. *Nature Medicine*. **18**, 807–815 (2012).

178. M. J. Osborn *et al.*, Evaluation of TCR Gene Editing Achieved by TALENs, CRISPR/Cas9, and megaTAL Nucleases. *Mol Ther*. **24**, 570–581 (2016).

179. E. C. Morris, H. J. Stauss, Optimizing T-cell receptor gene therapy for hematologic malignancies. *Blood*. **127**, 3305–3311 (2016).

180. J. Eyquem *et al.*, Targeting a CAR to the TRAC locus with CRISPR/Cas9 enhances tumour rejection. *Nature*. **543**, 113–117 (2017).

181. A. Seki, S. Rutz, Optimized RNP transfection for highly efficient CRISPR/Cas9-mediated gene knockout in primary T cells. *Journal of Experimental Medicine* (2018), doi:10.1084/jem.20171626.

182. T. L. Roth *et al.*, Reprogramming human T cell function and specificity with non-viral genome targeting. *Nature*. **559**, 405–409 (2018).

183. M. A. Cheever *et al.*, The prioritization of cancer antigens: a national cancer institute pilot project for the acceleration of translational research. *Clin. Cancer Res.* **15**, 5323–5337 (2009).

184. A. Johnsen, J. France, M. S. Sy, C. V. Harding, Down-regulation of the transporter for antigen presentation, proteasome subunits, and class I major histocompatibility complex in tumor cell lines. *Cancer Res*. **58**, 3660–3667 (1998).

185. B. Engels *et al.*, Relapse or eradication of cancer is predicted by peptide-major histocompatibility complex affinity. *Cancer Cell*. **23**, 516–526 (2013).

186. G. Segal, S. Prato, D. Zehn, J. D. Mintern, J. A. Villadangos, Target Density, Not Affinity or Avidity of Antigen Recognition, Determines Adoptive T Cell Therapy Outcomes in a Mouse Lymphoma Model. *The Journal of Immunology*. **196**, 3935–3942 (2016).

187. L. D. Shultz *et al.*, Generation of functional human T-cell subsets with HLA-restricted immune responses in HLA class I expressing NOD/SCID/IL2r gamma(null) humanized mice. *Proc. Natl. Acad. Sci. U.S.A.* **107**, 13022–13027 (2010).

188. M. Obenaus *et al.*, Identification of human T-cell receptors with optimal affinity to cancer antigens using antigen-negative humanized mice. *Nat. Biotechnol.* **33**, 402–407 (2015).

189. E. Strønen *et al.*, Targeting of cancer neoantigens with donor-derived T cell receptor repertoires. *Science*. **352**, 1337–1341 (2016).

190. A. Gros *et al.*, PD-1 identifies the patient-specific CD8(+) tumor-reactive repertoire infiltrating human tumors. *J. Clin. Invest.* **124**, 2246–2259 (2014).

191. A. Pasetto *et al.*, Tumor- and Neoantigen-Reactive T-cell Receptors Can Be Identified Based on Their Frequency in Fresh Tumor. *Cancer Immunol Res*. **4**, 734–743 (2016).

192. A. Gros *et al.*, Prospective identification of neoantigen-specific lymphocytes in the peripheral blood of melanoma patients. *Nature Medicine*. **22**, 433–438 (2016).

193. W. J. Falkenburg *et al.*, Allogeneic HLA-A*02-restricted WT1-specific T cells from mismatched donors are highly reactive but show off-target promiscuity. *The Journal of Immunology*. **187**, 2824–2833 (2011).

194. T. M. Schmitt *et al.*, Generation of higher affinity T cell receptors by antigen-driven differentiation of progenitor T cells in vitro. *Nat Immunol*. **35**, 1188–1195 (2017).

195. P. F. Robbins *et al.*, Single and dual amino acid substitutions in TCR CDRs can enhance antigen-specific T cell functions. *J Immunol*. **180**, 6116–6131 (2008).

196. A. S. Chervin, D. H. Aggen, J. M. Raseman, D. M. Kranz, Engineering higher affinity T cell receptors using a T cell display system. *J. Immunol. Methods*. **339**, 175–184 (2008).

197. P. S. Adusumilli *et al.*, Regional delivery of mesothelin-targeted CAR T cell therapy generates potent and long-lasting CD4-dependent tumor immunity. *Sci Transl Med*. **6**, 261ra151 (2014).

198. D. Sommermeyer *et al.*, Chimeric antigen receptor-modified T cells derived from defined CD8+ and CD4+ subsets confer superior antitumor reactivity in vivo. *Leukemia*. **30**, 492–500 (2016).

199. R. J. Salmond, A. Filby, I. Qureshi, S. Caserta, R. Zamoyska, T-cell receptor proximal signaling via the Src-family kinases, Lck and Fyn, influences T-cell activation, differentiation, and tolerance. *Immunol. Rev.* **228**, 9–22 (2009).

200. H. W. Kessels, K. Schepers, M. D. van den Boom, D. J. Topham, T. N. Schumacher, Generation of T cell help through a MHC class I-restricted TCR. *J Immunol*. **177**, 976–982 (2006).

201. R. A. Willemsen *et al.*, CD8 alpha coreceptor to improve TCR gene transfer to treat melanoma: down-regulation of tumor-specific production of IL-4, IL-5, and IL-10. *J Immunol*. **177**, 991–998 (2006).

202. Y. Zhao *et al.*, High-affinity TCRs generated by phage display provide CD4+ T cells with the ability to recognize and kill tumor cell lines. *J Immunol*. **179**, 5845–5854 (2007).

203. S. Mehrotra *et al.*, A coreceptor-independent transgenic human TCR mediates anti-tumor and anti-self immunity in mice. *The Journal of Immunology*. **189**, 1627–1638 (2012).

204. R. A. Morgan *et al.*, Cancer regression in patients after transfer of genetically engineered lymphocytes. *Science*. **314**, 126–129 (2006).

205. L. A. Johnson *et al.*, Gene therapy with human and mouse T-cell receptors mediates cancer regression and targets normal tissues expressing cognate antigen. *Blood*. **114**, 535–546 (2009).

206. P. F. Robbins *et al.*, Tumor regression in patients with metastatic synovial cell sarcoma and melanoma using genetically engineered lymphocytes reactive with NY-ESO-1. *J. Clin. Oncol.* **29**, 917–924 (2011).

207. P. F. Robbins *et al.*, A pilot trial using lymphocytes genetically engineered with an NY-ESO-1-reactive T-cell receptor: long-term follow-up and correlates with response. *Clin. Cancer Res.* **21**, 1019–1027 (2015).

208. S. Hammarstrom, The carcinoembryonic antigen (CEA) family: structures, suggested functions and expression in normal and malignant tissues. *Semin. Cancer Biol.* **9**, 67–81 (1999).

209. M. R. Parkhurst *et al.*, T cells targeting carcinoembryonic antigen can mediate regression of metastatic colorectal cancer but induce severe transient colitis. *Mol Ther*. **19**, 620–626 (2011).

210. M. Sang, Y. Lian, X. Zhou, B. Shan, MAGE-A family: attractive targets for cancer immunotherapy. *Vaccine*. **29**, 8496–8500 (2011).

211. P. van der Bruggen *et al.*, A gene encoding an antigen recognized by cytolytic T lymphocytes on a human melanoma. *Science*. **254**, 1643–1647 (1991).

212. N. Chinnasamy *et al.*, A TCR targeting the HLA-A*0201-restricted epitope of MAGE-A3 recognizes multiple epitopes of the MAGE-A antigen superfamily in several types of cancer. *The Journal of Immunology*. **186**, 685–696 (2011).

213. R. A. Morgan *et al.*, Cancer regression and neurological toxicity following anti-MAGE-A3 TCR gene therapy. *J. Immunother.* **36**, 133–151 (2013).

214. G. P. Linette *et al.*, Cardiovascular toxicity and titin cross-reactivity of affinity-enhanced T cells in myeloma and melanoma. *Blood*. **122**, 863–871 (2013).

215. B. J. Cameron *et al.*, Identification of a Titin-Derived HLA-A1-Presented Peptide as a Cross-Reactive Target for Engineered MAGE A3-Directed T Cells. *Sci Transl Med*. **5**, 197ra103 (2013).

216. M. C. Raman *et al.*, Direct molecular mimicry enables off-target cardiovascular toxicity by an enhanced affinity TCR designed for cancer immunotherapy. *Sci Rep*. **6**, 18851 (2016).

217. D. T. Harris *et al.*, Deep Mutational Scans as a Guide to Engineering High Affinity T Cell Receptor Interactions with Peptide-bound Major Histocompatibility Complex. *J. Biol. Chem.* **291**, 24566–24578 (2016).

218. J. J. Adams *et al.*, Structural interplay between germline interactions and adaptive recognition determines the bandwidth of TCR-peptide-MHC cross-reactivity. *Nat. Immunol.* **17**, 87–94 (2015).

219. C. Gerlach *et al.*, Heterogeneous differentiation patterns of individual CD8+ T cells. *Science*. **340**, 635–639 (2013).

220. L. Gattinoni *et al.*, A human memory T cell subset with stem cell-like properties. *Nature Medicine*. **17**, 1290–1297 (2011).

221. L. Gattinoni, C. A. Klebanoff, N. P. Restifo, Paths to stemness: building the ultimate antitumour T cell. *Nature Publishing Group*. **12**, 671–684 (2012).

222. V. R. Buchholz *et al.*, Disparate individual fates compose robust CD8+ T cell immunity. *Science*. **340**, 630–635 (2013).

223. V. R. Buchholz, T. N. M. Schumacher, D. H. Busch, T Cell Fate at the Single-Cell Level. *Annu Rev Immunol*. **34**, 65–92 (2016).

224. C. J. Turtle *et al.*, CD19 CAR-T cells of defined CD4+:CD8+ composition in adult B cell ALL patients. *J. Clin. Invest.* **126**, 2123–2138 (2016).

225. C. J. Turtle *et al.*, Immunotherapy of non-Hodgkin's lymphoma with a defined ratio of CD8+ and CD4+ CD19-specific chimeric antigen receptor-modified T cells. *Sci Transl Med*. **8**, 355ra116 (2016).

226. C. Stemberger *et al.*, Novel serial positive enrichment technology enables clinical multiparameter cell sorting. *PLoS ONE*. **7**, e35798 (2012).

227. C. M. Bollard *et al.*, Adapting a transforming growth factor beta-related tumor protection strategy to enhance antitumor immunity. *Blood*. **99**, 3179–3187 (2002).

228. R. Schlenker *et al.*, Chimeric PD-1:28 Receptor Upgrades Low-Avidity T cells and Restores Effector Function of Tumor-Infiltrating Lymphocytes for Adoptive Cell Therapy. *Cancer Res.* **77**, 3577–3590 (2017).

229. M. H. Kershaw, M. W. Teng, M. J. Smyth, P. K. Darcy, Supernatural T cells: genetic modification of T cells for cancer therapy. *Nature Reviews Immunology*. **5**, 928–940 (2005).

230. M. Sadelain, I. Riviere, S. Riddell, Therapeutic T cell engineering. *Nature*. **545**, 423–431 (2017).

231. L. Y. Han *et al.*, HLA class I antigen processing machinery component expression and intratumoral T-Cell infiltrate as independent prognostic markers in ovarian carcinoma. *Clin. Cancer Res.* **14**, 3372–3379 (2008).

232. J. Bukur, S. Jasinski, B. Seliger, The role of classical and non-classical HLA class I antigens in human tumors. *Semin. Cancer Biol.* **22**, 350–358 (2012).

233. R. Oren *et al.*, Functional Comparison of Engineered T Cells Carrying a Native TCR versus TCR-like Antibody-Based Chimeric Antigen Receptors Indicates Affinity/Avidity Thresholds. *The Journal of Immunology*. **193**, 5733–5743 (2014).

234. G. Zhang *et al.*, Anti-melanoma activity of T cells redirected with a TCR-like chimeric antigen receptor. *Sci Rep*. **4**, 591 (2014).

235. D. A. Bax *et al.*, EGFRvIII deletion mutations in pediatric high-grade glioma and response to targeted therapy in pediatric glioma cell lines. *Clin. Cancer Res.* **15**, 5753–5761 (2009).

236. A. A. Chekmasova *et al.*, Successful eradication of established peritoneal ovarian tumors in SCID-Beige mice following adoptive transfer of T cells genetically targeted to the MUC16 antigen. *Clin. Cancer Res.* **16**, 3594–3606 (2010).

237. E. Lanitis *et al.*, Redirected antitumor activity of primary human lymphocytes transduced with a fully human anti-mesothelin chimeric receptor. *Mol Ther*. **20**, 633–643 (2012).

238. M. Prapa *et al.*, A novel anti-GD2/4-1BB chimeric antigen receptor triggers neuroblastoma cell killing. *Oncotarget*. **6**, 24884–24894 (2015).

239. M. Hudecek *et al.*, The B-cell tumor-associated antigen ROR1 can be targeted with T cells modified to express a ROR1-specific chimeric antigen receptor. *Blood*. **116**, 4532–4541 (2010).

240. R. A. Morgan *et al.*, Case report of a serious adverse event following the administration of T cells transduced with a chimeric antigen receptor recognizing ERBB2. *Mol Ther*. **18**, 843–851 (2010).

241. T. Zhang, A. Barber, C. L. Sentman, Generation of Antitumor Responses by Genetic Modification of Primary Human T Cells with a Chimeric NKG2D Receptor. *Cancer Res*. **66**, 5927–5933 (2006).

242. P. Spear, A. Barber, A. Rynda-Apple, C. L. Sentman, NKG2D CAR T-cell therapy inhibits the growth of NKG2D ligand heterogeneous tumors. *Immunol. Cell Biol.* **91**, 435–440 (2013).

243. H. VanSeggelen *et al.*, T Cells Engineered With Chimeric Antigen Receptors Targeting NKG2D Ligands Display Lethal Toxicity in Mice. *Mol Ther*. **23**, 1600–1610 (2015).

244. M. L. Sentman *et al.*, Mechanisms of Acute Toxicity in NKG2D Chimeric Antigen Receptor T Cell-Treated Mice. *The Journal of Immunology*. **197**, 4674–4685 (2016).

245. K. S. Kahlon *et al.*, Specific recognition and killing of glioblastoma multiforme by interleukin 13-zetakine redirected cytolytic T cells. *Cancer Res*. **64**, 9160–9166 (2004).

246. G. Krenciute *et al.*, Characterization and Functional Analysis of scFv-based Chimeric Antigen Receptors to Redirect T Cells to IL13Ralpha2-positive Glioma. *Mol Ther*. **24**, 354–363 (2016).

247. C. E. Brown *et al.*, Bioactivity and Safety of IL13Rα2-Redirected Chimeric Antigen Receptor CD8+ T Cells in Patients with Recurrent Glioblastoma. *Clin. Cancer Res.* **21**, 4062–4072 (2015).

248. K. Tamada *et al.*, Redirecting gene-modified T cells toward various cancer types using tagged antibodies. *Clin. Cancer Res.* **18**, 6436–6445 (2012).

249. K. Kudo *et al.*, T lymphocytes expressing a CD16 signaling receptor exert antibody-dependent cancer cell killing. *Cancer Res.* **74**, 93–103 (2014).

250. K. Urbanska *et al.*, A universal strategy for adoptive immunotherapy of cancer through use of a novel T-cell antigen receptor. *Cancer Res.* **72**, 1844–1852 (2012).

251. Q. Ma *et al.*, A novel TCR-like CAR with specificity for PR1/HLA-A2 effectively targets myeloid leukemia in vitro when expressed in human adult peripheral blood and cord blood T cells. *Cytotherapy*. **18**, 985–994 (2016).

252. D. T. Harris *et al.*, Comparison of T Cell Activities Mediated by Human TCRs and CARs That Use the Same Recognition Domains. *The Journal of Immunology*. **200**, 1088–1100 (2018).

253. M. Hudecek *et al.*, Receptor Affinity and Extracellular Domain Modifications Affect Tumor Recognition by ROR1-Specific Chimeric Antigen Receptor T Cells. *Clin. Cancer Res.* **19**, 3153–3164 (2013).

254. R. C. Lynn *et al.*, High-affinity FRbeta-specific CAR T cells eradicate AML and normal myeloid lineage without HSC toxicity. *Leukemia : official journal of the Leukemia Society of America, Leukemia Research Fund, UK*. **30**, 1355–1364 (2016).

255. X. Liu *et al.*, Affinity-Tuned ErbB2 or EGFR Chimeric Antigen Receptor T Cells Exhibit an Increased Therapeutic Index against Tumors in Mice. *Cancer Res.* **75**, 3596–3607 (2015).

256. A. H. Long *et al.*, 4-1BB costimulation ameliorates T cell exhaustion induced by tonic signaling of chimeric antigen receptors. *Nature Medicine*. **21**, 581–590 (2015).

257. S. E. James *et al.*, Antigen sensitivity of CD22-specific chimeric TCR is modulated by target epitope distance from the cell membrane. *J. Immunol.* **180**, 7028–7038 (2008).

258. A. A. Hombach *et al.*, T cell activation by antibody-like immunoreceptors: the position of the binding epitope within the target molecule determines the efficiency of activation of redirected T cells. *J. Immunol.* **178**, 4650–4657 (2007).

259. R. D. Guest *et al.*, The role of extracellular spacer regions in the optimal design of chimeric immune receptors: evaluation of four different scFvs and antigens. *J. Immunother.* **28**, 203–211 (2005).

260. M. Hudecek *et al.*, The nonsignaling extracellular spacer domain of chimeric antigen receptors is decisive for in vivo antitumor activity. *Cancer Immunol Res*. **3**, 125–135 (2015).

261. A. Hombach, A. A. Hombach, H. Abken, Adoptive immunotherapy with genetically engineered T cells: modification of the IgG1 Fc 'spacer' domain in the extracellular moiety of chimeric antigen receptors avoids “off-target” activation and unintended initiation of an innate immune response. *Gene Ther.* **17**, 1206–1213 (2010).

262. M. Sadelain, I. Riviere, R. Brentjens, Targeting tumours with genetically enhanced T lymphocytes. *Nat. Rev. Cancer*. **3**, 35–45 (2003).

263. T. Brocker, K. Karjalainen, Signals through T cell receptor-zeta chain alone are insufficient to prime resting T lymphocytes. *J Exp Med*. **181**, 1653–1659 (1995).

264. L. J. N. Cooper *et al.*, T-cell clones can be rendered specific for CD19: toward the selective augmentation of the graft-versus-B-lineage leukemia effect. *Blood*. **101**, 1637–1644 (2003).

265. M. K. Jenkins, P. S. Taylor, S. D. Norton, K. B. Urdahl, CD28 delivers a costimulatory signal involved in antigen-specific IL-2 production by human T cells. *J Immunol*. **147**, 2461–2466 (1991).

266. B. Savoldo *et al.*, CD28 costimulation improves expansion and persistence of chimeric antigen receptor-modified T cells in lymphoma patients. *J. Clin. Invest.* **121**, 1822–1826 (2011).

267. D. M. Kofler *et al.*, CD28 costimulation Impairs the efficacy of a redirected t-cell antitumor attack in the presence of regulatory t cells which can be overcome by preventing Lck activation. *Mol Ther*. **19**, 760–767 (2011).

268. M. C. Milone *et al.*, Chimeric receptors containing CD137 signal transduction domains mediate enhanced survival of T cells and increased antileukemic efficacy in vivo. *Mol Ther*. **17**, 1453–1464 (2009).

269. O. U. Kawalekar *et al.*, Distinct Signaling of Coreceptors Regulates Specific Metabolism Pathways and Impacts Memory Development in CAR T Cells. *Immunity*. **44**, 380–390 (2016).

270. A. Balakrishnan *et al.*, Analysis of ROR1 Protein Expression in Human Cancer and Normal Tissues. *Clin. Cancer Res.* **23**, 3061–3071 (2017).

271. K. Chang, I. Pastan, Molecular cloning of mesothelin, a differentiation antigen present on mesothelium, mesotheliomas, and ovarian cancers. *Proceedings of the National Academy of Sciences*. **93**, 136–140 (1996).

272. K. Mujoo, D. A. Cheresh, H. M. Yang, R. A. Reisfeld, Disialoganglioside GD2 on human neuroblastoma cells: target antigen for monoclonal antibody-mediated cytolysis and suppression of tumor growth. *Cancer Res*. **47**, 1098–1104 (1987).

273. J. D. Pancook *et al.*, Expression and regulation of the neural cell adhesion molecule L1 on human cells of myelomonocytic and lymphoid origin. *J Immunol*. **158**, 4413–4421 (1997).

274. M. F. Press, C. Cordon-Cardo, D. J. Slamon, Expression of the HER-2/neu proto-oncogene in normal human adult and fetal tissues. *Oncogene*. **5**, 953–962 (1990).

275. Y. Wang *et al.*, MUC16 expression during embryogenesis, in adult tissues, and ovarian cancer in the mouse. *Differentiation*. **76**, 1081–1092 (2008).

276. M. A. Pule *et al.*, Virus-specific T cells engineered to coexpress tumor-specific receptors: persistence and antitumor activity in individuals with neuroblastoma. *Nature Medicine*. **14**, 1264–1270 (2008).

277. L. A. Johnson *et al.*, Rational development and characterization of humanized anti-EGFR variant III chimeric antigen receptor T cells for glioblastoma. *Sci Transl Med*. **7**, 275ra22 (2015).

278. A. D. Posey *et al.*, Engineered CAR T Cells Targeting the Cancer-Associated Tn-Glycoform of the Membrane Mucin MUC1 Control Adenocarcinoma. *Immunity*. **44**, 1444–1454 (2016).

279. K. Watanabe *et al.*, Target antigen density governs the efficacy of anti-CD20-CD28-CD3 ζ chimeric antigen receptor-modified effector CD8+ T cells. *The Journal of Immunology*. **194**, 911–920 (2015).

280. C. Berger *et al.*, Safety of targeting ROR1 in primates with chimeric antigen receptor-modified T cells. *Cancer Immunol Res*. **3**, 206–216 (2015).

281. B. G. Till *et al.*, Adoptive immunotherapy for indolent non-Hodgkin lymphoma and mantle cell lymphoma using genetically modified autologous CD20-specific T cells. *Blood*. **112**, 2261–2271 (2008).

282. M. C. Jensen *et al.*, Antitransgene rejection responses contribute to attenuated persistence of adoptively transferred CD20/CD19-specific chimeric antigen receptor redirected T cells in humans. *Biol. Blood Marrow Transplant.* **16**, 1245–1256 (2010).

283. C. H. Lamers *et al.*, Treatment of metastatic renal cell carcinoma with autologous T-lymphocytes genetically retargeted against carbonic anhydrase IX: first clinical experience. *J. Clin. Oncol.* **24**, e20–2 (2006).

284. C. H. Lamers *et al.*, Immune responses to transgene and retroviral vector in patients treated with ex vivo-engineered T cells. *Blood*. **117**, 72–82 (2011).

285. C. Berger, M. E. Flowers, E. H. Warren, S. R. Riddell, Analysis of transgene-specific immune responses that limit the in vivo persistence of adoptively transferred HSV-TK-modified donor T cells after allogeneic hematopoietic cell transplantation. *Blood*. **107**, 2294–2302 (2006).

286. S. R. Riddell *et al.*, T-cell mediated rejection of gene-modified HIV-specific cytotoxic T lymphocytes in HIV-infected patients. *Nature Medicine*. **2**, 216–223 (1996).

287. J. Maher, R. J. Brentjens, G. Gunset, I. Riviere, M. Sadelain, Human T-lymphocyte cytotoxicity and proliferation directed by a single chimeric TCRzeta /CD28 receptor. *Nat. Biotechnol.* **20**, 70–75 (2002).

288. R. J. Brentjens *et al.*, CD19-Targeted T Cells Rapidly Induce Molecular Remissions in Adults with Chemotherapy-Refractory Acute Lymphoblastic Leukemia. *Sci Transl Med*. **5**, 177ra38 (2013).

289. S. L. Maude *et al.*, Chimeric antigen receptor T cells for sustained remissions in leukemia. *N Engl J Med*. **371**, 1507–1517 (2014).

290. D. W. Lee *et al.*, T cells expressing CD19 chimeric antigen receptors for acute lymphoblastic leukaemia in children and young adults: a phase 1 dose-escalation trial. *Lancet*. **385**, 517–528 (2015).

291. M. L. Davila *et al.*, Efficacy and toxicity management of 19-28z CAR T cell therapy in B cell acute lymphoblastic leukemia. *Sci Transl Med*. **6**, 224ra25 (2014).

292. R. Gardner *et al.*, Acquisition of a CD19-negative myeloid phenotype allows immune escape of MLL-rearranged B-ALL from CD19 CAR-T-cell therapy. *Blood*. **127**, 2406–2410 (2016).

293. E. Sotillo *et al.*, Convergence of Acquired Mutations and Alternative Splicing of CD19 Enables Resistance to CART-19 Immunotherapy. *Cancer Discov*. **5**, 1282–1295 (2015).

294. S. L. Maude *et al.*, Tisagenlecleucel in Children and Young Adults with B-Cell Lymphoblastic Leukemia. *N Engl J Med*. **378**, 439–448 (2018).

295. J. N. Kochenderfer *et al.*, Eradication of B-lineage cells and regression of lymphoma in a patient treated with autologous T cells genetically engineered to recognize CD19. *Blood*. **116**, 4099–4102 (2010).

296. S. J. Schuster *et al.*, Chimeric Antigen Receptor T Cells in Refractory B-Cell Lymphomas. *N Engl J Med*. **377**, 2545–2554 (2017).

297. S. S. Neelapu *et al.*, Axicabtagene Ciloleucel CAR T-Cell Therapy in Refractory Large B-Cell Lymphoma. *N Engl J Med*. **377**, 2531–2544 (2017).

298. J. A. Burger *et al.*, Ibrutinib as Initial Therapy for Patients with Chronic Lymphocytic Leukemia. *N Engl J Med*. **373**, 2425–2437 (2015).

299. J. C. Byrd *et al.*, Acalabrutinib (ACP-196) in Relapsed Chronic Lymphocytic Leukemia. *N Engl J Med*. **374**, 323–332 (2016).

300. J. A. Jones *et al.*, Venetoclax for chronic lymphocytic leukaemia progressing after ibrutinib: an interim analysis of a multicentre, open-label, phase 2 trial. *Lancet Oncol.* **19**, 65–75 (2018).

301. A. W. Roberts *et al.*, Targeting BCL2 with Venetoclax in Relapsed Chronic Lymphocytic Leukemia. *N Engl J Med*. **374**, 311–322 (2016).

302. M. Kalos *et al.*, T cells with chimeric antigen receptors have potent antitumor effects and can establish memory in patients with advanced leukemia. *Sci Transl Med*. **3**, 95ra73 (2011).

303. C. J. Turtle *et al.*, Durable Molecular Remissions in Chronic Lymphocytic Leukemia Treated With CD19-Specific Chimeric Antigen Receptor-Modified T Cells After Failure of Ibrutinib. *J. Clin. Oncol.* **35**, 3010–3020 (2017).

304. D. W. Lee *et al.*, Current concepts in the diagnosis and management of cytokine release syndrome. *Blood*. **124**, 188–195 (2014).

305. J. Gust *et al.*, Endothelial Activation and Blood-Brain Barrier Disruption in Neurotoxicity after Adoptive Immunotherapy with CD19 CAR-T Cells. *Cancer Discov*. **7**, 1404–1419 (2017).

306. K. A. Hay *et al.*, Kinetics and biomarkers of severe cytokine release syndrome after CD19 chimeric antigen receptor-modified T-cell therapy. *Blood*. **130**, 2295–2306 (2017).

307. S. L. Maude, D. Barrett, D. T. Teachey, S. A. Grupp, Managing cytokine release syndrome associated with novel T cell-engaging therapies. *Cancer J*. **20**, 119–122 (2014).

308. S. S. Neelapu *et al.*, Toxicity management after chimeric antigen receptor T cell therapy: one size does not fit “ALL.” *Nature Reviews Clinical Oncology 2018 15:4*. **15**, 218–218 (2018).

309. X. Wang *et al.*, A transgene-encoded cell surface polypeptide for selection, in vivo tracking, and ablation of engineered cells. *Blood*. **118**, 1255–1263 (2011).

310. D. Gomes-Silva *et al.*, CD7-edited T cells expressing a CD7-specific CAR for the therapy of T-cell malignancies. *Blood*. **130**, 285–296 (2017).

311. Y. Yang *et al.*, TCR engagement negatively affects CD8 but not CD4 CAR T cell expansion and leukemic clearance. *Sci Transl Med*. **9**, eaag1209 (2017).

312. P. M. Maciocia *et al.*, Targeting the T cell receptor β-chain constant region for immunotherapy of T cell malignancies. *Nature Medicine*. **23**, 1416–1423 (2017).

313. C.-M. Wang *et al.*, Autologous T Cells Expressing CD30 Chimeric Antigen Receptors for Relapsed or Refractory Hodgkin Lymphoma: An Open-Label Phase I Trial. *Clin. Cancer Res.* **23**, 1156–1166 (2017).

314. C. A. Ramos *et al.*, Clinical and immunological responses after CD30-specific chimeric antigen receptor-redirected lymphocytes. *J. Clin. Invest.* **127**, 3462–3471 (2017).

315. A. P. Rapoport *et al.*, NY-ESO-1-specific TCR-engineered T cells mediate sustained antigen-specific antitumor effects in myeloma. *Nature Medicine*. **21**, 914–921 (2015).

316. A. L. Garfall *et al.*, Chimeric Antigen Receptor T Cells against CD19 for Multiple Myeloma. *N Engl J Med*. **373**, 1040–1047 (2015).

317. S. Lonial *et al.*, Elotuzumab Therapy for Relapsed or Refractory Multiple Myeloma. *N Engl J Med*. **373**, 621–631 (2015).

318. A. Palumbo *et al.*, Daratumumab, Bortezomib, and Dexamethasone for Multiple Myeloma. *N Engl J Med*. **375**, 754–766 (2016).

319. M. A. Dimopoulos *et al.*, Daratumumab, Lenalidomide, and Dexamethasone for Multiple Myeloma. *N Engl J Med*. **375**, 1319–1331 (2016).

320. T. Gogishvili *et al.*, SLAMF7-CAR T cells eliminate myeloma and confer selective fratricide of SLAMF7+ normal lymphocytes. *Blood*. **130**, 2838–2847 (2017).

321. E. Drent *et al.*, Pre-clinical evaluation of CD38 chimeric antigen receptor engineered T cells for the treatment of multiple myeloma. *Haematologica*. **101**, 616–625 (2016).

322. E. Drent *et al.*, A Rational Strategy for Reducing On-Target Off-Tumor Effects of CD38-Chimeric Antigen Receptors by Affinity Optimization. *Mol Ther*. **25**, 1946–1958 (2017).

323. A. J. Novak *et al.*, Expression of BCMA, TACI, and BAFF-R in multiple myeloma: a mechanism for growth and survival. *Blood*. **103**, 689–694 (2004).

324. Y.-T. Tai *et al.*, APRIL and BCMA promote human multiple myeloma growth and immunosuppression in the bone marrow microenvironment. *Blood*. **127**, 3225–3236 (2016).

325. R. O. Carpenter *et al.*, B-cell maturation antigen is a promising target for adoptive T-cell therapy of multiple myeloma. *Clin. Cancer Res.* **19**, 2048–2060 (2013).

326. A. Seckinger *et al.*, Target Expression, Generation, Preclinical Activity, and Pharmacokinetics of the BCMA-T Cell Bispecific Antibody EM801 for Multiple Myeloma Treatment. *Cancer Cell*. **31**, 396–410 (2017).

327. S. A. Laurent *et al.*, γ-Secretase directly sheds the survival receptor BCMA from plasma cells. *Nat Commun*. **6**, 7333 (2015).

328. S. A. Ali *et al.*, T cells expressing an anti-B-cell maturation antigen chimeric antigen receptor cause remissions of multiple myeloma. *Blood*. **128**, 1688–1700 (2016).

329. P. Otáhal *et al.*, Lenalidomide enhances antitumor functions of chimeric antigen receptor modified T cells. *Oncoimmunology*. **5**, e1115940 (2016).

330. H. Tashiro *et al.*, Treatment of Acute Myeloid Leukemia with T Cells Expressing Chimeric Antigen Receptors Directed to C-type Lectin-like Molecule 1. *Mol Ther*. **25**, 2202–2213 (2017).

331. F. Perna *et al.*, Integrating Proteomics and Transcriptomics for Systematic Combinatorial Chimeric Antigen Receptor Therapy of AML. *Cancer Cell*. **32**, 506–519.e5 (2017).

332. C. U. Louis *et al.*, Antitumor activity and long-term fate of chimeric antigen receptor-positive T cells in patients with neuroblastoma. *Blood*. **118**, 6050–6056 (2011).

333. N. Ahmed *et al.*, Human Epidermal Growth Factor Receptor 2 (HER2) -Specific Chimeric Antigen Receptor-Modified T Cells for the Immunotherapy of HER2-Positive Sarcoma. *J. Clin. Oncol.* **33**, 1688–1696 (2015).

334. Z. Grada *et al.*, TanCAR: A Novel Bispecific Chimeric Antigen Receptor for Cancer Immunotherapy. *Mol Ther Nucleic Acids*. **2**, e105 (2013).

335. E. Zah, M.-Y. Lin, A. Silva-Benedict, M. C. Jensen, Y. Y. Chen, T Cells Expressing CD19/CD20 Bispecific Chimeric Antigen Receptors Prevent Antigen Escape by Malignant B Cells. *Cancer Immunol Res*. **4**, 498–508 (2016).

336. Y. Cao *et al.*, Single-chain antibody-based immunotoxins targeting Her2/neu: design optimization and impact of affinity on antitumor efficacy and off-target toxicity. *Mol. Cancer Ther.* **11**, 143–153 (2012).

337. H. G. Caruso *et al.*, Tuning Sensitivity of CAR to EGFR Density Limits Recognition of Normal Tissue While Maintaining Potent Antitumor Activity. *Cancer Res.* **75**, 3505–3518 (2015).

338. S. Wilkie *et al.*, Dual Targeting of ErbB2 and MUC1 in Breast Cancer Using Chimeric Antigen Receptors Engineered to Provide Complementary Signaling. *J. Clin. Immunol.* **32**, 1059–1070 (2012).

339. C. C. Kloss, M. Condomines, M. Cartellieri, M. Bachmann, M. Sadelain, Combinatorial antigen recognition with balanced signaling promotes selective tumor eradication by engineered T cells. *Nat. Biotechnol.* **31**, 71–75 (2013).

340. M. E. Keir, M. J. Butte, G. J. Freeman, A. H. Sharpe, PD-1 and its ligands in tolerance and immunity. *Annu. Rev. Immunol.* **26**, 677–704 (2008).

341. V. D. Fedorov, M. Themeli, M. Sadelain, PD-1- and CTLA-4-Based Inhibitory Chimeric Antigen Receptors (iCARs) Divert Off-Target Immunotherapy Responses. *Sci Transl Med*. **5**, 215ra172 (2013).

342. A. Juillerat *et al.*, Design of chimeric antigen receptors with integrated controllable transient functions. *Nature Publishing Group*. **6**, 18950 (2016).

343. R. Sakemura *et al.*, A Tet-On Inducible System for Controlling CD19-Chimeric Antigen Receptor Expression upon Drug Administration. *Cancer Immunol Res*. **4**, 658–668 (2016).

344. C.-Y. Wu, K. T. Roybal, E. M. Puchner, J. Onuffer, W. A. Lim, Remote control of therapeutic T cells through a small molecule-gated chimeric receptor. *Science* (2015), doi:10.1126/science.aab4077.

345. E. R. Suarez *et al.*, Chimeric antigen receptor T cells secreting anti-PD-L1 antibodies more effectively regress renal cell carcinoma in a humanized mouse model. *Oncotarget* (2016), doi:10.18632/oncotarget.9114.

346. L. Cherkassky *et al.*, Human CAR T cells with cell-intrinsic PD-1 checkpoint blockade resist tumor-mediated inhibition. *J. Clin. Invest.* **126**, 3130–3144 (2016).

347. X. Liu *et al.*, A Chimeric Switch-Receptor Targeting PD1 Augments the Efficacy of Second-Generation CAR T Cells in Advanced Solid Tumors. *Cancer Res.* **76**, 1578–1590 (2016).

348. M. E. Prosser, C. E. Brown, A. F. Shami, S. J. Forman, M. C. Jensen, Tumor PD-L1 co-stimulates primary human CD8(+) cytotoxic T cells modified to express a PD1:CD28 chimeric receptor. *Mol. Immunol.* **51**, 263–272 (2012).

349. I. Caruana *et al.*, Heparanase promotes tumor infiltration and antitumor activity of CAR-redirected T lymphocytes. *Nature Medicine*. **21**, 524–529 (2015).

350. L. C. S. Wang *et al.*, Targeting Fibroblast Activation Protein in Tumor Stroma with Chimeric Antigen Receptor T Cells Can Inhibit Tumor Growth and Augment Host Immunity without Severe Toxicity. *Cancer Immunol Res*. **2**, 154–166 (2014).

351. S. P. Kerkar *et al.*, Tumor-specific CD8+ T cells expressing interleukin-12 eradicate established cancers in lymphodepleted hosts. *Cancer Res.* **70**, 6725–6734 (2010).

352. L. Zhang *et al.*, Improving Adoptive T Cell Therapy by Targeting and Controlling IL-12 Expression to the Tumor Environment. *Mol Ther*. **19**, 751–759 (2011).

353. M. Chmielewski, C. Kopecky, A. A. Hombach, H. Abken, IL-12 release by engineered T cells expressing chimeric antigen receptors can effectively Muster an antigen-independent macrophage response on tumor cells that have shut down tumor antigen expression. *Cancer Res.* **71**, 5697–5706 (2011).

354. M. Sukumar *et al.*, Mitochondrial Membrane Potential Identifies Cells with Enhanced Stemness for Cellular Therapy. *Cell Metab*. **23**, 63–76 (2016).

355. M. D. Buck *et al.*, Mitochondrial Dynamics Controls T Cell Fate through Metabolic Programming. *Cell*. **166**, 63–76 (2016).

356. S. Srivastava, S. R. Riddell, Engineering CAR-T cells: Design concepts. *Trends in Immunology*. **36**, 494–502 (2015).

357. J. N. Kochenderfer *et al.*, Chemotherapy-refractory diffuse large B-cell lymphoma and indolent B-cell malignancies can be effectively treated with autologous T cells expressing an anti-CD19 chimeric antigen receptor. *J. Clin. Oncol.* **33**, 540–549 (2015).

358. S. Terakura *et al.*, Generation of CD19-chimeric antigen receptor modified CD8+ T cells derived from virus-specific central memory T cells. *Blood*. **119**, 72–82 (2012).

359. H. Karlsson *et al.*, Evaluation of Intracellular Signaling Downstream Chimeric Antigen Receptors. *PLoS ONE*. **10**, e0144787 (2015).

360. V. Mayya *et al.*, Quantitative phosphoproteomic analysis of T cell receptor signaling reveals system-wide modulation of protein-protein interactions. *Sci Signal*. **2**, ra46–ra46 (2009).

361. V. Nguyen *et al.*, A new approach for quantitative phosphoproteomic dissection of signaling pathways applied to T cell receptor activation. *Mol. Cell Proteomics*. **8**, 2418–2431 (2009).

362. M. N. Navarro, J. Goebel, C. Feijoo-Carnero, N. Morrice, D. A. Cantrell, Phosphoproteomic analysis reveals an intrinsic pathway for the regulation of histone deacetylase 7 that controls the function of cytotoxic T lymphocytes. *Nat. Immunol.* **12**, 352–361 (2011).

363. P. Ruperez, A. Gago-Martinez, A. L. Burlingame, J. A. Oses-Prieto, Quantitative phosphoproteomic analysis reveals a role for serine and threonine kinases in the cytoskeletal reorganization in early T cell receptor activation in human primary T cells. *Mol. Cell Proteomics*. **11**, 171–186 (2012).

364. M. Salek *et al.*, Quantitative phosphoproteome analysis unveils LAT as a modulator of CD3ζ and ZAP-70 tyrosine phosphorylation. *PLoS ONE*. **8**, e77423 (2013).

365. R. T. Abraham, A. Weiss, Jurkat T cells and development of the T-cell receptor signalling paradigm. *Nature Reviews Immunology*. **4**, 301–308 (2004).

366. B. Jena *et al.*, Chimeric antigen receptor (CAR)-specific monoclonal antibody to detect CD19-specific T cells in clinical trials. *PLoS ONE*. **8**, e57838 (2013).

367. A. J. Davenport *et al.*, Chimeric antigen receptor T cells form nonclassical and potent immune synapses driving rapid cytotoxicity. *Proc. Natl. Acad. Sci. U.S.A.* **115**, E2068–E2076 (2018).

368. S.-E. Ong *et al.*, Stable isotope labeling by amino acids in cell culture, SILAC, as a simple and accurate approach to expression proteomics. *Mol. Cell Proteomics*. **1**, 376–386 (2002).

369. S.-E. Ong, M. Mann, A practical recipe for stable isotope labeling by amino acids in cell culture (SILAC). *Nat Protoc*. **1**, 2650–2660 (2006).

370. L. Liu *et al.*, Inclusion of Strep-tag II in design of antigen receptors for T-cell immunotherapy. *Nat. Biotechnol.* **34**, 430–434 (2016).

371. A. Thompson *et al.*, Tandem mass tags: a novel quantification strategy for comparative analysis of complex protein mixtures by MS/MS. *Anal. Chem.* **75**, 1895–1904 (2003).

372. A. Michalski, J. Cox, M. Mann, More than 100,000 detectable peptide species elute in single shotgun proteomics runs but the majority is inaccessible to data-dependent LC-MS/MS. *J. Proteome Res.* **10**, 1785–1793 (2011).

373. N. S. van Oers *et al.*, Constitutive tyrosine phosphorylation of the T-cell receptor (TCR) zeta subunit: regulation of TCR-associated protein tyrosine kinase activity by TCR zeta. *Mol Cell Biol*. **13**, 5771–5780 (1993).

374. D. Rueda *et al.*, Bcl10 controls TCR- and FcgammaR-induced actin polymerization. *J Immunol*. **178**, 4373–4384 (2007).

375. K. Ishiguro, T. Ando, H. Goto, R. Xavier, Bcl10 is phosphorylated on Ser138 by Ca2+/calmodulin-dependent protein kinase II. *Mol. Immunol.* **44**, 2095–2100 (2007).

376. M. J. Frigault *et al.*, Identification of Chimeric Antigen Receptors That Mediate Constitutive or Inducible Proliferation of T Cells. *Cancer Immunol Res*. **3**, 356–367 (2015).

377. G. K. Smyth, Linear models and empirical bayes methods for assessing differential expression in microarray experiments. *Stat Appl Genet Mol Biol*. **3**, Article3 (2004).

378. F. Sekiya, Y. S. Bae, D. Y. Jhon, S. C. Hwang, S. G. Rhee, AHNAK, a protein that binds and activates phospholipase C-gamma1 in the presence of arachidonic acid. *J. Biol. Chem.* **274**, 13900–13907 (1999).

379. D. Matza *et al.*, A scaffold protein, AHNAK1, is required for calcium signaling during T cell activation. *Immunity*. **28**, 64–74 (2008).

380. A. R. Sanchez-Paulete *et al.*, Deciphering CD137 (4-1BB) signaling in T-cell costimulation for translation into successful cancer immunotherapy. *Eur. J. Immunol.* **46**, 513–522 (2016).

381. J. S. Boomer, J. M. Green, An enigmatic tail of CD28 signaling. *Cold Spring Harb Perspect Biol*. **2**, a002436 (2010).

382. L. Sabbagh *et al.*, Leukocyte-specific protein 1 links TNF receptor-associated factor 1 to survival signaling downstream of 4-1BB in T cells. *J. Leukoc. Biol.* **93**, 713–721 (2013).

383. F. Baixauli *et al.*, The mitochondrial fission factor dynamin-related protein 1 modulates T-cell receptor signalling at the immune synapse. *EMBO J.* **30**, 1238–1250 (2011).

384. D. Röth, P. H. Krammer, K. Gülow, Dynamin related protein 1-dependent mitochondrial fission regulates oxidative signalling in T cells. *FEBS Lett.* **588**, 1749–1754 (2014).

385. M. A. Daniels, E. Teixeiro, TCR Signaling in T Cell Memory. *Front Immunol*. **6**, 617 (2015).

386. S. M. Kaech, W. Cui, Transcriptional control of effector and memory CD8+ T cell differentiation. *Nature Reviews Immunology*. **12**, 749–761 (2012).

387. J. M. Marchingo *et al.*, T cell signaling. Antigen affinity, costimulation, and cytokine inputs sum linearly to amplify T cell expansion. **346**, 1123–1127 (2014).

388. P. Rougerie *et al.*, Fam65b is a new transcriptional target of FOXO1 that regulates RhoA signaling for T lymphocyte migration. *The Journal of Immunology*. **190**, 748–755 (2013).

389. S. M. Kaech *et al.*, Selective expression of the interleukin 7 receptor identifies effector CD8 T cells that give rise to long-lived memory cells. *Nat Immunol*. **4**, 1191–1198 (2003).

390. Y. M. Kerdiles *et al.*, Foxo1 links homing and survival of naive T cells by regulating L-selectin, CCR7 and interleukin 7 receptor. *Nat Immunol*. **10**, 176–184 (2009).

391. D. Moogk *et al.*, Constitutive Lck Activity Drives Sensitivity Differences between CD8+ Memory T Cell Subsets. *The Journal of Immunology*. **197**, 644–654 (2016).

392. K. Nika *et al.*, Constitutively active Lck kinase in T cells drives antigen receptor signal transduction. *Immunity*. **32**, 766–777 (2010).

393. J. Dobbins *et al.*, Binding of the cytoplasmic domain of CD28 to the plasma membrane inhibits Lck recruitment and signaling. *Sci Signal*. **9**, ra75–ra75 (2016).

394. R. Tavano *et al.*, CD28 and lipid rafts coordinate recruitment of Lck to the immunological synapse of human T lymphocytes. *J Immunol*. **173**, 5392–5397 (2004).

395. V. Kalia *et al.*, Prolonged interleukin-2Ralpha expression on virus-specific CD8+ T cells favors terminal-effector differentiation in vivo. *Immunity*. **32**, 91–103 (2010).

396. M. E. Pipkin *et al.*, Interleukin-2 and inflammation induce distinct transcriptional programs that promote the differentiation of effector cytolytic T cells. *Immunity*. **32**, 79–90 (2010).

397. R. I. Klein Geltink *et al.*, Mitochondrial Priming by CD28. *Cell*. **171**, 385–397.e11 (2017).

398. J. H. Park *et al.*, Long-Term Follow-up of CD19 CAR Therapy in Acute Lymphoblastic Leukemia. *N Engl J Med*. **378**, 449–459 (2018).

399. P. Nguyen, I. Moisini, T. L. Geiger, Identification of a murine CD28 dileucine motif that suppresses single-chain chimeric T-cell receptor expression and function. *Blood*. **102**, 4320–4325 (2003).

400. J. Cox, M. Mann, MaxQuant enables high peptide identification rates, individualized p.p.b.-range mass accuracies and proteome-wide protein quantification. *Nat. Biotechnol.* **26**, 1367–1372 (2008).

401. S. Tyanova *et al.*, The Perseus computational platform for comprehensive analysis of (prote)omics data. *Nat. Methods*. **13**, 731–740 (2016).

402. M. E. Ritchie *et al.*, limma powers differential expression analyses for RNA-sequencing and microarray studies. *Nucleic Acids Res.* **43**, e47 (2015).

403. G. K. Smyth, J. Michaud, H. S. Scott, Use of within-array replicate spots for assessing differential expression in microarray experiments. *Bioinformatics*. **21**, 2067–2075 (2005).

404. A. Dobin *et al.*, STAR: ultrafast universal RNA-seq aligner. *Bioinformatics*. **29**, 15–21 (2013).

405. B. Li, C. N. Dewey, RSEM: accurate transcript quantification from RNA-Seq data with or without a reference genome. *BMC Bioinformatics*. **12**, 323 (2011).

406. M. D. Robinson, A. Oshlack, A scaling normalization method for differential expression analysis of RNA-seq data. *Genome Biol.* **11**, R25 (2010).

407. C. W. Law, Y. Chen, W. Shi, G. K. Smyth, voom: Precision weights unlock linear model analysis tools for RNA-seq read counts. *Genome Biol.* **15**, R29 (2014).

408. T. J. Fry *et al.*, CD22-targeted CAR T cells induce remission in B-ALL that is naive or resistant to CD19-targeted CAR immunotherapy. *Nature Medicine*. **24**, 20–28 (2018).

409. J. N. Brudno *et al.*, T Cells Genetically Modified to Express an Anti-B-Cell Maturation Antigen Chimeric Antigen Receptor Cause Remissions of Poor-Prognosis Relapsed Multiple Myeloma. *J. Clin. Oncol.*, JCO2018778084 (2018).

410. R. G. Majzner, C. L. Mackall, Tumor Antigen Escape from CAR T-cell Therapy. *Cancer Discov*. **8**, 1219–1226 (2018).

411. A. J. Walker *et al.*, Tumor Antigen and Receptor Densities Regulate Efficacy of a Chimeric Antigen Receptor Targeting Anaplastic Lymphoma Kinase. *Mol Ther*. **25**, 2189–2201 (2017).

412. Y. Sykulev, M. Joo, I. Vturina, T. J. Tsomides, H. N. Eisen, Evidence that a single peptide-MHC complex on a target cell can elicit a cytolytic T cell response. *Immunity*. **4**, 565–571 (1996).

413. J. Huang *et al.*, A single peptide-major histocompatibility complex ligand triggers digital cytokine secretion in CD4(+) T cells. *Immunity*. **39**, 846–857 (2013).

414. M. Chmielewski, A. Hombach, C. Heuser, G. P. Adams, H. Abken, T cell activation by antibody-like immunoreceptors: increase in affinity of the single-chain fragment domain above threshold does not increase T cell activation against antigen-positive target cells but decreases selectivity. *J. Immunol.* **173**, 7647–7653 (2004).

415. J. R. James, R. D. Vale, Biophysical mechanism of T-cell receptor triggering in a reconstituted system. *Nature*. **487**, 64–69 (2012).

416. Y. Y. L. Yu, N. Netuschil, L. Lybarger, J. M. Connolly, T. H. Hansen, Cutting edge: single-chain trimers of MHC class I molecules form stable structures that potently stimulate antigen-specific T cells and B cells. *J Immunol*. **168**, 3145–3149 (2002).

417. M. O. Butler *et al.*, Long-lived antitumor CD8+ lymphocytes for adoptive therapy generated using an artificial antigen-presenting cell. *Clin. Cancer Res.* **13**, 1857–1867 (2007).

418. F. Letourneur, R. D. Klausner, Activation of T cells by a tyrosine kinase activation domain in the cytoplasmic tail of CD3 epsilon. **255**, 79–82 (1992).

419. L. Li *et al.*, Ionic CD3-Lck interaction regulates the initiation of T-cell receptor signaling. *Proc. Natl. Acad. Sci. U.S.A.* **114**, E5891–E5899 (2017).

420. P. Tailor *et al.*, The proline-rich sequence of CD3epsilon as an amplifier of low-avidity TCR signaling. *J Immunol*. **181**, 243–255 (2008).

421. M. Mingueneau *et al.*, The proline-rich sequence of CD3epsilon controls T cell antigen receptor expression on and signaling potency in preselection CD4+CD8+ thymocytes. *Nat Immunol*. **9**, 522–532 (2008).

422. J. S. Bridgeman *et al.*, The optimal antigen response of chimeric antigen receptors harboring the CD3zeta transmembrane domain is dependent upon incorporation of the receptor into the endogenous TCR/CD3 complex. *The Journal of Immunology*. **184**, 6938–6949 (2010).

423. Y. Kagoya *et al.*, A novel chimeric antigen receptor containing a JAK-STAT signaling domain mediates superior antitumor effects. *Nature Medicine*. **5**, 177ra38 (2018).

424. S. L. Silins *et al.*, Selection of a diverse TCR repertoire in response to an Epstein-Barr virus-encoded transactivator protein BZLF1 by CD8+ cytotoxic T lymphocytes during primary and persistent infection. *Int. Immunol.* **9**, 1745–1755 (1997).

425. A. I. Salter *et al.*, Phosphoproteomic analysis of chimeric antigen receptor signaling reveals kinetic and quantitative differences that affect cell function. *Sci Signal*. **11**, eaat6753 (2018).

426. S. Srivastava, S. R. Riddell, Chimeric Antigen Receptor T Cell Therapy: Challenges to Bench-to-Bedside Efficacy. *The Journal of Immunology*. **200**, 459–468 (2018).

427. S. K. Oda *et al.*, A CD200R-CD28 fusion protein appropriates an inhibitory signal to enhance T-cell function and therapy of murine leukemia. *Blood*. **130**, 2410–2419 (2017).

428. K. T. Roybal, W. A. Lim, Synthetic Immunology: Hacking Immune Cells to Expand Their Therapeutic Capabilities. *Annu Rev Immunol*. **35**, 229–253 (2017).

429. A. O. Kamphorst *et al.*, Rescue of exhausted CD8 T cells by PD-1-targeted therapies is CD28-dependent. **355**, 1423–1427 (2017).

430. G. Rota *et al.*, Shp-2 Is Dispensable for Establishing T Cell Exhaustion and for PD-1 Signaling In Vivo. *Cell Rep*. **23**, 39–49 (2018).

431. L. Chen, X. Han, Anti-PD-1/PD-L1 therapy of human cancer: past, present, and future. *J. Clin. Invest.* **125**, 3384–3391 (2015).

432. E. Lázár-Molnár *et al.*, Crystal structure of the complex between programmed death-1 (PD-1) and its ligand PD-L2. *Proc. Natl. Acad. Sci. U.S.A.* **105**, 10483–10488 (2008).

433. D. Y.-W. Lin *et al.*, The PD-1/PD-L1 complex resembles the antigen-binding Fv domains of antibodies and T cell receptors. *Proc. Natl. Acad. Sci. U.S.A.* **105**, 3011–3016 (2008).

434. K. M. Zak *et al.*, Structure of the Complex of Human Programmed Death 1, PD-1, and Its Ligand PD-L1. *Structure/Folding and Design*. **23**, 2341–2348 (2015).

435. R. L. Maute *et al.*, Engineering high-affinity PD-1 variants for optimized immunotherapy and immuno-PET imaging. *Proc. Natl. Acad. Sci. U.S.A.* **112**, E6506–14 (2015).

436. E. Lázár-Molnár *et al.*, Structure-guided development of a high-affinity human Programmed Cell Death-1: Implications for tumor immunotherapy. *EBioMedicine*. **17**, 30–44 (2017).

437. E. K. Moon *et al.*, Multifactorial T-cell hypofunction that is reversible can limit the efficacy of chimeric antigen receptor-transduced human T cells in solid tumors. *Clin. Cancer Res.* **20**, 4262–4273 (2014).

438. C. Ankri, K. Shamalov, M. Horovitz-Fried, S. Mauer, C. J. Cohen, Human T cells engineered to express a programmed death 1/28 costimulatory retargeting molecule display enhanced antitumor activity. *The Journal of Immunology*. **191**, 4121–4129 (2013).

439. S. Kobold *et al.*, Impact of a New Fusion Receptor on PD-1-Mediated Immunosuppression in Adoptive T Cell Therapy. *J. Natl. Cancer Inst.* **107** (2015), doi:10.1093/jnci/djv146.

440. G. J. Freeman *et al.*, Engagement of the PD-1 immunoinhibitory receptor by a novel B7 family member leads to negative regulation of lymphocyte activation. *J Exp Med*. **192**, 1027–1034 (2000).

441. D. J. Andorsky *et al.*, Programmed death ligand 1 is expressed by non-hodgkin lymphomas and inhibits the activity of tumor-associated T cells. *Clin. Cancer Res.* **17**, 4232–4244 (2011).

442. L. E. Budde *et al.*, Truncated Cell-Surface CD19 As a Conditional Suicide Switch For Adoptive T Cell Immunotherapy. *Blood*. **122**, 1660–1660 (2013).

443. S. J. C. van der Stegen, M. Hamieh, M. Sadelain, The pharmacology of second-generation chimeric antigen receptors. *Nat Rev Drug Discov*. **14**, 499–509 (2015).

444. N. Nakamoto *et al.*, Functional restoration of HCV-specific CD8 T cells by PD-1 blockade is defined by PD-1 expression and compartmentalization. *Gastroenterology*. **134**, 1927–37– 1937.e1–2 (2008).

445. J. Zhou *et al.*, Potentiating functional antigen-specific $CD8^+$ T cell immunity by a novel PD1 isoform-based fusion DNA vaccine. *Mol Ther*. **21**, 1445–1455 (2013).

446. P. D. Greenberg, M. A. Cheever, Treatment of disseminated leukemia with cyclophosphamide and immune cells: tumor immunity reflects long-term persistence of tumor-specific donor T cells. *J Immunol*. **133**, 3401–3407 (1984).

447. M. Sadelain, R. Brentjens, I. Riviere, The basic principles of chimeric antigen receptor design. *Cancer Discov*. **3**, 388–398 (2013).

448. S. Rafiq *et al.*, Targeted delivery of a PD-1-blocking scFv by CAR-T cells enhances anti-tumor efficacy in vivo. *Nat. Biotechnol.* (2018), doi:10.1038/nbt.4195.

449. C. Lundegaard *et al.*, NetMHC-3.0: accurate web accessible predictions of human, mouse and monkey MHC class I affinities for peptides of length 8-11. *Nucleic Acids Res.* **36**, W509–12 (2008).

450. C. Ohlén *et al.*, CD8(+) T cell tolerance to a tumor-associated antigen is maintained at the level of expansion rather than effector function. *J Exp Med*. **195**, 1407–1418 (2002).

451. R. M. Teague *et al.*, Interleukin-15 rescues tolerant CD8+ T cells for use in adoptive immunotherapy of established tumors. *Nature Medicine*. **12**, 335–341 (2006).

452. C. H. Lamers *et al.*, Treatment of metastatic renal cell carcinoma with CAIX CAR-engineered T cells: clinical evaluation and management of on-target toxicity. *Mol Ther*. **21**, 904–912 (2013).

453. J. P. Snook, C. Kim, M. A. Williams, TCR signal strength controls the differentiation of CD4+ effector and memory T cells. *Sci Immunol*. **3**, eaas9103 (2018).

454. S. A. Rosenberg, N. P. Restifo, Adoptive cell transfer as personalized immunotherapy for human cancer. *Science*. **348**, 62–68 (2015).

455. J. N. Kochenderfer *et al.*, B-cell depletion and remissions of malignancy along with cytokine-associated toxicity in a clinical trial of anti-CD19 chimeric-antigen-receptor-transduced T cells. *Blood*. **119**, 2709–2720 (2012).

456. R. A. Gardner *et al.*, Intent-to-treat leukemia remission by CD19 CAR T cells of defined formulation and dose in children and young adults. *Blood*. **129**, 3322–3331 (2017).

457. C. A. Del Vecchio *et al.*, EGFRvIII gene rearrangement is an early event in glioblastoma tumorigenesis and expression defines a hierarchy modulated by epigenetic mechanisms. *Oncogene*. **32**, 2670–2681 (2013).

458. D. M. O apos Rourke *et al.*, A single dose of peripherally infused EGFRvIII-directed CAR T cells mediates antigen loss and induces adaptive resistance in patients with recurrent glioblastoma. *Sci Transl Med*. **9**, eaaa0984 (2017).

459. M. F. Rimawi, R. Schiff, C. K. Osborne, Targeting HER2 for the treatment of breast cancer. *Annu. Rev. Med.* **66**, 111–128 (2015).

460. G. Lammie, N. Cheung, W. Gerald, M. Rosenblum, C. Cordoncardo, Ganglioside gd(2) expression in the human nervous-system and in neuroblastomas - an immunohistochemical study. *Int. J. Oncol.* **3**, 909–915 (1993).

461. R. Hassan *et al.*, Mesothelin Immunotherapy for Cancer: Ready for Prime Time? *J. Clin. Oncol.* **34**, 4171–4179 (2016).

462. S. A. Richman *et al.*, High-Affinity GD2-Specific CAR T Cells Induce Fatal Encephalitis in a Preclinical Neuroblastoma Model. *Cancer Immunol Res*. **6**, 36–46 (2018).

463. H.-Y. H. Ho *et al.*, Wnt5a-Ror-Dishevelled signaling constitutes a core developmental pathway that controls tissue morphogenesis. *Proc. Natl. Acad. Sci. U.S.A.* **109**, 4044–4051 (2012).

464. H.-P. Chien *et al.*, Expression of ROR1 has prognostic significance in triple negative breast cancer. *Virchows Arch.* **468**, 589–595 (2016).

465. B. Cui *et al.*, High-level ROR1 associates with accelerated disease progression in chronic lymphocytic leukemia. *Blood*. **128**, 2931–2940 (2016).

466. Y.-Z. Zheng *et al.*, ROR1 is a novel prognostic biomarker in patients with lung adenocarcinoma. *Nat Immunol*. **6**, 36447 (2016).

467. J.-K. Zhou *et al.*, ROR1 expression as a biomarker for predicting prognosis in patients with colorectal cancer. *Oncotarget*. **8**, 32864–32872 (2017).

468. M. Y. Choi *et al.*, Pre-clinical Specificity and Safety of UC-961, a First-In-Class Monoclonal Antibody Targeting ROR1. *Clin Lymphoma Myeloma Leuk*. **15 Suppl**, S167–9 (2015).

469. P. Greaves, *Histopathology of Preclinical Toxicity Studies* (Academic Press, 2012).

470. J. Yang *et al.*, Therapeutic potential and challenges of targeting receptor tyrosine kinase ROR1 with monoclonal antibodies in B-cell malignancies. *PLoS ONE*. **6**, e21018 (2011).

471. J. Seita *et al.*, Gene Expression Commons: an open platform for absolute gene expression profiling. *PLoS ONE*. **7**, e40321 (2012).

472. B. A. Anthony, D. C. Link, Regulation of hematopoietic stem cells by bone marrow stromal cells. *Trends in Immunology*. **35**, 32–37 (2014).

473. C. N. Inra *et al.*, A perisinusoidal niche for extramedullary haematopoiesis in the spleen. *Nature*. **527**, 466–471 (2015).

474. A. M. Dimarino, A. I. Caplan, T. L. Bonfield, Mesenchymal stem cells in tissue repair. *Front Immunol*. **4**, 201 (2013).

475. J. Billiard *et al.*, The orphan receptor tyrosine kinase Ror2 modulates canonical Wnt signaling in osteoblastic cells. *Mol. Endocrinol.* **19**, 90–101 (2005).

476. Y. Liu, J. F. Ross, P. V. N. Bodine, J. Billiard, Homodimerization of Ror2 tyrosine kinase receptor induces 14-3-3(beta) phosphorylation and promotes osteoblast differentiation and bone formation. *Mol. Endocrinol.* **21**, 3050–3061 (2007).

477. Y. Liu *et al.*, The orphan receptor tyrosine kinase Ror2 promotes osteoblast differentiation and enhances ex vivo bone formation. *Mol. Endocrinol.* **21**, 376–387 (2007).

478. G. Liu *et al.*, Canonical Wnts function as potent regulators of osteogenesis by human mesenchymal stem cells. *The Journal of Cell Biology*. **185**, 67–75 (2009).

479. J. K. H. Tan, T. Watanabe, Stromal Cell Subsets Directing Neonatal Spleen Regeneration. *Sci Rep*. **7**, 40401 (2017).

480. L. Castagnaro *et al.*, Nkx2-5(+)islet1(+) mesenchymal precursors generate distinct spleen stromal cell subsets and participate in restoring stromal network integrity. *Immunity*. **38**, 782–791 (2013).

481. N. J. Krautler *et al.*, Follicular dendritic cells emerge from ubiquitous perivascular precursors. *Cell*. **150**, 194–206 (2012).

482. J. Potratz *et al.*, Receptor tyrosine kinase gene expression profiles of Ewing sarcomas reveal ROR1 as a potential therapeutic target in metastatic disease. *Mol Oncol*. **10**, 677–692 (2016).

483. H. Li, Y. Zhao, Increasing the safety and efficacy of chimeric antigen receptor T cell therapy. *Protein Cell*. **8**, 573–589 (2017).

484. M. Uhlén *et al.*, Proteomics. Tissue-based map of the human proteome. *Science*. **347**, 1260419–1260419 (2015).

485. B. Engels *et al.*, Retroviral vectors for high-level transgene expression in T lymphocytes. *Hum. Gene Ther.* **14**, 1155–1168 (2003).

486. C. BOURQUIN *et al.*, Bispecific antibody molecules with antigen-transfected t-cells and their use in medicine (2014).

487. S. Morita, T. Kojima, T. Kitamura, Plat-E: an efficient and stable system for transient packaging of retroviruses. *Gene Ther.* **7**, 1063–1066 (2000).

488. Y. Soneoka *et al.*, A transient three-plasmid expression system for the production of high titer retroviral vectors. *Nucleic Acids Res*. **23**, 628–633 (1995).

Appendix 1

Designing logic-gated chimeric antigen receptor expression systems to enable selective tumor targeting and reduce off-tumor toxicity

A version of this Appendix is undergoing revisions for publication at *Cancer Cell*:

Shivani Srivastava, Alexander I Salter, Denny Liggitt, Sushma Yechan-Gunja, Megha Sarvothama, Kirsten Cooper, Jarrod A Dudakov, Christoph Rader, Stanley R Riddell. “Logic-gated ROR1 chimeric antigen receptor expression rescues T cell-mediated toxicity to normal tissues and enables selective tumor targeting.”

Summary

Many targets in common epithelial cancers for chimeric antigen receptor (CAR)-modified T cells are also expressed in some normal tissues, raising concerns for on-target, off-tumor toxicity. We developed a model of CAR T cell-mediated toxicity targeting the tumor-associated antigen ROR1 to evaluate how off-tumor activity might be averted. In mice pre-conditioned with radiation or cyclophosphamide, the adoptive transfer of ROR1 CAR T cells exhibited anti-tumor activity but induced lethal bone marrow failure and splenic necrosis due to recognition of resident $ROR1^+$ stromal cells. To improve tumor selectivity, we engineered T cells with an EpCAM-specific synthetic Notch (synNotch) receptor that after ligand binding induces expression of a ROR1 CAR transgene. This strategy restricted ROR1 CAR expression to $EpCAM^+ROR1^+$ tumors and prevented toxicity from recognition of $EpCAM^-ROR1^+$ normal tissue. Unlike ROR1 CAR T cells, synNotch CAR T cells selectively accumulated in tumors but not spleen or bone marrow and controlled tumor growth. Combinatorial antigen recognition with synNotch receptors, thus, permits safe targeting of tumor-associated antigens that are expressed on normal tissues and that could result in fatal toxicity if targeted directly.

Signficance

The identification of tumor-specific antigens remains an obstacle for T cell therapy for common epithelial cancers, as most candidate target molecules are also expressed in some normal tissues, making off-tumor toxicity a significant risk of therapy. Our study shows that T cell-mediated toxicity to normal tissue can be context-dependent and cautions that the absence of toxicity in clinical trials targeting antigens expressed on normal tissues should be interpreted only within the context of the regimen and T cell dose administered. Moreover, our work illustrates that combinatorial antigen sensing using synNotch receptors can be a powerful tool for improving the safety of CAR T cells and may dramatically increase the number of cell surface molecules that can be targeted safely in cancer immunotherapy.

Introduction

Adoptive cell therapy (ACT) is a promising cancer treatment that involves transferring patient-derived or allogeneic T cells that are engineered with a synthetic chimeric antigen receptor (CAR) or exogenous T cell receptor (TCR) to redirect T cell activity toward a tumor antigen (*230*, *454*). CAR T cells have shown remarkable efficacy in B cell malignancies, where lineage markers like CD19 can be targeted without serious complications from depletion of normal B cells (*224*, *225*, *288-291*, *295*, *302*, *303*, *455*, *456*). Extending the success of CAR T

cells to solid tumors, however, has proven challenging (*426*). A major obstacle is identifying cell surface antigens that are preferentially and homogeneously expressed on tumor cells but not on critical normal tissues. The mutant EGFRvIII molecule in glioblastoma is tumor-specific, but heterogeneity in its expression has hindered therapeutic efficacy of EGFRvIII CAR T cells (*235*, *457*, *458*). The vast majority of other candidate CAR targets in solid tumors such as Her2, GD2, and mesothelin are over-expressed in tumors but are co-expressed on various normal tissues, making toxicity a risk of immunotherapy against such molecules (*459-462*).

Receptor tyrosine kinase-like orphan receptor 1 (ROR1) is expressed in embryonic development and exhibits high and homogenous cell surface expression in many common epithelial tumors and some B cell malignancies (*270*, *463*). In some tumors, ROR1 expression is associated with poor prognosis (*464-467*), and efforts to target ROR1 with immunotherapy are in progress (*468*). T cells that express a CAR comprised of a single-chain variable fragment (scFv) derived from the ROR1-specific antibody R12 and linked to 4-1BB and CD3ζ signaling domains, significantly improved survival in xenograft models of $ROR1^+$ human tumors (*253*). However, our lab demonstrated that ROR1 was expressed in normal adipocytes, parathyroid, pancreatic islets, esophagus, and gastric mucosa, raising concerns that targeting ROR1 may cause toxicity (*239*, *270*).

Several groups have suggested that molecules like ROR1 that are expressed on both tumor and normal tissues might be targeted safely using combinatorial antigen recognition, where engagement of two different tumor-associated antigens is required to elicit full T cell activity (*338*, *339*). One novel implementation of such an “AND” gate strategy was described by Roybal *et al.*, where a synthetic Notch (synNotch) receptor specific for antigen A induced expression of a second-generation CAR specific for antigen B, such that CAR T cell activity was only elicited against tumors where both antigens A and B were present (*9*). This study demonstrated that in principle, logic-gated CARs could discriminate single- and dual-positive tumors in a xenograft model using model antigens like GFP and CD19 but did not address whether such a design could provide sufficiently stringent regulation of CAR expression to prevent toxicity to normal endogenous tissue(s) in a clinically relevant model of off-tumor toxicity.

We sought to develop a model of CAR T cell toxicity to evaluate how T cells might be instructed to discriminate tumor cells and normal tissues. Adoptive transfer of murine CAR T cells that targeted a conserved epitope in murine ROR1 induced lethal hematopoietic toxicity and splenic necrosis in mice pre-conditioned with radiation or cyclophosphamide due to recognition of critical $ROR1^+$ bone marrow and splenic stromal cells. We used this model to test

whether regulated expression of the ROR1 CAR using synNotch receptors could mitigate toxicity to organs easily accessible to CAR T cells without impairing efficacy against a solid tumor.

Results

ROR1 CAR T cells induce lethal toxicity in mice pre-conditioned with radiation or cyclophosphamide

The R12 CAR targeting human ROR1 used in previous xenograft and non-human primate studies was not cross-reactive with murine ROR1 (mROR1) (*253*, *280*). Thus, to evaluate whether targeting ROR1 with CAR T cells in mice caused toxicity, we transduced murine T cells with a 4-1BB/CD3ζ CAR comprised of an scFv specific for an epitope in the Kringle domain of ROR1 that is conserved in mouse and human (**Figure 1A**) (*253*, *260*). A truncated murine CD19 (tCD19) transduction marker was co-expressed with the CAR using a 2A ribosomal skip sequence to enable detection of $tCD19^+$ CAR T cells by flow cytometry. Adoptive transfer of ROR1 CAR T cells or control T cells transduced with the tCD19 marker alone into C57BL/6 or BALB/c mice did not induce weight loss or clinical toxicity, but engraftment of donor T cells was poor (<0.02% of live cells) (**Figure 1B**). However, when mice were pre-conditioned with sub-lethal radiation (500R) to increase engraftment of adoptively transferred T cells (*100*), all mice receiving ROR1 CAR T cells but not control T cells progressively lost weight and died within two weeks of transfer (**Figure 1C**). Analysis of various tissues indicated that, relative to control T cells, ROR1 CAR T cells were present in higher number in spleen, bone marrow, peripheral lymph nodes, and liver, but not in lungs, kidney or pancreas and uniformly expressed high levels of PD-1 (**Figure 1D, Figure S1A**). Consistent with this pattern of T cell distribution, serum chemistry analysis of control and ROR1 CAR T cell-treated mice indicated normal pancreatic, kidney, and parathyroid function (**Figure S1B**). ROR1 CAR T cell-treated mice, however, exhibited a rapid and sustained decline in red blood cell (RBC) and platelet counts (**Figure 1E**) and elevated serum levels of ALT and AST by 10 days post-transfer (**Figure S1B**).

Analysis of organ histology from ROR1 CAR T cell-treated and control mice identified significant pathology in the spleen and bone marrow. Whereas spleen and bone marrow from control T cell-treated mice showed hyperplasia and recovery of all hematopoietic lineages following radiation, spleens from mice treated with ROR1 CAR T cells showed diffuse necrosis with a paucity of nucleated cells by 14 days after T cell transfer (**Figure 1F; Table S1**). Femurs from ROR1 CAR T cell-treated mice exhibited myelofibrosis at the epiphyseal ends of the bone

and markedly reduced hematopoiesis, with a striking absence of erythroid cells and megakaryocytes consistent with the marked decline in peripheral RBC and platelet counts (**Figure 1F**). By contrast, histologic changes in the lungs, pancreas, kidney, and small and large intestines were mild, and resolved to that observed with control T cells by 14 days after transfer (**Figure S1C,D**). Livers from control T cell-treated mice showed signs of extramedullary hematopoiesis (EMH), a normal mechanism of recovery from irradiation or chemotherapy, but livers from ROR1 CAR T cell-treated mice showed only focal coagulative necrosis (**Figure S1C,E),** consistent with ischemic and/or cytotoxic injury due to severe anemia or high serum IFNγ and IL-6 levels (**Figure 1E, Figure S1F**) (*469*). Notably, we observed the same development of weight loss, anemia, thrombocytopenia, severe splenic necrosis, and myelofibrosis in mice that were pre-conditioned with 200 mg/kg cyclophosphamide instead of radiation prior to ROR1 CAR T cell treatment (**Figure S2**). Thus, the adoptive transfer of ROR1 CAR T cells following lymphodepleting radiation or chemotherapy induced a consistent pattern of splenic and bone marrow toxicity.

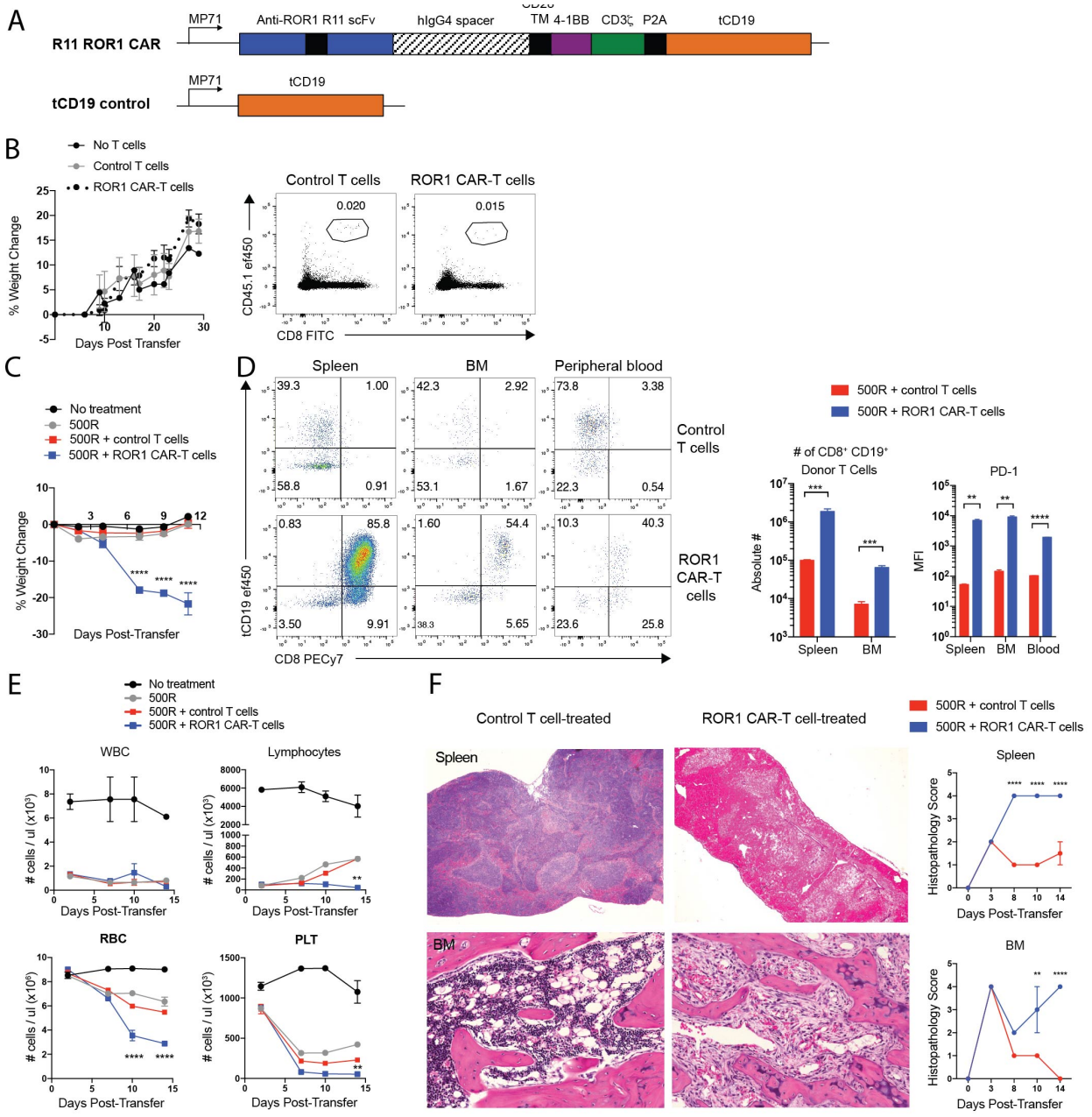

Figure 1. ROR1 CAR T cells induce lethal toxicity in mice pre-conditioned with radiation. A) Map of retroviral constructs used to generate ROR1 CAR and control T cells. TM = transmembrane. hIgG4 = human immunoglobulin G4. scFv = single chain variable fragment. B) Left: Percent change in body weight in BALB/c mice treated as indicated. Right: representative flow cytometric plots showing frequency of $CD8^+CD45.1^+$ donor T cells of live cells 7 days post-transfer. C) Percent change in body weight over time in BALB/c mice treated as indicated. N=4 mice per group. Two-way ANOVA with Tukey's post-test (ROR1 CAR T vs control T at D7, 9, 11: P<0.00001). D) Left: representative flow cytometric plots showing expression of tCD19 transduction marker and PD-1 on $CD8^+CD45.1^+$ donor T cells 4 days post-transfer. Right: summary of absolute number and PD-1 median fluorescence intensity (MFI) on $CD45.1^+CD8^+tCD19^+$ control or ROR1 CAR T cells 4 days post-transfer. N=4 mice per group. Unpaired Student's two-way t-test (Abs #: spleen, P=0.0004; BM, P=0.0002; PD-1: spleen, P=0.0007; BM, P=0.0007; blood, P=0.000008). E) White blood cell (WBC), lymphocyte, red blood cell (RBC), and platelet (PLT) counts in peripheral blood. N=4 mice per group. Two-way ANOVA with Tukey's post-test (ROR1 CAR T vs control T: Lymphocytes D14, P<0.005; RBC D10,14, P<0.00001; PLT D14, P<0.005). F) Left: representative H&E stains of spleen

and femur (BM) 14 days post-transfer. Right: histopathology scoring of control or ROR1 CAR T cell-treated tissues. N=4 mice per group. See Table S1 for histopathology scoring system. Two-way ANOVA with Sidak post-test (Spleen D8,10,14, P<0.00001; BM D10, P=0.004; BM D14, P<0.00001). *, P<0.05; **, P<0.005; ***, P<0.0005; ****, P<0.0001. Data are representative of 5 independent experiments. All data are presented as the mean values ± SEM.

Toxicity is dependent on the intensity of lymphodepletion and T cell dose

Lymphodepletion and cell dose have been shown to be factors determining engraftment and toxicity of adoptively transferred T cells in humans (*225*, *306*). To determine whether the toxicity of ROR1 CAR T cells was affected by the intensity of the lymphodepleting regimen, mice were given 100R or 500R of radiation, or 100 mg/kg or 200 mg/kg of cyclophosphamide prior to adoptive T cell transfer. Mice pre-conditioned with the lower dose of irradiation or cyclophosphamide exhibited reduced weight loss and all survived (**Figure 2A**). These mice had less robust CAR T cell expansion in the peripheral blood, suggesting that more intense lymphodepletion resulted in toxicity by enabling greater CAR T cell proliferation and accumulation (**Figure 2B**). Indeed, toxicity was dependent on the dose of CAR T cells administered, as giving a two-fold lower dose of ROR1 CAR T cells to mice conditioned with 500R induced intermediate weight loss, with all mice eventually recovering and surviving (**Figure 2C**)**.** Mice receiving a lower dose of CAR T cells showed lower expansion and faster contraction of CAR T cells in the peripheral blood (**Figure 2D**), and the CAR T cells upregulated PD-1 and TIM-3 earlier than high-dose CAR T cells (**Figure 2E**). These data demonstrate that toxicity from targeting ROR1 is dependent on achieving a threshold level of functional CAR T cells *in vivo*, which in immunocompetent mice is influenced by the intensity of lymphodepletion and cell dose.

Chemotherapy and radiation could have effects beyond inducing lymphodepletion that contribute to toxicity of ROR1 CAR T cells. Thus, we adoptively transferred control or ROR1 CAR T cells into RAG2-deficient mice without pre-conditioning to test whether lymphopenia alone was sufficient to induce toxicity. Interestingly, *Rag2*$^{-/-}$ mice did not develop weight loss, anemia, thrombocytopenia or mortality after CAR T cell infusion (**Figure 3A,B**). ROR1 CAR T cells accumulated in spleen and bone marrow to levels comparable to those in mice that received chemotherapy or radiation and were PD-1^{+}, suggesting that some ROR1^{+} target cells were being recognized in those tissues in the absence of pre-conditioning (**Figure 3C**). Although weight loss and hematopoietic toxicity were not observed, the splenic necrosis observed in WT irradiated mice receiving ROR1 CAR T cells did develop in *Rag2*$^{-/-}$ mice (**Figure 3D,E**). Femurs from ROR1 CAR T cell-treated mice showed only minor fibrosis at the epiphyseal ends but normal recovery of hematopoietic lineages throughout the shaft by 30 days

after transfer, consistent with the normal RBC and platelet counts in both control- and CAR Treated *Rag2*$^{-/-}$ mice (**Figure 3D**). Thus, lymphopenia was sufficient to induce ROR1 CAR-mediated splenic necrosis but not bone marrow failure or mortality, indicating that pre-conditioning created a context in which ROR1^{+} cells in the bone marrow were critical for hematopoietic recovery. Indeed, when *Rag2*$^{-/-}$ mice were pre-conditioned with 500R radiation prior to T cell transfer, ROR1 CAR T cells now induced rapid weight loss, anemia, thrombocytopenia, splenic necrosis and death in all mice (**Figure 3F,G,H**). These data demonstrate that the safety profile of CAR T cells specific for an antigen expressed on normal tissues can be highly context dependent, and identify both the dose of T cells and the intensity of lymphodepletion as critical variables for revealing toxicity.

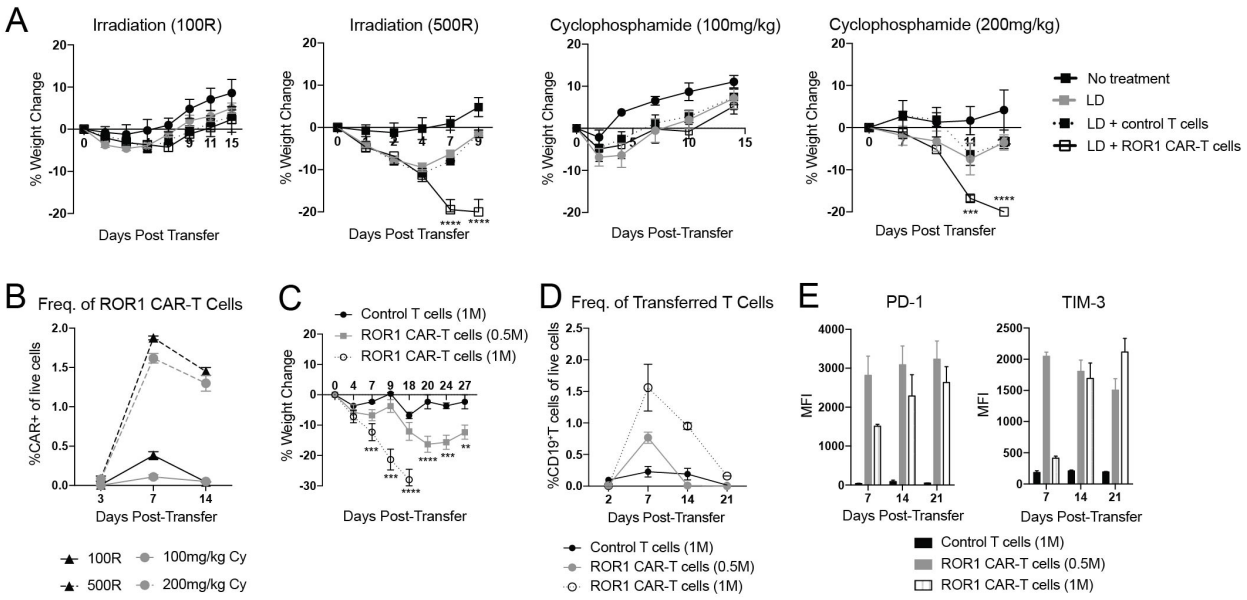

Figure 2. ROR1 CAR T cell-mediated toxicity is dependent on degree of lymphodepletion and dose of ROR1 CAR T cells. A) Percent change in body weight over time in BALB/c mice left untreated, lymphodepleted (LD), LD and given 1x10^{6} CD8^{+} control T cells, or LD and given 1x10^{6} CD8^{+} ROR1 CAR T cells. LD given was either 100R radiation, 500R radiation, 100mg/kg cyclophosphamide (Cy), or 200mg/kg Cy. N=4 mice per group. Two-way ANOVA with Tukey's post-test (ROR1 CAR T vs control T: 500R D7,9, P<0.00001; 200mg/kg Cy D7, P=0.0004; 200mg/kg Cy D9, P<0.00001). B) Frequency of CD8^{+}CD45.1^{+}tCD19^{+} ROR1 CAR T cells in peripheral blood over time in BALB/c mice receiving 100R, 500R, 100mg/kg Cy, or 200mg/kg Cy for lymphodepletion. N=4 mice per group. C-E) Percent change in body weight (C), frequency of CD8^{+}CD45.1^{+}tCD19^{+} donor T cells in peripheral blood (D), and PD-1 and TIM-3 expression on CD8^{+}CD45.1^{+}tCD19^{+} donor T cells in peripheral blood (E) over time in BALB/c mice irradiated 500R and treated with 1x10^{6} CD8^{+} control T cells (black), 5x10^{5} CD8^{+} ROR1 CAR T cells (gray), or 1x10^{6} CD8^{+} ROR1 CAR T cells (open circles/bars). N=4 mice per group. Two-way ANOVA with Tukey's post-test (1M CAR T vs control T: D7, P=0.0003; D9,18, P<0.00001; 0.5M CAR T vs control T: D20, P<0.00001; D24, P=0.0005; D27, P=0.0044). *, P<0.05; **, P<0.005; ***, P<0.0005; ****, P<0.0001. Data are representative of 2 independent experiments. All data are presented as the mean values ± SEM.

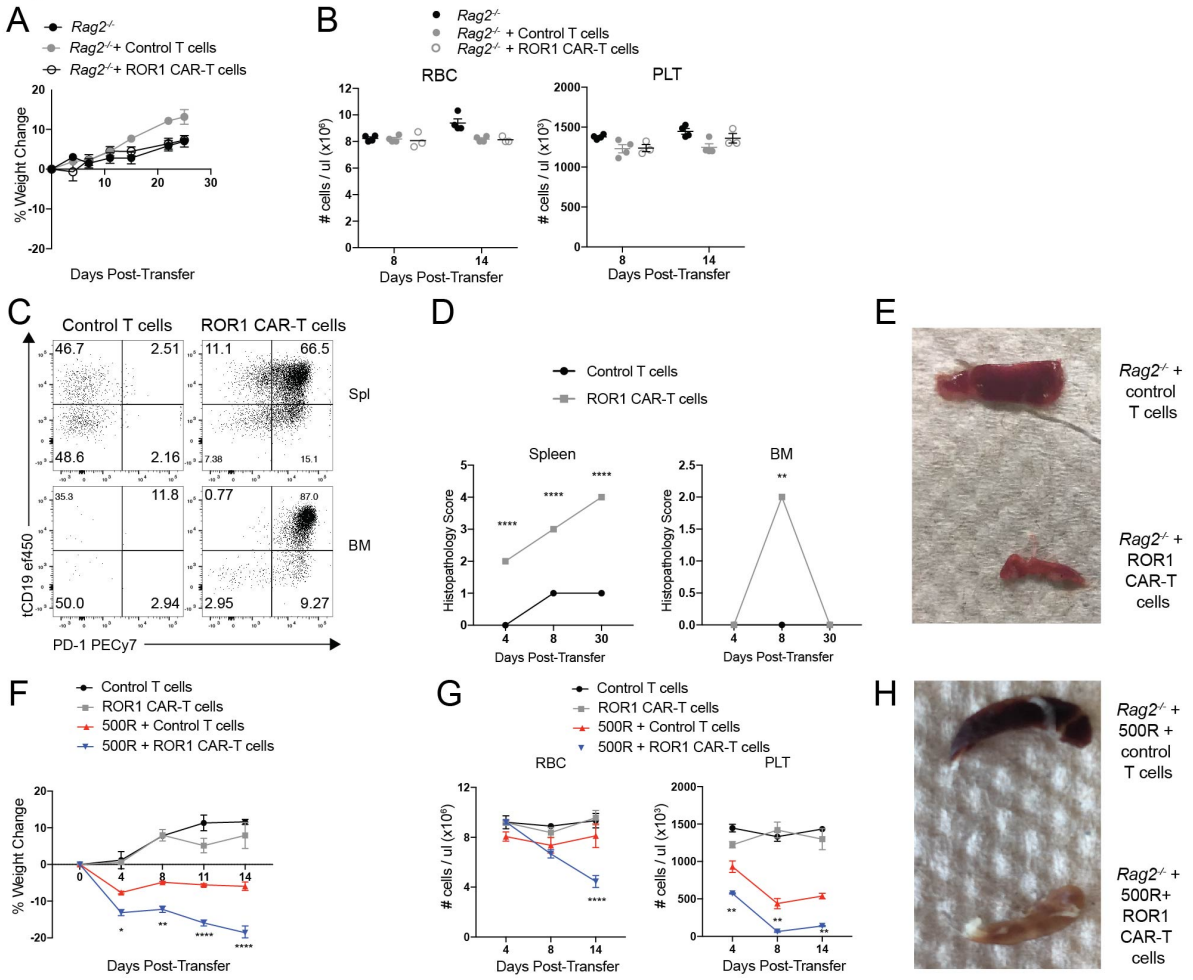

Figure 3. Lymphopenia is sufficient to induce minor myelofibrosis and splenic necrosis, but not anemia or lethal toxicity. A) Percent change in weight in BALB/c *Rag2*$^{-/-}$ mice left untreated, receiving 1x10^6 CD8$^+$ control T cells, or receiving 1x10^6 CD8$^+$ ROR1 CAR T cells. N=4 mice per group. B) Red blood cell (RBC) and platelet (PLT) counts from peripheral blood. N=4 mice per group. C) Representative flow cytometric plots showing expression of tCD19 CAR marker and PD-1 on CD8$^+$CD45.1$^+$ donor T cells 8 days post-transfer. D) Histopathology scoring of control or ROR1 CAR T cell-treated spleen and BM. See Table S1 for histopathology scoring system. N=4 mice per group. Two-way ANOVA with Sidak post-test (Spleen D4,8,30, P<0.00001; BM D8, P=0.0041). E) Representative picture of spleens from control and ROR1 CAR T cell-treated *Rag2*$^{-/-}$ mice 30 days post-transfer. F-H) Percent change in body weight (F), RBC and PLT count (G), and representative pictures of spleens 14 days post-transfer (H) in BALB/c *Rag2*$^{-/-}$ mice treated as indicated. N=4 mice per group. Two-way ANOVA with Tukey post-test: 500R+control T cells vs. 500R+ROR1 CAR T cells (Weight: D4, P=0.0265; D8, P=0.0018; D11, P<0.00001; D14, P<0.00001; RBC D14, P<0.00001; PLT D4, P=0.0043; PLT D8, P=0.0027; PLT D14, P=0.0014). *, P<0.05; **, P<0.005; ***, P<0.0005; ****, P<0.0001. Data are representative of 2 independent experiments. All data are presented as the mean values ± SEM.

ROR1 CAR T cell toxicity is dependent on ROR1 expression in non-hematopoietic cells

To understand the mechanism of CAR-mediated toxicity, we sought to identify the cell(s) being targeted by ROR1 CAR T cells. The ROR1 CAR we used is specific for an epitope in the extracellular Kringle domain of ROR1 and does not recognize ROR2 (*470*). Kringle domains

are, however, conserved in many proteins, and the toxicity of ROR1 CAR T cells could be due to off-target recognition of cells expressing a homologous protein. To confirm toxicity required recognition of ROR1^{+} cells, we generated ROR1 “knockout” (“ROR1-KO”) mice by crossing ROR1$^{fl/fl}$ mice to EIIα-Cre mice, which express Cre in the early mouse embryo, resulting in deletion of ROR1 in all tissues (*463*). WT or ROR1-KO mice were irradiated (500R) and received either control or ROR1 CAR T cells. ROR1-KO mice that received ROR1 CAR T cells did not exhibit any of the toxicities observed in WT mice, including weight loss, anemia, thrombocytopenia, and splenic necrosis, indicating that toxicity was due to targeting of ROR1 (**Figure 4A**).

To determine whether hematopoietic and/or nonhematopoietic cell types were targets of ROR1 CAR T cells, we constructed reciprocal bone marrow chimeras by lethally irradiating WT mice and reconstituting them with WT or ROR1-KO bone marrow. After allowing 8 weeks for full hematopoietic reconstitution, mice were irradiated (500R) and either control or ROR1 CAR T cells were adoptively transferred. A comparable decline in RBC and platelet counts, weight loss, splenic necrosis, and myelofibrosis was observed between WT>WT and KO>WT chimeras treated with ROR1 CAR T cells, indicating that hematopoietic ROR1 expression was not required for toxicity to spleen or bone marrow. CAR Treated KO>WT mice showed slightly less severe weight loss than CAR Treated WT>WT mice (**Figure 4B**), suggesting that ROR1 expression in the hematopoietic compartment may contribute to disease severity. This could be due to expression of ROR1 on pre-B cells (*239*), which in WT mice may provide an additional source of antigen to drive CAR T cell expansion.

The complementary experiment in which ROR1-KO mice were reconstituted with WT or ROR1-KO bone marrow showed that mice lacking ROR1 in non-hematopoietic cells were completely rescued from all toxicity, despite intact ROR1 expression in hematopoietic cells. WT>KO mice showed no significant weight loss, anemia, splenic necrosis or myelofibrosis, and all survived after receiving ROR1 CAR T cells (**Figure 4C**). Thus, ROR1 expression in non-hematopoietic cells is necessary and sufficient for the lethal toxicity mediated by ROR1 CAR T cells in mice.

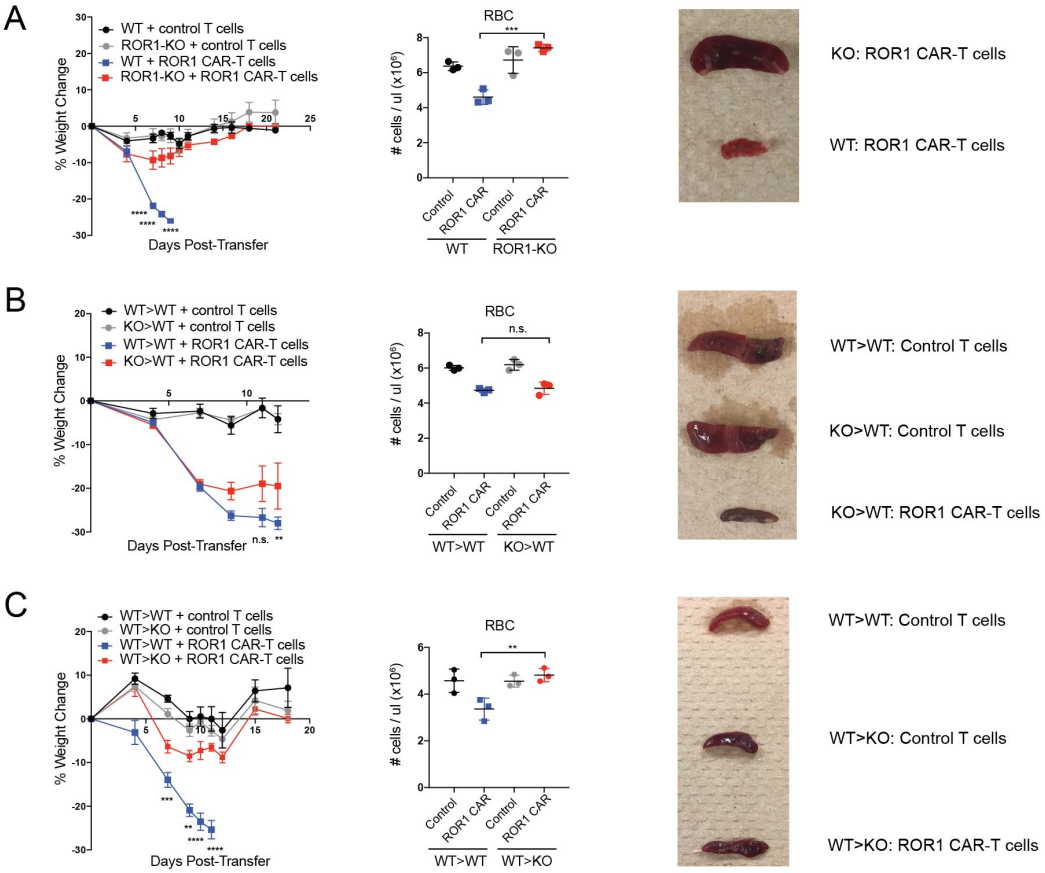

Figure 4. ROR1 CAR T cell-mediated toxicity is dependent on ROR1 expression in non-hematopoietic cells. A) Percent change in body weight (left), red blood cell (RBC) count in peripheral blood (middle), and representative pictures of spleens 9 days post-transfer (right) from B6 ROR1$^{fl/fl}$ (WT) or EIIα-Cre^{+}/ROR1$^{fl/fl}$ (KO) mice treated with 500R and 1x10^{6} CD8^{+} control T cells or ROR1 CAR T cells. N=3 mice per group. Left: two-way ANOVA with Tukey post-test (WT+CAR T vs. KO+CAR T: D7,8,9, P<0.00001). Middle: one-way ANOVA with Tukey post-test (P=0.0003). B) Percent change in body weight over time (left), RBC count in peripheral blood (middle), and representative pictures of spleens 15 days post-transfer (right) from WT>WT or ROR1-KO>WT bone marrow chimeric mice treated with 500R and 1x10^{6} CD8^{+} control T cells or ROR1 CAR T cells. N=3 mice per group. Left: two-way ANOVA with Tukey post-test (WT>WT CAR T vs. KO>WT CAR T: n.s. = not significant). Middle: one-way ANOVA with Tukey post-test. C) Percent change in body weight over time (left), RBC count in peripheral blood (middle), and representative pictures of spleens 40 days post-transfer (right) from WT>WT or WT>ROR1-KO bone marrow chimeric mice treated with 500R and 1x10^{6} CD8^{+} control T cells or ROR1 CAR T cells. N=3 mice per group. Left: two-way ANOVA with Tukey post-test (WT>WT CAR T vs. WT>KO CAR T: D7, P=0.00013; D9, P=0.0045; D10,11, P<0.00001). Middle: one-way ANOVA with Tukey post-test (P=0.0044). *, P<0.05; **, P<0.005; ***, P<0.0005; ****, P<0.0001. Data are representative of 2 independent experiments. All data are presented as the mean values ± SEM.

Bone marrow and splenic stromal cells express ROR1 and are targeted by ROR1 CAR T cells

We next examined what subset(s) of non-hematopoietic cells might be reognized by ROR1 CAR T cells. Data from the Gene Expression Commons shows *mROR1* is expressed in bone marrow stromal cells (*471*). A number of stromal cell types in the bone marrow, including endothelial cells, osteoblasts and mesenchymal stem cells (MSC), provide survival signals to

HSCs and promote hematopoiesis (*472*). We sorted different bone marrow stromal subsets from WT mice and found high levels of *mROR1* transcript by RT-PCR in osteoblasts and MSC but not in endothelial cells or hematopoietic progenitors, and transcript levels were further increased in MSC, but not osteoblasts or endothelial cells, 48 hours after irradiation (500R) (**Figure 5A**). ROR1 CAR T cells secreted high levels of IFNγ upon co-culture with primary MSC derived from WT mice but not after co-culture with MSC from ROR1-KO mice, indicating that WT MSC express sufficient ROR1 to activate CAR T cells (**Figure 5B**). CFU assays performed on femurs from control- and CAR T cell-treated mice revealed that the number of MSC was drastically reduced in CAR T cell-treated mice, providing further evidence these cells were targeted by ROR1 CAR T cells *in vivo* (**Figure 5C**). Pre-B cell progenitors, which are known to express ROR1 (*239*), were also completely absent from ROR1 CAR T cell-treated mice (**Figure 5C**). By contrast, we did not see any difference in erythrocyte, megakaryocyte, or granulocyte/macrophage progenitors in CFU assays between control and ROR1 CAR T cell-treated recipients, consistent with our bone marrow chimera data indicating that CAR-mediated toxicity was independent of ROR1 expression on hematopoietic progenitor cells (**Figure 4B**).

In the spleen, a population of $CD45^{-}Ter119^{-}VE\text{-}cadherin^{+}$ endothelial cells and $CD45^{-}Ter119^{-}Tcf21^{+}$ perivascular stromal cells play an analogous role to bone marrow stromal cells by producing Scf and CXCL12 that support splenic EMH in situations of stress to the bone marrow (*473*). Microarray data indicated that *mRor1* was enriched in Scf-producing spleen stromal cells relative to unenriched spleen cells, suggesting that elimination of these cells by ROR1 CAR T cells may be responsible for the splenic necrosis that we observed (*473*). Indeed, ROR1 CAR T cells became activated and secreted IFNγ upon co-culture with $CD45^{-}$ stromal but not $CD45^{+}$ hematopoietic splenic cells, indicating that ROR1 CAR T cells target a stromal population in the spleen (**Figure 5D**). To determine what stromal subset might be targeted by CAR T cells, we sorted different stromal populations and analyzed *mROR1* expression by RT-PCR. Most $Tcf21^{+}$ stromal cells were uniformly $PDGFR\beta^{+}$; therefore we sorted for $CD45^{-}VE\text{-}cadherin^{+}$ splenic endothelial cells and $CD45^{-}PDGFR\beta^{+}$ stromal cells from WT mice prior to and 48 hours after radiation and found *mROR1* transcripts in both splenic stromal subsets but not in $CD45^{+}$ hematopoietic cells from the spleen, with *mROR1* transcript levels selectively increased in $CD45^{-}PDGFR\beta^{+}$ stromal cells 48 hours after irradiation (**Figure 5E**). ROR1 CAR T cells, thus, target splenic stromal cells, resulting in splenic necrosis and failure of EMH, which together with targeting of MSC prevents hematopoietic recovery after cytotoxic therapy.

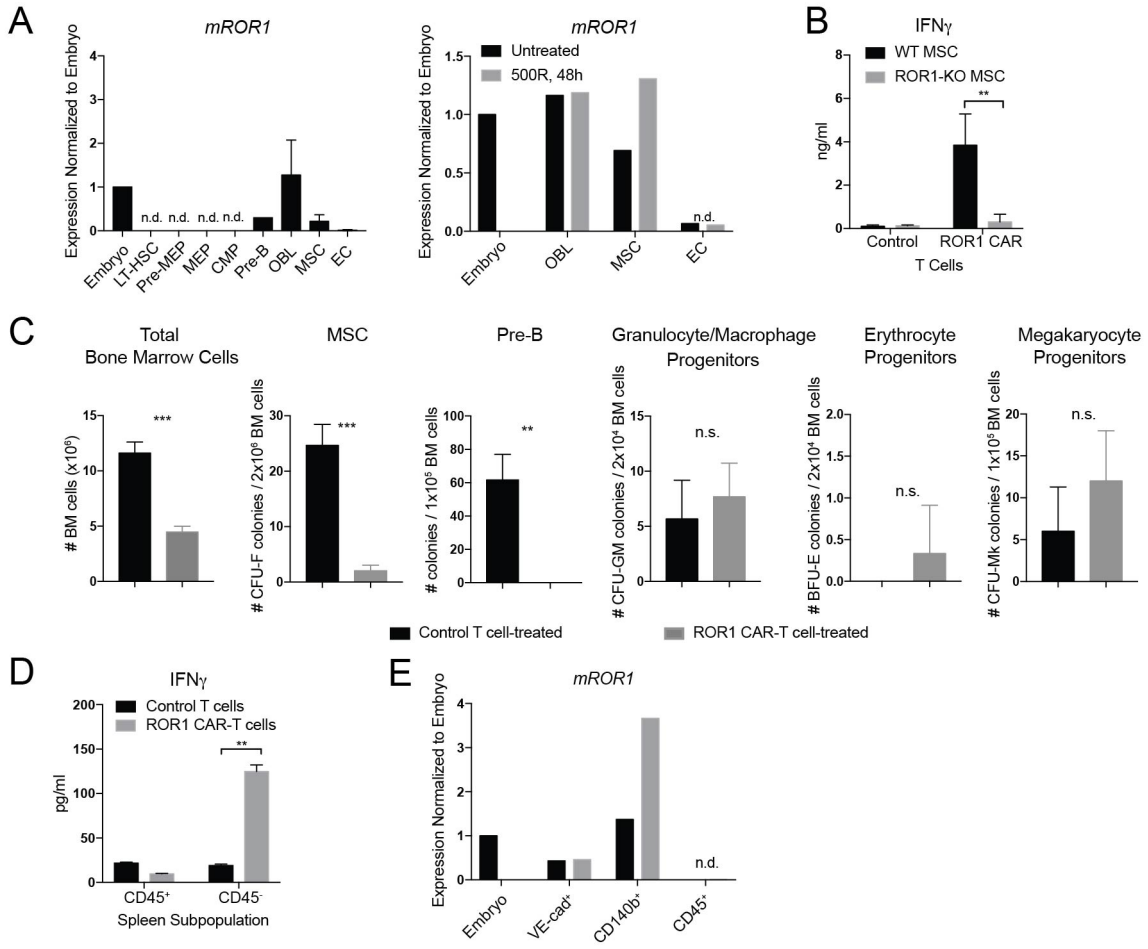

Figure 5. Bone marrow stromal cells express ROR1 and are targeted by ROR1 CAR T cells. A) Left: qPCR analysis of *mROR1* expression in sorted bone marrow populations from BALB/c mice. Right: qPCR analysis of *mROR1* expression in bone marrow populations sorted from BALB/c mice left untreated or irradiated 500R 48 hours prior to euthanasia. *mROR1* expression was normalized to *Actb* expression and expressed relative to *mROR1* expression in E10.5 embryos. N=3 mice per group. B) ELISA analysis of IFNγ production by $CD8^+$ control or ROR1 CAR T cells co-cultured for 48 hours with primary MSC derived from WT or ROR1-KO femurs and expanded *in vitro* for 14 days. Data are summarized from 3 independent experiments. Unpaired two-way Student's t-test (P=0.0041). C) Left: absolute number of cells in bone marrow flushed from femurs and tibia of control or ROR1 CAR T cell-treated mice 9 days post-transfer. Right: number of mesenchymal stem cell (MSC), pre-B cell, granulocyte/macrophage, erythrocyte, and megakaryocyte colonies formed after culture of bone marrow cells from femurs of control or ROR1 CAR T cell-treated BALB/c mice collected 9 days post-transfer. N=3 mice per group. Unpaired two-way Student's t-test (# BM cells, P=0.0004; MSC, P=0.0004; Pre-B, P=0.0023). D) ELISA analysis of IFNγ production by $CD8^+$ control or ROR1 CAR T cells co-cultured for 48 hours with $CD45^+$ or $CD45^-$ splenic cells. Data are summarized from 3 independent experiments. Unpaired two-way Student's t-test (P=0.0049). E) qPCR analysis of *mROR1* expression in splenic subpopulations sorted from BALB/c mice left untreated or irradiated 500R 48 hours prior to euthanasia. N.D. = not detected. *, P<0.05; **, P<0.005; ***, P<0.0005; ****, P<0.0001. Data are representative of 2-3 independent experiments. All data are presented as the mean values ± SEM.

SynNotch EpCAM-inducible ROR1 CAR T cells selectively target $EpCAM^+ROR1^+$ tumors but not $EpCAM^-ROR1^+$ normal tissues

Many candidate targets for ACT of solid tumors are expressed on some normal tissues, and identifying strategies that mitigate off-tumor toxicity to normal tissues without compromising on-tumor immune activity is an unresolved obstacle. An elegant combinatorial antigen-sensing approach was described recently in which recognition of one antigen by a synthetic Notch (synNotch) receptor releases an orthogonal transcription factor that drives expression of a CAR that is specific for a distinct antigen (*9*). This logic-gated expression system confined CAR recognition to dual-positive tumors when single-positive and dual-positive tumors expressing the model antigens CD19 and GFP were spatially separated by implantation on opposite flanks of a mouse. However, the half-life of CAR expression after disengagement of the synNotch receptor is ~8 hours, and T cells expressing sufficient levels of the CAR might migrate to neighboring tissues like the spleen and bone marrow where T cells frequently traffic, and mediate toxicity against single-positive normal cells in this time frame.

We searched for combinations of antigens to determine whether the synNotch approach could prevent toxicity mediated by ROR1 CAR T cell recognition of cells in bone marrow and spleen. We found that EpCAM is highly expressed on 4T1 mammary carcinoma cells that were transduced to express murine ROR1, but is absent from ROR1$^+$ bone marrow and splenic stromal cells (**Figure 6A**). We therefore constructed a lentiviral vector encoding a myc-tagged EpCAM-specific synNotch receptor bearing a Gal4-VP64 intracellular transcription activation domain. We made a second lentiviral vector in which the identical ROR1 4-1BB/CD3ζ CAR transgene used in prior experiments was placed under control of an inducible (UAS) promoter activated by the synNotch receptor, and a constitutively expressed blue fluorescent protein (BFP) was placed downstream as a transduction marker (**Figure S3A**). Truncated CD19 was included in the inducible CAR cassette as a surrogate marker of CAR expression to verify lack of CAR expression in the basal state and CAR induction after synNotch engagement.

Murine CD8$^+$ T cells were co-transduced with both lentiviral vectors and co-transduction was verified by myc and BFP expression (**Figure S3B**). Untouched synNotch T cells were enriched by FACS sorting BFP$^+$ T cells such that ~30-60% of T cells were myc$^+$BFP$^+$ and carried the full EpCAM-synNotch/UAS-ROR1-CAR circuit while 40-70% of cells were myc$^-$BFP$^+$ and incapable of binding EpCAM or inducing ROR1 CAR expression (**Figure S3B**). Notably, we did not observe any tCD19 expression in the absence of synNotch engagement, indicating minimal leakiness of CAR expression (**Figure S3B**). For *in vitro* and *in vivo* experiments, the transduction of ROR1 CAR T cells was adjusted to achieve a frequency of tCD19$^+$ ROR1 CAR T cells that was similar to the frequency of myc$^+$BFP$^+$ synNotch T cells (**Figure S3C**).

We cultured BFP-sorted synNotch T cells, ROR1 CAR T, and untransduced T cells with different combinations of K562, K562-mROR1, 4T1, and 4T1-mROR1 cells to test activity against ROR1 and EpCAM single- and dual-positive tumor cells. Whereas ROR1 CAR T cells killed both $EpCAM^{+}ROR1^{+}$ and $EpCAM^{-}ROR1^{+}$ tumors, synNotch T cells only showed lytic activity against tumor cells when both antigens were present (**Figure 6B**). SynNotch T cells were as efficient in lysing $EpCAM^{+}ROR1^{+}$ tumor cells by 24 hours after co-culture as ROR1 CAR T cells were after 6 hours of co-culture, consistent with previous reports showing synNotch T cells take 12-24 hours to fully upregulate CAR expression after engagement of the synNotch receptor (**Figure 6B**) (*9*). Additionally, whereas presence of EpCAM was sufficient to induce expression of the CAR marker tCD19 on synNotch T cells, $tCD19^{+}$ T cells only produced IFNγ when ROR1 antigen was also present (**Figure 6C**).

We next tested whether T cells co-transduced with synNotch EpCAM-inducible ROR1 CAR constructs could mediate antitumor effects against $ROR1^{+}$ breast cancer *in vivo* without toxicity to normal tissues *in vivo*. We inoculated mice with 4T1-mROR1 tumors in the mammary fat pad and after tumors were palpable, treated mice with 200 mg/kg cyclophosphamide to induce lymphodepletion and transferred untransduced, ROR1 CAR T cells, or BFP-sorted synNotch T cells. We used cyclophosphamide instead of irradiation as this regimen is more commonly used for lymphodepletion in clinical ACT studies. As previously observed, ROR1 CAR T cells induced rapid weight loss within one week of transfer and induced severe anemia, thrombocytopenia, and splenic necrosis (**Figure 7A-C**). By contrast, mice receiving synNotch T cells recovered their weight and RBC and platelet counts with the same kinetics and showed similar splenic morphology as mice that received untransduced T cells. Although synNotch T cells did not induce toxicity to normal $ROR1^{+}$ tissues, they mediated significant tumor control that was comparable to that observed with ROR1 CAR T cells (**Figure 7D**). ROR1 CAR T cells accumulated in spleen, bone marrow, and tumors, and expressed high levels of PD-1, consistent with local activation (**Figure 7E**). Transferred synNotch T cells were also detected in the spleen and bone marrow, but at least 10-fold fewer of these cells expressed the ROR1 CAR (**Figure 7E,F**). By contrast, in resected tumors synNotch T cells expressing the ROR1 CAR were present in the same high numbers as ROR1 CAR T cells, expressed similar levels of ROR1 CAR, and expressed markers of activation and proliferation, including PD-1 and Ki-67 (**Figure 7E,F**). Although spleen and bone marrow are readily accessible to CAR T cells that could migrate from the tumor, the few CAR^{+} T cells that were present in the spleen and bone marrow were below the threshold necessary to result in toxicity. Thus, synNotch T cells

exhibited tumor-selective accumulation, CAR expression, and anti-tumor activity without causing toxicity to critical ROR1$^+$ cells in bone marrow and spleen.

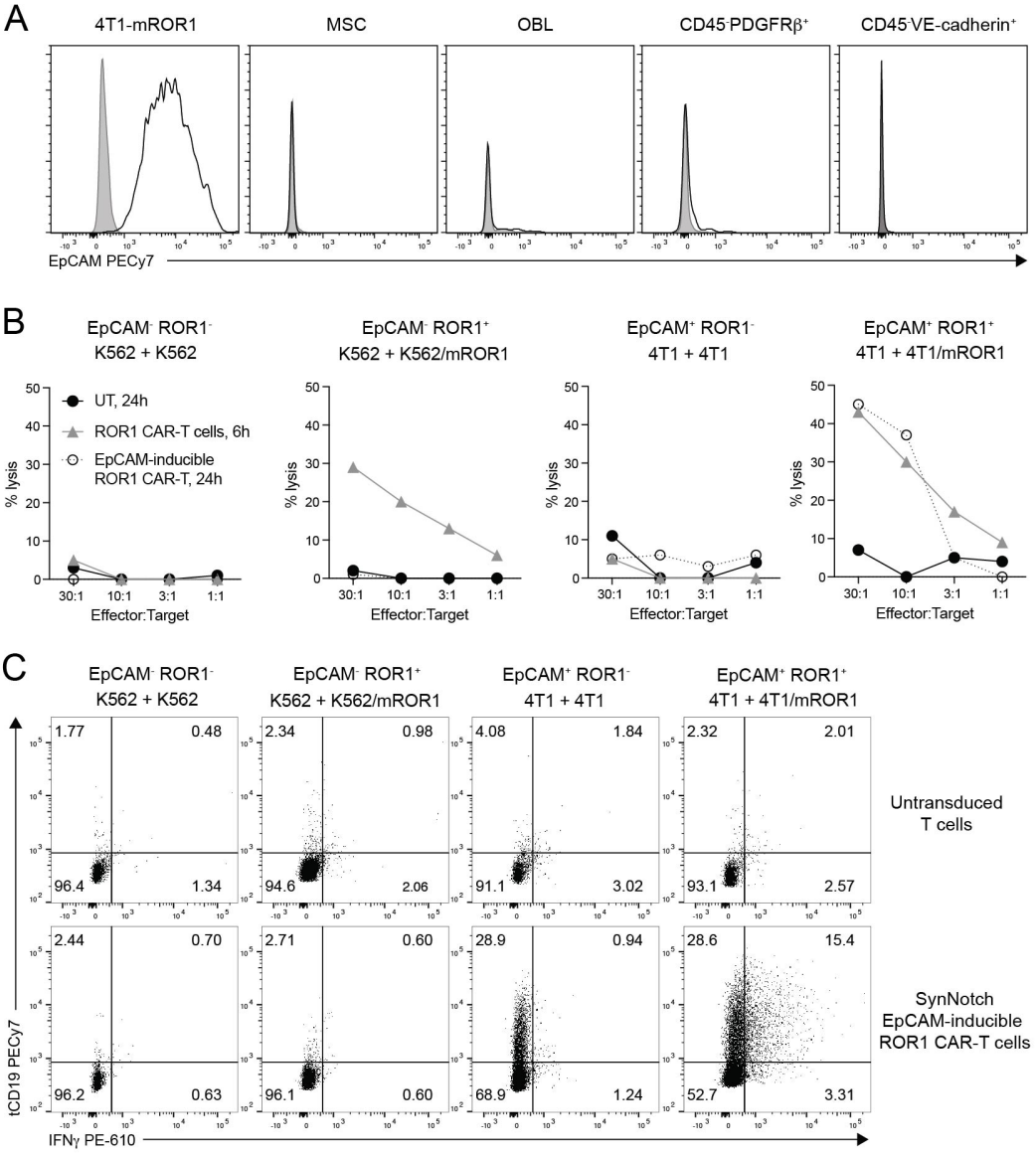

Figure 6. SynNotch EpCAM-inducible ROR1 CAR T cells selectively target EpCAM$^+$ROR1$^+$ cells but not EpCAM$^+$ROR1$^-$ or EpCAM$^-$ROR1$^+$ cells *in vitro*. A) Representative flow cytometric analysis of EpCAM expression on 4T1 tumor cells, MSC, osteoblasts (OBL), CD45$^-$Ter119$^-$PDGFRβ$^+$ spleen cells, and CD45$^-$Ter119$^-$VE-cadherin$^+$ spleen cells from WT BALB/c mice. B) Percent lysis of ^{51}Cr-labeled K562 (left), K562-mROR1 (left middle), 4T1 (right middle) or 4T1-mROR1 (right) tumor cells after 24 hours of co-culture with CD8$^+$ untransduced (black) or EpCAM-inducible ROR1 CAR T cells (open circles) or after 6 hours of co-culture with ROR1 CAR T cells (gray). C) Intracellular cytokine analysis of tCD19 CAR expression marker and IFNγ expression in CD8$^+$ untransduced or EpCAM-inducible ROR1 CAR T cells co-cultured for 72 hours with the indicated combinations of tumor cells in the presence of Brefeldin A for the last 24 hours of culture. Data are representative of two independent experiments.

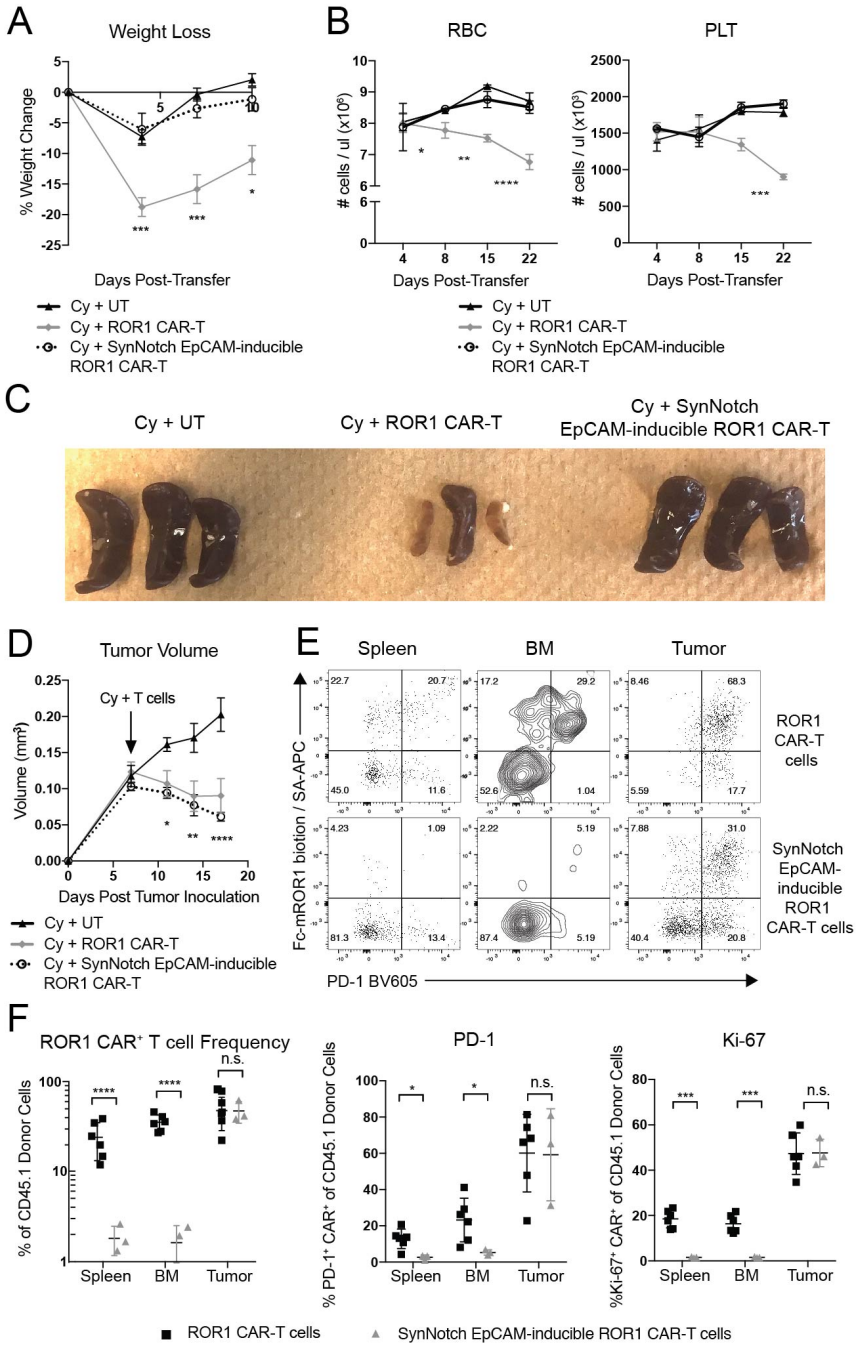

Figure 7. SynNotch EpCAM-inducible ROR1 CAR T cells rescue toxicity to ROR1⁺ normal tissues while maintaining activity against ROR1⁺ tumors. A) Percent change in body weight in BALB/c mice inoculated with 4T1-mROR1 tumors, treated with 200mg/kg cyclophosphamide (Cy) and untransduced (UT) T cells, ROR1 CAR T cells, or synNotch EpCAM-inducible ROR1 CAR T cells. N=3-6 mice per group. Two-way ANOVA with Tukey post-test (ROR1-CAR vs. EpCAM-inducible ROR1 CAR: D4, P=0.0004; D7, P=0.017; D9, P=0.0433). B) Red blood cell (RBC) and platelet (PLT) counts from peripheral blood of tumor-bearing mice treated as indicated. N=3-6 mice per group. Two-way ANOVA with Tukey post-test (ROR1-CAR vs. EpCAM-inducible ROR1 CAR: RBC D8, P=0.0322; RBC D15, P=0.001; RBC D22, P<0.00001; PLT D22, P=0.0004). C) Representative pictures of spleens 10 days post-transfer from tumor-bearing BALB/c mice treated as indicated. D) Tumor volume in mice treated as indicated. N=3-6 mice per group. Two-way ANOVA with Tukey post-test (ROR1-CAR vs. UT: D11, P=0.0405; D14, P=0.0013; D17,

P<0.00001; EpCAM-inducible ROR1 CAR vs. UT: D11, P=0.0381; D14, P=0.0025; D17, P<0.00001; ROR1-CAR vs EpCAM-inducible ROR1 CAR: n.s). E) Representative flow cytometric analysis of ROR1 CAR and PD-1 expression on $CD8^+CD45.1^+$ donor T cells from mice treated with Cy and ROR1 CAR T cells (top) or synNotch EpCAM-inducible ROR1 CAR T cells (bottom) 10 days post-transfer. F) Summary of frequency of ROR1 CAR^+, CAR^+Ki67^+, and $CAR^+PD\text{-}1^+$ T cells of $CD8^+CD45.1^+$ donor T cells from mice treated with 200mg/kg Cy and the indicated T cell groups 10 days post-transfer. N=3-6 mice per group. Unpaired two-way Student's t-test (Frequency: spleen, P<0.00001; BM, P<0.00001; PD-1: spleen, P=0.016; BM, P=0.0317; Ki67: spleen, P=0.00017; BM, P=0.00043). *, P<0.05; **, P<0.005; ***, P<0.0005; ****, P<0.0001. Data are representative of 2 independent experiments. All data are presented as the mean values ± SEM.

Discussion

The identification of truly tumor-specific target antigens remains a significant obstacle for treating common epithelial cancers with engineered T cells, and many groups are targeting molecules that are expressed by both tumor and normal cells. This approach can be problematic, as illustrated by the life-threatening toxicity observed in clinical trials with CAR T cells targeting CAIX or Her2 due to recognition of cognate antigen on bile duct and lung epithelia, respectively (*240*, *283*, *452*). ROR1 is an attractive target for CAR T cell therapy due to its expression in many common solid tumors; however expression on several normal tissues makes safety a major concern (*270*). We examined CAR-mediated toxicity to endogenous $ROR1^+$ normal tissue in a mouse model to define parameters where normal cells are susceptible to injury and to test strategies to improve safety. In this model, toxicity was dependent on the intensity of lymphodepletion prior to CAR T cell transfer and resulted from elimination of $ROR1^+$ bone marrow and splenic stromal cells that are critical for recovery from cytotoxic stress induced by lymphodepleting radiation or chemotherapy. Targeting these cells resulted in severe anemia, thrombocytopenia, splenic necrosis, and mortality. Despite the rapid onset, severity, and location of toxicity, logic-gated ROR1 CAR expression using a synNotch receptor completely rescued toxicity to spleen and bone marrow without diminishing anti-tumor activity against $ROR1^+$ breast tumors. This rigorous model of T cell-mediated toxicity illustrates that combinatorial antigen sensing can be a powerful tool for improving the safety of CAR T cell therapy.

Our results identify a vital role for $ROR1^+$ bone marrow and splenic stromal cells in supporting hematopoietic recovery from cytotoxic stress. MSC have been shown to play an important role in tissue repair and in supporting HSC survival and function following irradiation (*474*). Our data shows that bone marrow MSC upregulate ROR1 expression upon irradiation *in vivo*, are targets for CAR T cells *in vitro*, and decline drastically and selectively in CAR Treated mice. ROR1 has not previously been implicated in MSC function, but its homologue ROR2 is expressed on mouse and human MSC, and the ROR1/ROR2 ligand Wnt5a promotes MSC

differentiation into osteoblasts (*475-478*). Analogous to MSC in the bone marrow, PDGFRβ$^+$ stromal cells in the spleen support EMH under conditions of stress to the bone marrow and splenic regeneration following LCMV infection (*473*, *479*, *480*). Destruction of these splenic cells may prevent tissue regeneration and EMH after cytotoxic therapy, eventually resulting in necrosis of the entire tissue. Some studies suggest that PDGFRβ$^+$ stromal cells are mesenchymal in origin (*480*, *481*), suggesting that MSC and PDGFRβ$^+$ stromal cells are developmentally linked and may play parallel roles supporting hematopoiesis and tissue regeneration in their respective organs. Thus, their elimination by ROR1 CAR T cells destroys the niche for HSC both inside and outside the bone marrow, preventing hematopoietic recovery from cytotoxic stress that is necessary for survival.

In humans and non-human primates (NHP), ROR1 is expressed in pancreatic islets, parathyroid, esophagus, and gastric mucosa, and there is some evidence of ROR1 expression on human MSC (*270*, *482*). No toxicity was observed using ROR1 CAR T cells in NHP or with a monoclonal antibody targeting ROR1 in rats and cynomolgus monkeys *in vivo* (*280*, *468*), and both therapies have advanced to clinical trials. The lack of toxicity despite presence of ROR1$^+$ normal cells in these species may be due to insufficient levels of ROR1 on normal cells, poor T cell trafficking to ROR1$^+$ tissues, or the lack of lymphodepleting cytotoxic therapy. Toxicity in mice with CAR T cells targeting mROR1 was dependent on the intensity of lymphodepleting therapy, suggesting that toxicity may become apparent in clinical trials as T cell dose or intensity of preconditioning are increased. Our data caution that the absence of toxicity in clinical trials of ACT targeting antigens expressed on normal tissues should be interpreted only within the context of the regimen and T cell dose administered, and not taken to infer that the target is safe. Moreover, our data illustrates that T cell recognition of rare normal cells such as MSC that are not easily evaluated for target expression by qPCR analysis of whole tissues or IHC analysis of small subsections of tissue can be the cause of lethal toxicity.

Many strategies have been proposed to minimize off-tumor toxicity to normal tissues (*356*, *483*), but these have not tested in rigorous preclinical models of CAR or TCR therapy, or in patients. Combinatorial antigen sensing or “AND” logic gates exploit a principle of natural T cell biology by integrating multiple signals to regulate the state of T cell activation and/or effector function. “Split signaling” receptors are one incarnation of this strategy that spatially separate CAR CD3ζ and costimulatory domains and depend on the two receptors being non-functional on their own, but functional in combination when both receptors simultaneously bind antigen (*334*, *338*). We found a ROR1 CAR carrying only the CD3ζ signaling domain still induced toxicity in irradiated mice (unpublished), indicating that a “split signaling” approach would not

rescue toxicity without further modifications, such as lowering the affinity of the scFv to decrease the threshold for activation (*339*). Like “split signaling” receptors, logic-gated synNotch receptors can mediate activity against dual-positive but not single-positive tumors (*9*). However, whereas “split signaling” receptors require both antigens be engaged nearly simultaneously to co-deliver signals 1 and 2 of T cell activation, there is a significant temporal delay between engagement of the synNotch receptor, induction of CAR expression, and degradation of the CAR following disengagement of the synNotch receptor. Consequently, there is a less stringent requirement for both target antigens to be co-expressed on the same target cell. In fact, mixtures of target cells expressing only antigen A or antigen B still elicit activity from synNotch CAR T cells despite the absence of any dual-positive cells, indicating that spatial proximity is an important determinant of how well synNotch receptors discriminate single- and dual-positive cells (unpublished). While synNotch CAR T cells could discriminate dual-positive and single-positive tumors implanted on opposite flanks of the same mouse, whether this form of logic-gating is sufficiently stringent to prevent toxicity to more accessible normal tissues has not been previously tested in a model of CAR-mediated toxicity with clinically relevant target antigens. Here, we show that logic-gated synNotch CARs requiring dual recognition of EpCAM and ROR1 can be used to safely target $EpCAM^{+}ROR1^{+}$ breast tumors without toxicity to normal $EpCAM^{-}ROR1^{+}$ cells. Whereas targeting ROR1 directly with traditional CAR T cells resulted in marked accumulation of CAR T cells in bone marrow and spleen, the vast majority of synNotch T cells found in spleen and bone marrow did not express the ROR1 CAR, indicating limited recognition of $EpCAM^{+}$ cells in those tissues and/or limited migration of ROR1 CAR^{+} synNotch T cells out of the tumor. Spleen and bone marrow are easily accessible to T cells, and averting toxicity at these sites with synNotch logic-gated CARs provides a rigorous test of efficacy.

There are potential limitations of the synNotch system, which relies on a non-human orthogonal transcription factor that could be immunogenic. Alternative transcription factors or structure-guided deimmunization could be used if immunogenicity resulted in premature elimination of the synNotch T cells. There are also contexts where synNotch receptors may not be able to sufficiently distinguish tumor and normal tissue. For example, breast tumors often metastasize to bone marrow, and it is possible that the presence of tumor metastases in bone marrow would activate ROR1 CAR expression and enable recognition of normal $ROR1^{+}$ bone marrow stromal cells. The presence of metastatic disease in multiple distant organs may also complicate how best to screen for candidate antigen pairs for logic-gating. Further studies will be required to understand the limits of synNotch receptors and whether tighter regulation of

CAR degradation or additional logic gated control can improve tumor and normal cell discrimination.

Our results demonstrate that “AND” logic gates may dramatically increase the portfolio of cell surface molecules on solid tumors that can be targeted safely with CAR T cells. As ROR1 is expressed in several normal human tissues, logic-gating using synNotch receptors may be an effective strategy if toxicity is observed in an ongoing clinical trial with ROR1 CAR T cells (NCT02706392). Although EpCAM is not expressed on normal ROR1$^+$ stromal cells in the mouse, it is co-expressed on some ROR1$^+$ normal epithelial tissues in humans, and may not be the ideal target for the synNotch component of the logic gate (*484*). Attractive alternative candidates include L1CAM and B7H3 since these antigens are not co-expressed on the same normal tissues as ROR1, but are expressed on a subset of ovarian, breast and lung cancer, which are also frequently positive for ROR1 (*484*). One can envision many additional pairs and more complex logic gates that impart functions in the local tumor environment that would broaden both the applicability and efficacy of CAR T cells against solid tumors.

Materials and Methods

Experimental Design

The aim of this study was to understand the mechanism of ROR1 CAR T cell-mediated toxicity and to test whether logic-gated CAR expression using synNotch receptors could be used to avert toxicity without impairing anti-tumor efficacy. All experiments were performed *in vivo* in mice or *in vitro* using murine and/or human-derived cells. Sample size was estimated by pilot experiments that showed trends of effects and their sizes. In most cases, the effect size was large such that n=3-4 was the minimal number needed to detect 2 standard deviation difference with $P<0.05$. In all experiments, mice of similar age and size were used and randomly assignmed to treatment groups. For experiments in which tumor cells were implanted before T cell treatment, tumor size was very similar across all mice at the time of treatment, such that further randomization was unnecessary. The investigators were not blinded to treatments; however, histology was scored blinded. Figure legends include details of replicate experiments. No data were excluded from this study. All animal studies were approved and performed in accordance within the guidelines of the FHCRC Institutional Animal Care and Use Committee (protocols IR 50884 and IR 1806).

Mice

C57BL/6J (B6), B6 CD45.1, BALB/cByJ, BALB/cByJ CD45.1, BALB/cByJ *Rag2*$^{-/-}$, B6 EIIα-Cre and ROR1$^{f/f}$ mice were purchased from Jackson Laboratory. *Ror1*$^{f/f}$ mice were backcrossed for three generations to B6 mice and subsequently crossed to EIIα-Cre mice. All mice were housed and bred at the Fred Hutchinson Cancer Research Center.

Cell Lines

K562 and 4T1 cell lines were obtained from the American Type Culture Collection and maintained in RPMI 1640 with 5% FBS, 100U/ml penicillin/streptomycin and 2mM L-glutamine or RPMI 1640 with 10% FBS, 1mM sodium pyruvate, 1mM HEPES, 100U/ml penicillin/streptomycin, and 50μM β-mercaptoethanol, respectively. LentiX cells for lentiviral packaging were purchased from Clontech. Plat-E cells for retroviral packaging were purchased from Cell Biolabs. 4T1-mROR1 and K562-mROR1 cell lines were generated by retroviral transduction with full-length murine ROR1 cDNA (UniProt: Q9Z139) and subsequent FACS sorting of mROR1^{+} cells to >95% purity. All cells were tested bi-monthly for the absence of mycoplasma.

Cloning of Murine CAR Constructs

Retroviral MP71 vector was modified to encode truncated murine CD19 (MP71-tCD19, UniProt: P25918, amino acids 1-321) for transduction of control T cells (*485*). For the ROR1 CAR, MP71 vector was modified to encode the murine CD8α signal peptide (UniProt: P01731, amino acids 1-27) followed by the R11 scFv with a 4/2NQ modified IgG4 long spacer (*260*) fused to murine CD28 transmembrane (UniProt: P31041, amino acids 151-177) and murine 4-1BB (UniProt: P20334, amino acids 211-256) and CD3ζ signaling domains (UniProt: P24161, amino acids 52-164) and linked by a P2A ribosomal skip element to tCD19 (MP71-R11-41BB-CD3ζ-P2A-tCD19).

To generate the synNotch CAR, the EpCAM-specific monoclonal antibody G8.8 was synthesized as a single-chain variable fragment in VH-VL format with a $(G_4S)_3$ linker between heavy and light chains (*486*). A murine CD8α signal peptide and myc tag (EQKLISEEDL) were added to N-terminus of the G8.8 scFv during synthesis. The synthesized fragment was fused to the synNotch-Gal4VP64 receptor within a pHR lentiviral vector (Addgene plasmid #79125). The

previously described R11-41BB-CD3ζ-P2A-tCD19 ROR1 CAR was cloned into a pHR lentiviral vector under transcriptional control of the synNotch response element (Addgene plasmid #79123). In this system, myc-tag or BFP expression defines T cells transduced with each construct, and tCD19 expression identifies cells expressing the R11 ROR1 CAR. pHR_Gal4UAS_IRES-mC-pGK-tBFP and pHR_PGK_antiCD19_synNotch+Gal4VP64 were gifts from Wendell Lim (Addgene plasmids #79123 and #79125, respectively). To generate the constitutive ROR1 CAR as a control, the entire R11-41BBζ-P2A-tCD19 ROR1 CAR was cloned into the pHR backbone under control of the constitutive PGK promoter (Addgene plasmid #79125). Cloning was performed using fusion PCR, Gibson assembly, and/or restriction enzyme digest. All plasmids were verified by restriction digest and capillary sequencing prior to use.

Generation of Murine CAR T Cells

Retrovirus was produced by transient calcium phosphate transfection (Clontech) of the packaging cell line Plat-E with the indicated MP71 vectors (*485*, *487*). 48 hours after transfection, viral supernatant was harvested and filtered through a 0.45-μm syringe filter (Millipore). 24-well non-tissue culture plates were coated with 12.5μg/ml RetroNectin (TaKaRa) according to the manufacturer's protocol, and plates were loaded with 1ml filtered virus per well and centrifuged for 2 hours at 3000xg at 32°C. Murine $CD8^+$ and/or $CD4^+$ T cells were enriched from spleens and peripheral lymph nodes of congenic CD45.1 B6 or BALB/c mice using untouched negative isolation kits (Stem Cell) and stimulated with 1μg/ml each of plate-bound anti-CD3 and anti-CD28 (clone 145-2C11 and 37.51, respectively) for 24 hours in a 37°C, 5% CO_2 incubator in complete RPMI (RPM1 1640, 10% heat inactivated FBS, 1mM sodium pyruvate, 1mM HEPES, 100U/ml penicillin/streptomycin, 50μM β-mercaptoethanol) supplemented with 50U/ml recombinant murine IL-2 (Peprotech). Murine T cells were harvested from anti-CD3/28-coated plates, counted, and resuspended at $1x10^6$ cells/ml in complete RPMI supplemented with 50U/ml IL-2 and anti-CD3/28 mouse T-activator Dynabeads (ThermoFisher) at a bead to cell ratio of 1:1. Viral supernatant was aspirated from RetroNectin-coated plates, plates were rinsed with PBS, and 1ml ($1x10^6$) T cells were added to each virus-coated well. Plates were then centrifuged at 800xg for 30 mins at 32°C and returned to 37°C, 5% CO_2 incubators. A second transduction was performed as described the next day by harvesting another batch of viral supernatant from Plat-E cells 72 hours after transfection. T cells were subsequently harvested, counted, and resuspended in complete RPMI with 50ng/ml IL-15 every 1-2 days after. 4-5 days after transduction, magnetic beads were removed and T cell transduction was measured by flow cytometry staining for tCD19 and/or ROR1 CAR. Transduction rates between control and ROR1 CAR T cells were normalized by diluting cultures with untransduced T cells cultured in parallel such that the proportion of transduced cells was the same between control and CAR T cell populations, and control and CAR Treated mice received the same number of transduced and untransduced T cells.

For synNotch experiments, lentivirus was produced by transient calcium phosphate transfection of the packaging cell line LentiX with the indicated pHR lentiviral vectors, psPAX2 (Addgene #12260), and pHIT123 ecotropic envelope(*488*). Viral supernatant was harvested 48 and 72 hours after transfection and filtered through a 0.45-μm pore filter. Lentivirus was concentrated 40X by mixing filtered lentivirus with 40% polyethylene glycol (PEG, Sigma) at a PEG to virus ratio of 1:3 for 1-2 hours at 4°C. The virus/PEG mixture was then centrifuged at 1500xg for 45 minutes at 4°C, supernatant was aspirated, and the virus pellet was resuspended in 40X smaller volume of serum-free DMEM and snap-frozen in liquid nitrogen for long-term storage. Frozen virus was used to transduce murine T cells using the RetroNectin-based transduction protocol described above. When co-transduction of two constructs was desired, frozen virus from both vectors was mixed 1:1 and added to the same RetroNectin-coated well.

BFP$^+$ synNotch T cells were FACS sorted to enrich for T cells capable of inducing expression of the ROR1 CAR before adoptive transfer into mice.

In Vivo CAR T Cell Toxicity Model

Mice were pre-conditioned with sublethal radiation (100R or 500R) or with intraperitoneal injection with cyclophosphamide (100mg/kg or 200mg/kg) and 5-6 hours later were injected intravenously by retro-orbital injection with 1x10^6 CD8$^+$tCD19$^+$ control or ROR1 CAR T cells. Mice were weighed just prior to pre-conditioning and 1–2 times per week thereafter. Percent weight change was calculated as: (weight at time X – weight at time 0) / (weight at time 0). All mice in each experiment were sacrificed when any individual mice showed clinical signs of severe disease or 20 percent weight loss.

Cell Isolation, Sorting, and Transfer

Cell suspensions were prepared from spleen and peripheral lymph nodes by tissue disruption with glass slides and filtered through a 40µm filter. For bone marrow isolation, femurs and tibia were flushed with complete RPMI using a 27 gauge needle and cells were filtered with 40µm filter. Liver, kidney, pancreas, lungs, and tumors were digested with 10mg/ml collagenase type IV (Worthington) for 1hr at 37°C with gentle agitation and then filtered through a 40µm filter. Cells were lysed with ACK lysing buffer (Gibco) and resuspended as single cell suspensions for downstream analysis.

For sorting of hematopoietic bone marrow progenitors, bone marrow was isolated from femurs and tibia as described above, filtered through a 40µm filter, and ACK lysed. Cells were subsequently stained and FACS sorted for subpopulations using the following markers: LT-HSC (Lin$^-$Sca1$^+$ckit$^+$CD150$^+$CD48$^-$Flt3$^-$), pre-MEP (Lin$^-$Sca1$^-$ckit$^+$CD150$^+$CD34$^+$FcγR^{lo}), MEP (Lin$^-$Sca1$^-$ckit$^+$CD34$^-$FcγR$^-$CD150$^-$), CMP (Lin$^-$Sca1$^-$ckit$^+$CD150$^-$CD34$^+$FcγR^{lo}), pre-B cells (CD45$^+$Ter119$^-$B220$^+$), where lineage-negative (Lin$^-$) cells are defined as CD3$^-$CD4$^-$CD8$^-$B220$^-$CD11b$^-$CD11c$^-$Gr-1$^-$Ter119$^-$. For sorting of bone marrow stromal cells, femurs and tibia were crushed with a mortar and pestle and digested with 1mg/ml collagenase type I (Worthington) and 200U/ml DNase I (Stem Cell) for 1 hour at 37°C. Cells were filtered through a 40µm filter, ACK lysed, and depleted of CD45$^+$ cells using anti-CD45 microbeads (Miltenyi). Cells were subsequently stained and FACS sorted for subpopulations using the following markers: mesenchymal stem cells (CD45$^-$Ter119$^-$PDGFRα^+CD51$^+$CD31$^-$), endothelial cells (CD45$^-$Ter119$^-$PDGFRα^-CD51$^-$CD31$^+$), and osteoblasts (CD45$^-$Ter119$^-$PDGFRα^-CD51$^+$CD31$^-$). For sorting of splenic stromal cells, spleens were cut into ~1mm^3 fragments using scissors and digested with 1mg/ml collagenase type I (Worthington) and 200U/ml DNase I (Stem Cell) for 1 hour at 37°C. Cells were filtered through a 40µm filter, ACK lysed, and depleted of CD45$^+$ cells using anti-CD45 microbeads (Miltenyi). Cells were subsequently stained and FACS sorted for subpopulations using the following markers: PDGFRβ^+ spleen stromal cells (CD45$^-$Ter119$^-$PDGFRβ^+) and VE-cadherin$^+$ spleen stromal cells (CD45$^-$Ter119$^-$VE-cadherin$^+$). For analysis of endothelial cells, mice were injected intravenously into the retro-orbital venous sinus with 10 µg Alexa Fluor 660 conjugated anti-VE-cadherin antibody (BV13) 10 minutes before sacrifice. Samples were analyzed using a FACSAria II flow cytometer (BD Biosciences).

Co-Culture of Primary MSC and Splenic Stromal Cells with CAR T Cells

Bone marrow stromal cells were prepared from femurs and tibia of WT or ROR1-KO mice as described above, and MSCs were expanded *in vitro* using the MesenCult Expansion Kit (StemCell) by culturing in a hypoxic incubator (5% O_2, 5% CO_2, 37°C) for 14 days. For isolation of splenic stromal cells, spleens were digested as described above and separated into CD45$^+$ and CD45$^-$ fractions using anti-CD45 microbeads (Miltenyi). For co-culture experiments, 50,000 *in vitro*-expanded MSC or splenic cells were co-cultured with 50,000 CD8$^+$ control or ROR1

CAR T cells in 0.2ml of complete RPMI in triplicate in 96-well U-bottomed plates (Costar) at 37°C, 5% CO_2. After 48 hours, supernatant was harvested and frozen at -20°C for long-term storage and analyzed for IFNγ expression using the Ready-Set-Go Mouse IFNγ ELISA Kit (eBioscience).

CBC, Serum Cytokine, and Serum Chemistry Analysis
Peripheral blood was collected by retro-orbital bleeds into serum separator tubes or EDTA FACS tubes. Serum separator tubes were incubated at room temperature for 30 minutes to allow blood to clot and then centrifuged at 15800xg for 5 mins. Serum was either frozen at -80°C for multiple cytokine immunoassay by the FHCRC Immune Monitoring Core (Luminex) or submitted to Phoenix Central Labs for serum chemistry analysis. Blood in EDTA FACS tubes was submitted to Phoenix Central Labs for complete blood count analysis with differential.

Flow Cytometry
For live/dead staining, cells were stained using the Live/Dead Fixable Aqua Dead Cell stain kit (Invitrogen) according to the manufacturer's protocol. For surface staining, cells were incubated at 4°C for 30 minutes in staining buffer (PBS, 2% FBS) with the following directly conjugated antibodies for murine proteins (from Biolegend unless otherwise specified): anti-CD4 (RM4-5), -CD8 (53-6.7), -CD45.1 (A20), -CD3 (145-2C11), -CD19 (eBio1D3, eBioscience), -CD45 (30-F11), -PD-1 (29F.1A12), streptavidin (eBioscience), -Ter119 (TER119), -B220 (RA3-6B2), -PDGFRα (APA5), PDGFRβ (APB5), -CD51 (RMV7), -CD31 (390), -CD11b (M1/70), -CD11c (N418), -Gr-1 (RB6-8C5), -Sca1 (D7), -cKit (2B8), -CD150 (mShad150, eBioscience), -CD48 (HM48-1), -Flt3 (A2F10), -CD34 (RAM34, eBioscience), -FcγR (93), -EpCAM (G8.8, eBioscience), -myc (9B11, Cell Signaling), -TIM3 (RMT3-23). Biotinylated IgG1 R11 and biotinylated recombinant Fc-mROR1 were used to measure mROR1 and ROR1 CAR expression, respectively (*470*). For intracellular staining, cells were surface stained as described, washed and permeabilized for 20 minutes with eBioscience Fix/Perm buffer at 4°C. Cells were stained for 30 minutes at 4°C with anti-IFN-γ (XMG1; eBioscience) or -Ki67 (B56, BD Biosciences) in 1X Perm/Wash staining medium (eBioscience).

For intracellular cytokine staining following restimulation, 50,000 T cells were stimulated with the indicated combination of 25,000 K562, K562-mROR1, 4T1, or 4T1-mROR1 tumor cells each or with 50ng/ml PMA and 1μg/ml ionomycin in 0.2ml complete RPMI in triplicate in 96-well U-bottomed plates (Costar) at 37°C, 5% CO_2. After 48 hours, GolgiPlug (BD) was added to all wells according to the manufacturer's protocol and cells were cultured at 37°C, 5% CO_2 for an additional 24 hours before staining for flow cytometry as described above. Data were acquired on LSRII, Canto 2 or Symphony flow cytometers (BD Biosciences) and analyzed using FlowJo software (Treestar).

Histology and Disease Scoring
Tissues were immersion fixed in 10% neutral buffered formalin, paraffin embedded, cut into 5 μm sections, and stained with hematoxylin and eosin by the FHCRC Experimental Histopathology Core. Sections were scored semi-quantitatively from 0 to 4 for inflammation and toxicity in a blinded fashion. Changes typically associated with each grade for various tissues are described in Table S1.

Bone Marrow Chimeras
Femurs and tibia were isolated from B6 or EIIα-Cre/ROR1$^{f/f}$ mice and flushed using a 27 gauge needle to isolate bone marrow cells. Bone marrow cells were filtered using 40μm filters, ACK lysed, and depleted of $CD4^+$ and $CD8^+$ cells using anti-CD4 and anti-CD8 microbeads (Miltenyi Biotec). 2-4x10^6 T cell-depleted bone marrow cells were injected intravenously into lethally

irradiated (1000 Rad) B6 or EIIα-Cre/ROR1$^{f/f}$ mice. Mice were bled retro-orbitally 8 weeks after transplant and analyzed by flow cytometry to confirm reconstitution of hematopoietic lineages before use in adoptive transfer experiments.

CFU Assays
Femurs and tibia from control and ROR1 CAR T cell-treated mice were harvested 9 days post-T cell transfer and submitted to ReachBio Inc. for CFU-GM, BFU-E, CFU-Mk, Pre-B CFC, and CFU-F assays.

qPCR
Cell populations were sorted directly into buffer RLT and RNA was extracted using the RNeasy Micro kit (QIAGEN). cDNA was generated using the iScript cDNA Synthesis kit (BioRad) according to the manufacturer's instructions. Expression of *mRor1* was analyzed in triplicate and normalized to *mActb*. Amplifications were performed for 50 cycles on an ABI Prism 7900 (Applied Biosystems) in a 20ul reaction consisting of Power SYBR Green PCR Master Mix (Applied Biosystems), 5ng of cDNA, and 500nM gene-specific forward and reverse primers: *mROR1*, 5'-CAAAACCCGTCAGAGGACAGA-3' and 5'ATGAAACGCACAGCGGAAAG-3'; *mActb*, 5'-CTGTCCCTGTATGCCTCTG-3' and 5'-ATGTCACGCACGATTTCC-3'. The cycle threshold (Ct) was determined using SDS software (Applied Biosystems) and the level of gene expression calculated using the comparative Ct method (2(^Ct)).

Chromium Release Assay
K562, K562-mROR1, 4T1, and 4T1-mROR1 cells were labeled with ^{51}Cr (PerkinElmer) for 1 hour at 37°C and washed with complete RPMI. 1x10^3 ^{51}Cr-labeled target cells were plated with 1x10^3 unlabeled target cells per well in triplicate, and co-cultured with T-cells at various effector to target (E:T) ratios for 72 hours in a 37°C, 5% CO_2 incubator. Supernatants were harvested for γ-counting after 48 hours and 72 hours of incubation and specific lysis calculated by comparing counts to standardized wells where target cells were lysed with NP40-based soap solution.

4T1 Tumor Induction and Monitoring
1x10^5 4T1-mROR1 tumor cells were injected subcutaneously into the 4th right mammary fat pad of 6-8 week old BALB/c female mice. After 7 days, mice were injected intraperitoneally with 200mg/kg cyclophosphamide and 5-6 hours later injected with 5x10^5 CD8$^+$ and CD4$^+$ untransduced, ROR1 CAR, or synNotch EpCAM-inducible ROR1 CAR T cells intravenously. SynNotch T cells were enriched by untouched sorting for BFP$^+$ T cells, as described above, such that ~30% of sorted T cells were myc$^+$BFP$^+$ and carried the full EpCAM-synNotch/UAS-ROR1-CAR circuit. Transduction rate of constitutive ROR1 CAR T cells was equalized to ~30% by diluting cultures with untransduced T cells cultured in parallel such ROR1 CAR- and synNotch-treated mice each received the same number of T cells capable of expressing the ROR1 CAR and the same number of total T cells. Tumor size was monitored using calipers, and tumor volume was calculated as (length in mm)*(width in mm)^2.

Statistical Analysis
All data are presented as the mean values ± SEM. Statistical significance was determined by one-way ANOVA with Tukey's post-test, two-way ANOVA with Tukey's post-test, two-way ANOVA with Sidak post-test, or unpaired Student's two-way t-test as indicated in figure legends. Statistical significance was established at the levels of *, P<0.05; **, P<0.005; ***, P<0.0005; ****, P<0.0001.

Supplemental Figures

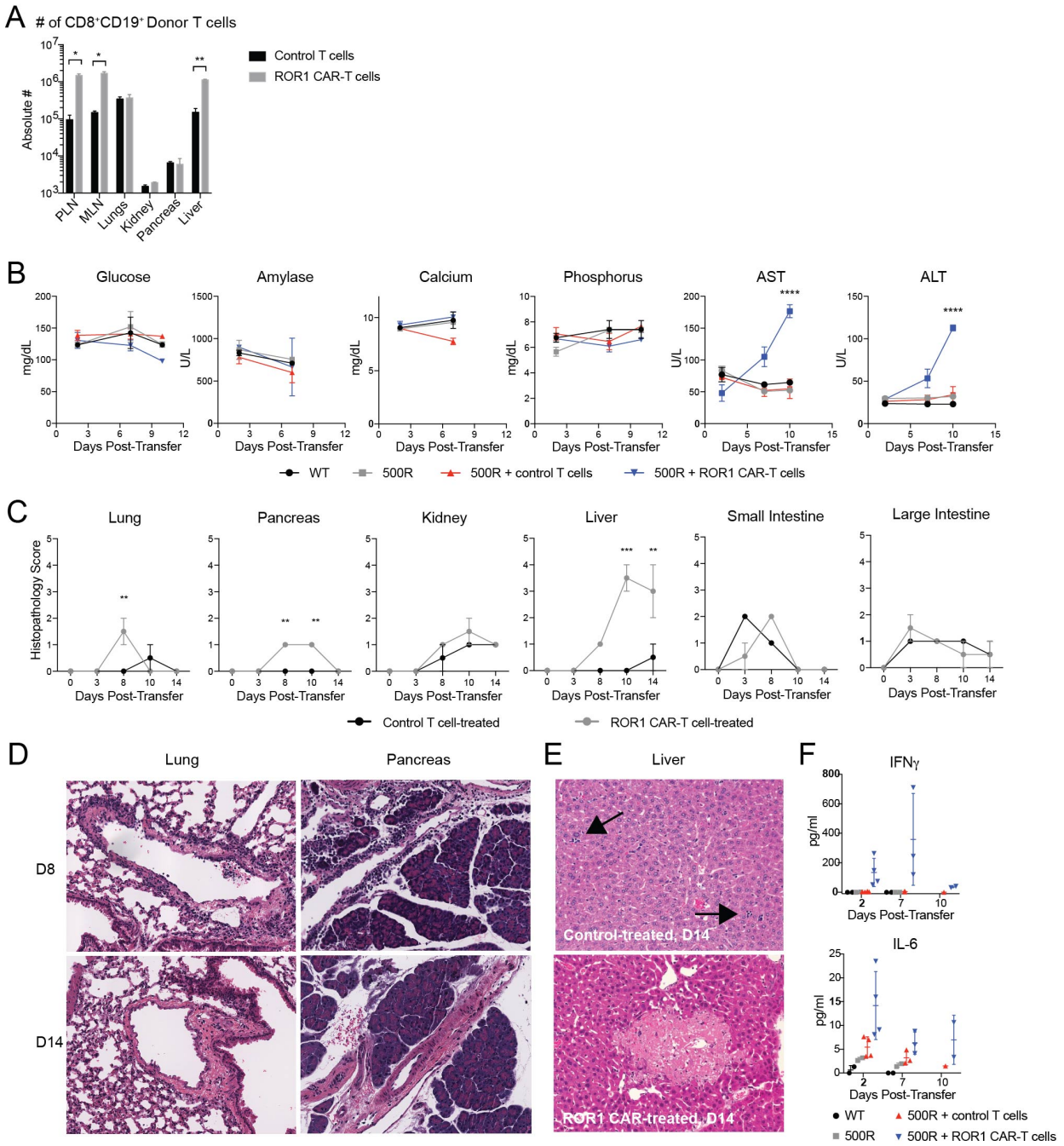

Figure S1. ROR1 CAR T cells induce transient inflammation in lungs, pancreas, and liver. A) Summary of absolute number of CD45.1$^+$CD8$^+$CD19$^+$ control or ROR1 CAR T cells 4 days post-transfer. N=4 mice per group. Unpaired Student's two-way t-test (PLN, P=0.0124; MLN, P=0.0153; Liver, P=0.0032). B) Serum chemistry analysis. N=4 mice per group. Two-way ANOVA with Tukey post-test (ALT D10, P<0.00001; AST D10, P<0.00001). C) Histopathology scoring of control or ROR1 CAR T cell-treated tissues. See Table S1 for histopathology scoring system. N=4 mice per group. Two-way ANOVA with Sidak post-test (Lung D8: P=0.0039; Pancreas D8, P=0.004; Pancreas D10, P=0.003; Liver D10, P=0.0004; Liver D14, P=0.0042). D) Representative H&E stains of lung and pancreas from ROR1 CAR T cell treated mice 8 and 14 days post-transfer. E) Representative H&E stains of livers 14 days post-transfer. Arrows indicate

examples of extramedullary hematopoiesis. F) Serum cytokine levels. N=4 mice per group. *, P<0.05; **, P<0.005; ***, P<0.0005; ****, P<0.0001. Data are representative of 5 independent experiments. All data are presented as the mean values ± SEM.

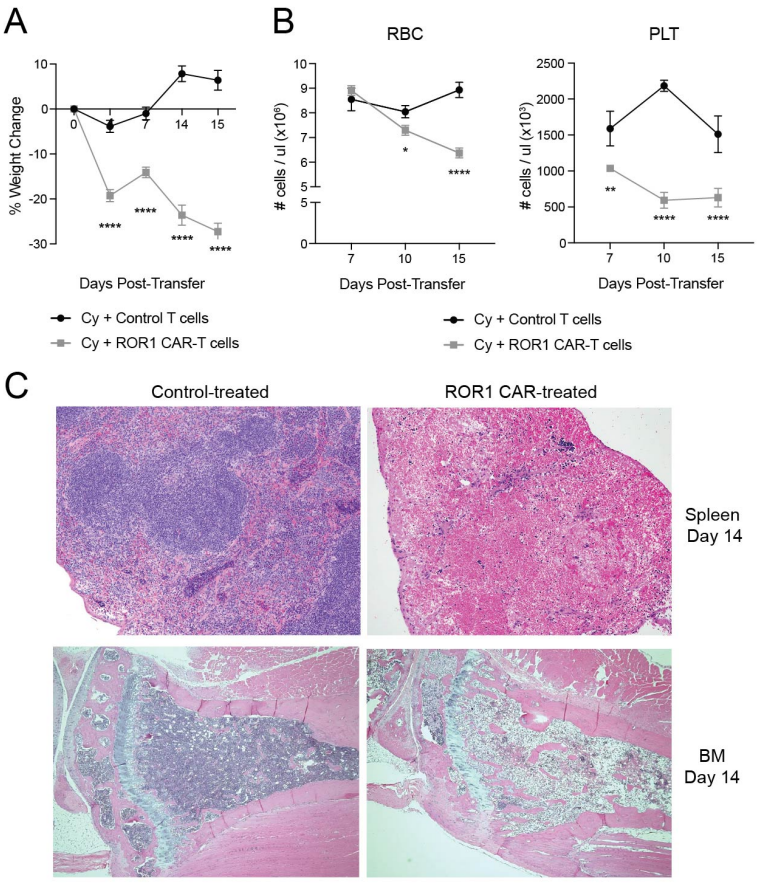

Figure S2. ROR1 CAR T cells induce lethal toxicity in mice preconditioned with 200mg/kg cyclophosphamide. A) Percent change in body weight over time in BALB/c mice treated with 200mg/kg cyclophosphamide (Cy) and receiving $1x10^6$ $CD8^+$ control T cells or $1x10^6$ $CD8^+$ ROR1 CAR T cells. N=4 mice per group. Two-way ANOVA with Tukey post-test (D4,7,14,15, P<0.00001). B) Red blood cell (RBC) and platelet (PLT) counts in peripheral blood from mice treated with Cy and control or ROR1 CAR T cells. N=4 mice per group. Two-way ANOVA with Tukey post-test (RBC D10, P=0.0212; RBC D15, P<0.00001; PLT D7, P=0.0038; PLT D10, P<0.00001; PLT D15, P<0.00001). C) Representative H&E stains of spleen and femur (BM) from control or ROR1 CAR T cell treated mice 14 days post-transfer. *, P<0.05; **, P<0.005; ***, P<0.0005; ****, P<0.0001. Data are representative of 2 independent experiments. All data are presented as the mean values ± SEM.

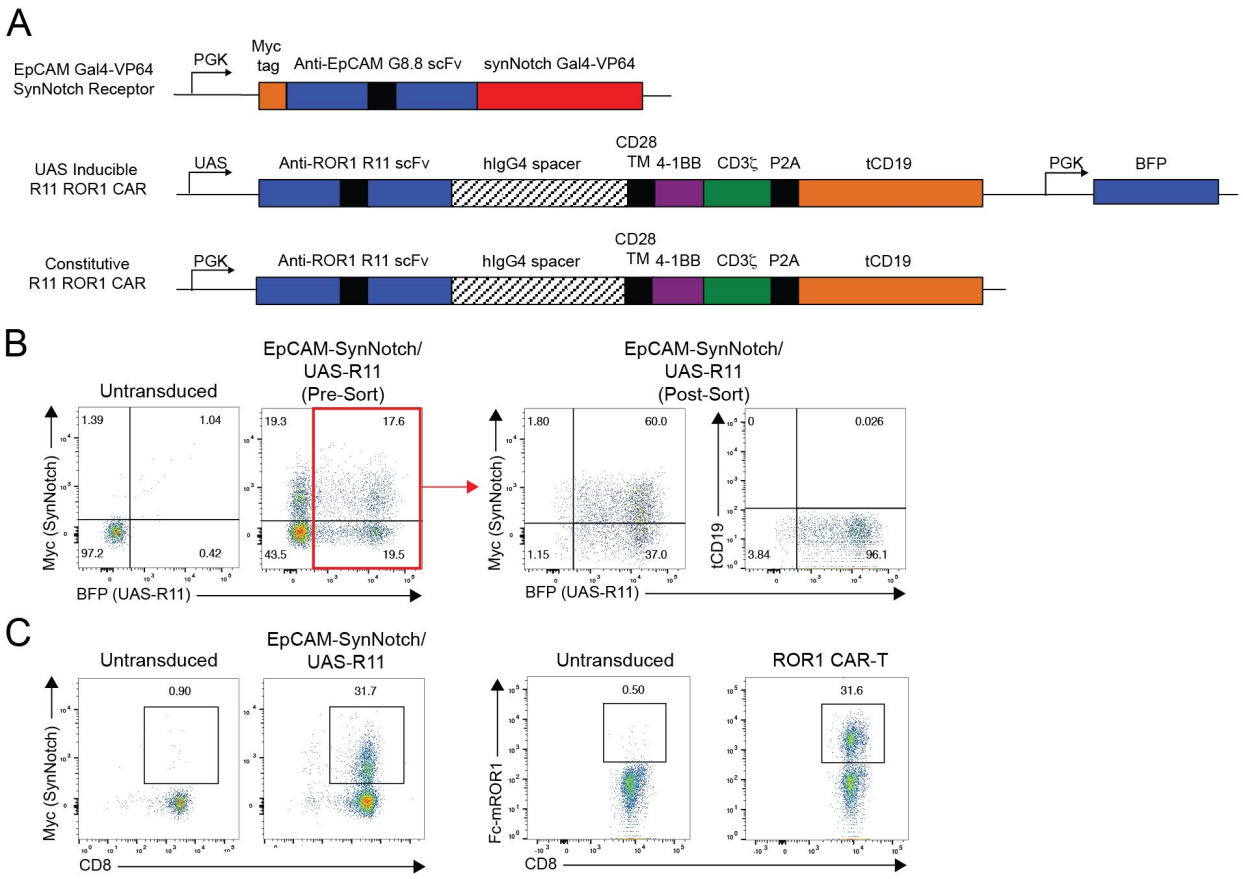

Figure S3. Design and generation of synNotch EpCAM-inducible ROR1 CAR T cells. A) Map of lentiviral constructs encoding EpCAM-Gal4VP64 synNotch Receptor, UAS inducible R11 ROR1 CAR, and constitutive R11 ROR1 CAR. Expression of the EpCAM synNotch receptor is detected by myc expression; transduction of the UAS inducible ROR1 CAR construct is detected by BFP expression; and induction of CAR expression is detected by tCD19 expression. B) Left: Representative flow cytometric analysis of myc and BFP expression in BALB/c $CD8^+$ T cells left untransduced or co-transduced with EpCAM synNotch and UAS inducible ROR1 CAR constructs prior to sorting. Right: representative flow cytometry analysis showing post-sort purity and tCD19 (ROR1 CAR) expression on EpCAM-synNotch/UAS-R11 co-transduced T cells sorted for BFP expression. C) Left: representative flow cytometry analysis showing EpCAM synNotch (myc) expression on $CD8^+$ untransduced and BFP-sorted synNotch T cells prior to adoptive transfer *in vivo*. Right: representative flow cytometry analysis showing ROR1 CAR expression on $CD8^+$ untransduced and ROR1 CAR T cells prior to adoptive transfer *in vivo*. TM = transmembrane. hIgG4 = human immunoglobulin G4. BFP = blue fluorescent protein.

Table S1. Histopathology scoring system of tissues from control and ROR1 CAR T cell-treated mice. RP = red pulp; WP = white pulp; EMH = extramedullary hematopoiesis.

	Histology Score				
	0	**1**	**2**	**3**	**4**
Spleen	Within normal limits	Minimal RP/WP atrophy with focal regeneration	Moderate RP/WP atrophy	Severe RP/WP atrophy and hyperplasia	Severe RP/WP atrophy and tissue necrosis
BM	Within normal limits	Minimal marrow atrophy with myeloid regeneration	Moderate marrow atrophy with myeloid regeneration	Moderate marrow atrophy with myelofibrosis and focal myeloid regeneration	Severe marrow atrophy with myelofibrosis and no myeloid or erythroid regeneration
Liver	Within normal limits	Minimal multifocal cholangiohepatitis	Moderate multifocal cholangiohepatitis with EMH	Moderate multifocal cholangiohepatitis with minimal focal necrosis and no EMH	Moderate multifocal cholangiohepatitis with moderate focal necrosis and no EMH
Lung	Within normal limits	Minimal multifocal perivasculitis	Moderate multifocal perivasculitis	*(not observed)*	*(not observed)*
Kidney	Within normal limits	Mesangial glomerulopathy	Moderate glomerulopathy with interstitial nephritis	*(not observed)*	*(not observed)*
Pancreas	Within normal limits	Multifocal interstitial pancreatitis	*(not observed)*	*(not observed)*	*(not observed)*
Small Intestine	Within normal limits	Moderate lymphoid atrophy	Severe lymphoid atrophy and villous atrophy/fibrosis	*(not observed)*	*(not observed)*
Large Intestine	Within normal limits	Moderate lymphoid atrophy	Severe lymphoid atrophy with focal ulcers	*(not observed)*	*(not observed)*

Leukemia (2017) **31,** 2191–2199

www.nature.com/leu

ORIGINAL ARTICLE

Fully human CD19-specific chimeric antigen receptors for T-cell therapy

D Sommermeyer[1], T Hill[1], SM Shamah[2], AI Salter[1], Y Chen[2], KM Mohler[2] and SR Riddell[1,3,4]

Impressive results have been achieved by adoptively transferring T-cells expressing CD19-specific CARs with binding domains from murine mAbs to treat B-cell malignancies. T-cell mediated immune responses specific for peptides from the murine scFv antigen-binding domain of the CAR can develop in patients and result in premature elimination of CAR T-cells increasing the risk of tumor relapse. As fully human scFv might reduce immunogenicity, we generated CD19-specific human scFvs with similar binding characteristics as the murine FMC63-derived scFv using human Ab/DNA libraries. CARs were constructed in various formats from several scFvs and used to transduce primary human T-cells. The resulting CD19-CAR T-cells were specifically activated by CD19-positive tumor cell lines and primary chronic lymphocytic leukemia cells, and eliminated human lymphoma xenografts in immunodeficient mice. Certain fully human CAR constructs were superior to the FMC63-CAR, which is widely used in clinical trials. Imaging of cell surface distribution of the human CARs revealed no evidence of clustering without target cell engagement, and tonic signaling was not observed. To further reduce potential immunogenicity of the CARs, we also modified the fusion sites between different CAR components. The described fully human CARs for a validated clinical target may reduce immune rejection compared with murine-based CARs.

Leukemia (2017) **31,** 2191–2199; doi:10.1038/leu.2017.57

INTRODUCTION

Adoptive immunotherapy with gene-modified T-cells expressing a tumor-reactive CAR has rapidly evolved with the most impressive clinical results using autologous T-cells expressing a CD19-specific CAR to treat B-cell malignancies such as acute lymphoblastic leukemia, chronic lymphocytic leukemia (CLL) and non-Hodgkin's lymphoma.[1–9] Tumor regression has correlated with the level of CAR T-cell proliferation and the duration of their persistence in the blood.[4–11] The length of time that CAR T-cells must persist *in vivo* to attain complete disease eradication has not been established. However, in patients with acute lymphoblastic leukemia the loss of CAR T-cells after an initial expansion phase coincided with the return of normal B-cells and an increased risk of relapse with $CD19^+$ malignancy.[3] Multiple mechanisms may be responsible for the inability of certain CAR T-cells to survive *in vivo*. One such mechanism is the development of an HLA-restricted T-cell mediated immune response against epitopes derived from the murine scFv used as the antigen-binding domain of the CAR. We previously described T-cell responses to foreign transgene products in patients receiving modified T-cells expressing hygromycin-phosphotransferase and herpes-simplex-virus thymidine-kinase,[12,13] and recently reported that some patients treated with CD19-CAR T-cells developed an immune response specific for epitopes in the murine scFv and rendered subsequent T-cell infusions ineffective.[3]

CARs are synthetic proteins consisting of an antigen-binding moiety, usually an scFv derived from non-human mAbs, linked by hinge/spacer and transmembrane sequences to an intracellular signaling module. CARs may contain unique peptide sequences that could be presented by major histocompatibility complex (MHC) and potentially be immunogenic. Such epitopes could come from a non-human scFv, fusion sites between different human CAR components, and any additional amino acid (aa) modifications to the CAR. In addition to T-cell responses, CAR-specific Abs, including IgE responses that have induced anaphylaxis, may develop after adoptive transfer of CAR T-cells, particularly those not targeting B-cells, as with CD19-CARs.[14–16] Reducing immunogenicity of CARs by using humanized[17–19] or fully human scFvs[20–22] may improve the longevity of CAR T-cell persistence and enhance their therapeutic efficacy in patients.

All published clinical trials targeting CD19 have utilized scFvs derived either from the murine FMC63 or SJ25C1 mAbs.[3–5,7] Here we describe the successful generation and isolation of anti-human CD19 scFvs from human Ab/DNA libraries with similar binding characteristics as an scFv derived from FMC63. When tested in CAR formats, certain human scFvs showed improved *in vitro* functions against tumor cell lines and primary CLL and were more efficient in eliminating lymphoma xenografts in immunodeficient mice than the FMC63-CAR. These data indicate that functional fully human CARs against an antigen that has been successfully targeted in patients can be generated to potentially overcome the immunologic barriers that exist with CARs constructed from scFvs that are not fully human in origin.

MATERIALS AND METHODS

Cells

HEK293T (ATCC_CRL-11268), HEK293 (ATCC_CRL-1573) and CD19-transfected HEK293 (HEK293/CD19) cells were cultured in Dulbecco's modified Eagle's medium, 10% fetal calf serum and 100 U/ml

[1]Fred Hutchinson Cancer Research Center, Clinical Research Division, Program in Immunology, Seattle, WA, USA; [2]Juno Therapeutics, Inc., Seattle, WA, USA; [3]Department of Medicine, University of Washington, Seattle, WA, USA and [4]Technical University of Munich, Institute for Advanced Study, Munich, Germany. Correspondence: Dr SR Riddell, Fred Hutchinson Cancer Research Center, 1100 Fairview Ave N., D3-100, Seattle, WA 98109, USA.
E-mail: sriddell@fredhutch.org
Received 4 November 2016; revised 23 January 2017; accepted 1 February 2017; accepted article preview online 16 February 2017; advance online publication, 21 March 2017

penicillin/streptomycin. K562 (ATCC_CCL-243), K562/CD19,[23] Raji (ATCC_CCL-86) and Raji/ffluc[24] cells were cultured in RPMI-1640, 5% fetal calf serum and 100 U/ml penicillin/streptomycin. Truncated rhesus macaque CD19 (including the extracellular and transmembrane regions) and chimeric rhesus/human versions of truncated CD19 were cloned into the retroviral plasmid pMP71.[25] K562 cells were transduced with genes encoding rhesus CD19 and rhesus/human CD19 chimeric molecules, and transgene-positive cells were enriched by fluorescence activated cell sorting after staining with an anti-CD19 mAb (BD Bioscience, San Jose, CA, USA; #555415). The absence of mycoplasma was confirmed for all cell lines by monthly testing. T-cells were isolated and cultured as described.[26] Peripheral blood mononuclear cells isolated from blood of CLL patients with high circulating tumor burdens were used as primary CLL samples.

Screening for human anti-CD19 scFvs from human Ab-chain libraries

DsDNA-displayed fusion libraries were purified, and eluted in binding buffer containing 1 mg/ml bovine serum albumin (Life Technologies, Carlsbad, CA, USA) and 0.1 mg/ml of ssDNA (Life Technologies) as blocking reagents. Counter-selections were carried out three times with parental HEK293 or K562 cells, each with 10^7 pre-blocked cells for 1 h at 4 °C followed by centrifugation. Unbound library members were transferred to a new tube, incubated with 10^7 pre-blocked HEK293/CD19 or K562/CD19 cells for 1 h on ice to prevent internalization and then washed with binding buffer. Enriched pools were generated by addition of murine FMC63 IgG to elute binders from the cell surface that recognize overlapping epitopes as the murine reference antibody.

After six rounds of enrichment, the scFv pools were subcloned into the periplasmic expression vector pET-22b (Life Technologies) and transformed into BL21(DE3) bacterial cells for expression. Supernatants from several hundred clones were screened in a flow cytometry-based binding assay. ScFvs specifically binding to $CD19^+$ cells were then scaled up for production and purified through a C-terminal His-tag.

Binding and competition flow cytometry assays

2×10^5 K562/CD19 cells were incubated for 1 h at 4 °C with the indicated concentration of His-tagged anti-CD19 scFvs for binding assays and with a mixture of 10 nM myc-tagged FMC63-scFv and the indicated concentration of His-tagged human scFvs for competition binding assays, respectively. Following two washes, cells were stained with an anti-His mAb (Qiagen, Hilden, Germany; #35370) for binding assays or an anti-myc mAb (EMD Millipore, Darmstadt, Germany; clone 9E10) for competition binding assays. Mean fluorescence intensity was measured using a Guava flow cytometer (EMD Millipore).

Lentiviral vector construction, virus preparation, transduction of T-cells and *in vitro* functional assays

The CD19-specific FMC63-CAR was described previously.[26] Sequences encoding human anti-CD19 scFvs were linked to a modified IgG4 hinge region with a serine to proline substitution at position 10, the CD28-derived transmembrane region, a 4-1BB-derived costimulatory domain and intracellular CD247. Codon-optimized *CAR* genes were combined with a sequence encoding truncated epidermal growth factor receptor (EGFRt) by a T2A sequence and cloned into the lentiviral vector epHIV7.[27] To generate *CAR-eGFP* fusion genes, eGFP was linked in frame to CD247 replacing T2A-EGFRt. To generate 35-G01S HL mutant, one threonine and two serines were mutated to alanine in a predicted *O*-glycosylation site of 35-G01S by site-directed mutagenesis. The new fusion site between CD28 transmembrane and 4-1BB signaling domain that extended the CD28 sequence by two aa was created by overlapping PCRs. Lentivirus was generated by transient transfection of HEK293T-cells[28] using psPAX2 and pMD2G packaging plasmids. Primary human T-cells were activated, transduced, enriched and expanded as described.[26] Cytotoxicity was analyzed by a standard 4 h chromium release assay, cytokine concentrations were determined by enzyme-linked immunosorbent assay and proliferation was measured by carboxyfluorescein succinimidyl ester dilution as described.[29]

Flow cytometry

Transduced T-cells were stained with biotin-conjugated (EZ-Link Sulfo-NHS-Biotin; Thermo Scientific, Waltham, MA, USA) anti-EGFR mAb (ImClone Systems Incorporated, New York, NY, USA) and streptavidin-PE (BD Biosciences; #554061). T-cells were stained with anti-PD-1 mAbs and matched isotype control (Biolegend, San Diego, CA, USA; #329907, #400119). Flow cytometry was performed on a FACSCanto II and data were analyzed with FlowJo (Treestar, Ashland, OR, USA).

Western blot

5×10^6 CAR T-cells were lysed and 10 µg of protein were separated on a 10% polyacrylamide gel. After blotting, membranes were incubated with an anti-CD247 mAb (BD Biosciences; #556366) followed by a horseradish peroxidase conjugated rabbit anti-mouse secondary Ab (Cell Signaling Technology, Danvers, MA, USA; #7076 S). To remove *N*-linked glycosylations, protein lysates were incubated with PNGaseF (New England Biolabs, Ipswich, UK) for 1 h at 37 °C.

Fluorescence microscopy

Live cells were imaged with a DeltaVision microscope (GE Healthcare, Pittsburgh, PA, USA) and data were analyzed using ImageJ software (National Institutes of Health, Bethesda, MD, USA). Raji and K562 cells were stained with Hoechst33342 (NucBlue Live reagent; ThermoFisher, Waltham, MA, USA) for 20 min, washed and then co-cultured with CAR T-cells for 10 min at 37 °C.

MHC-binding prediction

Binding affinities of 9-mer peptides derived from the CAR sequence that are not encoded by the human genome were predicted using NetMHC.[30]

NOD/SCID/$\gamma c^{-/-}$ (NSG) mouse model

Six- to eight-week-old female NSG mice were engrafted with 5×10^5 Raji/ffluc cells via tail vein injection. One week later, CAR- or control T-cells that had been expanded with CD19+ Epstein Barr virus lymphoblastoid cells for 9 days were injected intravenously. Bioluminescence imaging was performed as described.[29] For experiments where differences between individual mice were expected, at least five mice per experimental group were used for data analysis to provide 81% power to detect an effect size of 1.75, based on a *t*-test with a one-sided 0.05 level of significance. The investigator was blinded to group allocation.

Study approval

Blood donors provided written informed consent for research protocols approved by the Institutional Review Board of the Fred Hutchinson Cancer Research Center. The Fred Hutchinson Cancer Research Center Institutional Animal Care and Use Committee approved all mouse experiments.

RESULTS

Selection of human CD19-specific scFvs with similar binding characteristics as FMC63 from human Ab-chain libraries

Highly diverse human VH and VL libraries were constructed by reverse transcription-PCR from bone marrow and peripheral blood mononuclear cells samples from 20 donors and displayed in a cell-free system as dsDNA-Ab libraries.[31] A VH-library was selected through three rounds for binding to HEK293/CD19 cells, but not to HEK293 cells. The enriched VH-library containing ~10^4–10^5 different sequences was then converted to a scFv-library by shuffling with the naïve VL-library in a VH-$(G4S)_3$-VL format. This scFv-library comprising at least 10^9 sequences was further enriched by two rounds of negative selections on HEK293 or K562 cells followed by positive selections on HEK293/CD19 or K562/CD19 cells. Bound scFvs were displaced off the cell surface by competition with FMC63 with the objective of deriving scFvs that targeted a CD19 epitope overlapping with that recognized by FMC63. The obtained scFv pool was then again negatively selected for members not binding HEK293 and K562 cells, followed by a final positive selection for binding to HEK293/CD19 cells. After this extensive selection, the scFv sequences were cloned into a bacterial vector and crude bacterial supernatants from several hundred randomly picked colonies were screened for scFv binding to CD19/K562 cells.

ScFvs from 60 clones that displayed elevated binding to CD19-expressing cells compared with negative cells were purified

Table 1. Binding affinity (EC_{50}) and competitive binding activity with FMC63 (IC_{50}) of selected scFvs

scFv	*EC_{50} (nM)*	*IC_{50} (nM)*
FMC63	6.1 ± 0.7 ($n=10$)	15.6 ± 2.6 ($n=11$)
35-G01	4.1 ± 0.6 ($n=7$)	20.1 ± 5.6 ($n=4$)
35-G01S	4.9 ± 0.8 ($n=7$)	32.1 ± 2.4 ($n=4$)
35-C03	11.6 ± 1.1 ($n=5$)	37.1 ± 2.9 ($n=3$)
62-B01	7.0 ± 1.4 ($n=5$)	18.2 ± 1.5 ($n=2$)
33-E03	>200 ($n=4$)	Not done

and characterized for binding affinity (EC_{50}) to CD19 by flow cytometry. We selected three scFvs (35-G01, 35-C03, 62-B01) with a comparable binding affinity to that of the FMC63-scFv (~5 nM), and one scFv (33-E03) with a significantly lower binding activity (Table 1 and Figure 1a). All scFvs included an identical VH paired with different VLs. Analysis of the aa sequence of the 35-G01 scFv identified a cysteine residue in the VL-CDR3, which was not suspected to be involved in target binding as it is the first residue of the VL-CDR3 sequence. This residue represented a potential concern for aggregation due to indiscriminate disulfide bond formation and was therefore converted by site-directed mutagenesis to a serine residue. This derivative scFv (35-G01S) had a similar binding affinity as the original scFv (Table 1 and Figure 1a).

An objective was to identify human scFvs that bind CD19 at epitopes shared by FMC63. We therefore analyzed the competitive binding activity (IC_{50}) of individual human scFvs with FMC63. All tested human scFvs displayed 100% competition with FMC63 for binding to K562/CD19 cells with IC_{50} values in the range of 20–40 nM (Table 1 and Figure 1b). Thus, a number of CD19-specific human scFvs that competed with FMC63 for binding and had a similar affinity as FMC63 were successfully generated for CAR construction.

In vitro function of T-cells expressing CD19-specific CARs constructed with human scFvs

We incorporated each of the five human CD19-specific scFvs shown in Figure 1 into CARs and compared their ability to redirect T-cell function with that of a CAR containing a murine FMC63-scFv that is currently used in a number of clinical trials.[3,5,7–9] The human VH and VL chains of individual scFvs were linked by a $(G_4S)_3$-linker with either the VH at the N-terminus (HL) or the VL at the N-terminus (LH). All CARs contained an extracellular IgG4-hinge region, a CD28 transmembrane region and an intracellular 4-1BB costimulatory domain linked to the cytoplasmic domain of CD247. Thus, apart from containing human scFv-binding regions, the CARs were otherwise comparable to an FMC63-CAR construct used in clinical trials at the FHCRC. The constructs were encoded in lentiviral vectors that coexpressed an EGFRt to permit purification of transduced T-cells. $CD8^+$ T-cells were isolated from normal donors, transduced with different CAR vectors, and transduction efficiencies were analyzed based on expression of EGFRt. $CD8^+$ T-cells were efficiently transduced with all CAR vectors and transgene-positive T-cells were enriched by sorting based on expression of EGFRt (Figure 2a). T-cells expressing the FMC63-CAR and each of the human scFv CARs specifically lysed K562 cells transduced with CD19 (K562/CD19) but not control K562 cells, and lysed $CD19^+$ lymphoma cells (Raji; Figure 2b). T-cells transduced with human scFv CARs in the HL configuration, which was the original configuration of the scFv-library, were more effective in lysing $CD19^+$ target cells compared with T-cells with LH CARs. These results were consistent with flow cytometry binding assays with purified LH scFvs on K562/CD19 cells that showed reduced or no binding compared with HL scFvs (data not shown).

Human HL CAR T-cells also produced higher cytokine levels and proliferated more after activation with $CD19^+$ cells as compared with LH CAR T-cells (Figures 2c and d). When evaluated against Raji lymphoma cells, which express lower levels of CD19 than K562/CD19 cells, we observed superior cytolytic activity, cytokine production and proliferation of T-cells expressing all of the human scFv CARs in the HL configuration compared with T-cells expressing the FMC63-CAR (Figures 2b–d). The superior effector function of human HL CARs compared with FMC63 observed in this assay was also seen when primary CLL samples were used as target cells (Figure 2e). Interestingly, T-cells expressing the 33-E03-CAR that contained an scFv with a lower affinity than FMC63 showed significantly more IFN-γ production and proliferation compared with those expressing the FMC63-CAR.

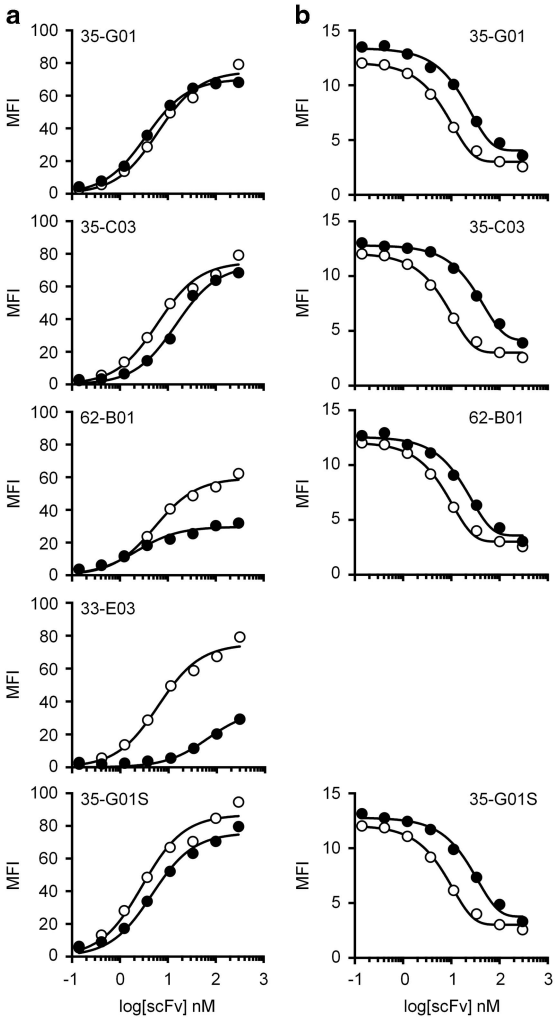

Figure 1. Human CD19-specific scFv with similar binding characteristics as FMC63 were isolated from a human Ab-chain library. (**a**) ScFv titration to assess binding to K562/CD19 cells. (**b**) Competition binding assay of each scFv with FMC63. Binding of FMC63 and competition with itself (open symbols) are shown as a comparison in each graph.

CD19-CARs are expressed at similar levels but differentially glycosylated

To examine whether the functional differences observed between HL, LH and FMC63-CARs were due to different expression levels, we analyzed the total amount of CAR protein. Western blot analysis of cell lysates with a CD247-specific Ab showed that all CARs were expressed at similar levels (Figure 3a). Although the CARs should have similar molecular weights based on their

sequences, western blot results revealed bands for all HL CARs of a slightly larger molecular weight compared with the LH CARs. In addition, lysates from T-cells expressing the 62-B01 CAR showed two bands. Analysis of the 62-B01 sequence revealed a predicted *N*-glycosylation site (NetNGlyc 1.0 Server) and treatment of the lysate with PNGaseF, which removes *N*-glycosylations, resulted in

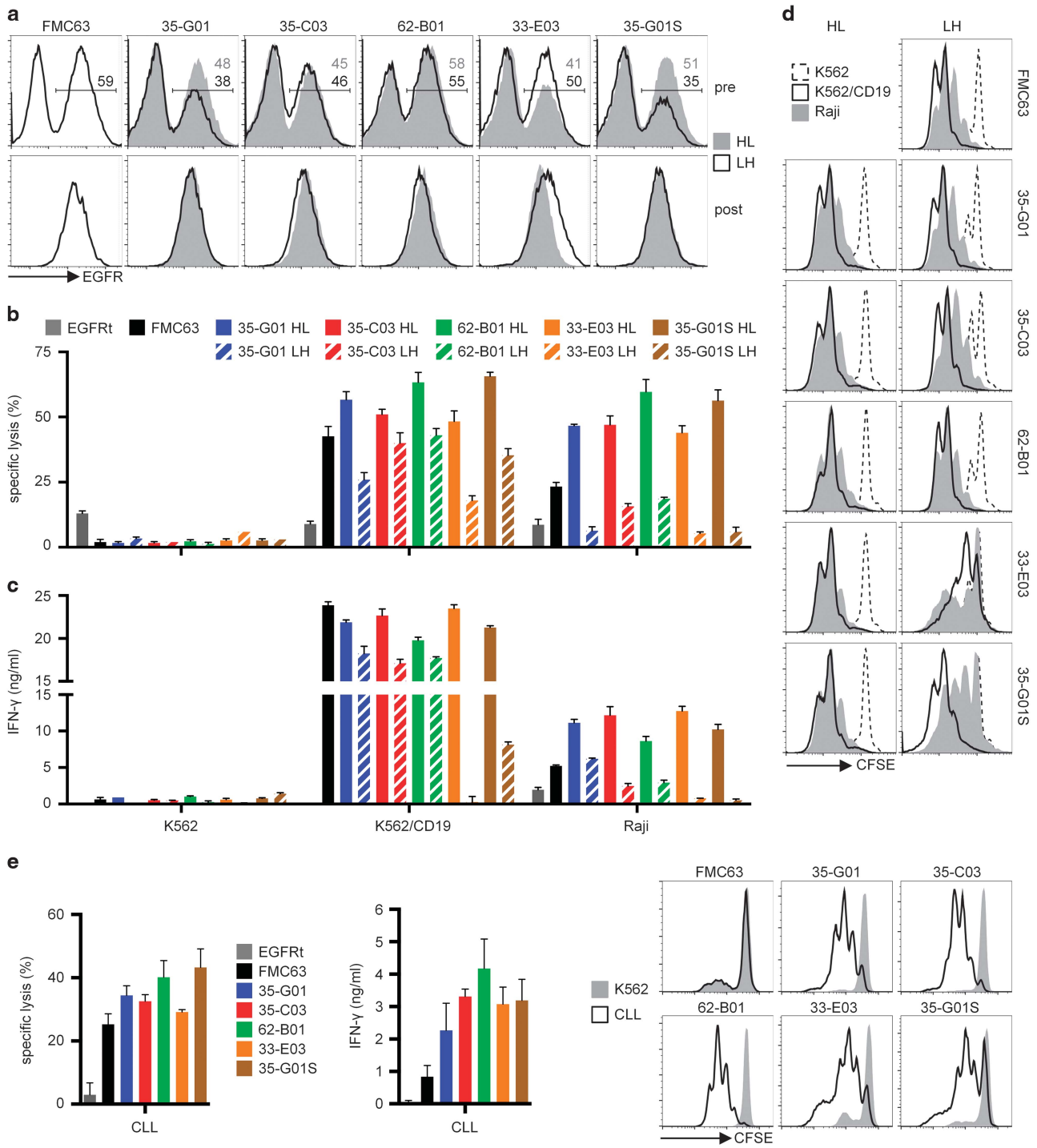

Figure 2. CARs with human CD19-specific scFvs recognize CD19$^+$ tumor cells. (**a**) EGFRt expression on CD8$^+$ T-cells transduced with CD19-CAR-EGFRt constructs before enrichment (pre) and after enrichment and expansion (post). (**b**) Cytolytic activity of EGFRt$^+$ CD19-CAR T-cells against CD19$^+$ (K562/CD19, Raji) and control (K562) target cells analyzed by a 4 h chromium release assay at an E:T ratio of 30:1. (**c**) IFN-γ concentrations in supernatants of CD19-CAR-T-cells after stimulation with K562, K562/CD19 and Raji cells for 24 h analyzed by enzyme-linked immunosorbent assay. Data in (**a**–**c**) are representative of at least five experiments with T-cells prepared from different donors. Differences between HL and LH constructs are significant ($P < 0.05$) for each CAR. (**d**) Proliferation of CD19-CAR-T-cells after stimulation with K562, K562/CD19 and Raji cells for 72 h analyzed by a carboxyfluorescein succinimidyl ester dilution assay. Data are representative of at least three experiments with T-cells prepared from different donors. (**e**) Cytolytic activity, IFN-γ production and proliferation of CD19-CAR-T-cells after co-culture with primary CLL or K562 cells. Data for cytolytic activity and IFN-γ production are shown as means of three CLL samples isolated from different patients. Proliferation data are representative for three CLL samples.

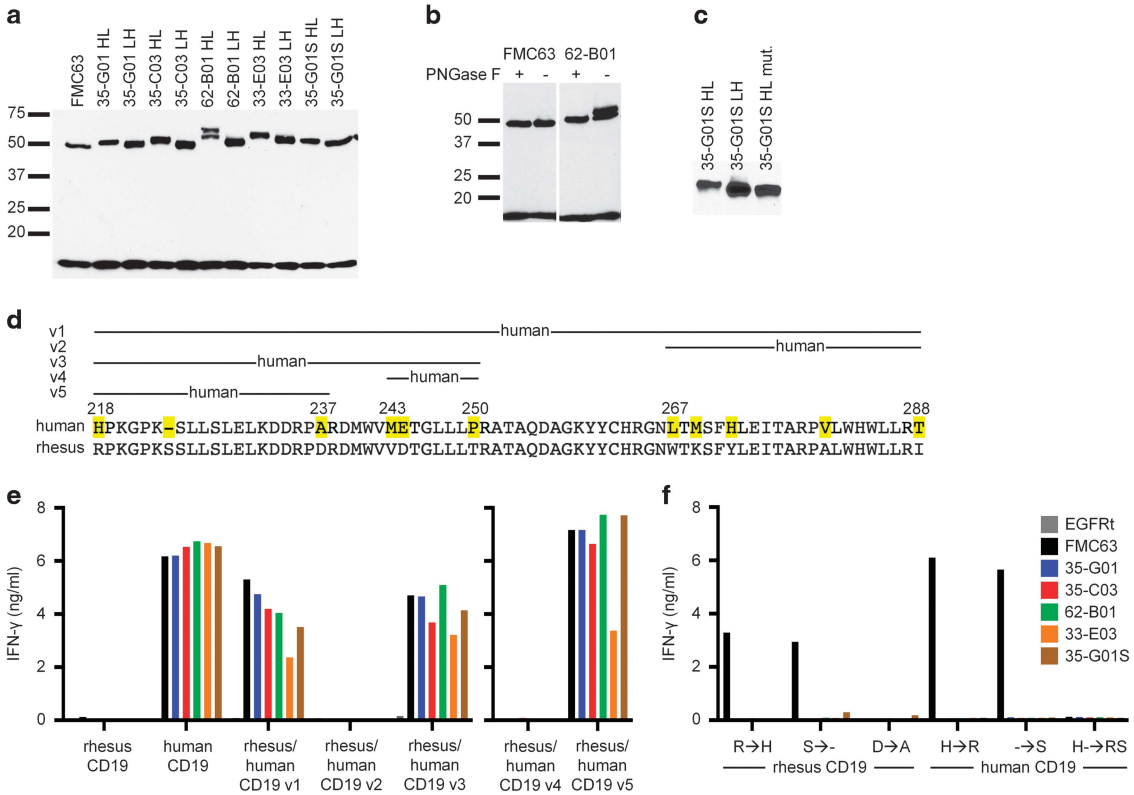

Figure 3. (**a**–**c**) Western blot analysis of CAR protein (~50 kDa) based on CD247 staining. Endogenous CD247 (18 kDa) was used as a loading control. Data are representative of at least two experiments. (**d**) Sequences of human and rhesus macaque CD19 are shown for aa 218–288. aa that are different are marked in the human sequence. (**e**) IFN-γ concentrations in supernatants of CD19-CAR-T-cells after co-culture with K562 cells expressing either rhesus macaque, human or chimeric versions of CD19. (**f**) IFN-γ concentrations in supernatants of CD19-CAR-T-cells after co-culture with K562 cells expressing either rhesus macaque or human CD19 with single or double mutations to the other species. Data in (**e**, **f**) are representative of at least two experiments.

disappearance of the second higher molecular weight band for 62-B01, whereas FMC63 was not affected (Figure 3b). A potential *O*-glycosylation site was identified in each of the human HL CARs but not in any of the LH CARs (NetOGlyc 4.0 Server[32]), and we speculated that the size difference in the western blot results might be due to *O*-glycosylation at this site. We mutated the site in the 35-G01S HL CAR and showed that the mutated protein had the same apparent size as 35-G01S LH on a western blot, which suggested that *O*-glycosylation in HL constructs explained their slightly higher molecular weights (Figure 3c). However, the additional *O*-glycosylation did not seem to explain the enhanced function of HL compared with LH CARs, as the *in vitro* function of 35-G01S HL CARs with and without the glycosylation site was comparable (data not shown).

The fully human CD19-CARs recognize the same region of CD19 as FMC63 but require distinct aa for recognition

The human CD19-CARs in the HL configuration exhibited superior function against CD19$^+$ tumor cells *in vitro* compared with the FMC63-CAR, despite having similar affinity for CD19. To analyze whether the superior function might be due to differences in the epitope on CD19, we examined the sequences of CD19 that were important for recognition by making human/rhesus chimeric CD19 molecules. The extracellular domains of human and rhesus macaque CD19 are 88% homologous; however, neither FMC63 nor the human CD19-CARs recognized K562 cells expressing rhesus CD19 (Figures 3d and e). We first replaced aa 218–288 of rhesus CD19 by the human sequence because the epitope for FMC63 is assumed to be located in this region.[33] CD8$^+$ T-cells expressing either the FMC63- or a human CAR recognized K562 cells transduced with this chimeric CD19 version (rhesus/human CD19_v1), consistent with the requirement for this sequence for recognition (Figures 3d and e). We next subdivided this region into two parts and constructed CD19 chimeras with the human sequence in either of the two parts (v2: 267–288, v3: 218–250). All CAR T-cells recognized K562 cells expressing the chimera including aa 218–250 from the human sequence (v3), whereas the other version (v2) was not recognized by any of the CARs (Figures 3d and e). The region 218–250 was further divided into constructs containing human CD19 sequences corresponding to 243–250 (v4) and 218–237 (v5). All human CARs and FMC63 recognized version 5 but not 4, suggesting that all of the human CARs that we assessed recognize a highly similar region on CD19 as FMC63, a result that is consistent with the results of competition assays performed with the scFvs.

There are only three differences between the human and rhesus sequences within aa 218–237. The residue in each such position in the rhesus sequence was individually mutated to the corresponding aa in the human sequence and these mutant rhesus CD19 molecules were expressed in K562 cells to allow comparison of the fine specificities of the human CARs and the FMC63-CAR. FMC63-CAR T-cells recognized K562 cells expressing rhesus CD19 with a mutation at position 218 from arginine to histidine or with a deletion of the serine at position 224, but did not recognize rhesus CD19 with only the aspartic acid to alanine substitution (Figure 3f). None of the human CARs recognized any of the single mutation constructs demonstrating that the fine specificity of these CARs was different than FMC63. To confirm these results, we mutated human CD19 at position 218 from histidine to arginine and/or added a serine at position 224. Here again, the results indicated that each of these CD19 single aa variants was recognized by

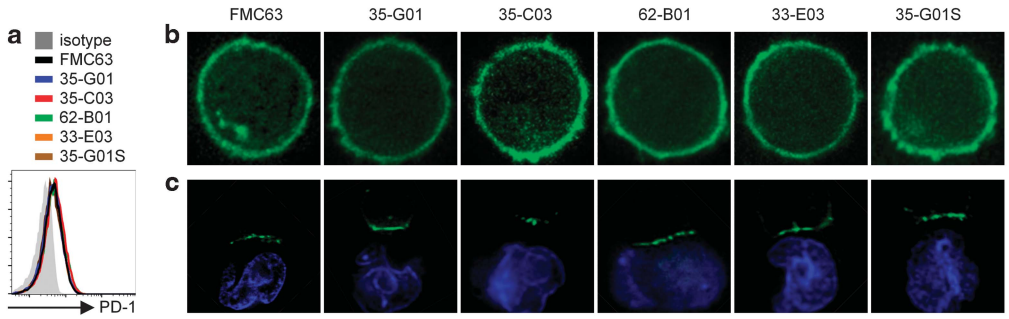

Figure 4. (**a**) Flow cytometric analysis of PD-1 expression on CD19-CAR T-cells 10 days after re-stimulation with CD19$^+$ Epstein Barr virus lymphoblastoid cells. (**b**, **c**) Fluorescence microscopy images of T-cells expressing CD19-CAR-eGFP fusion proteins in the absence (**b**) or presence (**c**) of Hoechst33342-labeled (blue) Raji cells. Data in (**a**–**c**) are representative of at least two experiments.

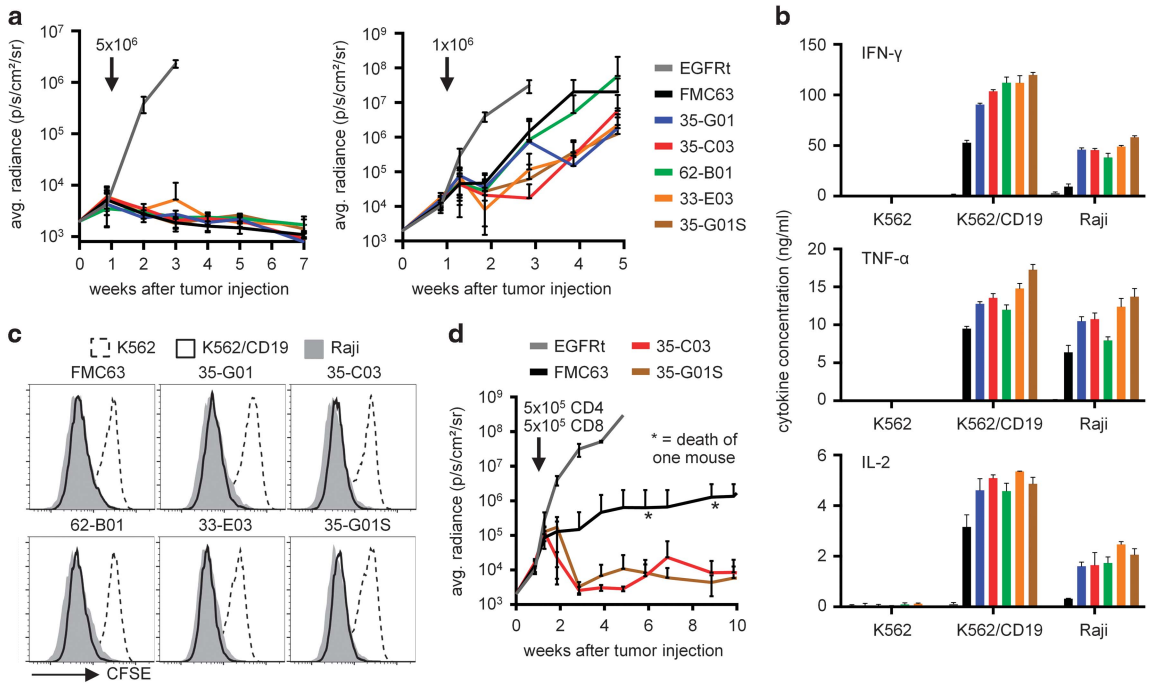

Figure 5. CAR-T-cells with a human CD19-specific scFv eradicate tumors *in vivo*. (**a**) Bioluminescence imaging of Raji/ffluc tumor growth in NSG mice that received 5×10^6 (4 mice per group) and 1×10^6 (9 mice per group) CD8$^+$ CD19-CAR T-cells, respectively. EGFRt-T-cells were used as control (four mice per group). Arrows mark the day of T-cell transfer. (**b**) Cytokine concentrations in supernatants of CD4$^+$ CD19-CAR T-cells after stimulation with K562, K562/CD19 and Raji cells for 24 h. (**c**) Proliferation of CD4$^+$ CD19-CAR T-cells after stimulation with K562, K562/CD19 and Raji cells for 72 h. Data in (**b**, **c**) are representative of three experiments with T-cells prepared from different donors. (**d**) Bioluminescence imaging of Raji/ffluc tumor growth in NSG mice (five mice per group) that received a mixture of 5×10^5 CD4$^+$ and 5×10^5 CD8$^+$ CAR T-cells. EGFRt-T-cells were used as a control (four mice per group). The arrow marks the day of T-cell transfer.

the FMC63-CAR but not by any of the human CARs (Figure 3f). A variant containing both arginine and serine substitutions was not recognized by FMC63 or any of the human scFv CARs. Together, these results show that either the presence of histidine at residue 218 or the absence of serine at residue 224 was necessary for FMC63 recognition, but insufficient to restore recognition by the human CD19-CARs. These results demonstrated that the same region encoded by exon 4 of CD19 was required for recognition by both the human CD19-CARs and the FMC63-CAR, but indicated that the particular aa important in this region for recognition by the different CARs were distinct.

Human CD19-CARs lack tonic signaling and cell surface clustering

It has been reported that some CARs when expressed in human T-cells result in tonic signaling in the absence of antigen and lead to an exhausted T-cell phenotype, characterized by sustained cell surface expression of PD-1 and loss of function in NSG tumor xenograft models.[34] We examined the expression of PD-1 on primary T-cells expressing each of the human CD19-CARs 10 days after T-cell stimulation and observed only low levels of PD-1 that were comparable to those on T-cells expressing FMC63 (Figure 4a).

Tonic signaling has also been linked to clustering of CAR molecules on the T-cell surface,[34] which may preclude their efficient recruitment to synapses with tumor cells. To examine the distribution of CD19-CARs on T-cells, we linked eGFP to the cytoplasmic tail of CD247 and expressed these constructs in CD8$^+$ T-cells. All human CD19-CARs showed a uniform surface distribution on T-cells comparable to the FMC63-CAR, and no evidence of CAR clustering was observed (Figure 4b). To analyze whether the CARs could cluster in an immunological synapse, we co-cultured

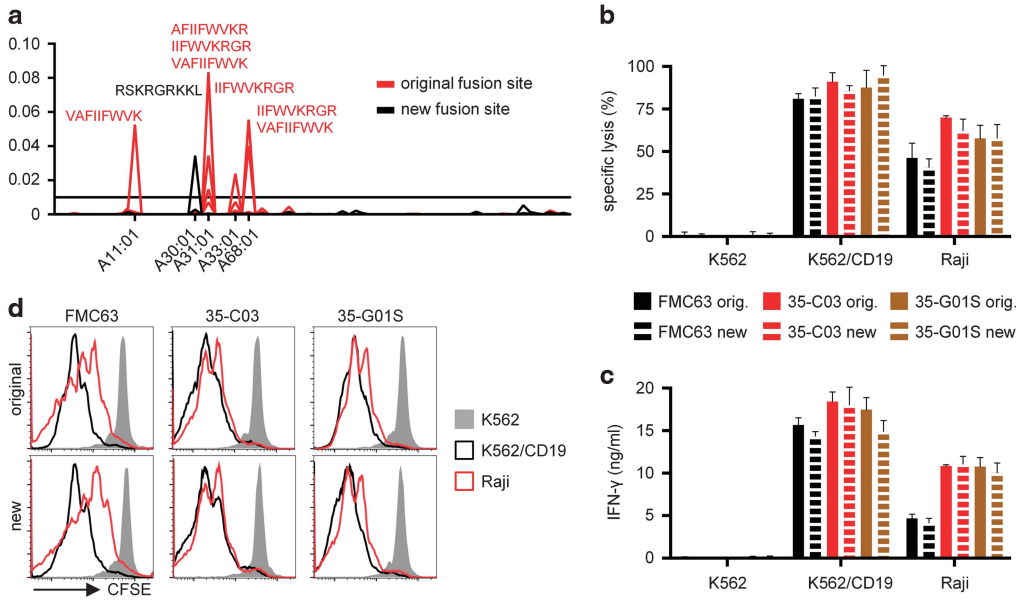

Figure 6. The CD28/4-1BB fusion site can be modified to reduce the probability of creating an immunogenic peptide. (**a**) Predicted affinities to MHC I of 9-mer peptides derived from the CD28/4-1BB fusion site. Reciprocals of predicted affinities in nM were plotted for all tested MHC types. A predicted affinity of < 100 nM (> 0.01) was chosen as a threshold. Peptides above the threshold and corresponding HLA types are specified. (**b**) Cytolytic activity, (**c**) IFN-γ production and (**d**) proliferation of $CD8^+$ T-cells expressing CARs with either the original or the new CD28/4-1BB fusion site after co-culture with K562, K562/CD19 and Raji cells. Data in (**b**–**d**) are representative of at least two experiments with T-cells prepared from different donors.

the CAR T-cells with $CD19^+$ Raji cells for 10 min at 37 °C before imaging. All CARs concentrated at the interface between the T-cells and target cells, indicating that they could efficiently form an immunological synapse with ligand expressing tumor cells (Figure 4c). No CAR clustering in synapses was observed when T-cells were co-cultured with $CD19^-$ K562 cells (data not shown). In addition, we did not observe constitutive proliferation in the absence of T-cell stimulation as has been reported for c-Met-specific CARs[35] (data not shown).

Human CD19-CARs eliminate tumors *in vivo*

Our *in vitro* data suggested that the human HL CARs were functionally superior to LH CARs and to the murine FMC63-CAR in tumor recognition assays. To determine if the HL CARs were functional *in vivo* and to compare their activity to FMC63, NSG mice that had been injected with 5×10^5 Raji/ffluc cells 1 week before were treated with 5×10^6 or 1×10^6 $CD8^+$ T-cells expressing each of the human scFv CARs or FMC63. At the high dose, T-cells expressing FMC63 and the human CARs eliminated the Raji tumors whereas control T-cells were ineffective; however, at the 1×10^6 cell dose, tumors progressed and progression was more rapid in mice treated with T-cells expressing FMC63 or 62-B01 CARs (Figure 5a).

Our initial functional studies were performed only using transduced $CD8^+$ T-cells, and we have previously shown that CAR T-cell products containing both $CD4^+$ and $CD8^+$ CAR T-cells are more potent than either subset alone, and can allow complete tumor eradication at very low cell doses.[26] To confirm that the human scFv CARs functioned in $CD4^+$ T-cells, we transduced $CD4^+$ T-cells and analyzed their function *in vitro*. All $CD4^+$ CAR T-cells released substantial amounts of Th1 cytokines and proliferated after stimulation with $CD19^+$ cells (Figures 5b and c). Consistent with the results in $CD8^+$ T-cells, $CD4^+$ T-cells expressing the human CARs released significantly more cytokines than $CD4^+$ T-cells expressing the FMC63-CAR.

We then treated Raji/ffluc-bearing NSG mice with 1×10^6 CAR T-cells comprised of a 1:1 mixture of $CD4^+$ and $CD8^+$ CAR T-cells and analyzed tumor growth. These experiments compared the FMC63-CAR currently in the clinic with 35-C03 and 35-G01S, which were potent in the experiments with $CD8^+$ T-cells alone. Raji tumors were rejected in mice treated with the mixture of $CD4^+$ and $CD8^+$ CAR T-cells expressing the human scFvs at this low cell dose, and mice remained tumor free without side effects for > 10 weeks. Both human CD19-CARs exhibited better antitumor activity than FMC63 (Figure 5d). Collectively, the data showed that CARs constructed from the fully human CD19-specific scFvs exhibited superior function *in vitro* and *in vivo* compared with the FMC63-CAR utilized in clinical trials.

Modifying the CD28/4-1BB fusion site to reduce MHC class I binding peptides

The rationale for replacing murine with human scFvs in CAR design is to reduce the immunogenicity in patients, since it is expected that human T-cells will be tolerant to the peptide sequences of human scFvs, and that Ab responses are less likely to develop. However, even if all individual segments of a CAR are of human origin, fusion sites between these segments could potentially be immunogenic. We have previously shown that $CD8^+$ but not $CD4^+$ T-cells are cytotoxic to transgene-positive T-cells in patients.[13] Because binding to MHC I molecules is a prerequisite for a peptide to be recognized by cytotoxic T-cells, we analyzed all 9-mer peptides located in the regions spanning each of the fusion sites (H-chain/G4S/L-chain, L-chain/IgG4-hinge, IgG4-hinge/CD28 transmembrane, CD28 transmembrane/4-1BB, 4-1BB/CD247, CD247/T2A) of the CD19-CARs for their potential to bind to human MHC I alleles using the NetMHC prediction algorithm (Figure 6a and Supplementary Figure S1A). We identified the fusion site between the CD28 transmembrane and the 4-1BB costimulatory domain as a region of concern that contained seven 9-mer peptide sequences with an affinity to several MHC class I molecules of < 100 nM based on MHC-binding prediction (Figure 6a). To reduce the potential of this fusion site to provide immunogenic epitopes, we extended the CD28 sequence by two additional aa (Supplementary Figure S1B), which resulted in only one predicted 9-mer peptide for HLA-A30:01 with an

affinity of < 100 nM (Figure 6a). FMC63, 35-C03 and 35-G01S CARs with this new fusion site were constructed and analyzed for *in vitro* function. We observed no significant differences between CARs with the original and the new fusion site in cytotoxicity, cytokine release and proliferation (Figures 6b–d), demonstrating that highly functional CARs with an optimized fusion site between the CD28 transmembrane and the 4-1BB signaling domains can be generated.

DISCUSSION

Adoptive transfer of T-cells engineered to express a receptor that re-directs T-cell specificity to a molecule expressed on malignant cells has shown potent antitumor effects in patients with B-cell malignancies and is being investigated for common epithelial tumors.[19,36,37] T-cells expressing CARs constructed from scFvs of murine mAbs specific for CD19 have resulted in durable remissions in a subset of patients with relapsed or refractory acute lymphoblastic leukemia, CLL and non-Hodgkin's lymphoma.[3–5,7,8] Relapse with tumor cells that have lost expression of the CD19 epitope targeted by the CAR is a cause of failure;[38] however, some of the patients have relapsed with $CD19^+$ tumor cells after an initial response to therapy, and relapse in these patients has been observed to coincide with a loss of detectable CAR T-cells in the blood.[3,9,39] The duration that transferred T-cells persist could reflect cell intrinsic properties of the infused T-cells, the costimulatory domain used in the CAR,[40] inhibitory effects of the patient's tumor on CAR T-cell survival and/or the development of immune responses to the foreign transgene product. Prior work has demonstrated that the transfer of autologous human T-cells expressing foreign proteins, including CARs derived from murine scFvs, can elicit cellular and humoral immune responses.[14,15] In patients treated with CD19-CAR T-cells, normal B-cells are eliminated, thereby compromising humoral immunity, but T-cell responses that primarily targeted peptide epitopes derived from the murine scFv have been detected in patients in whom CAR T-cells were lost.[3] Thus, the immunologic barrier to cells expressing foreign proteins represents a challenge for using CAR T-cells for cancer therapy, where a long duration of persistence may be required to eliminate all sites of metastatic disease. Immune responses to CAR T-cells may be even more problematic for patients earlier in their disease course when the immune system has not been suppressed by extensive prior chemotherapy, and for targets other than CD19, where Ab responses to the CAR are more likely.

Using a human or humanized scFv in CAR design should reduce the immunogenicity of synthetic CARs, but this approach has not yet been applied successfully to a clinically validated target. Alonso-Camino *et al.*[22] used lymphocyte display of a lentivirally encoded human scFv-library in a CAR format to screen for human Abs that recognized cell surface molecules on tumor cells. This approach may be useful as an initial screen to identify candidate human scFvs that recognize cancer cells but requires substantial validation to characterize the target and determine potential expression on normal tissues. Fully human anti-folate receptor-alpha and anti-mesothelin scFvs were isolated by guided selection and chain shuffling from phage and yeast display human scFv libraries.[20,21] These fully human scFvs were functional *in vitro* and in NSG mouse models;[20,21] however, whether these molecules can be targeted safely or effectively with CAR T-cells in the clinic remains to be established. The folate-receptor alpha is expressed on ovarian cancer and on the apical surface of normal epithelial cells, and an initial study of CAR T-cells derived from murine scFvs was not successful.[15] Mesothelin is expressed on mesothelioma, lung, ovarian and pancreatic cancers, but also on normal pericardium and pleura.[41,42] Analysis of the safety in patients of mesothelin-CARs constructed from murine and human scFvs, respectively, has been initiated by multiple groups.[16,43] Both humanized and human scFvs that target EGFR variant III, which is expressed on a subset of glioblastoma, have been described and are effective in animal models *in vivo*.[19] However, efforts to target EGFRvIII in clinical trials with CAR T-cells have thus far been ineffective.[44]

We focused on developing fully human scFv CARs for CD19 as a target because CARs with murine scFvs are effective in inducing remissions in patients with relapsed and refractory B-cell malignancies. We screened highly diverse human VH and VL libraries with the goal of isolating human scFvs that recognized the same epitope of CD19 as FMC63 and with a similar affinity. We identified 60 candidate scFvs and selected 5 with an identical VH paired with different VL to design CARs with identical spacer, transmembrane, costimulatory and signaling domains as present in our FMC63-CAR construct.[3] All scFvs were efficiently expressed as CARs, and in the HL configuration conferred superior recognition of $CD19^+$ tumor cell lines and primary human leukemia compared with the FMC63-CAR. We did not observe evidence of tonic signaling, and cell surface imaging using eGFP fusion constructs showed uniform distribution, similar to FMC63. T-cells expressing the human CD19-CARs were more potent than those expressing FMC63 in eliminating lymphoma xenografts in NSG mice. The superior efficacy of the human scFv CARs was unexpected since they were selected to have similar CD19 binding properties to FMC63. Expression of all CARs was also similar as measured by western blot and the level of co-expressed eGFP for the fusion constructs. Mapping of sequences involved in recognition of CD19 demonstrated that the same 19 aa region encoded by exon 4 of CD19 was required for recognition by all of the human scFvs and FMC63, but identified a distinct role for specific aa within this region. This difference in fine specificity or slight differences in CAR surface expression may account for the improved function of CARs constructed from the human scFvs.

A comprehensive assessment of the potential for immunogenicity of synthetic receptors requires analysis of all foreign peptide sequences that are present, including fusion sites between human components of the CAR. Prior studies have suggested that $CD8^+$ T-cells that recognize peptides from foreign transgene products presented by HLA class I molecules on transduced T-cells are a major mediator of immune-mediated elimination.[12] We used bioinformatics to evaluate the potential for peptides comprising the fusion sites to bind to human HLA class I alleles, and identified candidate immunogenic sequences between CD28 and 4-1BB that could be removed by altering the site of the fusion.

In conclusion, we describe the derivation, characterization and function of CD19-specific CARs derived from fully human scFvs. These novel CARs can be used for reprogramming T-cells against a validated clinical target. Using fully human CARs may reduce the risk of developing anti-CAR immune responses that have contributed to their premature elimination and a higher risk of relapse in prior trials. A fully human CD19-CAR may also allow repeat infusions enabling dose escalation of T-cells to reduce the severity of cytokine release syndrome and other toxicities of CAR T-cells.

CONFLICT OF INTEREST

SRR is founder and shareholder of Juno Therapeutics, Inc.

ACKNOWLEDGEMENTS

We thank Melissa Comstock and Don Parilla (Shared Resources, Fred Hutchinson Cancer Research Center) for expertise in performing mouse experiments. This work was supported by grants from the National Institutes of Health CA136551 and CA114536 (to SRR) and Juno Therapeutics, Inc.

AUTHOR CONTRIBUTIONS

DS designed and performed research, analyzed data, and wrote the manuscript; TH, SMS and AIS designed and performed research and analyzed data; YC and KMM provided expert advice and analyzed data; and SRR designed research, analyzed data and wrote the manuscript.

REFERENCES

1 Jensen MC, Riddell SR. Design and implementation of adoptive therapy with chimeric antigen receptor-modified T cells. *Immunol Rev* 2014; **257**: 127–144.
2 Kochenderfer JN, Rosenberg SA. Treating B-cell cancer with T cells expressing anti-CD19 chimeric antigen receptors. *Nat Rev Clin Oncol* 2013; **10**: 267–276.
3 Turtle CJ, Hanafi LA, Berger C, Gooley TA, Cherian S, Hudecek M *et al.* CD19 CAR-T cells of defined CD4+:CD8+ composition in adult B cell ALL patients. *J Clin Invest* 2016; **126**: 2123–2138.
4 Davila ML, Riviere I, Wang X, Bartido S, Park J, Curran K *et al.* Efficacy and toxicity management of 19-28z CAR T cell therapy in B cell acute lymphoblastic leukemia. *Sci Transl Med* 2014; **6**: 224ra225.
5 Grupp SA, Kalos M, Barrett D, Aplenc R, Porter DL, Rheingold SR *et al.* Chimeric antigen receptor-modified T cells for acute lymphoid leukemia. *N Engl J Med* 2013; **368**: 1509–1518.
6 Kalos M, Levine BL, Porter DL, Katz S, Grupp SA, Bagg A *et al.* T cells with chimeric antigen receptors have potent antitumor effects and can establish memory in patients with advanced leukemia. *Sci Transl Med* 2011; **3**: 95ra73.
7 Kochenderfer JN, Dudley ME, Feldman SA, Wilson WH, Spaner DE, Maric I *et al.* B-cell depletion and remissions of malignancy along with cytokine-associated toxicity in a clinical trial of anti-CD19 chimeric-antigen-receptor-transduced T cells. *Blood* 2012; **119**: 2709–2720.
8 Porter DL, Levine BL, Kalos M, Bagg A, June CH. Chimeric antigen receptor-modified T cells in chronic lymphoid leukemia. *N Engl J Med* 2011; **365**: 725–733.
9 Maude SL, Frey N, Shaw PA, Aplenc R, Barrett DM, Bunin NJ *et al.* Chimeric antigen receptor T cells for sustained remissions in leukemia. *N Engl J Med* 2014; **371**: 1507–1517.
10 Savoldo B, Ramos CA, Liu E, Mims MP, Keating MJ, Carrum G *et al.* CD28 costimulation improves expansion and persistence of chimeric antigen receptor-modified T cells in lymphoma patients. *J Clin Invest* 2011; **121**: 1822–1826.
11 Brentjens RJ, Riviere I, Park JH, Davila ML, Wang X, Stefanski J *et al.* Safety and persistence of adoptively transferred autologous CD19-targeted T cells in patients with relapsed or chemotherapy refractory B-cell leukemias. *Blood* 2011; **118**: 4817–4828.
12 Riddell SR, Elliott M, Lewinsohn DA, Gilbert MJ, Wilson L, Manley SA *et al.* T-cell mediated rejection of gene-modified HIV-specific cytotoxic T lymphocytes in HIV-infected patients. *Nat Med* 1996; **2**: 216–223.
13 Berger C, Flowers ME, Warren EH, Riddell SR. Analysis of transgene-specific immune responses that limit the in vivo persistence of adoptively transferred HSV-TK-modified donor T cells after allogeneic hematopoietic cell transplantation. *Blood* 2006; **107**: 2294–2302.
14 Lamers CH, Willemsen R, van Elzakker P, van Steenbergen-Langeveld S, Broertjes M, Oosterwijk-Wakka J *et al.* Immune responses to transgene and retroviral vector in patients treated with ex vivo-engineered T cells. *Blood* 2011; **117**: 72–82.
15 Kershaw MH, Westwood JA, Parker LL, Wang G, Eshhar Z, Mavroukakis SA *et al.* A phase I study on adoptive immunotherapy using gene-modified T cells for ovarian cancer. *Clin Cancer Res* 2006; **12**(20 Pt 1): 6106–6115.
16 Maus MV, Haas AR, Beatty GL, Albelda SM, Levine BL, Liu X *et al.* T cells expressing chimeric antigen receptors can cause anaphylaxis in humans. *Cancer Immunol Res* 2013; **1**: 26–31.
17 Zhao Y, Wang QJ, Yang S, Kochenderfer JN, Zheng Z, Zhong X *et al.* A herceptin-based chimeric antigen receptor with modified signaling domains leads to enhanced survival of transduced T lymphocytes and antitumor activity. *J Immunol* 2009; **183**: 5563–5574.
18 Sun M, Shi H, Liu C, Liu J, Liu X, Sun Y. Construction and evaluation of a novel humanized HER2-specific chimeric receptor. *Breast Cancer Res* 2014; **16**: R61.
19 Johnson LA, Scholler J, Ohkuri T, Kosaka A, Patel PR, McGettigan SE *et al.* Rational development and characterization of humanized anti-EGFR variant III chimeric antigen receptor T cells for glioblastoma. *Sci Transl Med* 2015; **7**: 275ra222.
20 Lanitis E, Poussin M, Hagemann IS, Coukos G, Sandaltzopoulos R, Scholler N *et al.* Redirected antitumor activity of primary human lymphocytes transduced with a fully human anti-mesothelin chimeric receptor. *Mol Ther* 2012; **20**: 633–643.
21 Song DG, Ye Q, Poussin M, Liu L, Figini M, Powell DJ Jr. A fully human chimeric antigen receptor with potent activity against cancer cells but reduced risk for off-tumor toxicity. *Oncotarget* 2015; **6**: 21533–21546.
22 Alonso-Camino V, Sanchez-Martin D, Compte M, Nunez-Prado N, Diaz RM, Vile R *et al.* CARbodies: human antibodies against cell surface tumor antigens selected from repertoires displayed on T cell chimeric antigen receptors. *Mol Ther Nucleic Acids* 2013; **2**: e93.
23 Terakura S, Yamamoto TN, Gardner RA, Turtle CJ, Jensen MC, Riddell SR. Generation of CD19-chimeric antigen receptor modified CD8+ T cells derived from virus-specific central memory T cells. *Blood* 2012; **119**: 72–82.
24 Hudecek M, Sommermeyer D, Kosasih PL, Silva-Benedict A, Liu L, Rader C *et al.* The nonsignaling extracellular spacer domain of chimeric antigen receptors is decisive for in vivo antitumor activity. *Cancer Immunol Res* 2015; **3**: 125–135.
25 Engels B, Cam H, Schuler T, Indraccolo S, Gladow M, Baum C *et al.* Retroviral vectors for high-level transgene expression in T lymphocytes. *Hum Gene Ther* 2003; **14**: 1155–1168.
26 Sommermeyer D, Hudecek M, Kosasih PL, Gogishvili T, Maloney DG, Turtle CJ *et al.* Chimeric antigen receptor-modified T cells derived from defined CD8(+) and CD4(+) subsets confer superior antitumor reactivity in vivo. *Leukemia* 2016; **30**: 492–500.
27 Wang X, Chang WC, Wong CW, Colcher D, Sherman M, Ostberg JR *et al.* A transgene-encoded cell surface polypeptide for selection, in vivo tracking, and ablation of engineered cells. *Blood* 2011; **118**: 1255–1263.
28 Leisegang M, Engels B, Meyerhuber P, Kieback E, Sommermeyer D, Xue SA *et al.* Enhanced functionality of T cell receptor-redirected T cells is defined by the transgene cassette. *J Mol Med* 2008; **86**: 573–583.
29 Hudecek M, Lupo-Stanghellini MT, Kosasih PL, Sommermeyer D, Jensen MC, Rader C *et al.* Receptor affinity and extracellular domain modifications affect tumor recognition by ROR1-specific chimeric antigen receptor T cells. *Clin Cancer Res* 2013; **19**: 3153–3164.
30 Lundegaard C, Lamberth K, Harndahl M, Buus S, Lund O, Nielsen M. NetMHC-3.0: accurate web accessible predictions of human, mouse and monkey MHC class I affinities for peptides of length 8-11. *Nucleic Acids Res* 2008; **36**(Web Server issue): W509–W512.
31 Wagner RW, Litovchick A, Chen Y. Protein screening methods. US Patent No: US9134304 B2 2015.
32 Steentoft C, Vakhrushev SY, Joshi HJ, Kong Y, Vester-Christensen MB, Schjoldager KT *et al.* Precision mapping of the human O-GalNAc glycoproteome through SimpleCell technology. *EMBO J* 2013; **32**: 1478–1488.
33 De Oliveira SN, Wang J, Ryan C, Morrison SL, Kohn DB, Hollis RP. A CD19/Fc fusion protein for detection of anti-CD19 chimeric antigen receptors. *J Transl Med* 2013; **11**: 23.
34 Long AH, Haso WM, Shern JF, Wanhainen KM, Murgai M, Ingaramo M *et al.* 4-1BB costimulation ameliorates T cell exhaustion induced by tonic signaling of chimeric antigen receptors. *Nat Med* 2015; **21**: 581–590.
35 Frigault MJ, Lee J, Basil MC, Carpenito C, Motohashi S, Scholler J *et al.* Identification of chimeric antigen receptors that mediate constitutive or inducible proliferation of T cells. *Cancer Immunol Res* 2015; **3**: 356–367.
36 Morello A, Sadelain M, Adusumilli PS. Mesothelin-targeted CARs: driving T cells to solid tumors. *Cancer Discov* 2016; **6**: 133–146.
37 Berger C, Sommermeyer D, Hudecek M, Berger M, Balakrishnan A, Paszkiewicz PJ *et al.* Safety of targeting ROR1 in primates with chimeric antigen receptor-modified T cells. *Cancer Immunol Res* 2015; **3**: 206–216.
38 Sotillo E, Barrett DM, Black KL, Bagashev A, Oldridge D, Wu G *et al.* Convergence of acquired mutations and alternative splicing of CD19 enables resistance to CART-19 immunotherapy. *Cancer Discov* 2015; **5**: 1282–1295.
39 Lee DW, Kochenderfer JN, Stetler-Stevenson M, Cui YK, Delbrook C, Feldman SA *et al.* T cells expressing CD19 chimeric antigen receptors for acute lymphoblastic leukaemia in children and young adults: a phase 1 dose-escalation trial. *Lancet* 2015; **385**: 517–528.
40 Kawalekar OU, O'Connor RS, Fraietta JA, Guo L, McGettigan SE, Posey AD Jr *et al.* Distinct signaling of coreceptors regulates specific metabolism pathways and impacts memory development in CAR T cells. *Immunity* 2016; **44**: 380–390.
41 Lamberts LE, de Groot DJ, Bense RD, de Vries EG, Fehrmann RS. Functional genomic mRNA profiling of a large cancer data base demonstrates mesothelin over-expression in a broad range of tumor types. *Oncotarget* 2015; **6**: 28164–28172.
42 Chang K, Pastan I. Molecular cloning of mesothelin, a differentiation antigen present on mesothelium, mesotheliomas, and ovarian cancers. *Proc Natl Acad Sci USA* 1996; **93**: 136–140.
43 Adusumilli PS, Cherkassky L, Villena-Vargas J, Colovos C, Servais E, Plotkin J *et al.* Regional delivery of mesothelin-targeted CAR T cell therapy generates potent and long-lasting CD4-dependent tumor immunity. *Sci Transl Med* 2014; **6**: 261ra151.
44 O'Rourke D, Desai A, Morrissette J, Martinez-Lage M, Nasrallah M, Brem S *et al.* Abstracts from the 20th Annual Scientific Meeting of the Society for Neuro-Oncology, November 19–22, 2015, San Antonio, Texas: IMCT-15 pilot study of T cells redirected to EGFRvIII with a chimeric antigen receptor in patients with EGFRvIII+ glioblastoma. *Neuro-Oncology* 2015; **17**(suppl 5): v110–v111.

Supplementary Information accompanies this paper on the Leukemia website (http://www.nature.com/leu)